FERMILAB-Proposal-0570

Fermilab Experimental
Proposal 570
Spokesperson: Irwin A. Pless
Massachusetts Institute of Technology
Laboratory for Nuclear Science
575 Technology Square, Room 408
Cambridge, Massachusetts 02139
Telephone: (617) 253-6081
8 September 1977

PROPOSAL FOR A STUDY OF PARTICLE PRODUCTION AND DYNAMICS FROM X = 0 TO X = 1 AND THE DEPENDENCE ON INCIDENT QUANTUM NUMBERS

Brown University
Providence, Rhode Island 02912
D. Brick
A. M. Shapiro
M. Widgoff

CERN
Geneva, Switzerland
F. Bruyant
L. Montanet

Illinois Institute of Technology
Chicago, Illinois 60616
R. A. Burnstein
H. A. Rubin

Indiana University
Bloomington, Indiana 47401
E. D. Alyea, Jr.

Johns Hopkins University
Baltimore, Maryland 21218
A. Pevsner
L. Bachman

Massachusetts Institute of Technology
Cambridge, Massachusetts 03139
F. Barreiro
O. Benary
E. S. Hafen
R. I. Hulsizer
V. Kistiakowsky
I. A. Pless
P. Trepagnier
R. K. Yamamoto

University of Mons
Mons, Belgium
P. Gillis
F. Grard
V. Henri
P. Herquet
J. Skura
R. Windmolders

University of Nijmegen
Nijmegen, The Netherlands
F. Crijns
W. Kittel
W. Metzger
C. Pols
J. Schotanus
R. Van de Walle

299 pgs.

Fermilab Experimental
Proposal 570
Spokesperson: Irwin A. Pless
Massachusetts Institute of Technology
Laboratory for Nuclear Science
575 Technology Square, Room 408
Cambridge, Massachusetts 02139
Telephone: (617) 253-6081
8 September 1977

PROPOSAL FOR A STUDY OF PARTICLE PRODUCTION AND DYNAMICS FROM X = 0 TO X = 1 AND THE DEPENDENCE ON INCIDENT QUANTUM NUMBERS

Brown University Providence, Rhode Island 02912	D. Brick A. M. Shapiro M. Widgoff
University of Cambridge Cambridge, England	R. E. Ansorge J. R. Carter W. W. Neale J. G. Rushbrooke D. R. Ward B. A. Webber T. O. White
CERN Geneva, Switzerland	F. Bruyant L. Montanet
~~Fermilab~~ ~~Batavia, Illinois 60510~~	~~D. Bogert~~ ~~J. Wolfson~~
Illinois Institute of Technology Chicago, Illinois 60616	R. A. Burnstein H. A. Rubin
Indiana University Bloomington, Indiana 47401	E. D. Alyea, Jr.
Johns Hopkins University Baltimore, Maryland 21218	A. Pevsner L. Bachman
Massachusetts Institute of Technology Cambridge, Massachusetts 03139	F. Barreiro O. Benary E. S. Hafen R. I. Hulsizer V. Kistiakowsky I. A. Pless P. Trepagnier R. K. Yamamoto
University of Mons Mons, Belgium	P. Gillis F. Grard V. Henri P. Herquet J. Skura R. Windmolders

University of Nijmegen Nijmegen, The Netherlands	F. Crijns W. Kittel W. Metzger C. Pols J. Schotanus R. Van de Walle
Oak Ridge National Laboratory Oak Ridge, Tennessee 37830	H. O. Cohn R. D. McCulloch
University of Padova Padova, Italy	A. Bettini M. Cresti M. Mazzucato L. Peruzzo P. Rossi G. Sartori S. Sartori L. Ventura A. Zudori G. Zumerle
University of Pavia Pavia, Italy	S. Alborghetti R. Attendoli E. Calligarich G. Cecchet R. Dolfini L. Mapelli S. Ratti
University of Rome Rome, Italy	L. Barone R. Bizzarri G. Bressi G. Ciapetti D. Dionisi P. F. Loverre D. Zanello L. Zanello
Rutgers University New Brunswick, New Jersey 08903	P. F. Jacques R. J. Plano T. L. Watts
Stevens Institute of Technology Hoboken, New Jersey 07030	E. B. Brucker E. L. Koller P. E. Stamer S. Taylor
Technion Haifa, Israel	S. Dado J. Goldberg S. Toaff

Tel-Aviv University Tel-Aviv, Israel	G. Alexander S. Dagan J. Grunhaus A. Levy D. Lissauer Y. Oren
University of Tennessee Knoxville, Tennessee 37916	W. M. Bugg G. T. Condo T. Handler E. L. Hart
University of Trieste Trieste, Italy	E. Castelli C. Omero P. Poropat M. Sessa
Weizmann Institute of Science Rehovot, Israel	Y. Eisenberg B. Haber D. Hochman U. Karshon E. E. Ronat A. Shapira R. Yaari G. Yekutieli
Yale University New Haven, Connecticut 06520	H. Kraybill D. Ljung T. Ludlam H. D. Taft

Summary

We propose a study of the production of π^0, $\pi^\pm$, Λ^0, K^0, K^+, K^-, p, $\bar{p}$ in multiparticle final states, with tagged positive and negative beams of 200 GeV/c particles incident on protons. In addition, a new phenomenon in which a large amount of electromagnetic energy is emitted in the forward direction will be investigated. Evidence for this phenomenon was observed in Experiment 154.

This experiment is to be carried out with the advanced hybrid spectrometer system, with the bubble chamber as target, and with the downstream portion of the spectrometer including two powerful new tools, an ISIS system to identify charged particles and a forward gamma detector (FGD) to study the production of electromagnetic energy. The beam momentum and the ISIS design are such as to give high efficiency for identification of particles produced in the central region of x and y, where most particle production takes place. The two instruments will allow us to study for the first time correlations among neutral particles and between neutral and charged particles, and also questions of local conservation of transverse momentum and of quantum numbers.

We wish to achieve a positive beam with 10% K^+, the remainder being equally divided between p and π^+, and a negative beam composition of 20% $\bar{p}$, the remainder π^-. We propose 1×10^6 pictures in each of the two beams. This will allow us to study the details of the production processes as a function of the quantum numbers of the projectile particle under identical experimental conditions, with good statistics.

Introduction

We propose a comprehensive experiment to examine the dynamics of hadronic production utilizing the full analyzing power of the advanced 30-inch hybrid bubble chamber system for a variety of incident beams with downstream instrumentation for the identification of heavy charged particles (ISIS) and for the measurement of electromagnetic decays of forward-going neutral particles (Forward Gamma Detector).

Presently available data, consisting primarily of momentum distributions of charged secondary pions, have revealed a pattern in which short-range phenomena characteristic of asymptotic models coexist with strong fragmentation effects. At Fermilab energies the nature of the beam and target particles is reflected in the major fraction of particle production; not only the diffraction component, but also the high-multiplicity component and the (presumably) deeply inelastic production of J/ψ show a marked dependence on the quantum numbers of the incident channel. In the latter cases the observed effects may be a direct consequence of the kinematic distribution of quarks among the incident particles.

In order to extract new information regarding these features of the strong interaction mechanism, we propose an experiment with the full retinue of charged hadron beams available to the 30-inch chamber for the widest spectrum of incident channel quantum numbers, employing the ISIS detector to isolate heavy charged particles (K's and protons) in the final state, and the forward gamma detector for a more nearly complete accounting of the total energy into pions. These new capabilities will allow a much more complete examination of the generalized charge structure of events than has been possible in the past and in turn will require longer exposures. The physics topics will emphasize multiparticle production in the central region. The parameters of the experiment have been chosen to optimize the effectiveness of the ISIS detector in this range of center-of-mass momenta.

We request 1.0×10^6 pictures with a tagged negative beam and 1.0×10^6 pictures with a tagged positive beam, both at 200 GeV/c momentum. The positive beam will be composed of approximately 10% K^+, with remainder consisting of equal numbers of π^+ and p, while the negative beam will consist of about 20% $\bar{p}$ and 80% π^-. The use of these tagged beams will enable us to study the dependence of the interaction characteristics on the quantum numbers of the incident particle with minimum systematic errors and minimum set-up time. These areas of investigation will include single particle distributions for identified charged and neutral particles, multiplicity studies, and correlation studies, including the question of neutral-charged particle correlations about which little is known. The ω, η^0, $\rho^{\pm}$ and other resonances which decay into π^0's will now be studied in detail and their connection with clusters will be clarified. Also, local conservation of transverse momentum, strangeness and other quantum numbers will be checked with much more complete information. The forward gamma detector will also permit the investigation of the large amounts of forward going neutral energy observed in low multiplicity events, a new phenomenon which has been observed at Fermilab energies (E154). Four-constraint fits will be extended to events with one, two, and possibly three π^0's, and events with charged K's. In addition, we will engage in more speculative searches: a search for a possibly new phenomenon where both projectile and target end up near x=0; a search for new particles that decay into one or more heavy particles and several pions; a study of four-constraint physics; and a study of pairs of identical heavy particles to compare with the Bose-like behavior seen in identical-pion pairs.

Physics of the Experiment

The primary object of this experiment is the study of the production characteristics of particles and resonances in interactions with target protons, and the dependence of these production characteristics on the quantum numbers of the projectile particle.

We will be able to detect, identify and measure γ, π^0, $\pi^{\pm}$, K^0, $K^{\pm}$, p, $\bar{p}$, Λ^0, with sufficient accuracy to isolate and study the resonances they form.

Figure 1 shows the main features of the downstream spectrometer system which makes these studies possible.

Specific physics topics we will explore are:

1. Study of π^0 Production

In order to study π^0 production, we have built a lead glass shower detector-hodoscope with good energy and spatial resolution. A prototype has been extensively tested and used in E299; the result of these tests as well as a description of the full scale forward gamma detector (FGD) are included in Appendix I.

With this device we will be able to reconstruct π^0 and η^0 mesons and to distinguish up to six gamma rays ($3\pi^0$). Thus, we shall be able to perform a study of the two, four, six, and eight charged prong topologies where one, two and possibly three π^0's are observed, allowing four constraint (4C) fits. There have been no previous studies of these channels. This experiment, together with E154 and E299, also will permit high statistics studies of the four, six, and eight charged prong topologies with no neutral particles, and comparison with the corresponding channels with π^0 mesons should prove extremely fruitful. For example, our E154 study of the four charged-particle 4C sample[1] has shown that more than 92% of the cross section is due to beam and target diffraction dissociation. $\rho^0\pi^-$ events make an important contribution to the beam dissociation cross section in the A_1 and A_2 mass region and there is some evidence for a contribution from $f^0\pi^-$. Higher statistics should permit a resolution of the latter question as well as yielding a better understanding of the three-pion system in all invariant mass regions. In this experiment it will be possible also to obtain results for the four charged-prong, one π^0 channel at a similar level of statistics.

This experiment will also permit an inclusive study of π^0 production as a function of rapidity in the forward hemisphere. Such a study is extremely important in order to verify the previous evidence for the existence of clusters and to determine whether they consist mainly of two pions ("ρ" like) or three pions ("ω" like) and indeed whether clusters <u>are</u> the well-known resonances. Rigorous tests of local transverse momentum conservation will be carried out, whereas with charged-particle rapidity studies only, definitive tests of this sort are not possible.

Another facet of this experiment is the examination of the forward going neutral energy associated with the production of two charged particles. Our interest in this phenomenon stems from our observations in Exp. 154 ($\pi^- p$ at 150 GeV/c). For this experiment we had in our PWC system a crude gamma ray detector consisting of a two-radiation length thick piece of lead followed by three PWC planes. This counter permitted a rough measurement of the intensity of electromagnetic energy incident on the lead converter in each event. In the two-prong inelastic data we found a significant class of events in which most of the incident momentum went into the forward electromagnetic shower [refer to proposal for E393, Appendix III]. Monte Carlo calculations emulating known diffractive processes were not able to reproduce the observed results. We believe that these observations indicate a new phenomenon occurring in the 2-prong events, and that a detailed study of the electromagnetic energy associated with the two-prong events is required. Data from the forward gamma detector in the experiment proposed here will allow us to determine π^0 four-vectors and form relevant invariant mass distributions. If there are narrow structures in this final state, we will be able to detect them. In any event, we will be able to determine the character of this final state in an exclusive manner and determine if there are any new physical phenomena involved.

2. Multi-Particle Production with Charged Particle Identification

In order to identify charged particles which leave the bubble chamber in the forward direction, we will use the Fermilab ISIS system which is described in Appendix II. This is the relativistic rise particle identifier which was first discussed in the September 1975 Bubble Chamber Symposium[2] and which was further specified during a workshop held at Fermilab in May 1976[3]. This device is designed to have good acceptance for particles produced in the central region, near x=0, where most particle production occurs, and is essential to the study of the following questions.

a) Single Particle Inclusive Distributions

K^+, K^-, p, $\bar{p}$ production as functions of t, x and y will be measured. These will be the first complete data of this kind at these energies. K^0 and Λ^0 distributions will also be studied. It is important to determine where in the rapidity chain these heavy particles tend to lie - are they produced in association with either the target or projectile, or does production simply peak in the central region. By comparison of measurements made with the different projectile particles under identical circumstances, it will be possible to see over what range of rapidity the nature of the incident particle affects the production of these particles.

Comparison of $K^{\pm}K^{\mp}$, $K^{\pm}\Lambda^0$, $K^{\pm}K^0$ production for different incident beam particles will allow a search for a strangeness = 0 plateau. The existence of such a plateau would be interesting, in view of the fact that no charge = 0 plateau exists in π^-p interactions.[4]

b) Correlations

Rapidity correlations between pairs of charged pions have yielded much information leading to our current understanding of the nature of multiparticle production. The observed short-range correlations have stimulated great interest in the question of cluster formation and the concept of local quantum number conservation near y = 0[5].

Specific identification of $K^{\pm}$ *and* $p^{\pm}$ *with good efficiency in the central region will* greatly extend the correlation information and allow a study of baryon number and strangeness compensation in addition to that of electric charge. Also of prime interest would be the study of π^0 creation near the central rapidity region. Measurements of the π^0 mesons will permit the more complete study of local conservation of transverse momentum. To date, there is very little information regarding the correlation between neutral and charged pions. The distribution of π^0 production and correlations between π^0's have yet to be studied. In addition, identical particle effects which have been studied for charged pion pairs will be investigated for K^+K^+, K^-K^- and $\pi^0\pi^0$ pairs.

This experiment, by virtue of π^0 detection and charged kaon identification, should provide a rich variety of new opportunities for the study of correlations in effective mass of multiparticle systems (e.g., resonance production), and the study of multiparticle correlations treating resonance states as single prompt particles.

c) Braking Collisions

There appears to be some experimental evidence from the ISR that a cross section approaching one millibarn exists for a process where both incident protons stop in the center-of-mass.[6] The number and distribution of the associated particles (presumably mostly pions) is of great interest. No data exist on these questions. There are two speculations about the origin of this phenomenon. The first is that the two protons stop due to a mutually catastrophic bremsstrahlung of pions. This would manifest itself by the emission of two large jets of pions, forward and backward. The second speculation is that the protons stop due to a coherent central collision of the fundamental constituents (quarks, partons), and this type of reaction might yield an isotropic distribution of pions. Establishing that the ISR result is real and measuring the distributions of the outgoing particles would establish a totally new phenomenon which should yield fundamental information on elementary hadronic properties.

d) Resonance Production

The capability for detecting charged K mesons as well as neutral strange particle decays over momentum ranges which encompass the central region, coupled with the π^0 detection capability of the forward gamma detector, will provide the means for a systematic study of the following matrix of inclusive reactions:

$$\begin{bmatrix} \pi^{\pm} \\ K^{+} \\ p^{\pm} \end{bmatrix} + p \longrightarrow \begin{bmatrix} \eta \\ \rho^{\pm},\ \rho^{0} \\ K^{*\pm},\ K^{*0} \\ \Phi^{0} \\ \omega^{0} \\ \Delta,\ y^{*} \end{bmatrix} + \text{anything}$$

The initial analysis goal will be to determine the cross sections as functions of the kinematic variables x, y, t, etc. The contribution of resonances, especially the meson resonances, to the whole of multiparticle production is important in its own right, and has obvious implications for the understanding of clustering phenomena. Of the reactions listed above, only those leading to ρ^0 and Δ^{++} have been studied in any detail in collisions at Fermilab energies.

In terms of the generalized charge structure of events, we expect that the kinematic distribution of resonance states will be far more sensitive to the nature of reaction mechanisms than is the distribution of their decay products. The proposed experiment will afford a broad investigation of the kinematic behavior of identifiable resonances in terms of the resonance quantum numbers and the quantum numbers of the incident beam. Existing data for the production of ρ, K^*, and J/ψ show a marked dependence on the nature of the incident particles, with central production observed in pp or p-nucleus collisions and forward, beam-like production observed in collisions of mesons with nucleons. This could be the result of the usual hierarchy of coupling strengths for the various quantum number exchanges in a multiperipheral mechanism, or it could result from the intrinsic constituent structure of beam and target. Although the absolute cross sections for ρ^0 production are nearly equal for π meson and proton beams incident[7], the relative cross sections for J/ψ production are very different[8], and recent measurements of J/ψ induced by meson, proton and anti-proton beams at 40 GeV/c[9] point to a significant contribution from valence quark annihilation. Of particular interest in this context will be a systematic examination of the production of the low-mass meson resonances ρ, ω, Φ, K* for π, K, p and $\bar{p}$ beams incident.

Data of this sort will be important as well for the emerging phenomenology of hadronic interactions via hard collisions of constituents. While such models emphasize the high-P_T regime beyond the reach of bubble chamber data, it is clear that more complete and precise data on the resonance structure of "normal" events will be of great value in the interpretation of experiments which probe the structure of large transverse momentum phenomena.

e) $\bar{p}p$ Annihilation

Our primary interest in an enriched $\bar{p}$ component of the negative beam arises from our desire to have the widest possible spectrum of incident channel quantum numbers (or valence quark configurations) available for a systematic study of the dynamics of particle production. The importance of a $\bar{p}$ beam in the context of such a program is discussed in the subsections above.

In addition, it would be of great interest to measure the total $\bar{p}p$ annihilation cross section. An attempt will be made to do so in this experiment in spite of the major difficulties involved in estimating the cross section for $\bar{p}p \to \bar{n}n + X$. While this cross section can be estimated in principle by assuming factorization and applying this assumption to measurements of the channels $\bar{p}p \to \bar{n}p + X$, $\bar{p}p \to \bar{p}n + X$, and $\bar{p}p \to \bar{p}p + X$, meaningful results can only be obtained if the factorization assumption is reliable to considerably better than 5%. This is because the interesting difference $\sigma_T(\bar{p}p) - \sigma_T(pp)$ is expected to be of the order of 2mb[10], which is 5% of either cross section and the correction for $\bar{n}n$ production must be known considerably better than the difference itself. It is obvious that inefficiencies in measuring any of the three cross sections will reduce the reliability of the estimate of the annihilation cross section. It is clearly important, however, to establish the measurable cross sections as accurately as possible.

Beam and Experimental Apparatus

As has been discussed, the experiment will require the Fermilab hybrid 30-inch bubble chamber - PWC spectrometer, with the addition of an ISIS system and the FGD in the downstream portion of the spectrometer, as shown in Fig. 1. These devices are described in detail in Appendices I and II.

A prototype of the FGD has been intensively and successfully tested in use and its performance is described in Appendix I. Results of these measurements show that we are able to locate the shower centers within a standard deviation of 1.4 mm, and to measure the shower energy with a resolution $\Delta E/E = .27/\sqrt{E}$ where ΔE is the full width at half maximum of the measured energy distribution for incident electrons of nominal energy E. The prototype has been tested with incident electrons of energies ranging from 26 GeV/c to 100 GeV/c. The angular acceptance of the full FGD is 125 mr.

The full scale FGD is now being assembled at Fermilab.

The Fermilab ISIS is well matched to the spectrum of charged particles leaving the bubble chamber, since the beginning of the relativistic rise region for protons is at about 5 GeV/c and that for kaons and pions is lower. The acceptance of the Fermilab ISIS is also quite well matched to the angular spread of the particles leaving the bubble chamber (see Appendix II).

As discussed in Appendix II, the resolution of the Fermilab ISIS decreases above 10 GeV/c with increasing momentum and kaon identification becomes poor above 40 GeV/c. Thus the momentum resolution of the hybrid system ($\Delta p/p = 0.06p\%/\mathrm{GeV}/c$) is sufficient so as not to be a limitation on the Fermilab ISIS over the momentum range where it has good resolution, particle identification in this device requiring momenta measured to better than 10%.

A primary interest of this experiment is the study of reactions which yield protons nearly at rest in the center of mass and mesons in the central region of rapidity. As can be seen in Figs. 2 and 3, the corresponding laboratory momenta of these secondary particles fall in a region where the resolution of the Fermilab ISIS is very good.

The first module of the Fermilab ISIS (ISIS-1) is being assembled. After preliminary testing it will be shipped to Fermilab the beginning of October where it is scheduled for a beam test starting October 27.

Preliminary studies have shown that, with an accelerator beam of 400 GeV/c, the desired ratio of 10% K^+ is achievable in the 200 GeV/c positive beam, with the remainder approximately equally divided between π^+ and p. Theoretical calculations indicate that one should be able to achieve the desired $\bar{p}/\pi^-$ ratio of 1/4 in the negative 200 GeV/c beam. Beam tests will have to be made to determine the actual beam compositions. With these beams, enriched in K^+ and $\bar{p}$, an intensity of about 10^{10} particles per ping will yield the desired 8 tracks per picture.

<u>Equipment Costs</u>

New equipment will be required for this experiment. All electronic items shown in fig. 1, i.e., P1, D1, I1, D2, I2, D3, and FGD, will be used for the first time in this experiment. The following list describes these items, their cost and who will furnish them.

Description	Cost	Responsibility
P1 - 3,500 wire PWC system	$125,000	Universities
	85,000	Fermilab
D1 - 80 channel Drift Chamber system	25,530	Fermilab
	45,000	Universities
I1 - ISIS 1	40,000	Fermilab
	225,000	Universities
D2 - 80 channel Drift Chamber system	25,530	Fermilab
	49,000	Universities
I2 - ISIS 2	146,200	Fermilab
	187,000	Universities
D3 - 80 channel Drift Chamber system	70,530	Universities
FGD - Forward Gamma Ray Detector	250,000	Universities
	100,000	Fermilab
Computer		Fermilab

As noted before, the FGD is complete and hence requires no new money. ISIS I is actually under construction and test and does not require new money. ISIS II, the PWC and Drift Chamber systems do require new money. Note that the above figures are approximate. Detailed figures will be furnished and negotiated for the agreement.

REFERENCES

1) "The Exclusive Channel $\pi^-\pi^-\pi^+p$ in π^-p Interactions at 147 GeV/c", D. Fong et al., Nuovo Cim. 34A, 659 (1976).

2) Bubble Chamber Symposium, September 1975. Reported by T. Groves, NALREP, December 1975.

3) Particle Identifiers for Hadron Physics, May 1976. Reported by V. Kistiakowsky, NALREP, July 1976.

4) "Evidence for Charged Cluster Emission in 147 GeV/c π^-p Collisions", D. Fong et al., Phys. Lett. 61B, 99 (1976).

5) "Local Quantum-Number Compensation in Multiple Production", C. Quigg, Phys. Rev. D12, 834 (1975).

6) M. Jacob, private communication.

7) "Inclusive and Semi-Inclusive ρ^0 Production in π^-p Interaction at 147 GeV/c", D. Fong et al., Phys. Lett, 60B, 124 (1975); "ρ^0 Production in 205 GeV/c pp Production", R. Singer et al., Phys. Lett. 60B, 385 (1976).

8) "Measurement of ψ (3.1) Meson Production by Pions and Protons", G. J. Blanar et al., Phys. Rev. Lett. 35, 346 (1975); "Production of Muon Pairs by 150 GeV/c π^+ and Protons", K. J. Anderson et al., Phys. Rev. Lett. 36, 237 (1976).

9) "Experimental Comparison of j/ψ Production by $\pi^\pm$, $K^\pm$, p and $\bar{p}$ Beams at 39.5 GeV/c", M. J. Corden et al., Phys. Lett. 68B, 96, (1977).

10) "Total Cross Sections of p and $\bar{p}$ on Protons and Deuterons Between 50 and 200 GeV/c", A. S. Carroll et al., Phys. Rev. Lett. 33, 928 (1974).

Fig. 1

Downstream Hybrid Spectrometer System

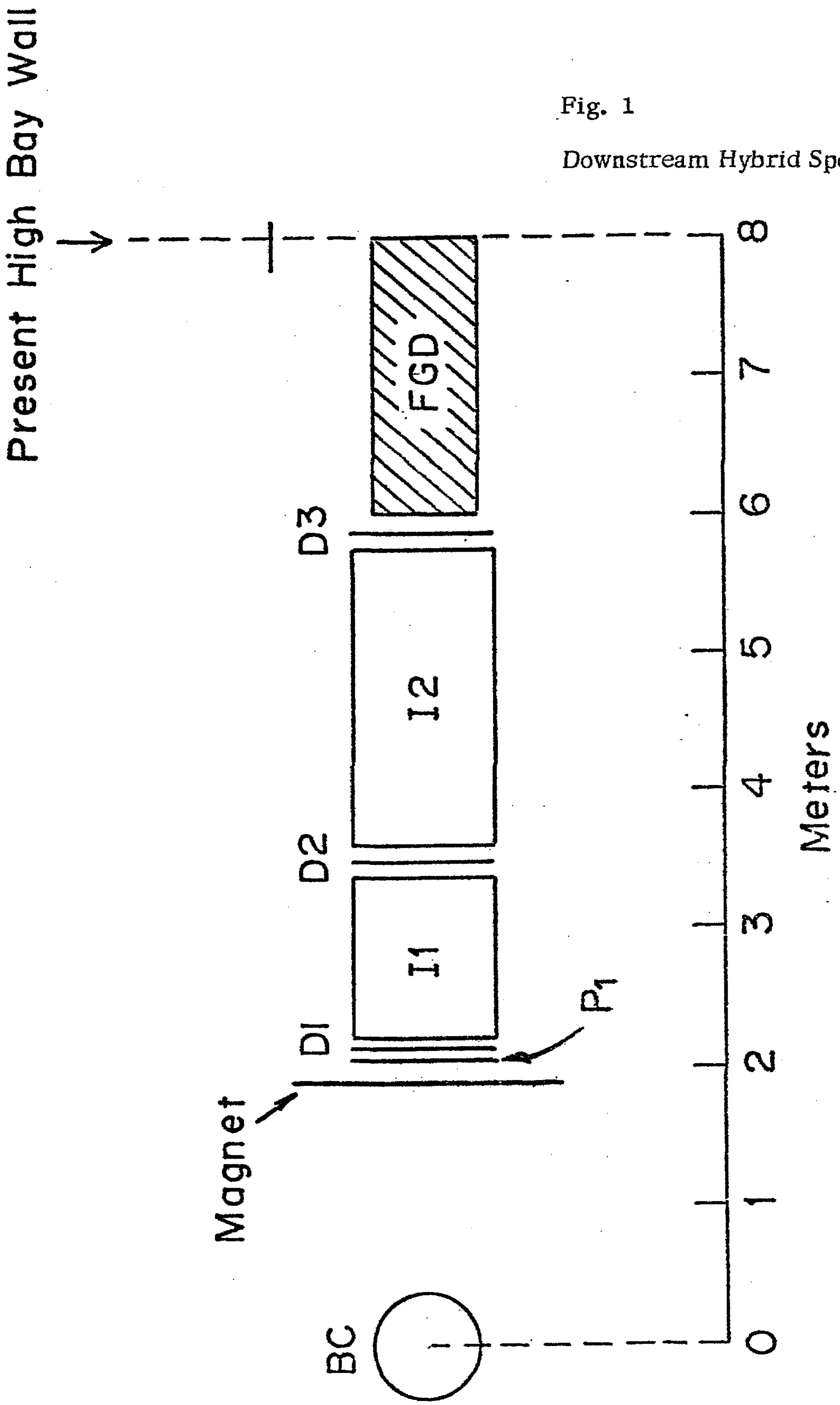

Fig. 2

Protons at 200 GeV/c

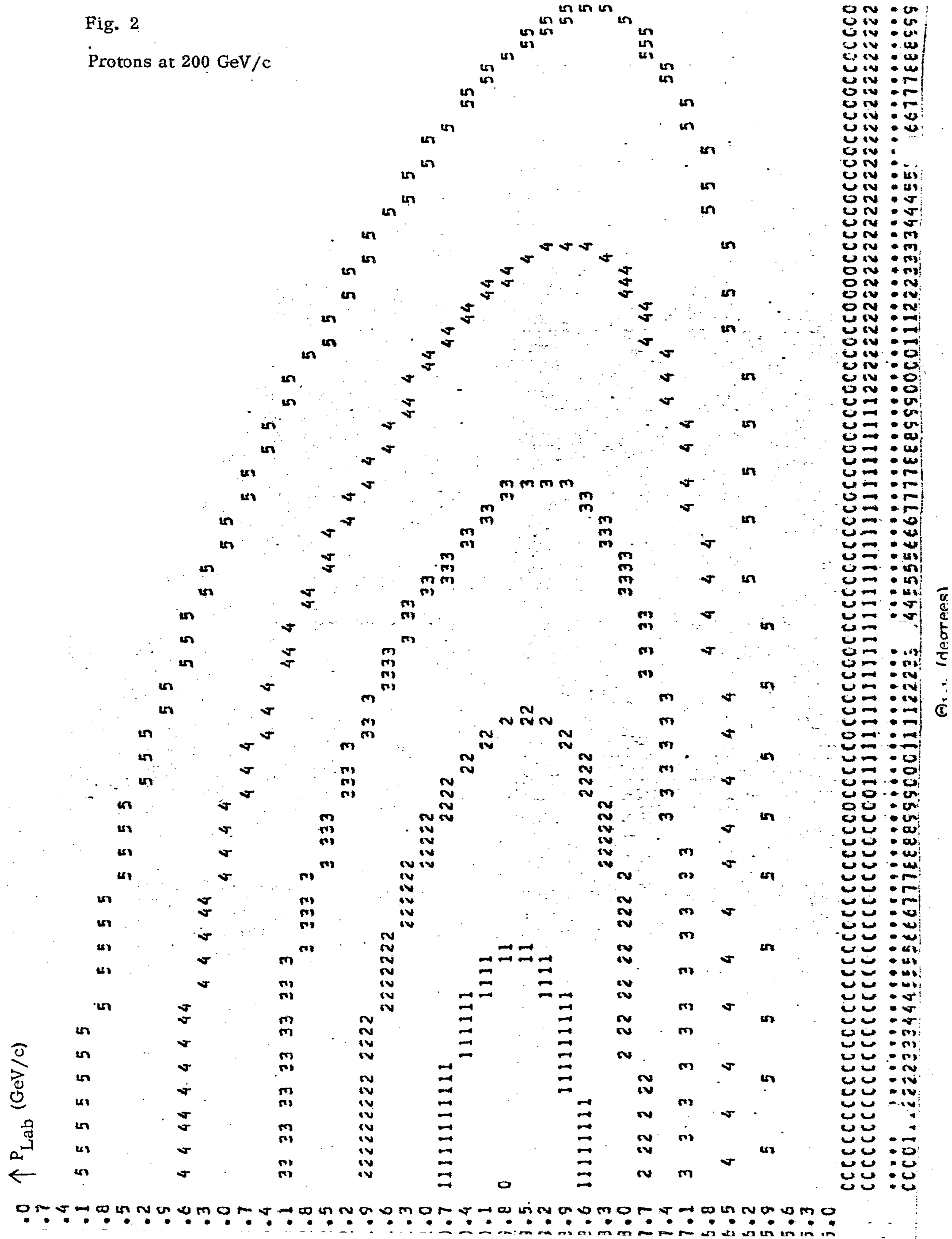

Fig. 3

Kaons at 200 GeV/c

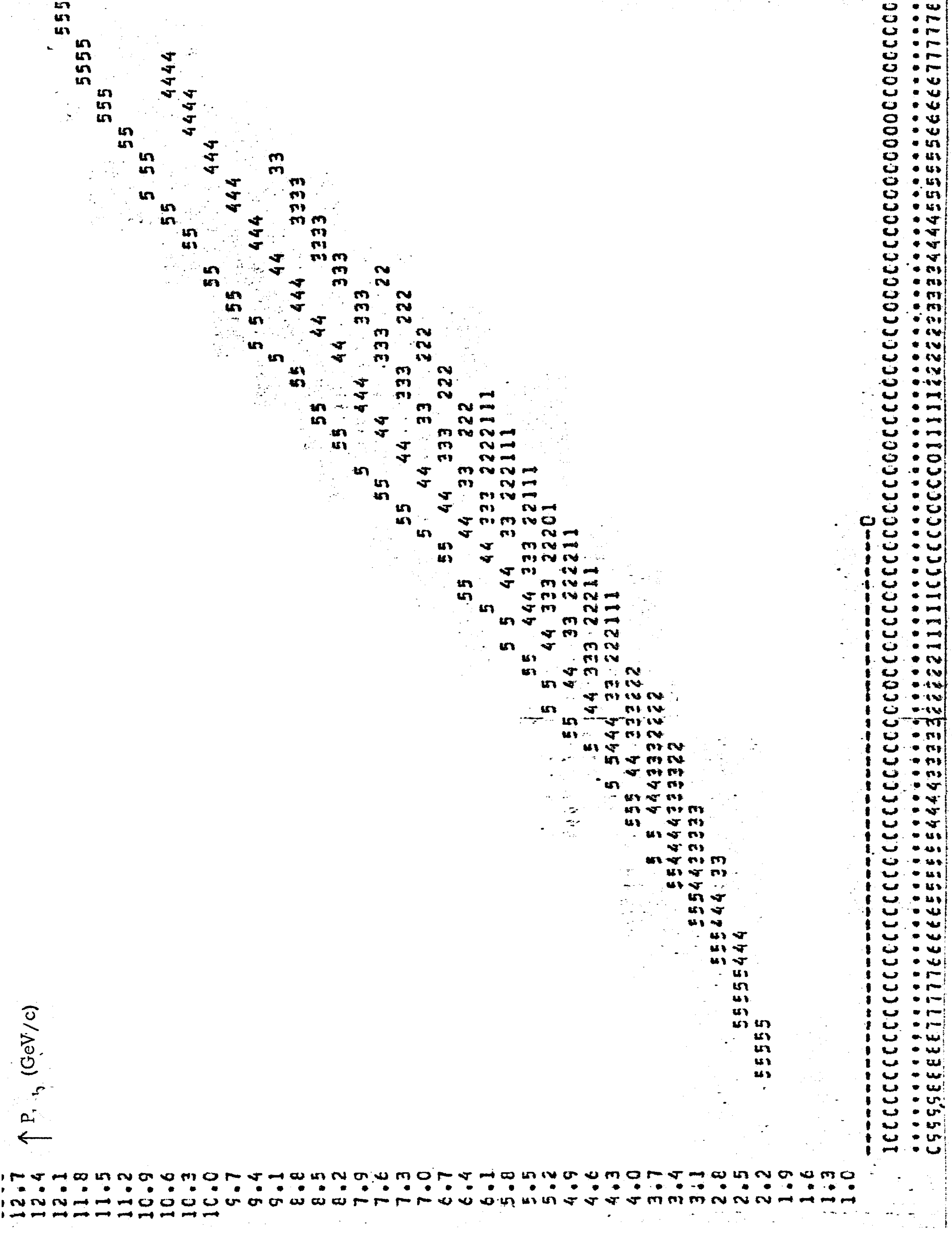

APPENDIX I

Test Results of a 31 cm x 31 cm Lead Glass Electromagnetic Shower Detector

IHSC Consortium

To be Submitted to Nuclear Instruments and Methods

Introduction

Preliminary test runs of a lead-glass Cerenkov electromagnetic shower detector have been carried out using a tagged negative electron beam at the Fermi National Accelerator Laboratory, with nominal beam energies of 30, 40, 50, 60, 75, and 100 GeV. The detector tested here is a reduced scale version of the shower detector to be used with the Hybrid Spectrometer[1] at Fermilab and the Forward Gamma Detector at CERN. Several workers have studied and used various types of lead glass shower detectors[2] and lead-scintillator sandwich detectors.[3, 4] The novel feature of this system is that the electromagnetic shower converter, as well as the absorber, consists of active elements, ensuring negligible unobserved energy loss and good energy resolution.

The Detector

The detector (Fig. 1) consists of three sections: (1) converter, (2) shower hodoscope, and (3) absorber. Photons or electrons incident on the converter develop a cascade electromagnetic shower which then passes through the shower hodoscope. The shower hodoscope is then able to measure the profile of the shower allowing for determination of the shower centroid. Finally, the shower is totally absorbed by the absorber and the energy deposited in it is measured along with the energy deposited in the converter.

The converter is constructed of two layers of lead glass bars, each bar being 6.25cm x 6.25cm x 75cm and of type F-2[5]. Each layer consists of five bars with the axes of the bars in the different layers situated at 90^0 to each other and overlapping with an area of 31cm x 31cm (see Fig. 1). There are a total of four radiation lengths presented to the beam (two radiation lengths per layer). These bars are each viewed by an AMPEREX 56 AVP[6] photomultiplier with clear silicone resin wafers[7] used for optical contact.

The bars are wrapped with 1/4 mil. aluminized mylar and the entire coverter unit is housed in a light tight wooden box. The box (Fig. 2) is made of clear pine, notched, glued, and screwed together to afford maximum strength. The interior corners were sealed and all surfaces were painted black to minimize light leaks.

The photomultipliers were spring loaded against the glass to ensure good optical contact between the glass and the encapsulating resin coat on the phototube faces.

The calibration package shown schematically in Fig. 3 is essentially a two-compartment light-tight container. One compartment contains the argon strobe lamp, which is mounted at the center of a spherical support for fiber optic light guides which are illuminated by the strobe. These guides carry light from the strobe to the detector phototubes, and it is this light standard against which the gain stability of the tubes is determined. To monitor the stability of the strobe, one of the light guides is directed into the second compartment of the calibration package and is viewed, together with a collimated Am^{241}-doped NaI(Tl) scintillator source[8], by a reference phototube. The strobe signal is attenuated by a neutral filter to a level comparable to that of the Am^{241}.

The shower hodoscope consists of three plastic scintillator planes, made of "fingers" 1cm thick and 1.5cm wide of type NE100[9]. The central plane has vertical fingers with the other two planes set at $\pm 45^0$ to it. Each scintillator finger is viewed by low cost RCA 931A[10] photomultipliers which are adequate for the large amount of light produced by the high flux electron showers. To increase the light acceptance of the internal photocathode through the lateral window, each finger is equipped with light guide heads of cylindrical shape which focus the light on the photocathode. The 78 photomultipliers (29 for each diagonal plane and 20 for the vertical plane) are enclosed in a single light-tight aluminum box. Figure 4 is a photograph displaying the light guides for the three scintillator planes.

The linearity of the 931A photomultiplier was measured in a separate test and found to be linear within 1% up to 20 mA, and at 40 mA the deviation from linearity was found to be 10%. The output charge from each 931A photomultiplier for the fingers is digitized in order to establish the spatial position of the shower as described in detail below.

In order to equalize the gains of the photomultipliers used with the finger hodoscope, a light diffusing, graded Lucite bar is used for the three planes. Light from a pulsed cold-cathode Krytron (EG&G KN-22)(11) is diffused by a white painted band on the surface of the Lucite bar facing the end of the fingers (see Fig. 5). The pink light from the KN-22 is incident on a scintillator bar, made of the same scintillator plastic as used in the hodoscope, which induces fluorescent light with the same spectrum as the actual scintillations. This induced light is then incident on the diffusing bar which distributes the proper amount of light to each finger. The grading of the shape of the Lucite bar and the variation in width of the painted diffuser band were empirically determined to ensure the uniformity of diffused light accepted by each finger. To compensate for the attenuation of light flux with distance, both the thickness of the Lucite bar and the width of the painted diffusing band were tapered. The result is a "saber" 1.5 meters long with a thickness of 4.5cm at the beginning and 1.5cm at the end with the diffusing band starting with a width of 0.7mm and increasing linearly to 2.0mm. Within a length of 1 meter the variation in the light output is less than 2%.

The shower absorber is made up of 4 lead glass blocks of type SF5(5), each being 15cm x 15cm x 60cm in dimension. These blocks are placed behind the finger hodoscope with their longitudinal axis perpendicular to the plane of the finger hodoscope, thus presenting ~ 25.4 radiation lengths for shower absorption. Each absorber block is equipped with a 5 inch EMI 9530R(12) photomultiplier, coupled to the glass with optical grease[13]. These blocks are wrapped with aluminized mylar and opaque tape and are not housed, but stacked in the open. The identical scheme for equalizing photomultiplier gains is used for these absorber blocks as for the converter blocks, described earlier.

The Beam Description

The test was carried out in the Fermilab Neutrino Section N5 hadron beam line, which is normally used in conjunction with the 15 foot bubble chamber. A 30cm x 5mm x 5mm Be target having ~ 1 absorption length as well as ~ 1 radiation length was used. A semi-differential gas Cerenkov counter was used to tag electrons in the beam but no attempt was made to incorporate the electron trigger in the gate logic, since the Cerenkov counter was located too far upstream. This being the case, a trigger having reasonably high rejection of π^-'s and μ^-'s was devised by adding the photomultiplier signals from the second layer of the converter with a linear fan-in. The output signal of the fan-in was then discriminated at a level to insure an electron count when registered as such by the Cerenkov counter. This allowed a relatively small amount of high energy hadronic showers to be registered with virtually no loss of electron events. The fraction of good triggers (i.e., electrons) ranged from 60% at 30 GeV/c to 30% at 50 GeV/c and only a few percent at 100 GeV/c due to the decreasing electron content in the beam with increasing energy.

The beam was dispersed over an area of $\sim$ 10cm (horizontal) by 6cm (vertical) at the apparatus, allowing for showers to develop throughout several converter and absorber components. The beam was directed over various regions of the entire active area of the apparatus. A triplet set of proportional wire chamber planes was situated just in front of the detector to enable off-line position determination of each incident particle.

The momentum bite of the beam including systematic uncertainties due to beam monitoring resulted in a $\frac{\Delta p}{p} \approx 1\%$.

Data Acquisition

A master gate was formed by two-fold coincidence between two scintillators separated by 2 meters and situated immediately before the apparatus. This gate was then fanned out to the Proportional Wire Chamber (PWC) gating and storage logic and the Analog to Digital Converter (ADC) units for the lead glass and scintillator hodoscope components. The PWC system is capable of storing information for 16 particles with dead time during storage of ~150 nsec. The ADC units for the lead-glass system were operated with an integrating gate of ~ 400 nsec, during which time the master gate generator was locked out by a latch. Thus the maximum hardware dead time of the system during data storage was ~ 400 nsec. The ADC units used were LeCroy 2249A CAMAC modules[14] with 10 bit digital readout and least count of 1/4 p C. The overall deadtime of the system was dictated by the PDP-11/45 computer[15] which read out the ADC units through direct memory access. Upon completion of the ADC readout, the master gate lockout latch was cleared to allow continuation of data acquisition. This was repeated for a maximum of 16 particles or until the end of spill, whichever came first. Thus, each event consisted of ADC information along with the corresponding PWC information which allowed for off-line determination of beam position, shower-core position and energy, on an event by event basis.

After each beam spill which resulted in the storage of information for up to 16 beam events, up to 16 calibration events originating from the triggering of the various light sources (EG&G KN22 for the scintillator hodoscope, Kerns[16] flash lamps for the lead glass converter and absorber blocks and the Am^{241} doped NaI) were recorded.

Energy Determination

As a shower develops through the system, some of its energy is deposited in the first two layers of lead glass converter blocks and the remainder of energy is deposited in the absorber blocks. The amount of energy deposited in the hodoscope scintillators is negligible and is not taken into account in this study. Thus there are 14 active components, 10 converters and 4 absorbers, whose photo-multiplier output charge represents energy deposited in the system. The coefficient α_k for each component which relates charge to energy is determined by a least square analysis using the expression:

$$\chi^2 = \sum_i (E_i - \sum_k^{14} \alpha_k C_{ki})^2$$

E_i = energy of the electron for the i^{th} event.

α_k = charge to energy conversion factor to be determined.

C_{ki} = charge from the k^{th} component of the i^{th} event.

The fit was carried out at 50 GeV to determine the α_k coefficients which in turn were used to obtain the shower energy $E_i = \sum \alpha_k C_{ki}$ for the 30, 40, 60, 75, and 100 GeV runs.

In this report, no attempt was made to compensate for photomultiplier (EMI 9530 for absorbers, AMPEREX 56 AVP for converters) gain drifts due to temperature change. The analysis is as elementary as possible.

Figure 6 displays the sum of the energy distribution in the first two converter layers summed for each event whereas fig. 7 shows the distribution of energy deposited in the absorber blocks for the same sample at 50 GeV. Figure 8 displays the distribution of total shower energy determined for each event in the 50 GeV run which includes hadronic as well as electronic showers (no Cerenkov electron tag was imposed). The major portion of hadronic showers was eliminated by selectively setting the threshold of a discriminator into which the OR'ed output of the second layer of converter blocks was fed.

Figure 9 displays the 50 GeV distribution with the Cerenkov electron tag imposed. The remainder of the hadronic shower is then seen to be eliminated.

The entire remaining low energy tail may be due to π's with a delta ray in the Cerenkov counter registering as a beam electron.

Figures 10-14 display the shower energy distributions for 100-30 GeV incoming electrons. In all cases the Cerenkov electron tag was imposed.

Figure 15 is a plot of the actual beam energy versus measured energy. As can be seen, the linearity is good up to the highest energy value. The resolution, in terms of FWHM, for the various energies is shown in fig. 16 and its energy dependence is given by:

$$\frac{\Delta E}{E}\,(\mathrm{FWHM}) = \frac{27 \pm 2\,\%}{\sqrt{E}}$$

or

$$\sigma = (11.4 \pm 0.8)\ 10^{-2}\sqrt{E}$$

where E is the energy of the shower in units of GeV.

Position Determination

The center of an electron shower whose radial distribution is (closely) exponential and which has a characteristic width of 2.3cm is determined by evaluating the weighted average of the signals from the hodoscope fingers. This method introduces a systematic error due to the exponential behavior of the shower profile and the discrete sampling of the fingers[4]. This systematic shift to the finger center has been corrected by the following function:

$$\Delta x = 0.075 \sin\left[\frac{2\pi}{w}\,(\bar{x} - x_c)\right]$$

w = 1.5cm width of finger.

x_c = coordinate of finger center closest to $\bar{x}$.

$\bar{x}$ = weighted average coordinate.

A plot of the quantity $d = x + y + \sqrt{2}v$ where x, y, and v are the finger coordinates allows us to estimate the resolution of our detector. Elementary geometric considerations dictate d is constant and the standard deviation of its measurement is twice that of each coordinate, assuming x, y, and v are measured with the same accuracy. The final shower position is determined by a least square fit to x and y along with the geometric constraint given by d.

Figure 17 shows the distribution of d at 50 GeV. FWHM is 6.3 mm which leads to the conclusion that each coordinate has a resolution of $\sigma = 2.7$ mm.

Figures 18a and 18b show the x and y distributions of the difference between the shower center determined by the hodoscope fit and the position of the incident electron as given by the PWC. The distributions are consistent with the 1.4 mm hodoscope resolution since the PWC has 2 mm wire spacings.

Conclusion

The results of this test show that an electromagnetic shower detector can be built without the use of inactive components, such as lead. This allows for better shower energy determination and simplifies the overall construction. The plastic scintillator hodoscope is used solely for determining the position and not the energy of the showers and thus does not require extreme measures to insure pulse height integrity. The charge to digital converter units used with the position hodoscope were probably much better than required, only because of their availability. Cheaper units could be substituted for this task. Temperature control and temperature compensation in the electronics were not considered for this test. Although effects due to temperature variation were found to be negligible, the final system will be monitored for temperature variations.

The energy resolution for this prototype system was found to be $\sigma = (11.4 \pm 0.8) \times 10^{-2} \sqrt{E}$ GeV and shower-core positions were determined with $\sigma = 1.4$ mm resolution. By periodically calibrating the phototube gains with a known energy electron beam, it is conceivable that a system such as this could be used with systematic errors known and correctable to better than a percent.

Acknowledgments

We would like to thank Fermilab and its Neutrino Section for their support and use of the N5 beam line and the use of the 15' bubble chamber tagging system. Particular thanks go to J. C. Walker and C. Needles of the Neutrino Section for their help throughout the entire test.

REFERENCES

1) D. G. Fong et al., Nucl. Phys. B102, 386(1976); Phys. Lett. 53B, 290(1974).

2) J. S. Beale et al., NIM 117, 501(1974).

L. M. Lederman and R. A. Vidal, NIM 129, 65(1975).

B. J. Blumenfeld et al., NIM 97, 427(1971).

M. Holder et al., Phys. Lett. 40B, 141(1972).

J. A. Appel et al., NIM 127, 495(1975).

R. G. Astratsaturov et al., NIM 107, 105(1973).

3) A. V. Barnes et al., Phys. Rev. Lett. 37, 76(1976).

G. Donaldson et al., Phys. Rev. Lett. 36, 1110(1976).

4) Yu. Bushnin et al., NIM 106, 493(1973).

Yu. Bushnin et al., NIM 120, 391(1974).

5) Schott Optical Glass Inc.
York Avenue
Duryea, Pennsylvania 18642
U. S. A.

	F-2	SF-5
Radiation Length (cm)	3.06	2.36
Critical Energy (MeV)	18.4	15.8
Density (gr/cm^2)	3.60	4.08
Refractive Index	1.62	1.6727

6) Amperex Electronic Corp.
230 Duffy Avenue
Hicksville, N. Y. 11802

56AVP - 2 inch head-on photomultiplier tube with 14 stages.

7) Dow Corning Corp.
Midland, Michigan 48640
U. S. A.

Sylgard 184, Encapsulating Resin

8) The Harshaw Chemical Company
Crystal-Solid State Division
1945 East 97th Street
Cleveland, Ohio 44106

Am^{241} Doped NaI (Tℓ) Light Pulser $\sim$ 200 counts/sec.

9) Nuclear Enterprises
931 Terminal Way
San Carlos, California 94070

10) RCA Electronic Components
Harrison, N. J. 07029

931A - 1 1/8" Diameter Side-on photomultiplier tube with 9 stages.

11) E G & G Inc.
Electro-Optics Division
35 Congress Street
Salem, Massachusetts 01970

KN-22 Cold Cathode, Gas-filled Krytron

12) EMI Gencom Inc.
80 Express Street
Plainview, New York 11803, U. S. A.

9530R - 5" diameter, "super" S-11 cathode, 11 dynodes

13) Dow Corning Corp.
Midland, Michigan 48640
U. S. A.

Optical Grease

14) LeCroy Research Systems Corp.
Spring Valley, N. Y. 10977
U. S. A.

CAMAC Model 2249A, 12-channel A to D converter

15) Digital Equipment Corp.
Maynard, Massachusetts 01754
U. S. A.

PDP-11/45 Computer

16) Private communication
Kerns, Gordon
Physics Department
Fermilab
P. O. Box 500
Batavia, Illinois 60510, USA

These flash lamps were designed by C. Kerns and loaned to us during the test.

Figure Captions

Figure 1	Schematic of the converter, hodoscope and absorber layout.
Figure 2	Photograph of the converter and its light-tight box.
Figure 3	Schematic of the light calibration package.
Figure 4	Photograph of the light pipes from the scintillator hodoscope.
Figure 5	Schematic of the "saber" light diffusing bar used for the hodoscope calibration.
Figure 6	Energy distributions of the showers in the converter, from 50 GeV/c electrons.
Figure 7	Energy distributions of the showers in the absorber, from 50 GeV/c electrons.
Figure 8	Energy distributions of the showers detected by the entire system from 50 GeV/c negatives. The long tail on the low energy side is due to hadrons.
Figure 9	Energy distributions of the showers detected by the entire system, from 50 GeV/c electrons, with the Cerenkov counter electron tag invoked.
Figure 10a	Energy distribution of the showers as detected by the system, from 100 GeV/c negatives. The Cerenkov counter electron tag is not used here since the counter efficiency is low at this energy.
Figure 10b	Energy distribution of the same sample as shown in fig. 10a, except the electron tag from the Cerenkov counter is used. Due to the low efficiency, the sample is depreciated.
Figures 11-14	Energy distributions for electrons at 75, 60, 40 and 30 GeV/c, respectively.
Figure 15	Measured shower energy versus actual electron beam energy.

Figure 16 Energy resolution (% FWHM) versus $E^{\frac{1}{2}}$ for the various shower energies.

Figure 17 Distribution of $d = u + v + \sqrt{2}\, x$ for shower cores. See text for definition of d.

Figure 18a Distribution of x coordinate differences between shower core and beam electron positions.

Figure 18b Distribution of y coordinate differences between shower core and beam electron positions.

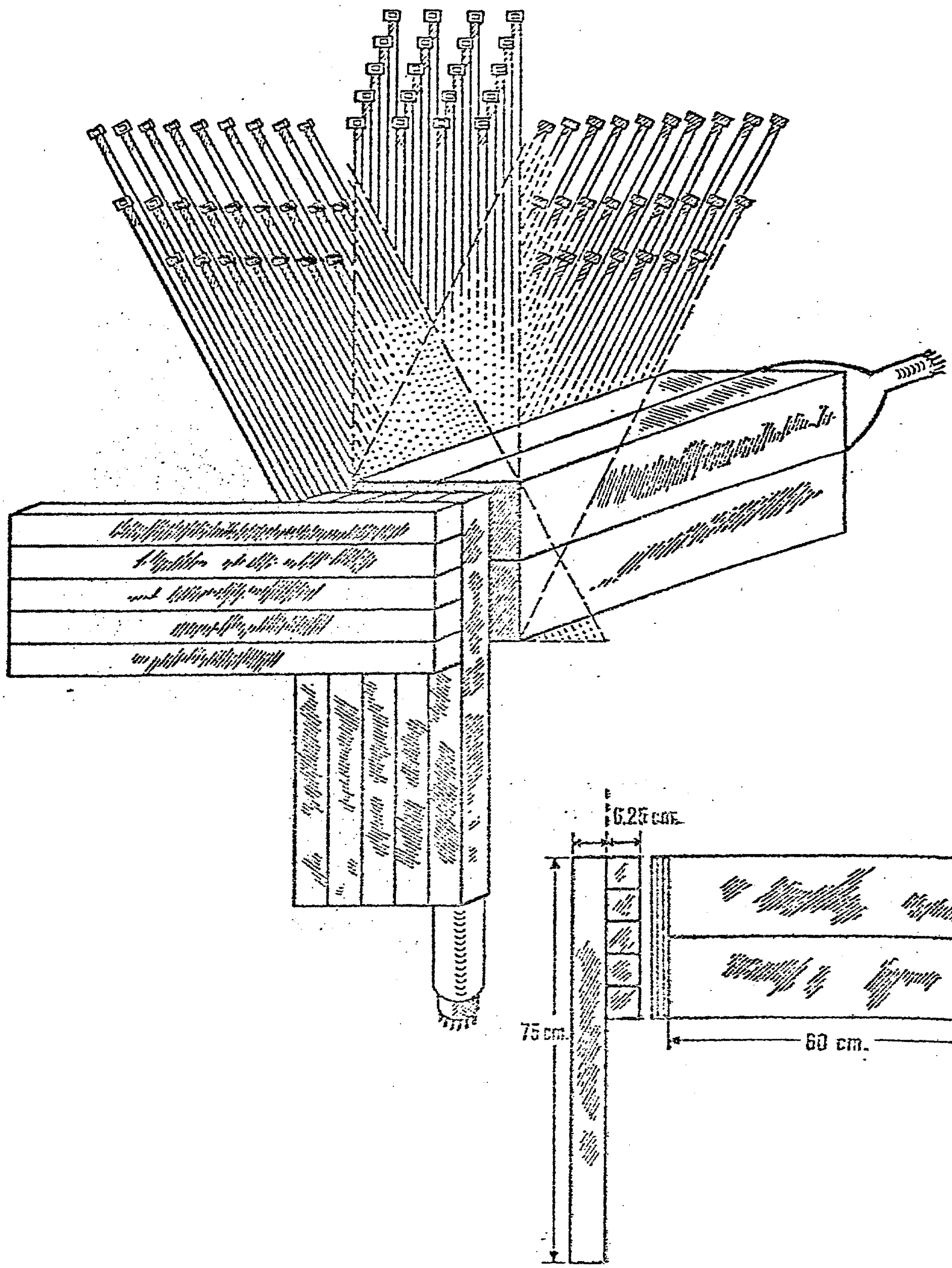

Fig 1

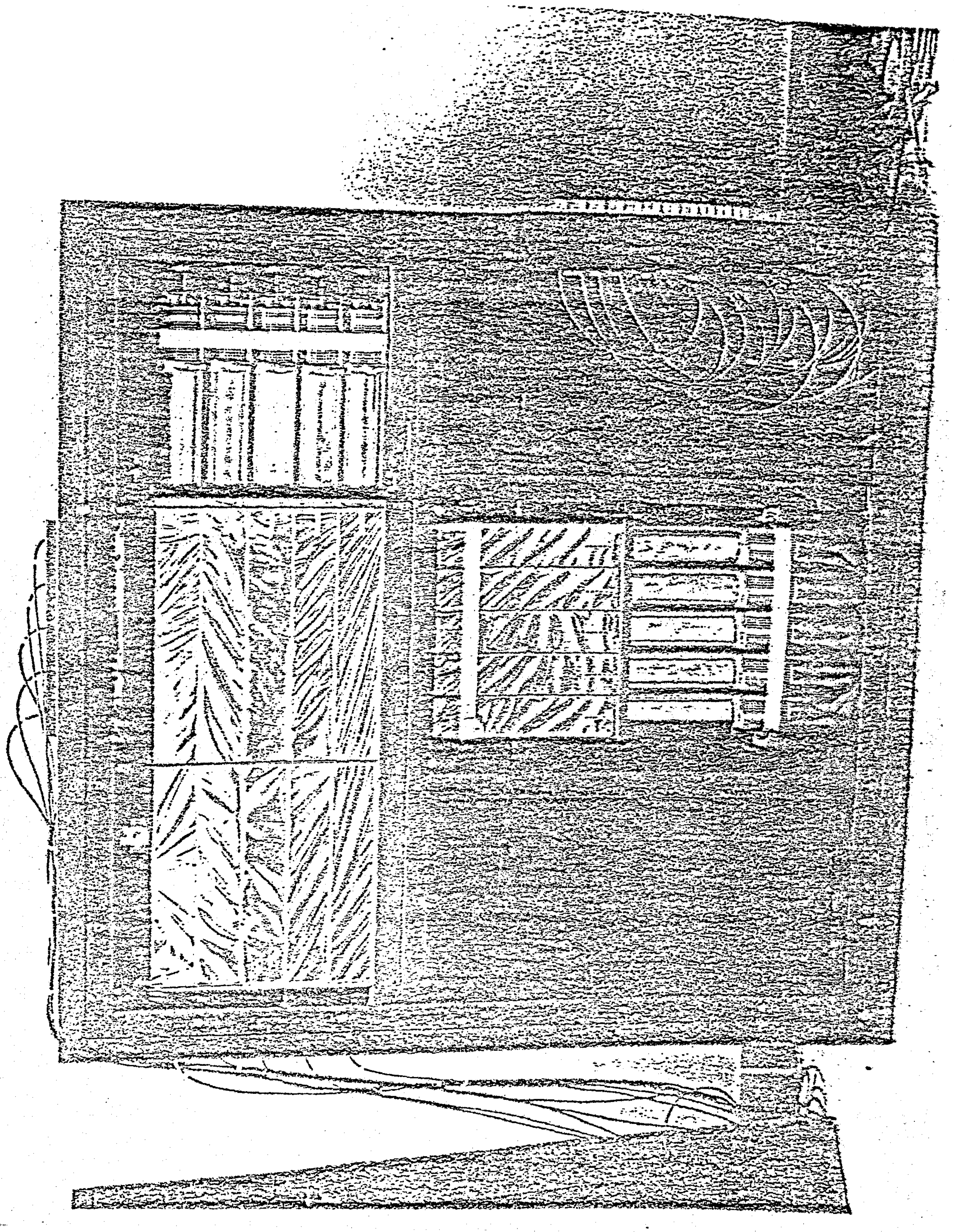

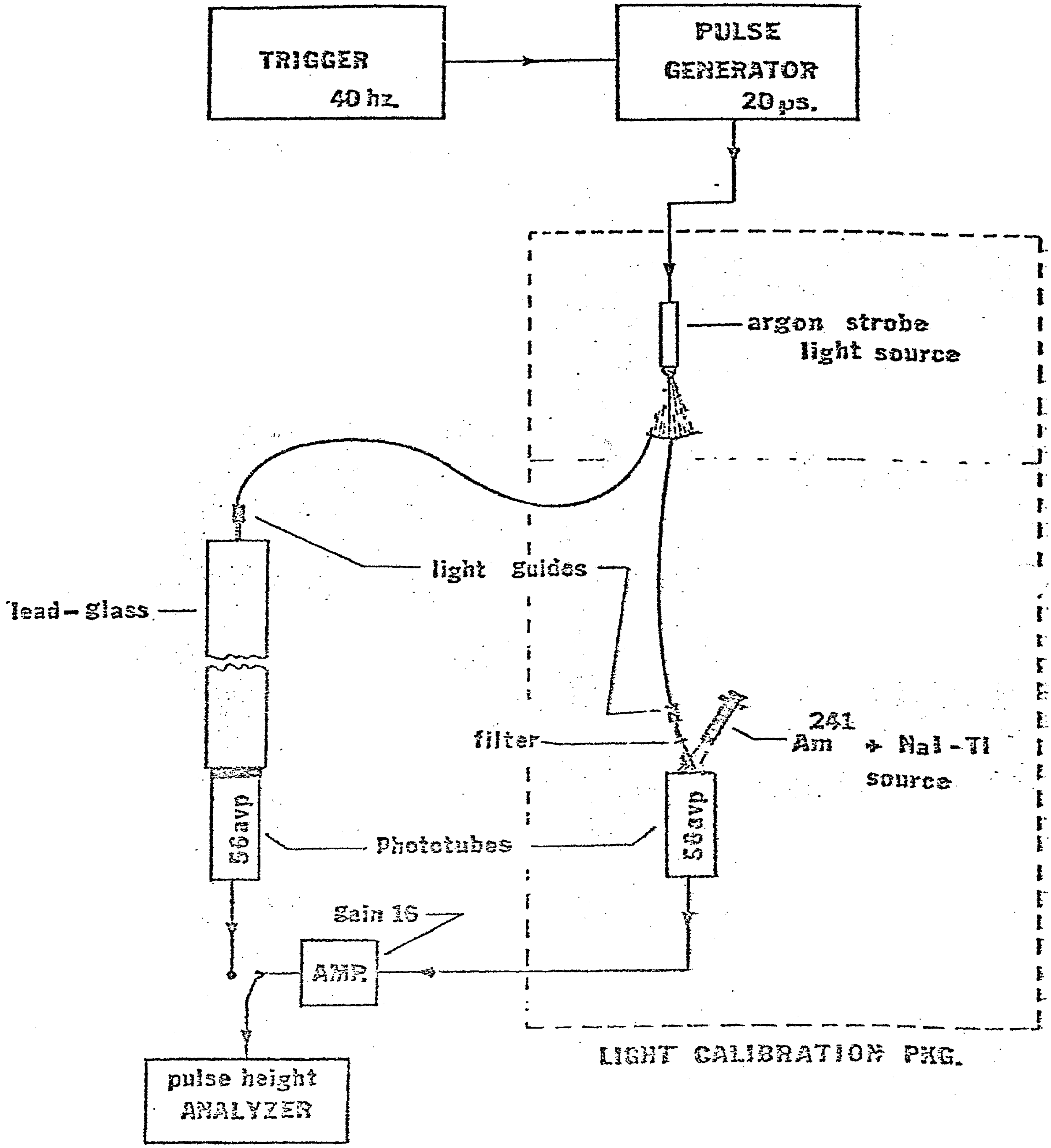
TRIGGER
40 hz.
PULSE
GENERATOR
20 μs.
argon strobe
light source
light guides
lead-glass
filter
241
Am + NaI-Tl
source
56avp
Phototubes
56avp
gain 16
AMP.
pulse height
ANALYZER
LIGHT CALIBRATION PKG.

FIG. 3

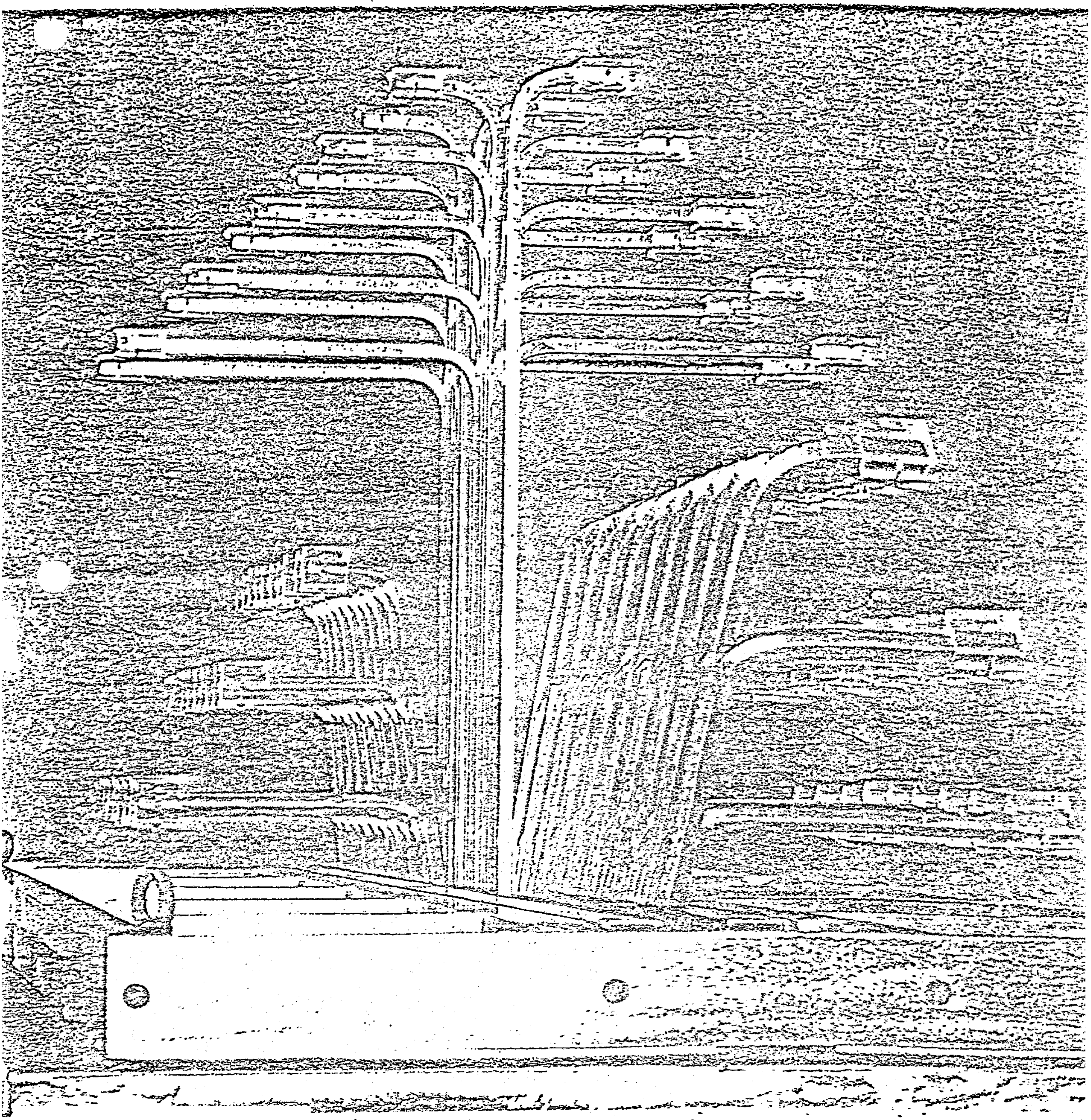

FIG 4

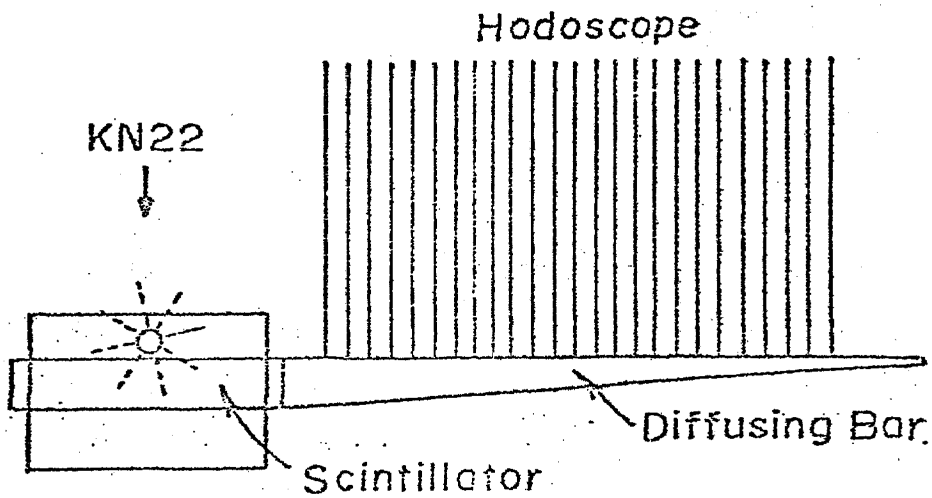

Schematic of Light Calibration System for Hodoscope

FIG 5

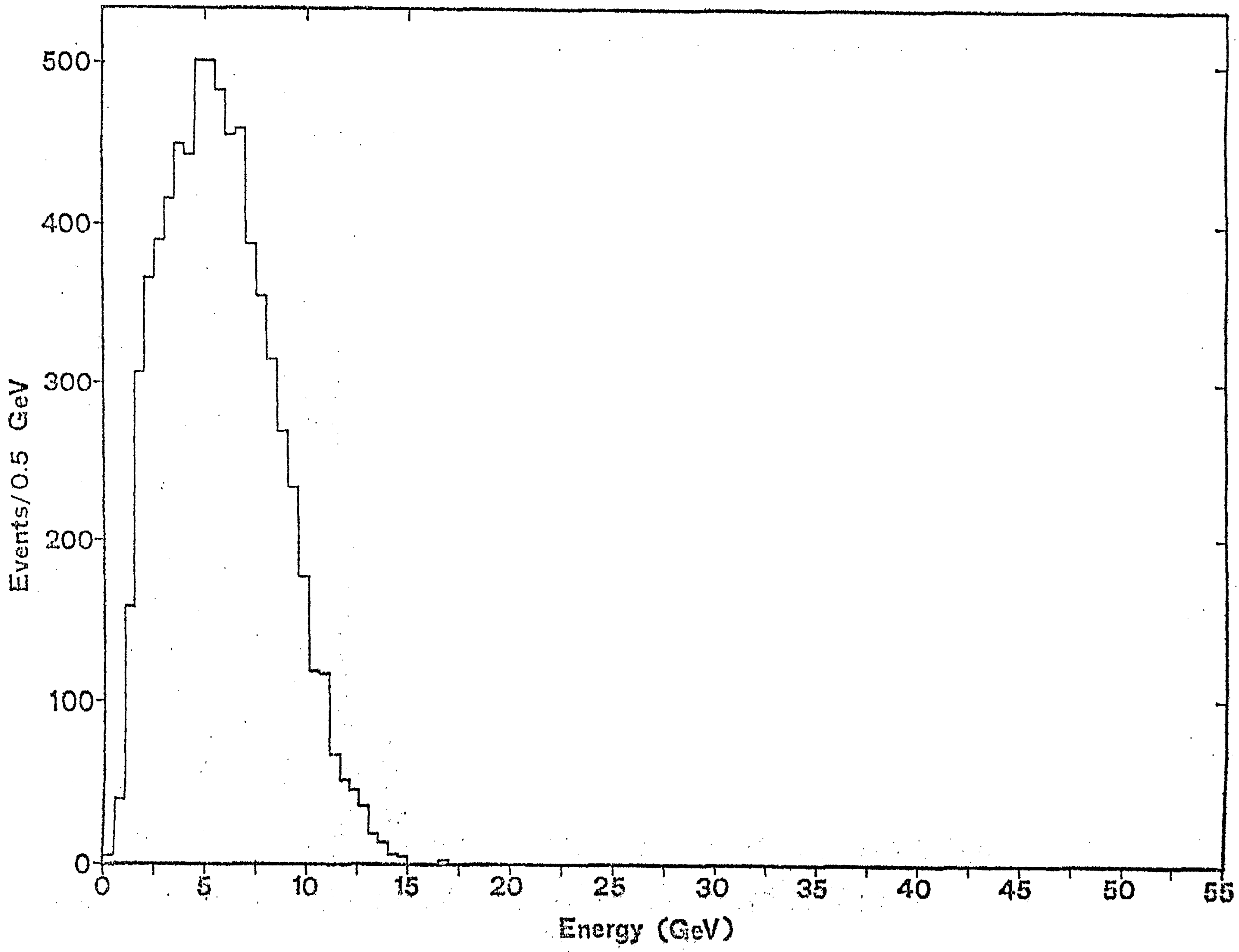

Events/0.5 GeV
500
400
300
200
100
0
0
5
10
15
20
25
30
35
40
45
50
55
Energy (GeV)

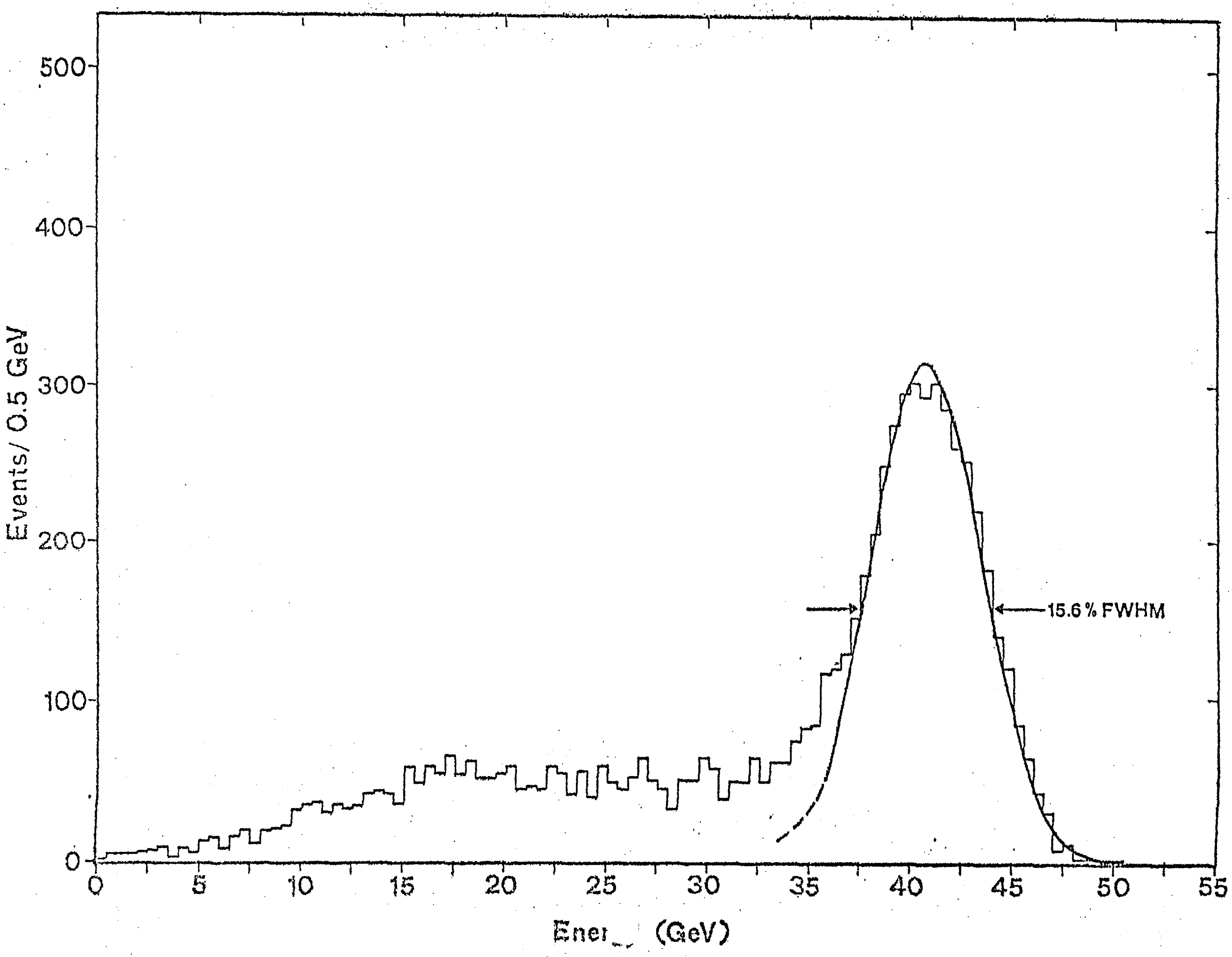

Events/ 0.5 GeV
0
100
200
300
400
500
0
5
10
15
20
25
30
35
40
45
50
55
15.6 % FWHM
(GeV)

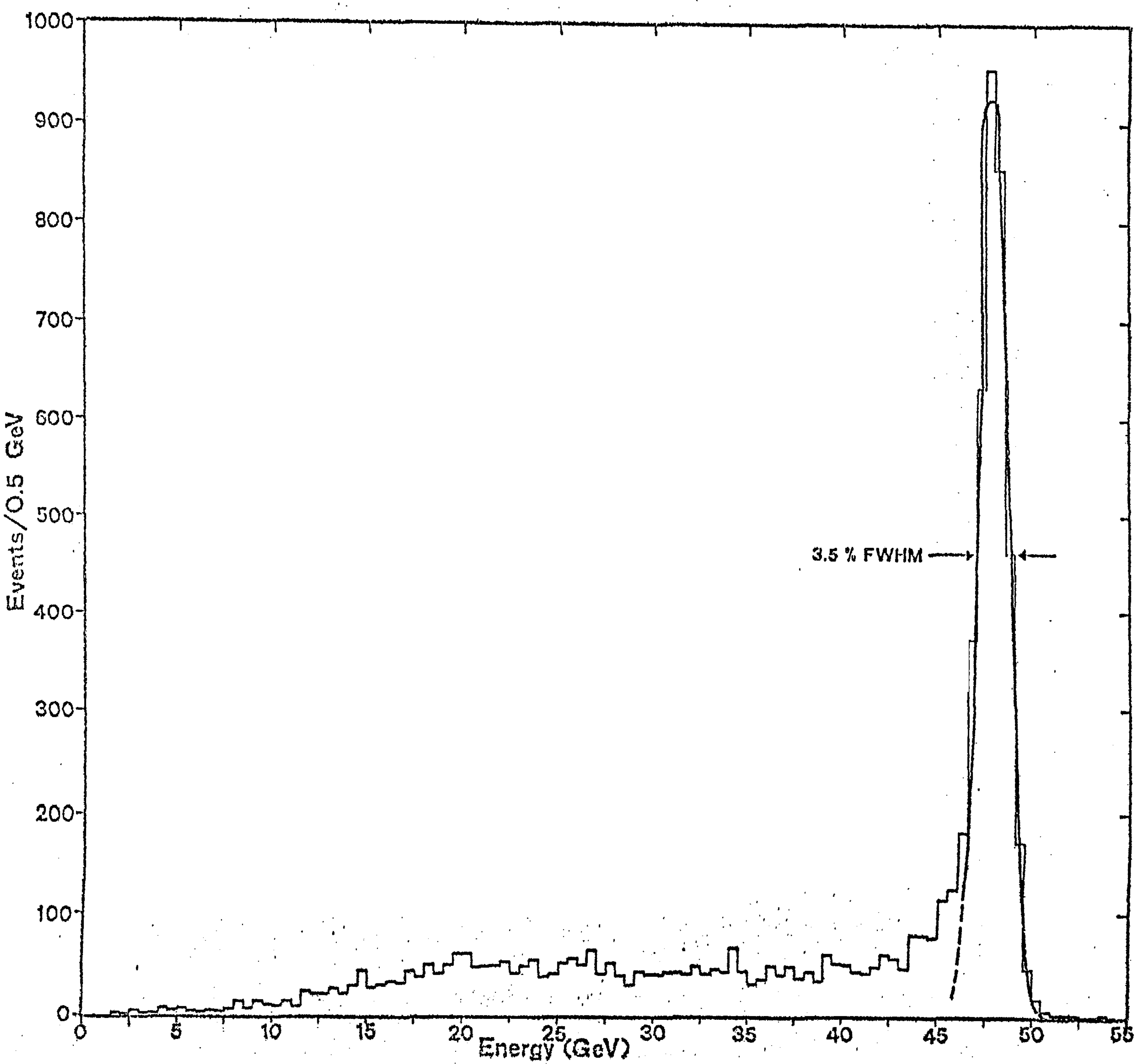

Events/0.5 GeV
Energy (GeV)
3.5 % FWHM
0
100
200
300
400
500
600
700
800
900
1000
0
5
10
15
20
25
30
35
40
45
50
55

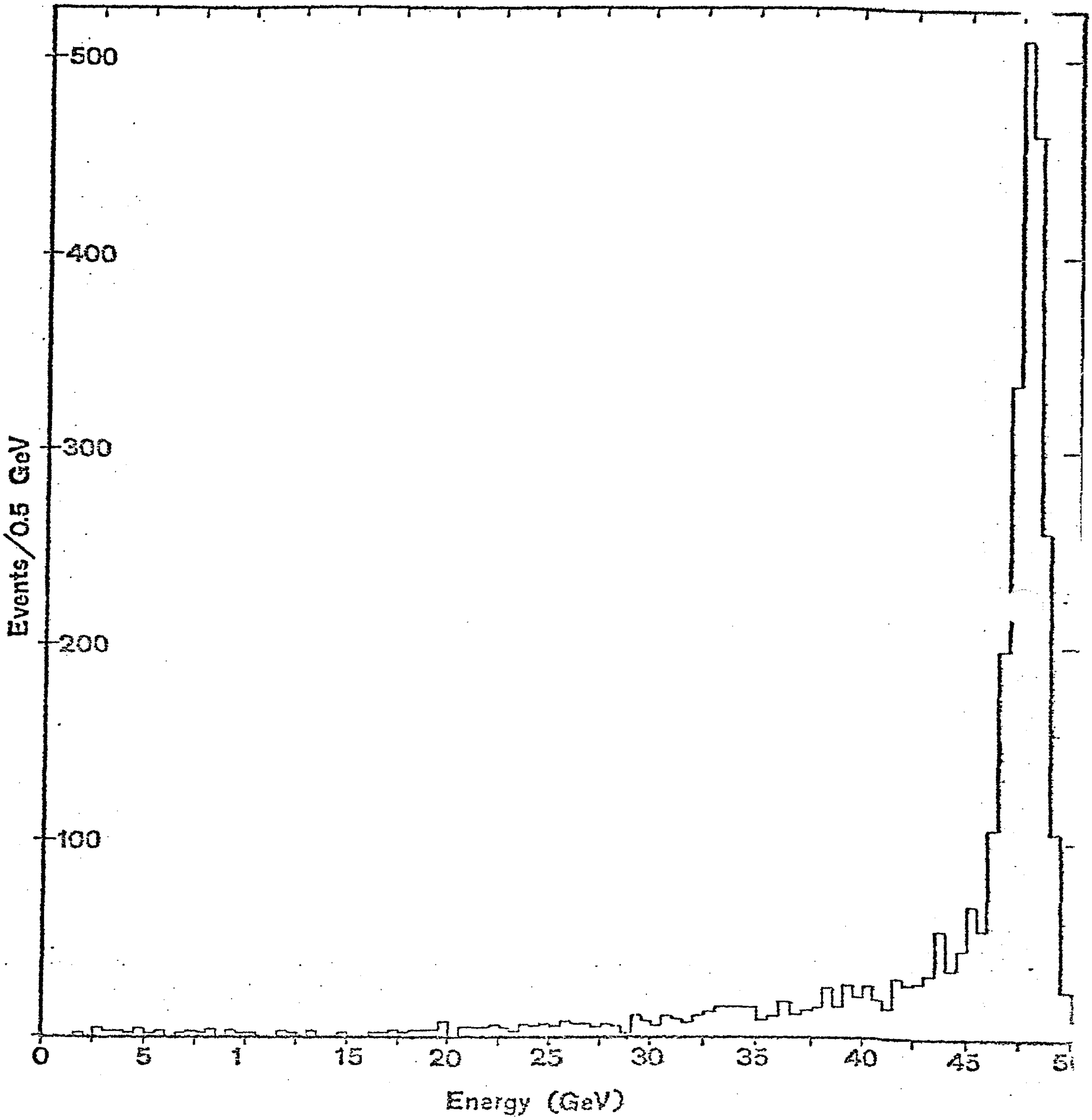
Events/0.5 GeV
500
400
300
200
100
0
5
1
15
20
25
30
35
40
45
5
Energy (GeV)

FIG 9

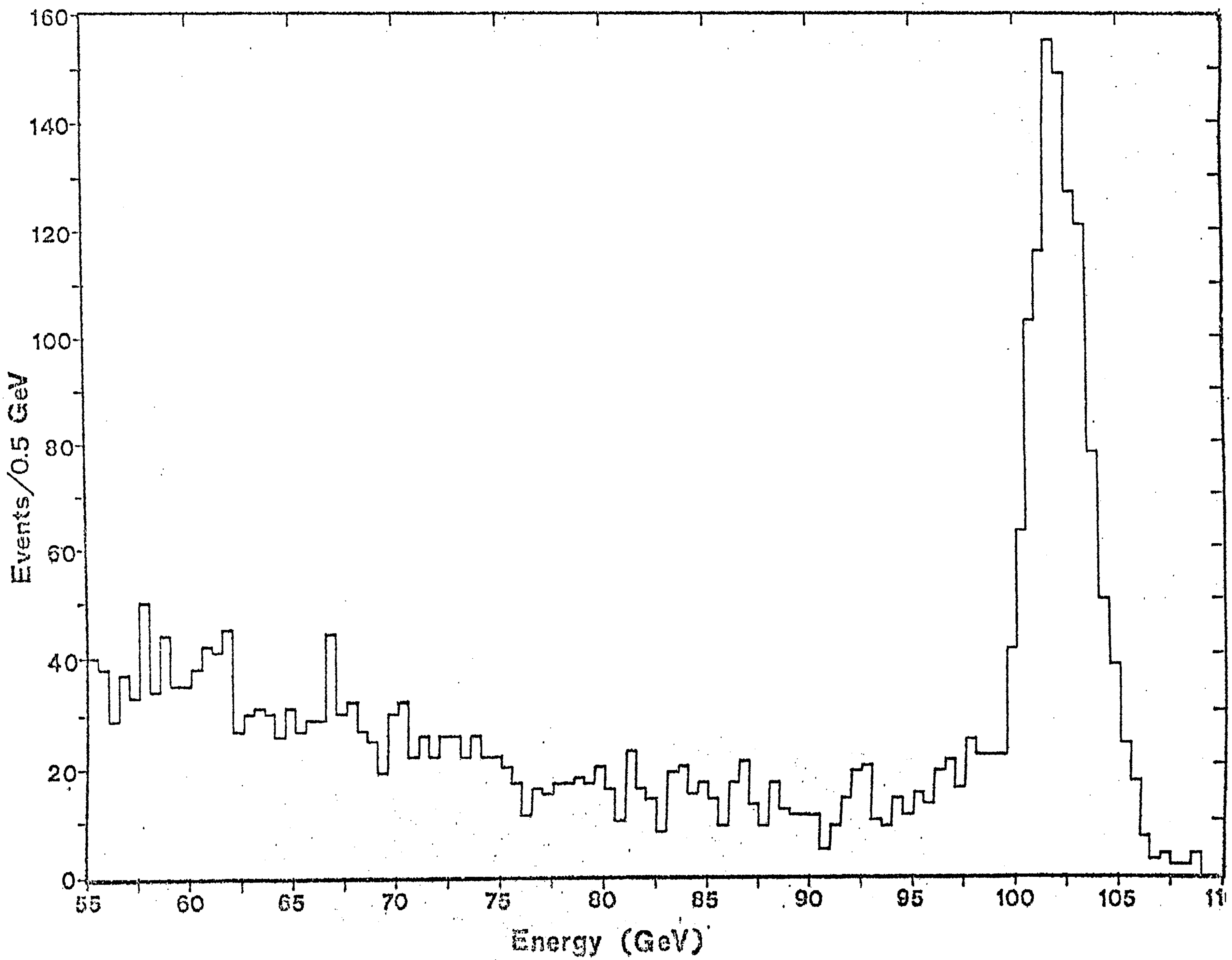

Events/0.5 GeV
0
20
40
60
80
100
120
140
160
55
60
65
70
75
80
85
90
95
100
105
Energy (GeV)

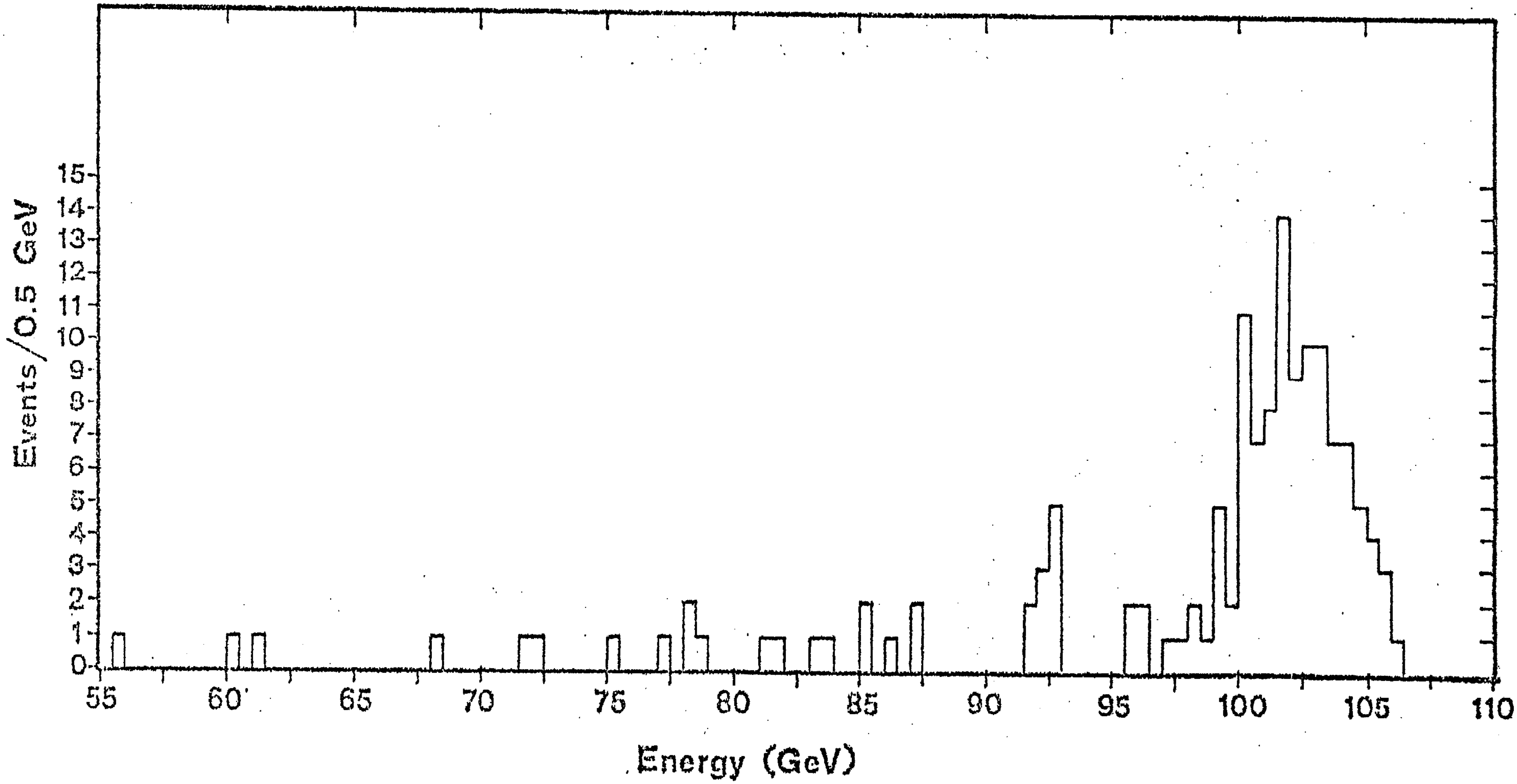
Events/0.5 GeV
15
14
13
12
11
10
9
8
7
6
5
4
3
2
1
0
55
60
65
70
75
80
85
90
95
100
105
110
Energy (GeV)

FIG 10b

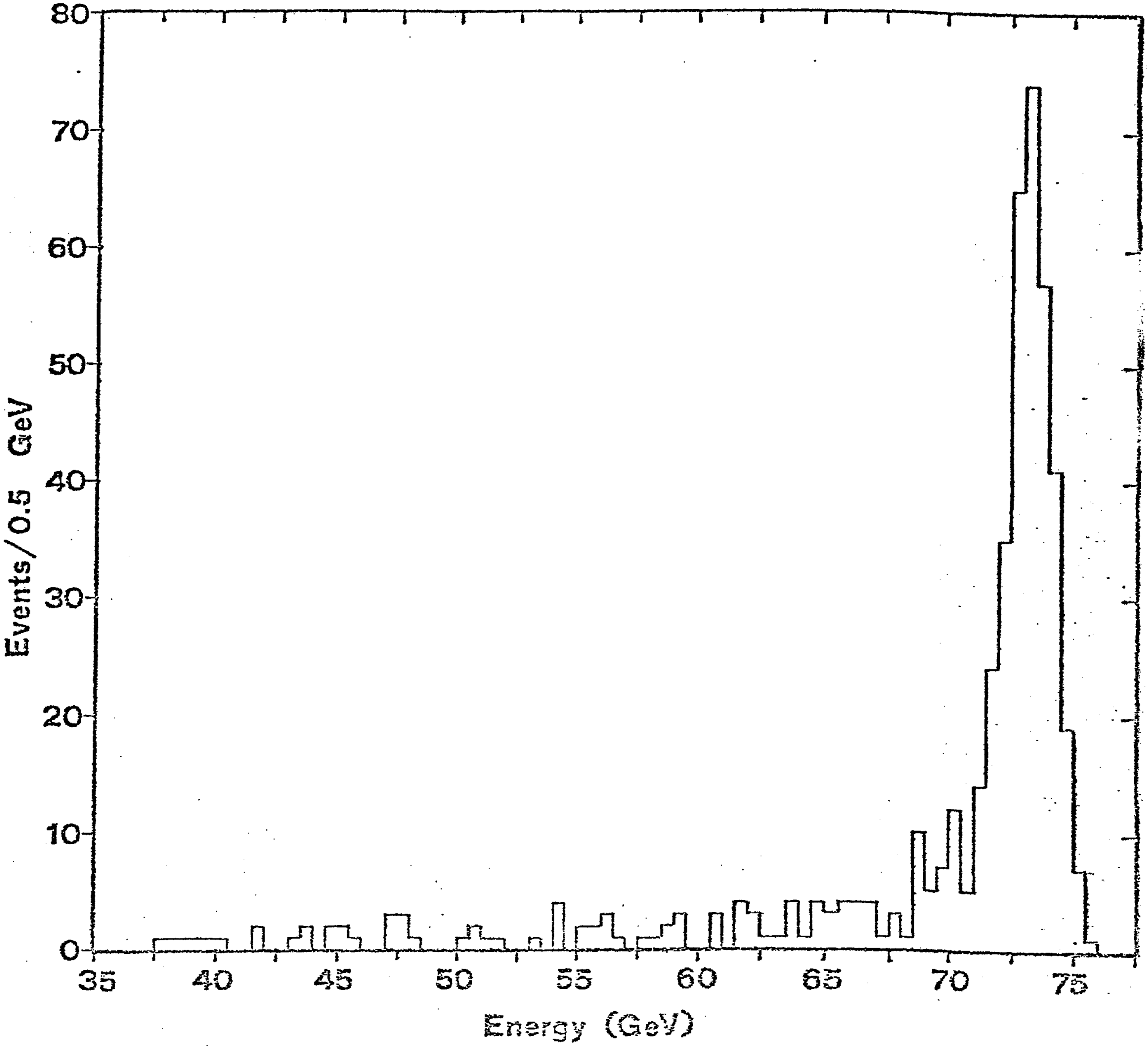

80
70
60
50
40
30
20
10
0
Events/0.5 GeV
35
40
45
50
55
60
65
70
75
Energy (GeV)

FIG 11

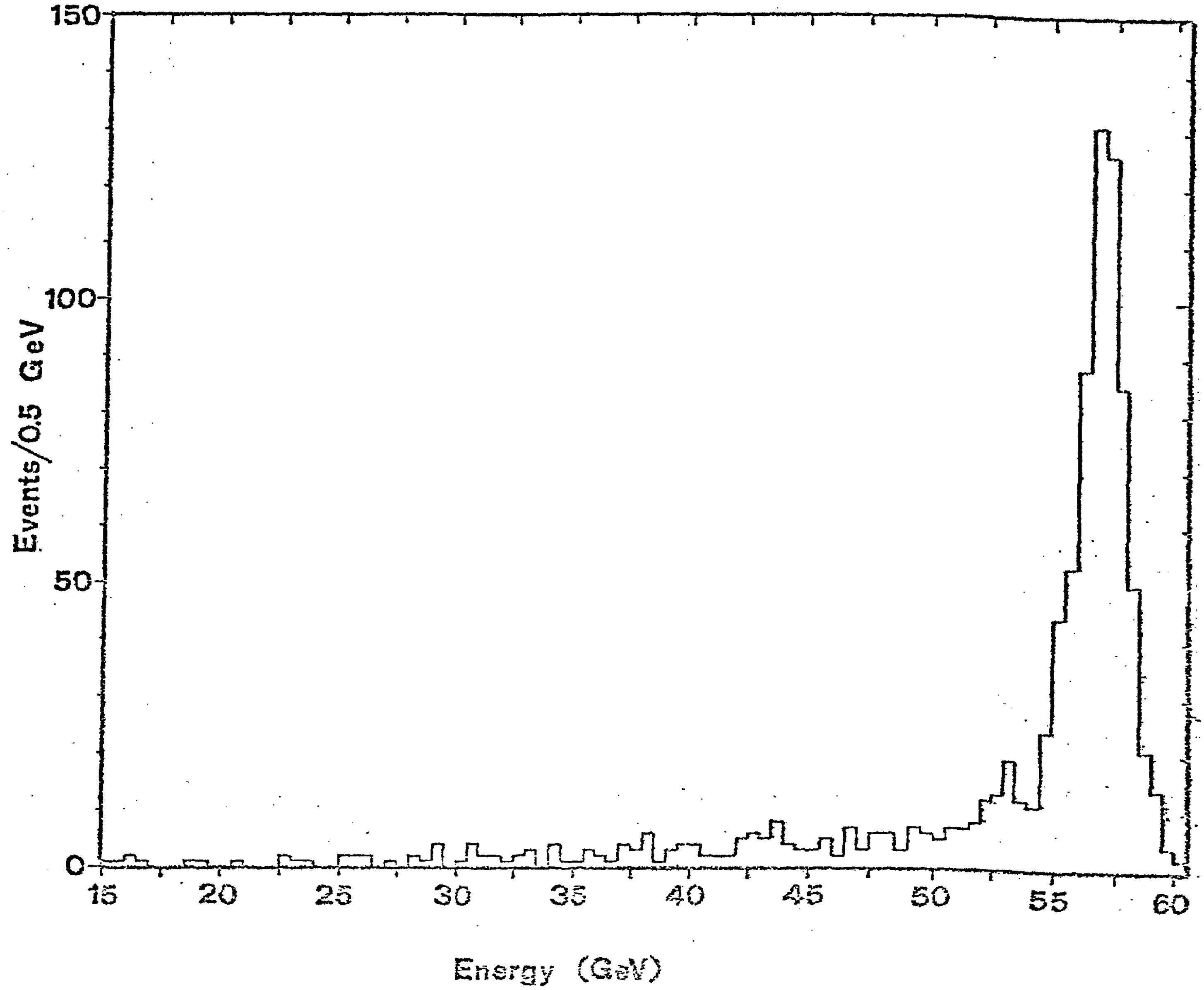

FIG 12

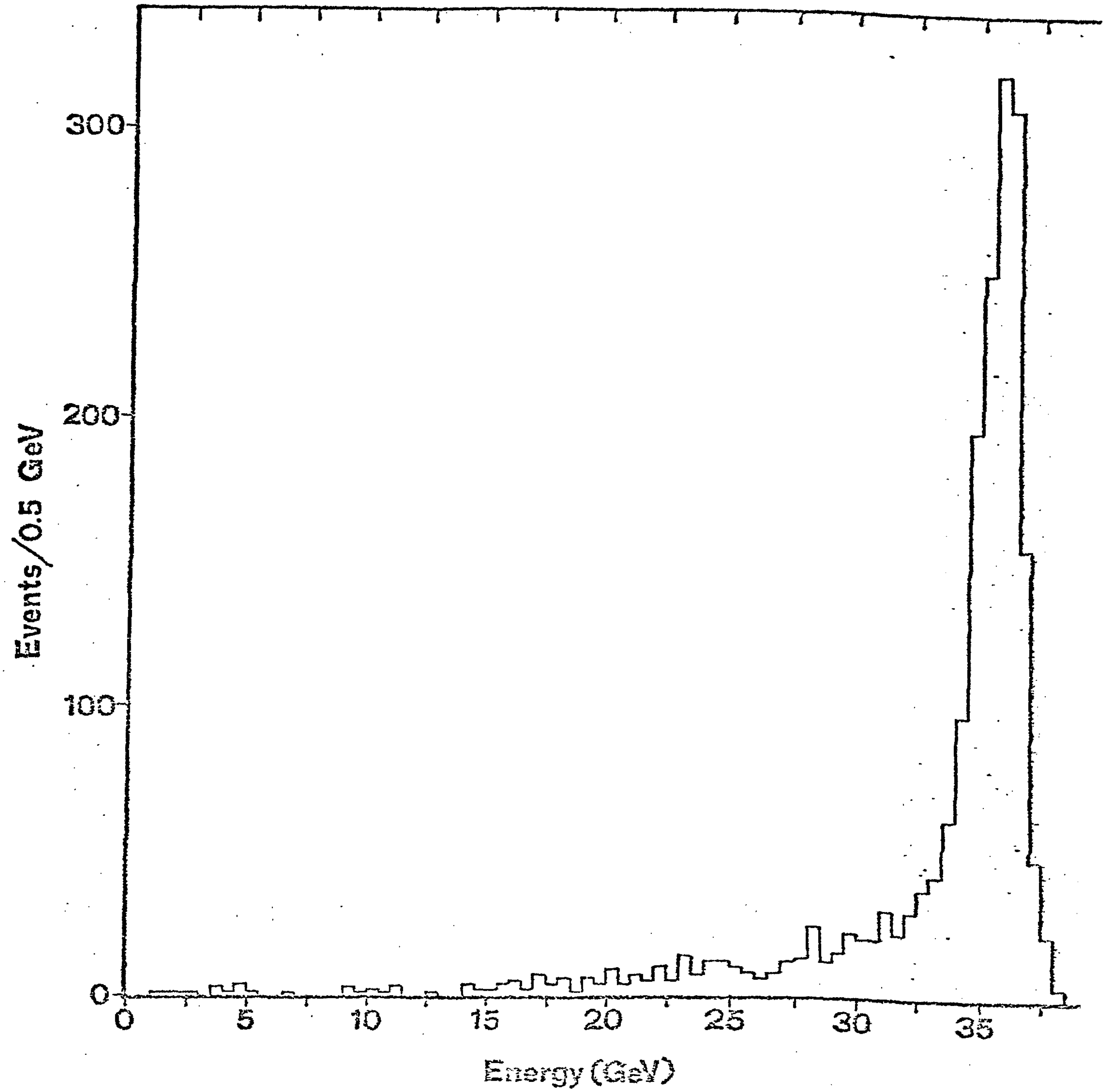

Figure 13

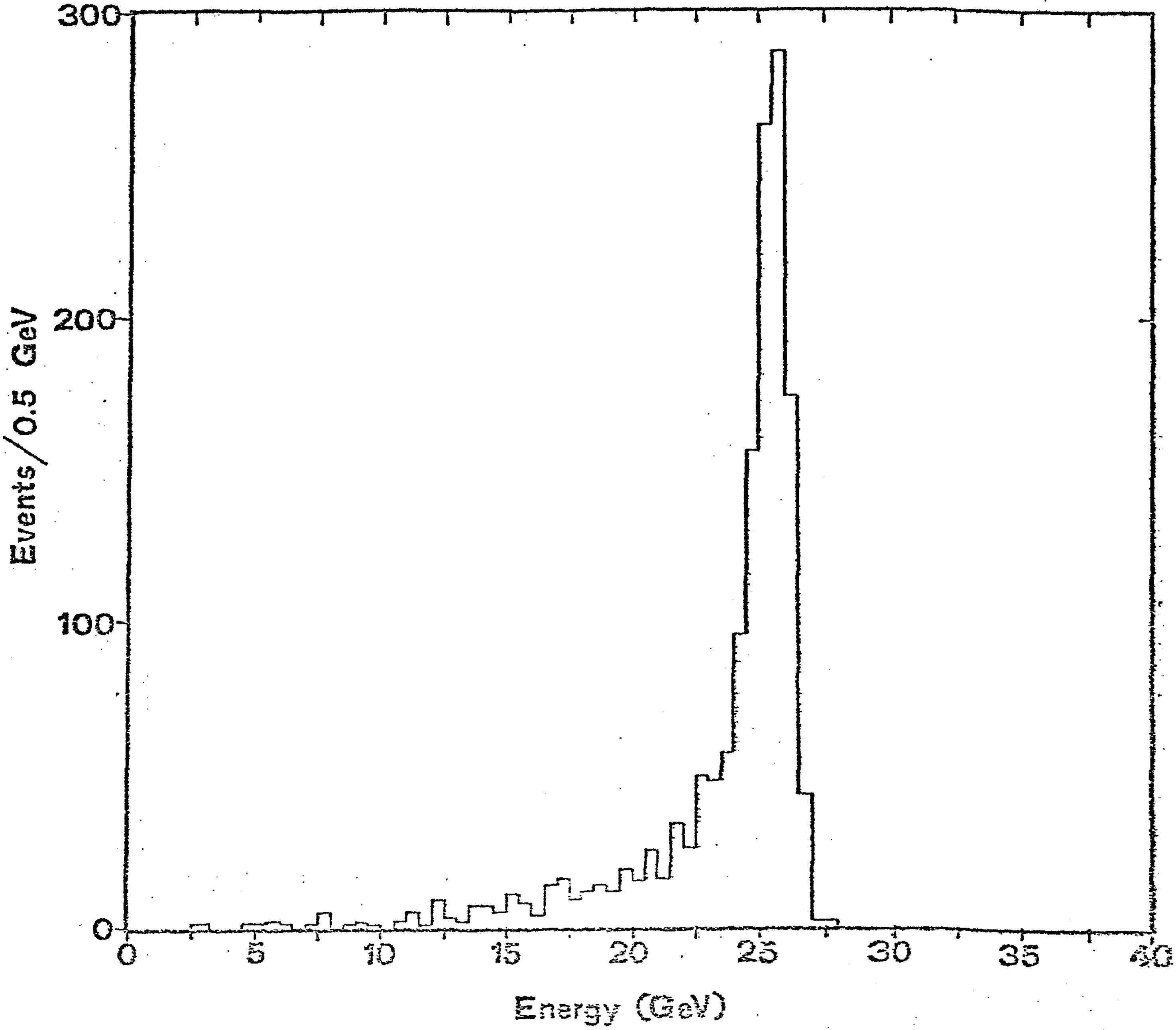

figure 14

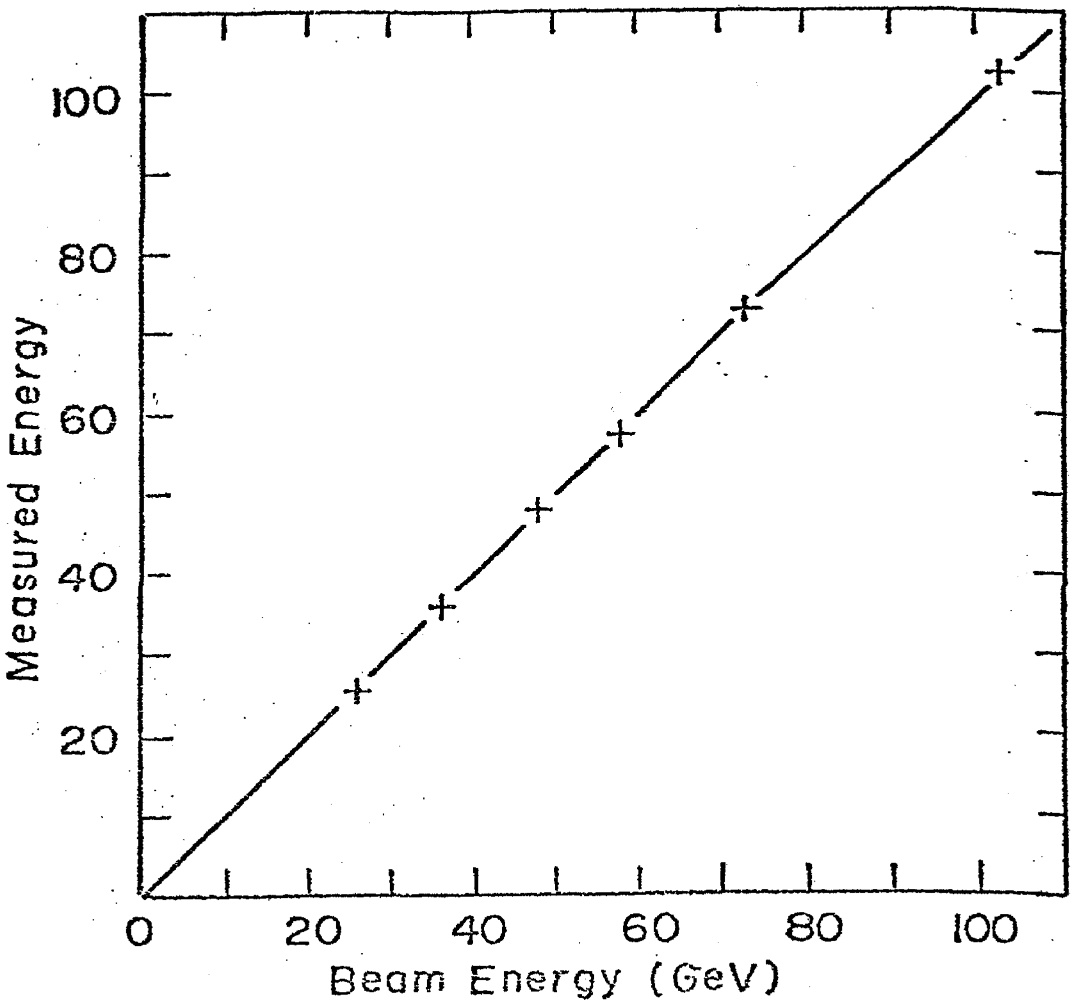

100
80
60
40
20
Measured Energy
0
20
40
60
80
100
Beam Energy (GeV)

figure 15

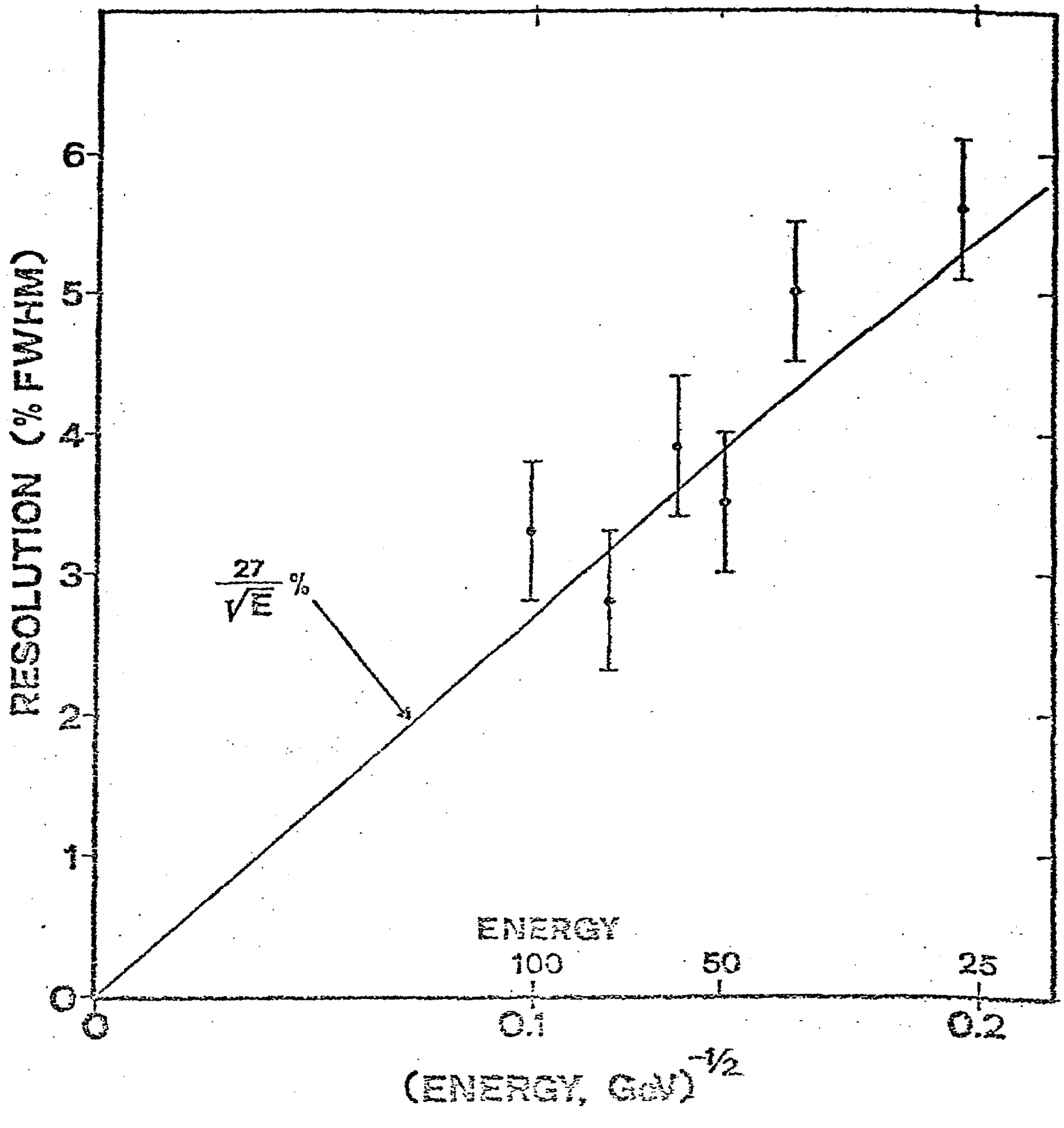
RESOLUTION (% FWHM)
6
5
4
3
2
1
0
$\frac{27}{\sqrt{E}}$ %
ENERGY
100
50
25
0
0.1
0.2
(ENERGY, GeV)$^{-1/2}$

figure 16

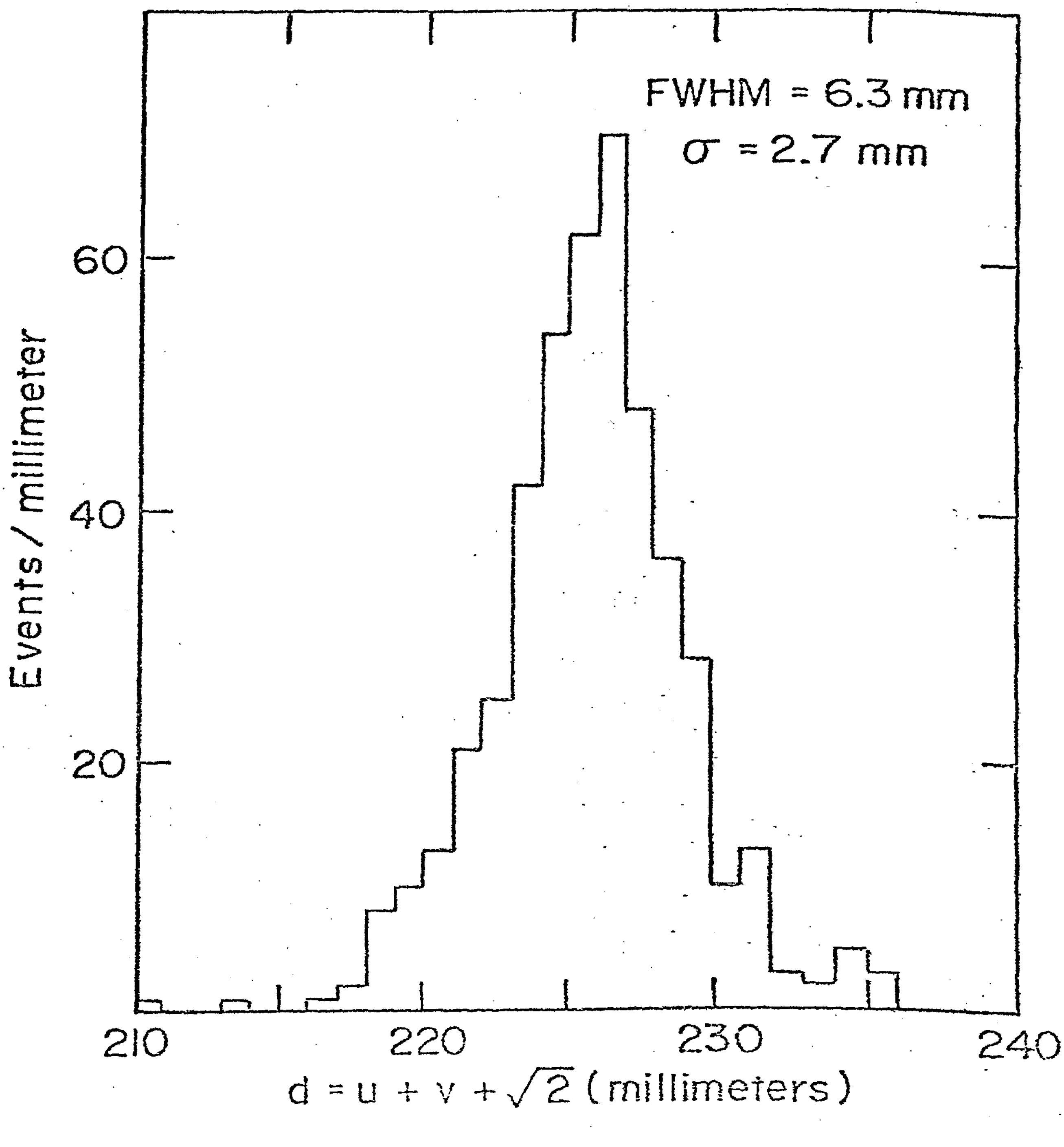
FWHM = 6.3 mm
σ = 2.7 mm
60
40
20
Events / millimeter
210
220
230
240
d = u + v + √2 (millimeters)

figure 17

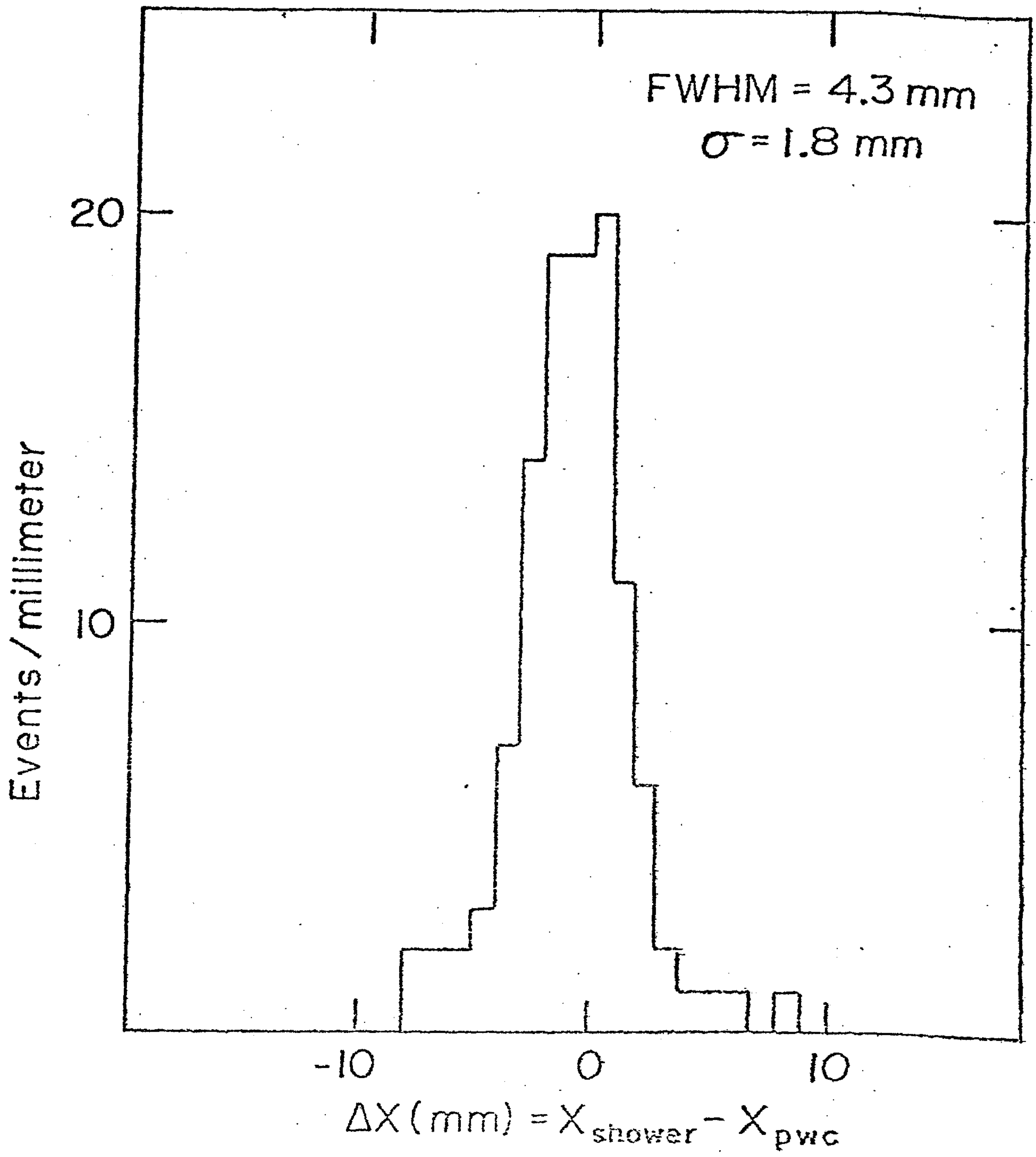
FWHM = 4.3 mm
σ = 1.8 mm
20
10
Events / millimeter
-10
0
10
ΔX (mm) = X shower − X pwc

figure 18

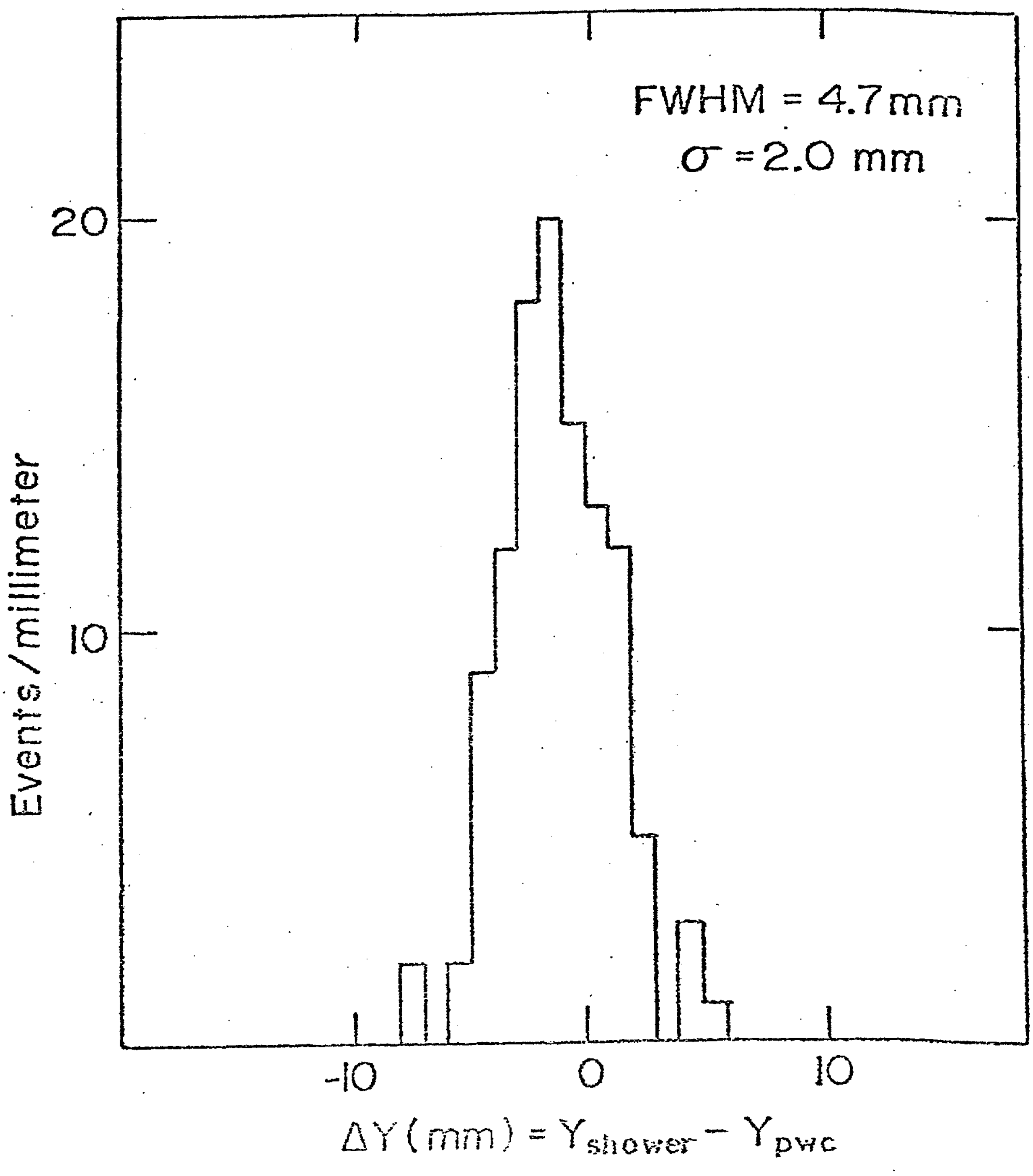

FWHM = 4.7mm
σ = 2.0 mm
20
10
Events / millimeter
-10
0
10
ΔY (mm) = Y shower − Y pwc

figure 18 b

Acceptance and Resolution Studies for the Fermilab ISIS

T. B. Stoughton, T. Ludlam, and V. Kistiakowsky

Introduction

Studies have been carried out previously of the acceptance and resolution anticipated for an ISIS-like device by R. Plano (Rutgers), W. Bugg (Tennessee), and J. Brau and V. Kistiakowsky (MIT). Some of these results were presented at the May 1976 Fermilab Workshop on Particle Identifiers for hadron physics and their consideration was partly the basis for choosing ISIS as a component of the downstream charged particle identifier. Appendix 1 of this note contains results obtained by W. Bugg for 147 GeV/c π^-p interactions (E-154) and references will be made to these figures and tables.

The present study was carried out for 300 GeV/c π^-p interactions because of the proposal to use ISIS for such an experiment (Fermilab proposal, P-488). The study attempts to answer some questions raised during and subsequent to the workshop.

The results given in the following sections are based on a sample of 147 GeV/c π^-p events (E-154) which have been modified to simulate 300 GeV/c events. The analysis was carried out independently at MIT (VK, TS) and at Yale (TL) with somewhat different assumptions and the results were in agreement where direct comparison was possible.

The quasi-300 GeV/c events were obtained from 147 GeV/c events by multiplying the longitudinal component of the center of mass momentum of every charged particle by $\sqrt{s(300)/s(147)}$ where s(300) and s(147) are the center of mass energy for 300 GeV/c and 147 GeV/c $\pi^- p$ interactions, respectively. The particles were then transformed into a frame in which the transformed target proton was at rest.

At MIT, the particles were swum downstream from their experimental vertex positions. At Yale, the incident pions were assumed to be parallel to the x-axis and the production vertices were distributed randomly in a volume of the bubble chamber defined as follows in the usual coordinate system:

$$-.20 < x < .10\text{m}$$

$$.035 < y < .085\text{m}$$

$$-.195 < z < -.185\text{m}$$

The accuracy of the swimming program was verified by swimming particles from 147 GeV/c events to the position along the beam-line of a proportional wire plane in the existing hybrid system and comparing the y and z coordinates obtained in this fashion with the experimental positions.

Studies were made both with and without background. Five noninteracting beam tracks were randomly distributed in an area of the bubble chamber defined as follows:

$$.015 < y < .105\text{m}$$

$$.210 < z < -.170\text{m}$$

The event and the five noninteracting beam tracks were randomly distributed in a 250 μsec spill. The effect of this background on the track resolution was negligible. The major source of background results from the interaction of low momentum event tracks with the magnet and other material. W. Bugg (Tenn.) has measured the event related background for 147 GeV/c and found an average of 7 tracks at the entrance of ISIS-1 and only two tracks at the exit of ISIS-2. It was attempted to simulate this highly divergent background by randomly distributing 147 GeV/c events on the surface of the magnet aperture. This background resulted in an average of 5.5 tracks at ISIS-1 and 4.5 tracks at ISIS-2. Since a slowly diverging background track is more likely to interfere with an event track (also slowly diverging), this simulated background has a very pessimistic effect on track resolution.

Figure 1 gives the momentum distribution for all particles from simulated 300 GeV/c events and for those which escape through the B. C. magnet aperture into the downstream system. These distributions may be compared with figure A-4 (figure 4 in Appendix A). The main effect of the transformation to 300 GeV/c is an understandable shift to higher momenta.

Figure 2 gives the rapidity distribution for A) all particles from the simulated 300 GeV/c events, B) the particles which escape the magnet, C) the particles with $p > 5$ GeV/c which escape the magnet, and D) the particles with $p > 5$ which pass through a 1mx1mx3m long ISIS ending at x=6.125m. These figures may be compared with figures A-10 through A-20 (figures in the appendix) and the main effect of the transformation is seen to be a widening of the rapidity region and as expected a depletion of the number of events with $y < 0$ and $p > 5$ GeV/c which escape the magnet.

Figure 3 shows the distribution of the number of events which result in a given number of charged particles in ISIS-1 and figure 4 that for ISIS-2. The averaged charged multiplicities are 3.0 for ISIS-1 and 2.6 for ISIS-2. These numbers are obtained from the 147 GeV/c events, scaled up in energy as described, which have a total charge multiplicity of 7.40 ± 0.04.[1] The average total charge multiplicity at 300 GeV/c, obtained by interpolating data at 147, 200, and 360 GeV/c, is 8.5/event. In the studies at Yale, the 360 GeV/c data of Firestone et al.[2] were used for the purpose of summing or averaging over all multiplicities. This multiplicity distribution is reproduced in figure 5. Figure 6 shows the frequency of charged tracks entering ISIS-1 and ISIS-2 as a function of primary multiplicity.

I. Acceptance

Since design considerations seem to dictate that ISIS consist of two modules rather than the three originally proposed, this study was carried out for a 1 meter long ISIS module (ISIS-1) with an entrance plane at x=2.375m and a 2 meter long ISIS module (ISIS-2) with an entrance plane at x=4.125m.

Due to voltage breakdown and gas purity considerations it is undesirable to increase the dimension of ISIS beyond 1 meter in the direction perpendicular to the plane of signal wires. However, the criteria limiting the dimension of ISIS in the direction parallel to the signal wires is less restrictive so tests were made to determine the fraction of particles gained by extending the dimension of ISIS beyond 1 meter in this direction.

Table I shows the fraction of the tracks which escape the magnet and traverse the entire length of ISIS-1 for various y and z dimensions. Table II shows the same fraction for the second module of ISIS. The tests show that virtually nothing is gained by increasing the dimension of ISIS beyond 1 meter in the z-direction, but a 5% increase in the fraction of tracks which traverse the entire length of ISIS-2 occurs by increasing the dimension in the y-direction by 20cm. The reason for this is that the bubble chamber magnetic field points in the z-direction and so the tracks are more spread out in the y-direction. However, due to the lower density of tracks in the y-direction, track resolution is so much more efficient with the wires parallel to the z-axis (which will be discussed in the next section) that the acceptance gained by having the extended wires perpendicular to the z-axis is negligible compared to the loss in track resolution. Therefore, the wires should be parallel to the z-axis (direction of the B. C. magnetic field) and thus the dimension of ISIS is limited to approximately 1 meter in the y-direction. As Tables I and II show, no significant gain in acceptance is obtained by increasing the dimension of ISIS in the z-direction. Therefore in all further tests ISIS is assumed to be 1 meter in both the y and z-direction.

II. Track Overlap

The effectiveness of ISIS in identifying a given track is determined by the number of cells the track traverses in which it can be resolved from neighboring tracks in the event. Since it is necessary to make an accurate determination of the ionization, it is necessary to integrate the pulse arriving at the wire for a long enough time so that all the charge is collected. W. W. M. Allison et al.[3] have found that this time varies from ~0.25 μsec to ~0.4 μsec, corresponding to spacial resolutions of 1cm to 1.7cm for a drift velocity of 4cm/μsec. The lower limit is for tracks passing close to the sense wire and the upper limit for tracks where the charge has drifted 2m. For this study, two tracks were considered to be unresolvable in those regions where their projections on the x-y plane were within 1cm of each other.

In the studies carried out at Yale, ISIS-1 was divided into 62 cells and ISIS-2 into 125 cells corresponding approximately to the number of data samples from each module. That study determined the average number of "clear" cells for each track and the fraction of tracks with 90% of the track clear. In the MIT study ISIS-1 was divided into 100 "cells" and ISIS-2 into 200 "cells" and the study determined the fraction of each track which was clear. Histograms were made giving the percentage of tracks with a given fraction of the track clear. The results of the two approaches were in qualitative agreement.

The original design of ISIS consisted of a sense wire plane at beam height sandwiched between two high voltage planes at a distance of 50cm. Because the symmetry of the configuration results in the fact that the single sense wire plane may receive signals from both the upper and lower halves of ISIS at the same time, the probability of track interference is approximately doubled. Table III shows the effect of this reflection symmetry. In this table f_{160} is the fraction of tracks with 160 of 187 cells clear as a function of momentum and primary multiplicity. The improvement in resolution by eliminating this reflection symmetry is quite dramatic. Studies were made in an attempt to eliminate or reduce the effect of this reflection symmetry. These studies resulted in a modification to the high voltage - sense wire plane configuration of ISIS.

It was suggested at the Fermilab workshop in May 1976 that a way to improve the acceptance of ISIS without increasing the drift distance would be to position the device with lengthened sense wires perpendicular to the magnetic field and where the largest aperture is necessary. Table IV compares the track overlap characteristics for ISIS-1 and ISIS-2 with wires parallel to and perpendicular to the magnetic field. The loss in track resolution indicates that the orientation of ISIS with the sense wires parallel to the magnetic field is desirable. All succeeding test results will be given only for the case with the wires parallel to the B. C. magnetic field.

In an attempt to improve resolution, tests were made by offsetting the signal wire plane from beam height and also by rotating by angles between $\pm 6^{\circ}$ about the axis parallel to the sense wires through the center of each ISIS module. All of these tests resulted in a decrease in track resolution.

Since track resolution is seen to be a serious problem and no improvement is obtained by trying different orientations of the original design, tests were run to compare the original design, A) signal wire plane at beam height with high voltage planes at $\pm$ 50cm, with the following alternatives, B) high voltage plane at beam height with two separately analyzed signal planes at $\pm$ 50cm, and C) high voltage plane at beam height with two separately analyzed signal planes at $\pm$ 25cm and two more high voltage planes at $\pm$ 50cm (see figure 7). Design B eliminates the problem of reflection symmetry. Design C eliminates the reflection symmetry problem about the y=0 plane but introduces reflection symmetry about the planes $y=\pm 25$cm. However design C is an improvement over the original design since each sense plane receives signals from only half the volume of ISIS and thus the probability of track overlap is reduced. Table V gives the fraction of tracks entering the full ISIS as a function of the amount of the track which is clearly resolved for each of the three designs. Designs B and C are a substantial improvement over the original design A.

Design C has the additional attractive feature that the maximum drift distance is reduced by a factor of 2 and thus the chamber may be operated at half the voltage originally anticipated for ISIS. Since high voltage tests in Argon (20%) CO_2 have shown that breakdown and corona may be a problem in a device with a 50cm drift space, design C, with a 25cm drift space, is especially attractive. Therefore, since the track resolution of design C is at an acceptable level, this design has been proposed for ISIS.

Table VI gives the fraction of tracks of a given momentum and primary multiplicity entering the full ISIS as a function of the amount of track which is clearly resolved for design C. Table VII gives the same data with the event-related background described in section I. Since this slowly diverging background has been found to be rather pessimistic, the actual results should be somewhere between those of Tables VI and VII. Nevertheless, in view of the difference between Tables VI and VII, it clearly would be very desirable to reduce the background by increasing the aperture in the magnet.

Since it may be possible to improve the spacial resolution because of the smaller drift space, a study has been made of the track overlap characteristics for a spacial resolution of 0.5cm. Table VIII gives these results together with those for 1.0cm spacial resolution. The factor of two in track resolution is seen to give an approximately 13% increase in the fraction of tracks which are at least 90% clear.

Additional studies were made to determine the effect of connecting signal wires from the two signal wire planes in a systematic way to reduce the amount of electronics required for analysis. The following two schemes were tested, 1) wires in the upper plane were successively connected from the front to wires in the lower plane from the back, and 2) wires from the front half of the upper plane were successively connected to wires in the back half of the lower plane and wires from the back half of the upper plane were successively connected to wires in the front half of the lower plane (see figure 8). Both tests gave virtually identical results. Table IX compares these tests with the test of design C. In view of these results it is not desirable to connect signal wires from the two sense wire planes.

III. Particle Identification

The ability of ISIS to identify particles rests on an accurate determination of the ionization loss dE/dx. Figure 9 taken from W. W. M. Allison et al.[(4)] shows the mean ionization of a π, k, and p in A(20%) CO_2 as a function of particle momentum. However, since a series of measurements of dE/dx will be distributed in a Landau distribution such as that shown in figure 10, a large number of measurements will be needed to get an accurate determination of the mean ionization. If one then plots a distribution of the calculated mean ionization for all particles seen by ISIS for a given momentum one will obtain peaks corresponding to different particle types. The locations of these peaks will correspond to their relative ionizations and their widths to the expected resolution of ISIS. This resolution depends both on the statistics of the amount of ionization in each sample and on the number of samples. Thus it is proportional to the square root of the number of samples used in calculating the mean. W. W. M. Allison et al. have shown that 6.2% full width at half maximum (FWHM) may be obtained with 330 samples. Since the Fermilab ISIS will provide a maximum of 192 samples the expected width of these peaks with maximum track resolution is 8.1% FWHM. Figures 11, 12, 13 and 14 show results for several momenta assuming that the ratio of $\pi/k/p$ is 10/1/1.

For the purposes of this study, a particle identification was made from figures 11 through 14 by making two partitions in the mean ionization loss corresponding to the point where a particle is as likely to be a kaon as a proton and the point where a particle is as likely to be a kaon as a pion. All particles with a mean ionization loss less than the first partition are identified as protons and all particles with a mean ionization loss greater than the second partition are identified as pions. The remaining particles with mean ionization loss between the two partitions are identified as kaons.

Figure 15 gives the percentage of pions, protons and kaons which are correctly identified with 192 ionization samples for all particles. The efficiency of ISIS for identifying protons is $\gtrsim$ 80% for the entire range from 5 to 80 GeV/c. The percentage of kaons which are correctly identified falls from 75% at 7 GeV/c to 50% at 43 GeV/c.

An important parameter in the analysis of ISIS data will be the probability that a given particle is correctly identified. For this purpose figure 16 gives the percentage of the particles called kaons which are correctly identified. Corresponding curves for protons and pions are also given. Although figure 15 states that only 50% of the kaons will be correctly identified at 43 GeV/c, figure 16 states that of those particles identified as kaons 62% will actually be kaons at 43 GeV/c. The apparent discrepancy between figure 15 and 16 results from the fact that in figure 16 the number of particles called a given type is not independent of momentum. Although more kaons are misidentified at higher momenta which results in the fast fall of the kaon curve in figure 15, the fall is less drastic in figure 16 because fewer particles are called kaons at higher momenta. Figure 16 indicates that the Fermilab ISIS will be a useful kaon identifier up to at least 40 GeV/c.

In conclusion it should be stated that although these last figures are a realistic estimate of the ultimate resolution of the Fermilab ISIS based on the current state of the technique, we are looking into the possibility of improving the particle identification by looking not only at the mean ionization, but also at the width of the Landau distributions of the ionization samples. Others have found that such considerations should lead to a significant improvement in resolution.[5]

IV. Conclusion

The Fermilab ISIS will be a two module device. The first module, ISIS-1, will be 1x1x1m with its entrance plane at x=2.375m. The second module, ISIS-2, will be 1x1x2m with its entrance plane at x=4.125m. 97% of the particles which escape the aperture of the bubble chamber magnet traverse the entire length of ISIS-1 while 80% of the particles traverse the entire length of ISIS-2.

The Fermilab ISIS will consist of a sandwich of two signal wire planes and three high voltage planes. The high voltage plane in the center of the sandwich will be at beam height. For this configuration an average of approximately 80% of the ionization samples for tracks with momentum between 5 and 80 GeV/c will be useful if there is no background. For a pessimistic simulated background this average falls to approximately 70%. Again for the case with no background, the average percentage of useful ionization samples varies from 60% at 5 GeV/c to 85% at 80 GeV/c.

Particle identification studies have shown that for 192 ionization samples between 85 and 80% of the protons are correctly identified in the range from 5 to 80 GeV/c. The percentage of kaons which are correctly identified falls approximately linearly from 75% at 7 GeV/c to 37% at 60 GeV/c. Nevertheless the Fermilab ISIS will be a useful kaon identifier up to at least 40 GeV/c. The particle identification may be improved, as others have found, by looking not only at the mean ionization, but also at the width of the Landau distributions of the ionization samples. This possibility will be studied.

REFERENCES

1. D. Fong et al., Nucl. Phys. B102, 386 (1974)

2. A. Firestone et al., Phys. Rev. D14, 2902 (1976)

3. W. W. M. Allison and R. W. Pleming, ISIS note 25

4. W. W. M. Allison et al., Nucl. Inst. and Meth. 119, 499 (1974)

5. Time Projection Chamber Group Proposal to PEP

Figure 1 Momentum distribution for all particles from simulated 300 GeV/c events and for those which escape through the bubble chamber magnet aperture into the downstream system (unshaded).

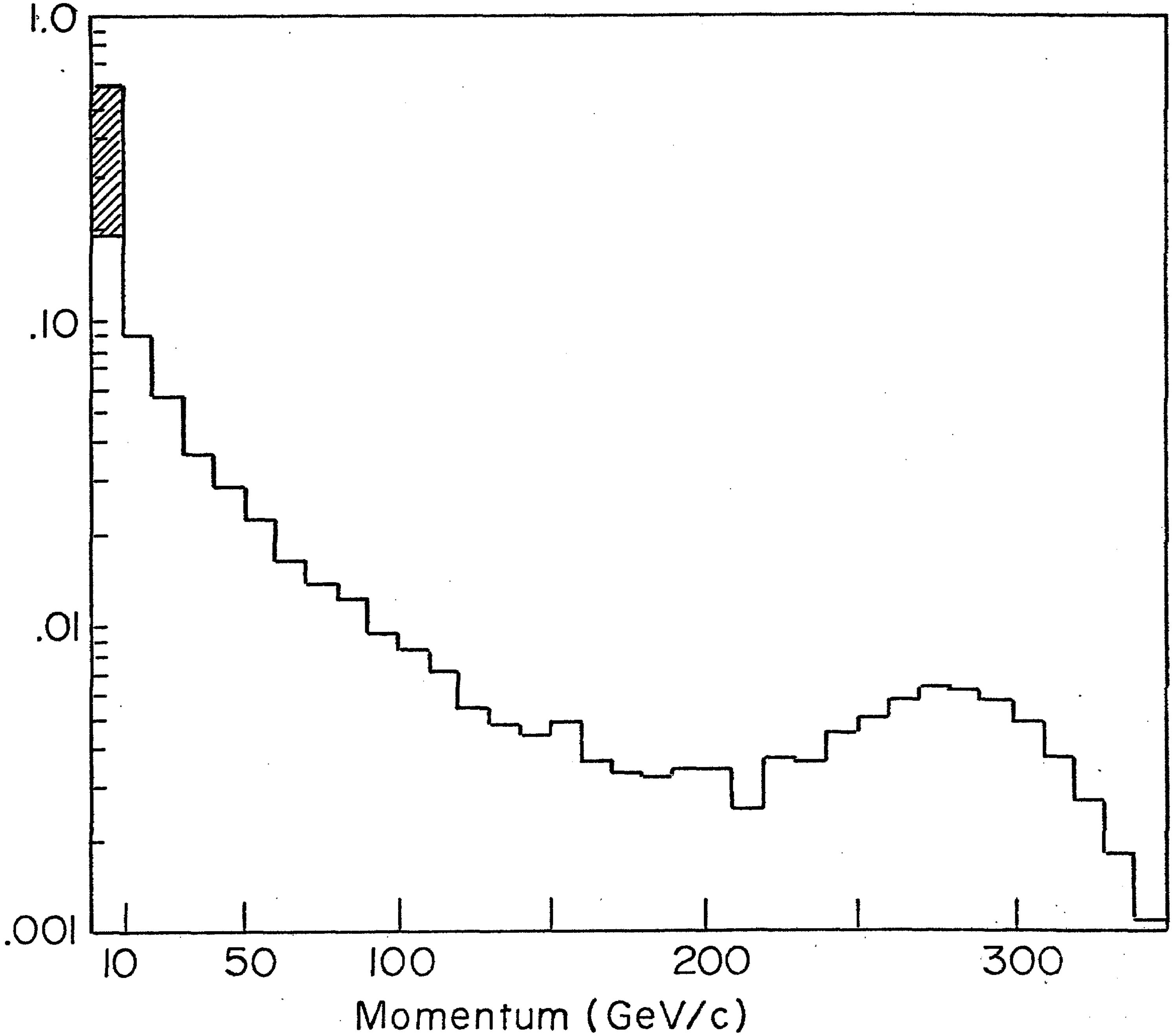

1.0
.10
.01
.001
10
50
100
200
300
Momentum (GeV/c)

Figure 2 Rapidity distribution for A) all particles from the simulated 300 GeV/c events, B) the particles which escape the magnet, C) the particles with p >5 GeV/c which escape the magnet, and D) the particles with p > 5 which pass through a 1m x 1m x 3m long ISIS ending of x = 6. 125m.

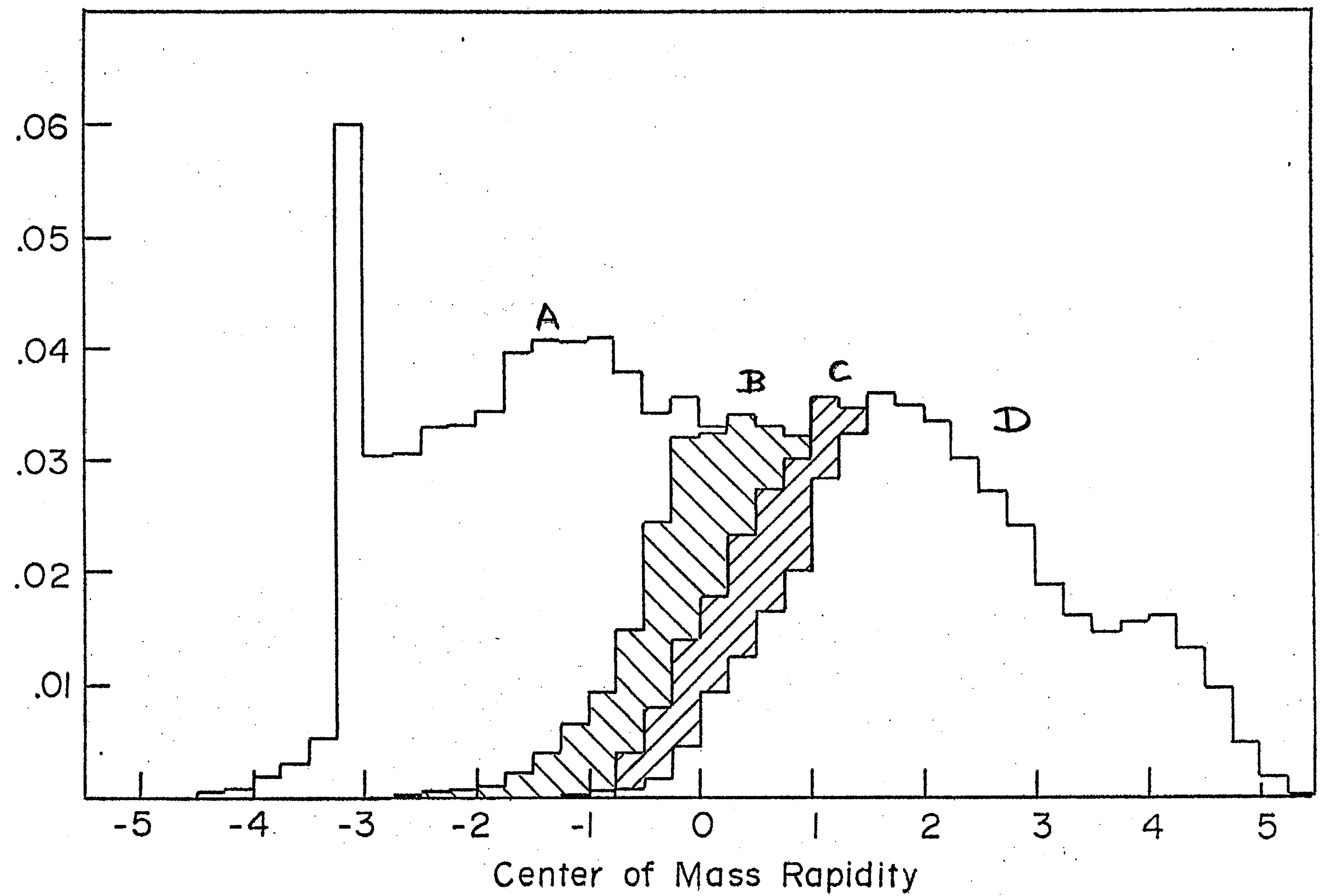

.06
.05
.04
.03
.02
.01
A
B
C
D
-5
-4
-3
-2
-1
0
1
2
3
4
5
Center of Mass Rapidity

Figure 3 Distribution of the number of events which result in a given number of charged particles in ISIS-1.

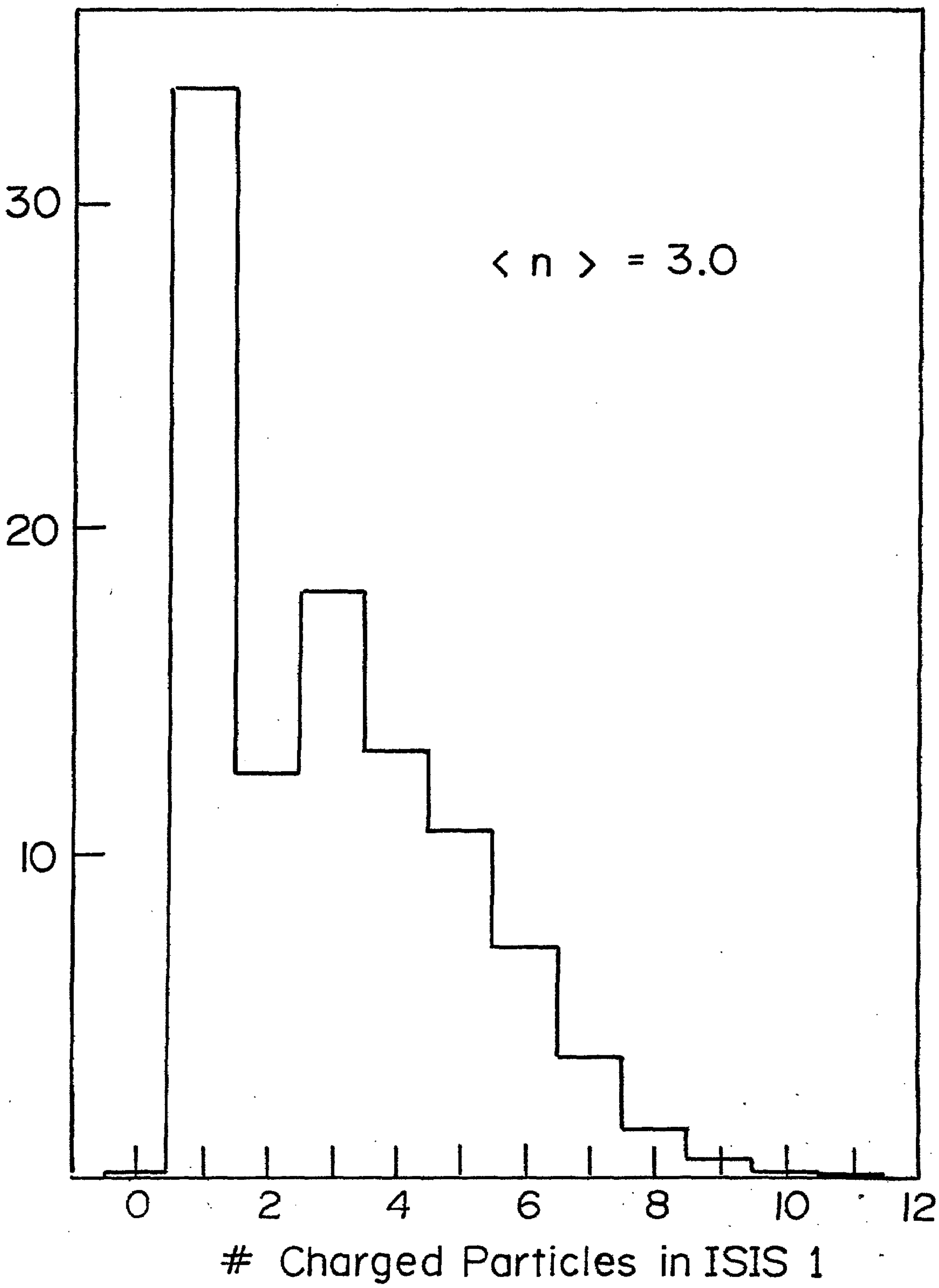

30
20
10
< n > = 3.0
0
2
4
6
8
10
12
Charged Particles in ISIS 1

Figure 4 Distribution of the number of events which result in a given number of charged particles in ISIS-2.

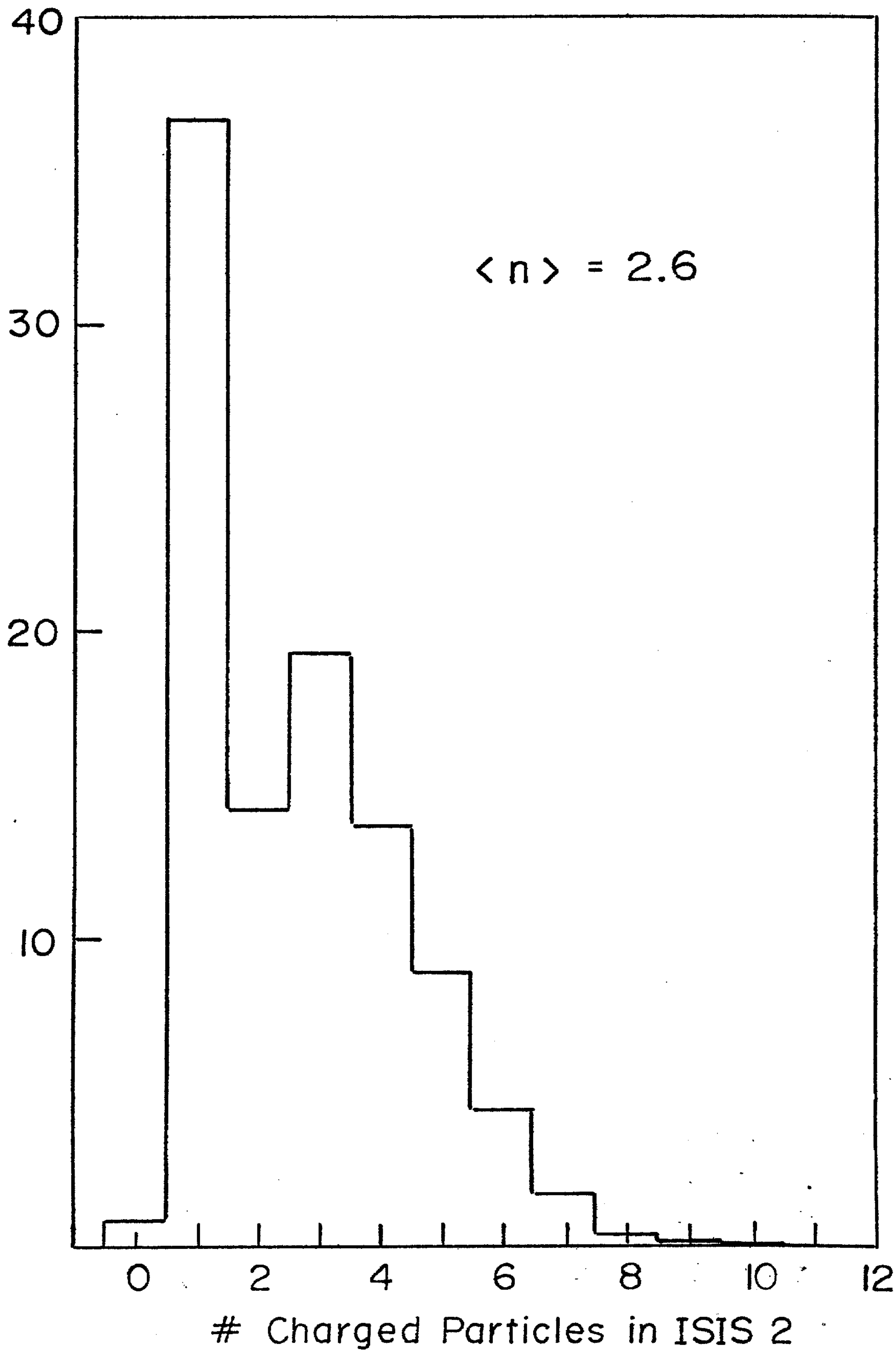

40
30
20
10
⟨n⟩ = 2.6
0
2
4
6
8
10
12
Charged Particles in ISIS 2

Figure 5 Charged prong multiplicity distribution 360 GeV/c $\pi^- p$ [3]

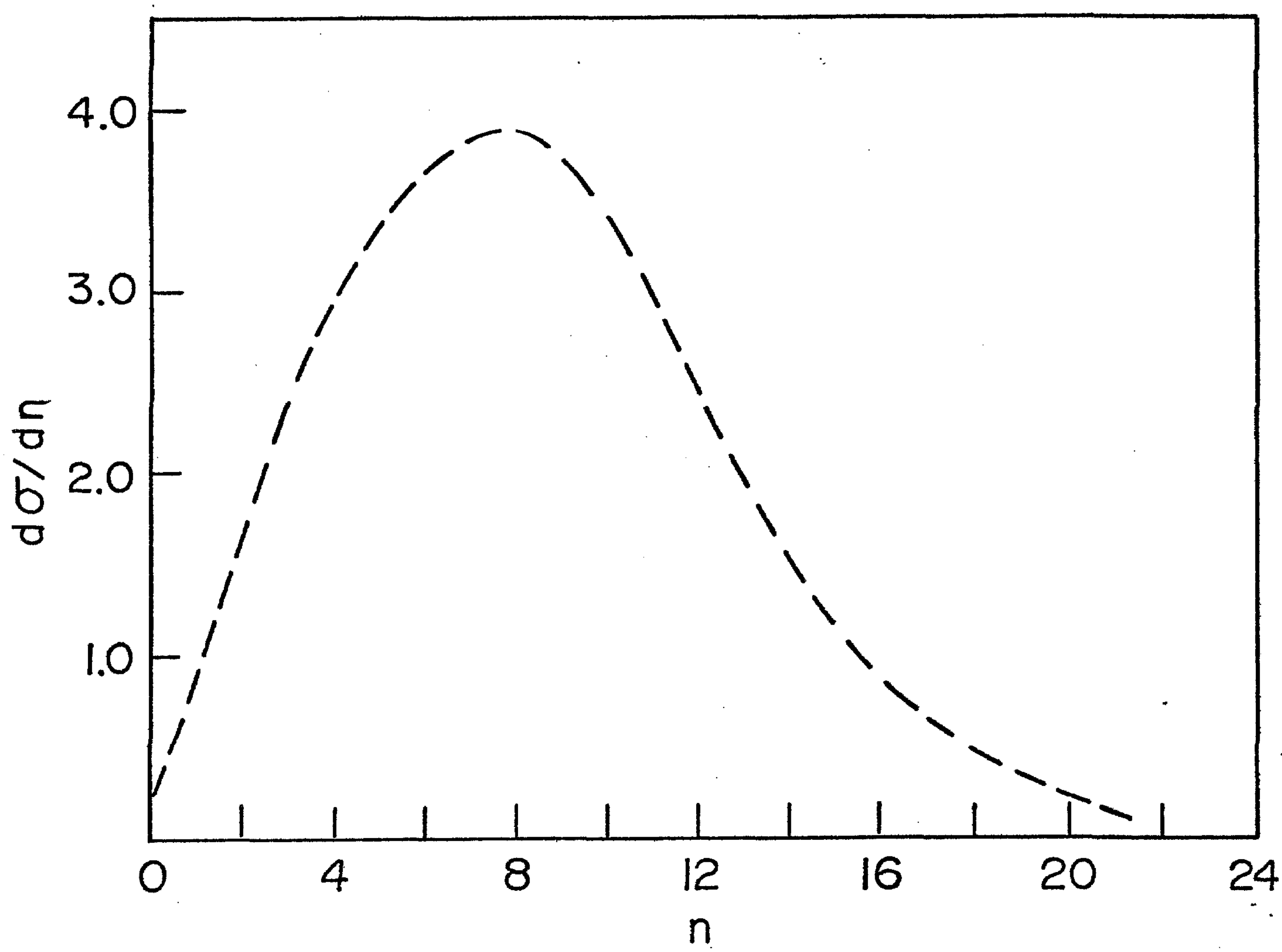

4.0
3.0
2.0
1.0
dσ/dη
0
4
8
12
16
20
24
η

Figure 6 Number of tracks as a function of multiplicity for 300 GeV/c $\pi^- p$.

Solid line-entrance to ISIS-1. Dashed line-entrance to ISIS-2.

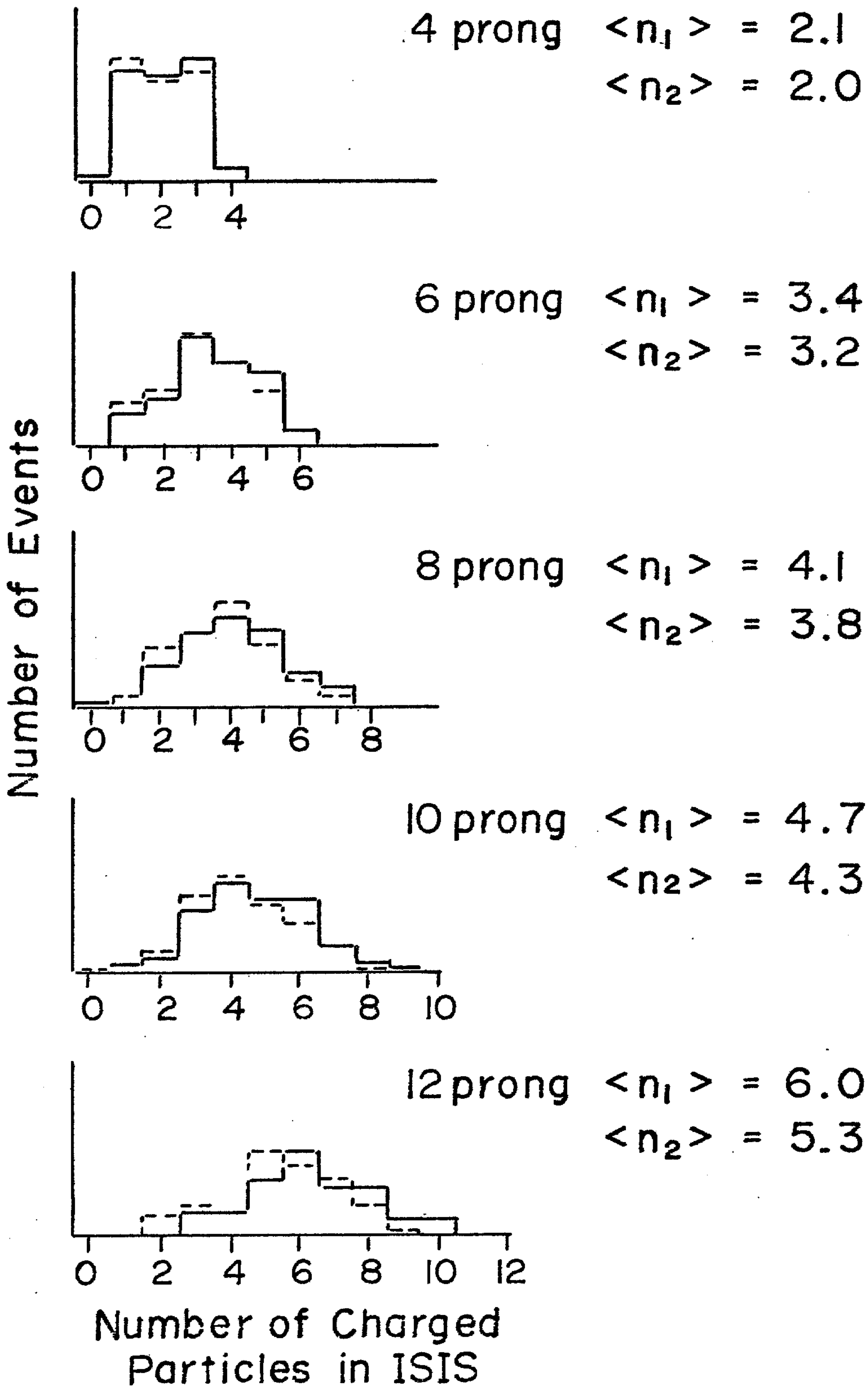

4 prong $\langle n_1 \rangle = 2.1$
$\langle n_2 \rangle = 2.0$
6 prong $\langle n_1 \rangle = 3.4$
$\langle n_2 \rangle = 3.2$
8 prong $\langle n_1 \rangle = 4.1$
$\langle n_2 \rangle = 3.8$
10 prong $\langle n_1 \rangle = 4.7$
$\langle n_2 \rangle = 4.3$
12 prong $\langle n_1 \rangle = 6.0$
$\langle n_2 \rangle = 5.3$
Number of Events
0 2 4
0 2 4 6
0 2 4 6 8
0 2 4 6 8 10
0 2 4 6 8 10 12
Number of Charged Particles in ISIS

Figure 7: Configuration of the high voltage and signal wire planes for the three designs of ISIS which were tested. For a comparison of these designs, see Table V.

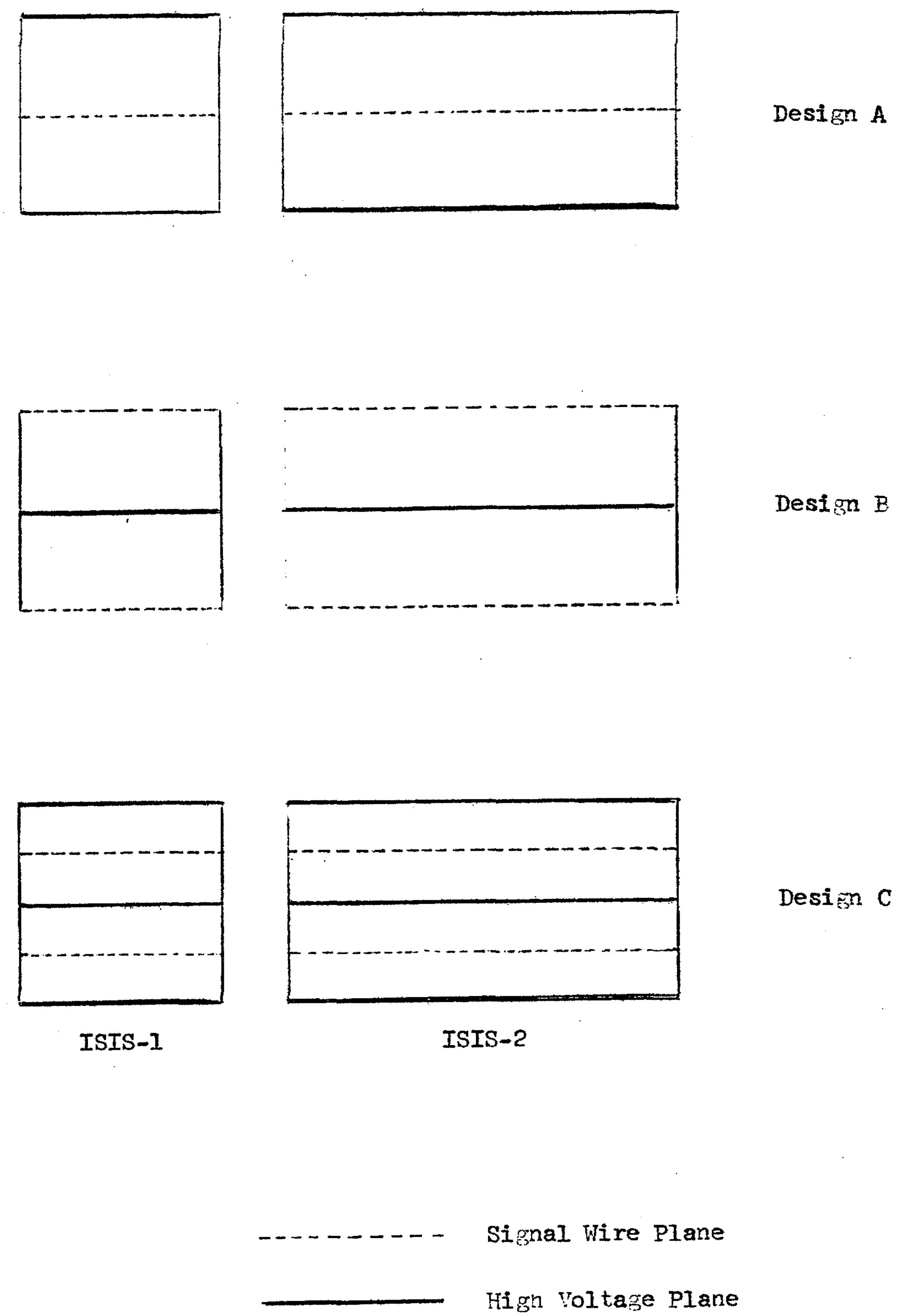
Design A
Design B
Design C
ISIS-1
ISIS-2
Signal Wire Plane
High Voltage Plane

Figure 8: Drawings showing how the signal wires could be connected to reduce the amount of required electronics. For a comparison of these two configurations with design C of Figure 7, see Table IX.

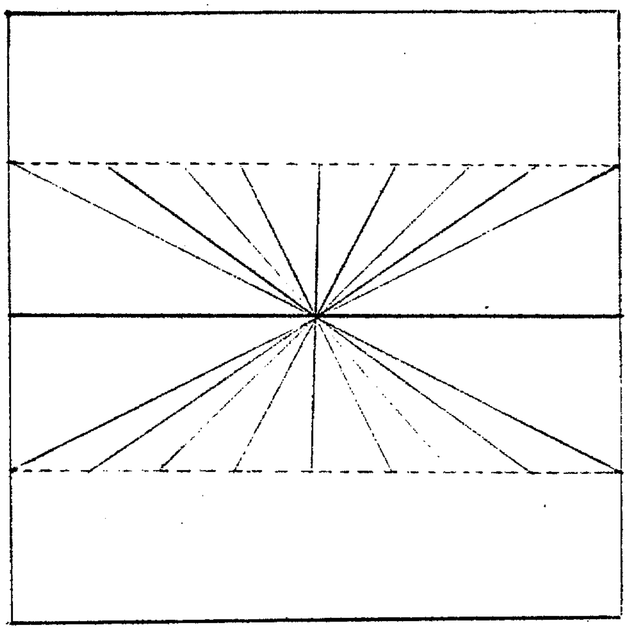

Test 1

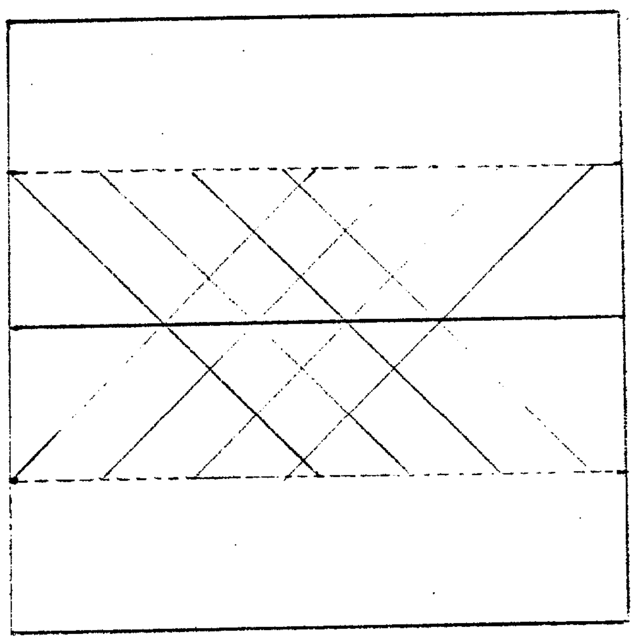

Test 2

Diagonal Lines Denote Wire Conections

Figure 9 Mean ionization loss in 80% A-20% CO_2 as a function of momentum for pions, kaons, and protons (taken from ref. 4).

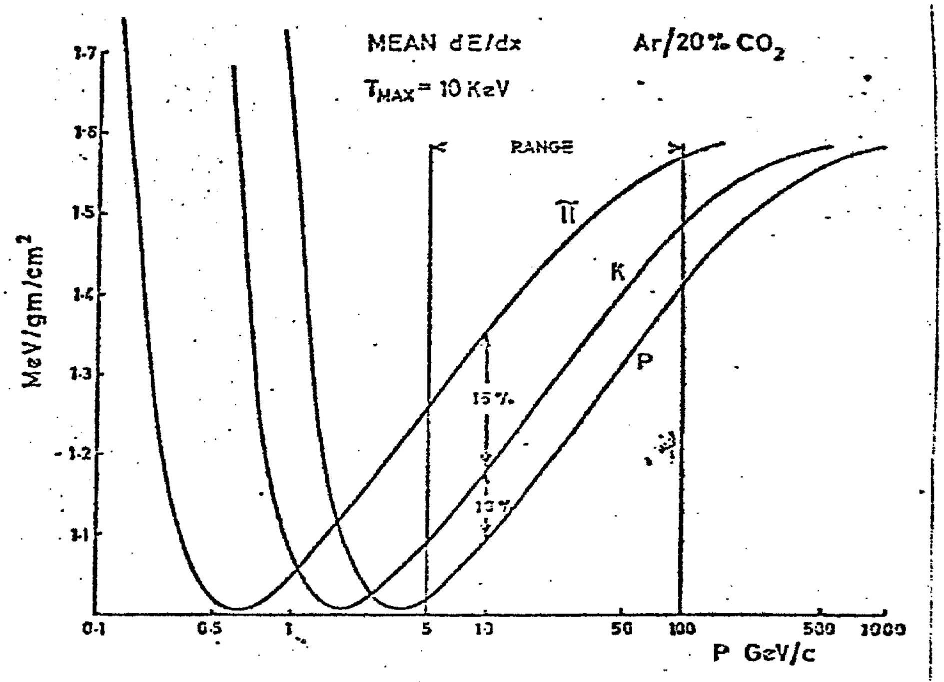

MEAN dE/dx
Ar/20% CO2
TMAX = 10 KeV
RANGE
π
K
P
15%
13%
MeV/gm/cm2
1·7
1·6
1·5
1·4
1·3
1·2
1·1
0·1
0.5
1
5
10
50
100
500
1000
P GeV/c

Figure 10: Ionization loss for 3 GeV/c pions in 1.5cm of 93% A-7% CH_4 (taken from ref. 4).

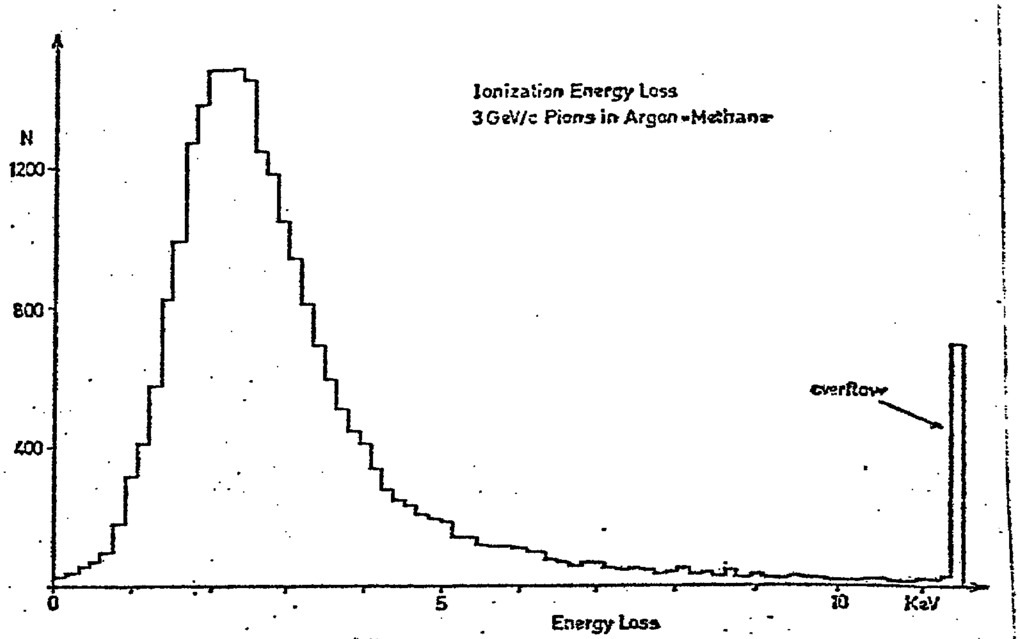
Ionization Energy Loss
3 GeV/c Pions in Argon-Methane
N
1200
800
400
0
5
10
KeV
Energy Loss
overflow

Figure 11: Mean ionization loss in ISIS for 5 Gev/c protons, kaons and pions ($p:k:\pi = 1:1:10$).

SCATTERPLOT NUMBER 1   5 GEV/C   198 WIRES CLEAN

0   3   0
0 297   0
0   0   0   123456789ABCDEFGHIJKLMNOPQRSTUVWXYZ

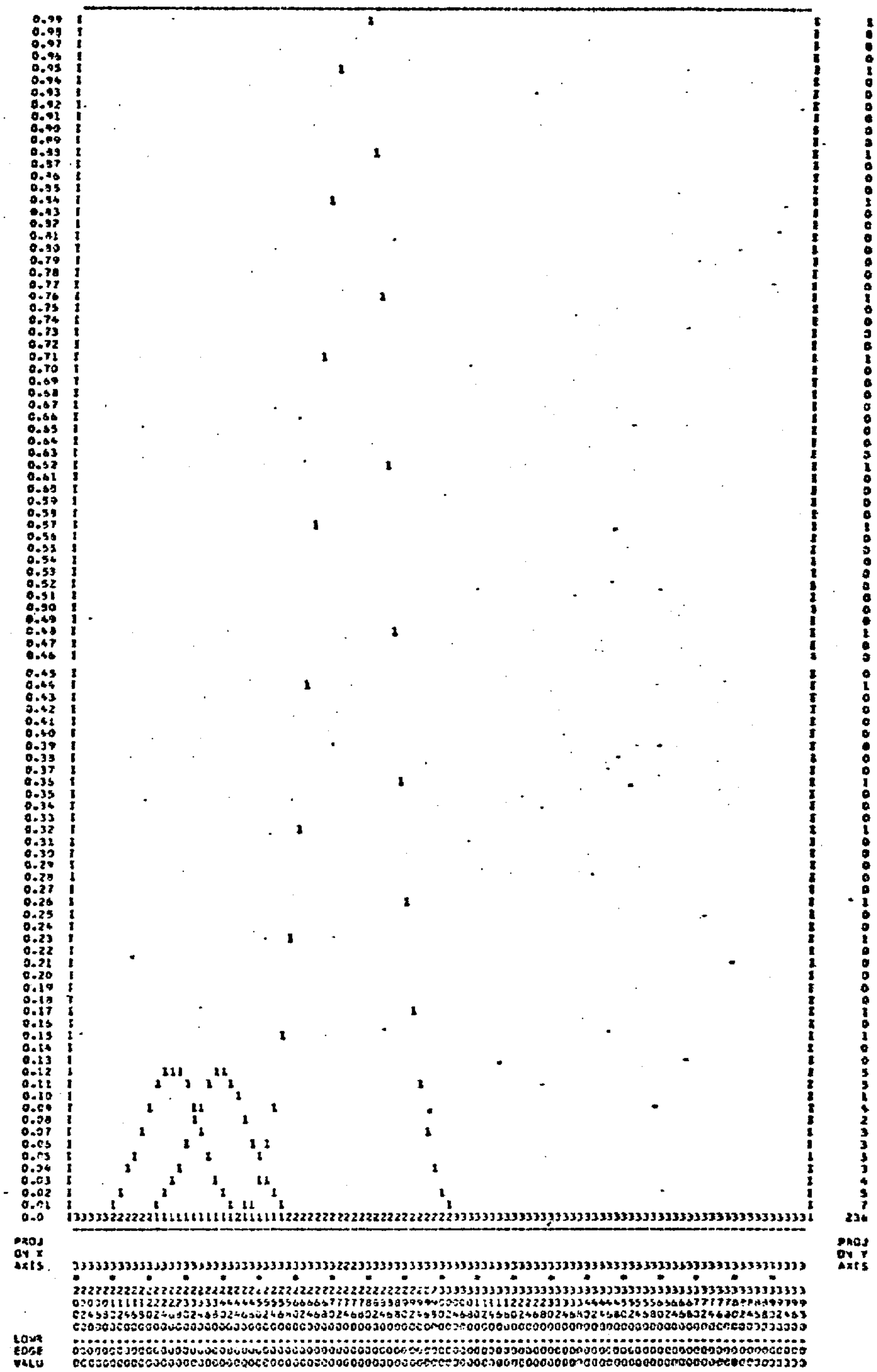

Figure 12: Mean ionization loss in ISIS fo 10 Gev/c protons, kaons and pions ($p:k:\pi = 1:1:10$).

SCATTERPLOT NUMBER 3 10 GEV/C 198 WIRES CLEAN

```
0    0   0
0  300   0
0    0   0     123456789ABCDEFGHIJKLMNOPQRSTUVWXYZ
```

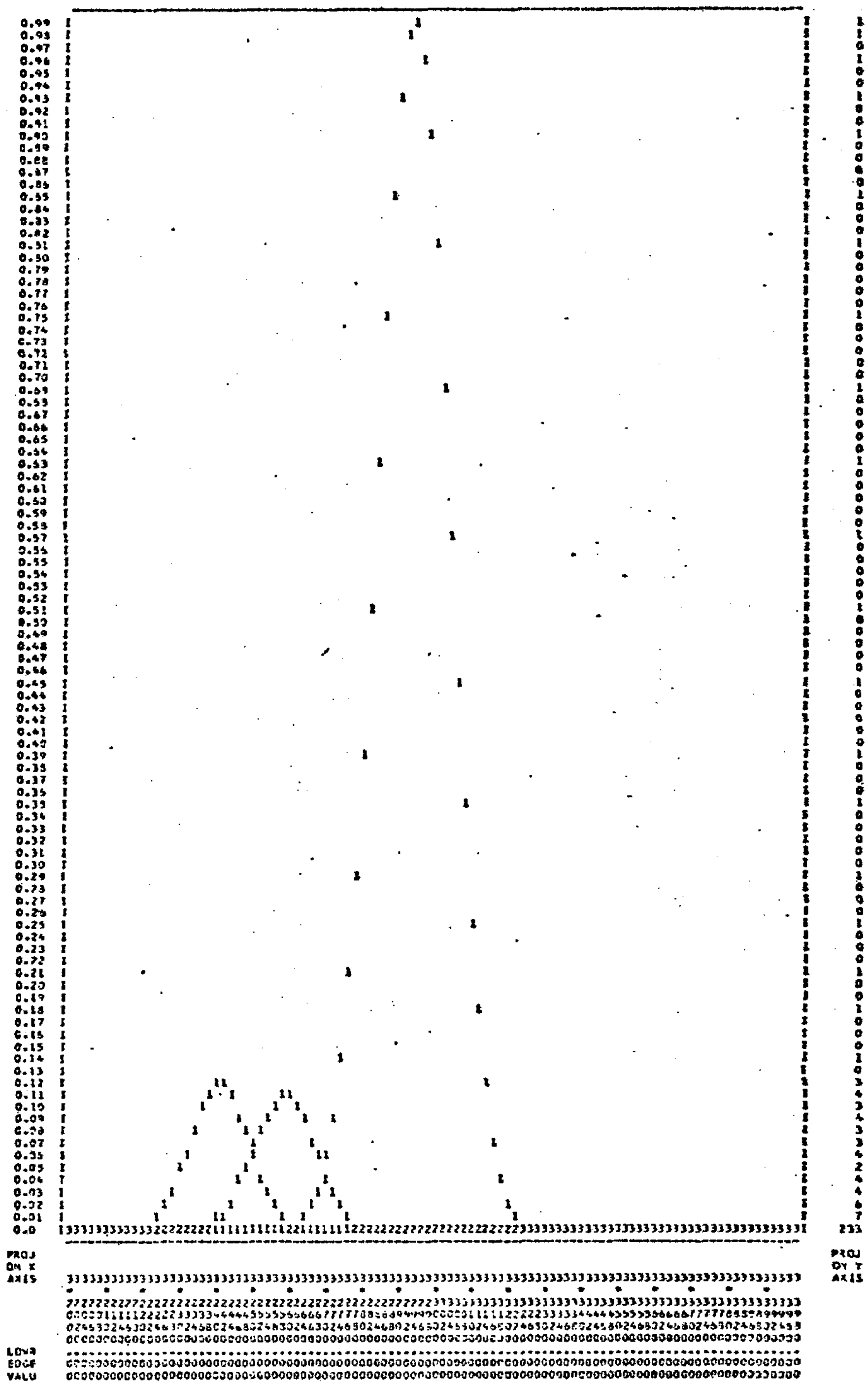

Figure 13: Mean ionization loss in ISIS for 20 Gev/c protons, kaons and pions ($p:k:\pi = 1:1:10$).

SCATTERPLOT NUMBER 5   20 GEV/C 198 WIRES CLEAN

0 0 0
0 300 0
0 0 0   123456789ABCDEFGHIJKLMNOPQRSTUVWXYZ

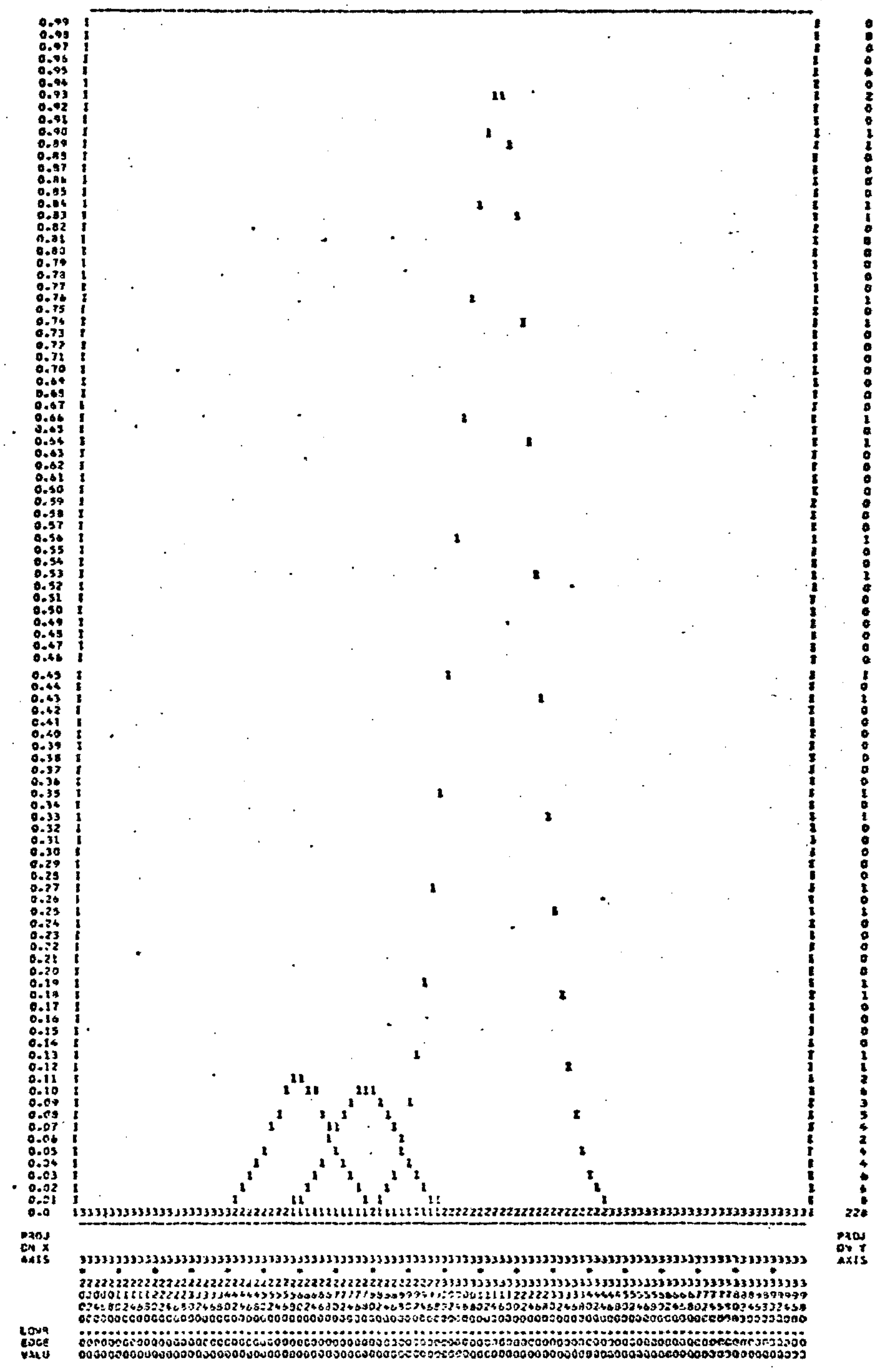

Figure 14: Mean ionization loss in ISIS for 60 Gev/c protons, kaons and pions ($p:k:\pi = 1:1:10$).

SCATTERPLOT NUMBER 9   60 GEV/C 148 WIRES CLEAN

```
0    0    0
0  300    0
0    0    0     123456789ABCDEFGHIJKLMNOPQRSTUVWXYZ
```

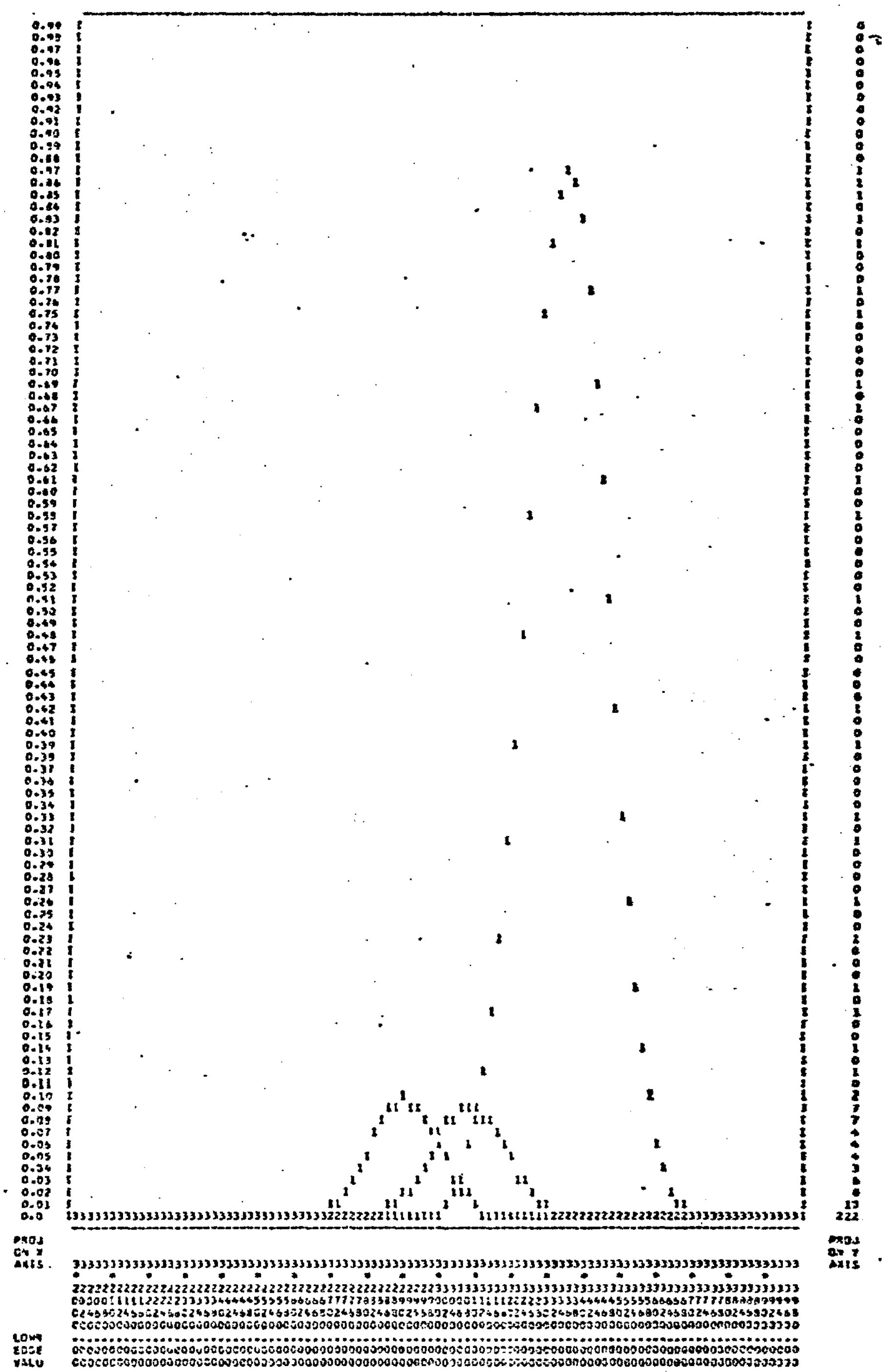

Figure 15: Percentage of particles of a given type which are correctly identified assuming that the ratio of $\pi/k/p$ is 10/1/1 for all momenta.

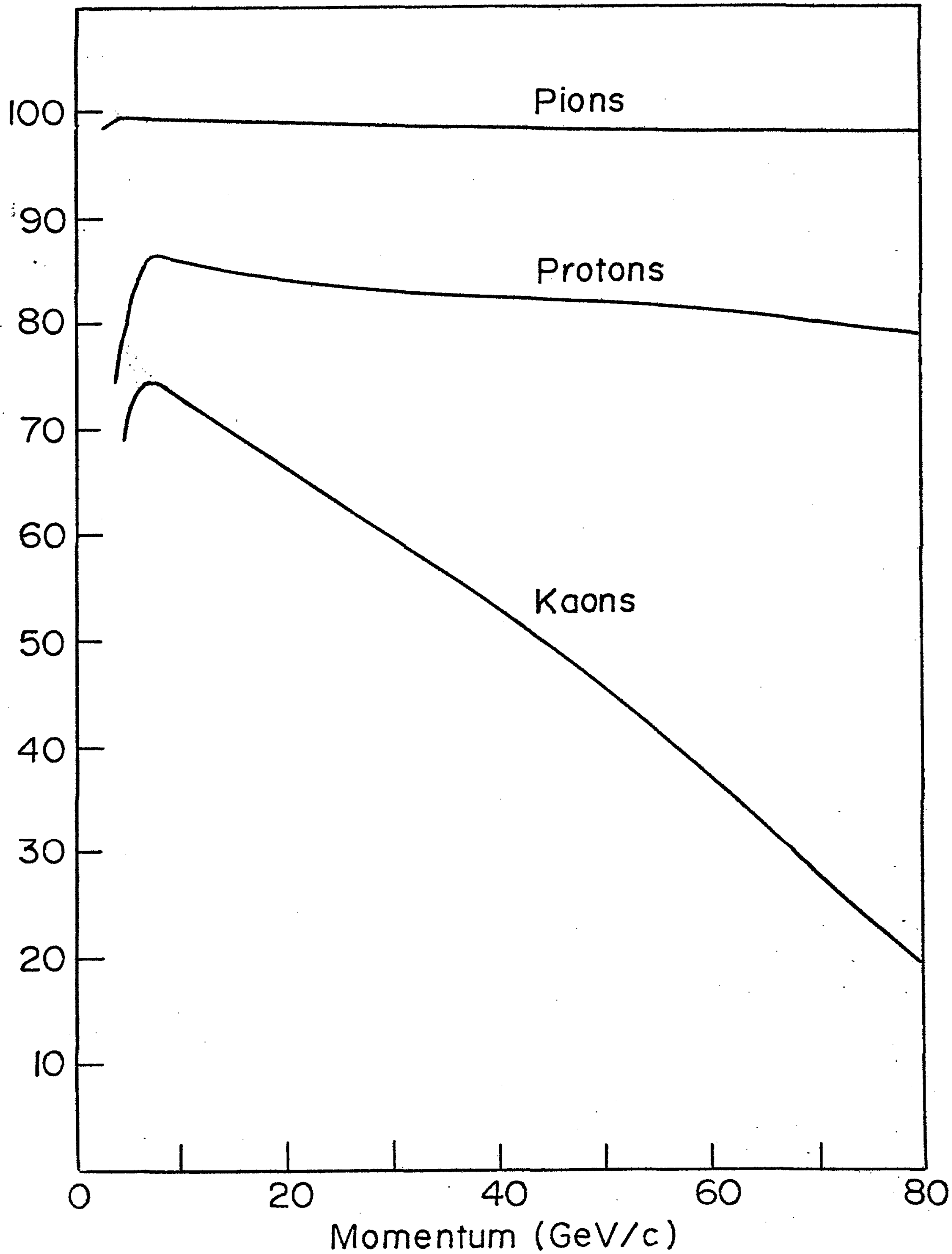
Pions
Protons
Kaons
100
90
80
70
60
50
40
30
20
10
0
20
40
60
80
Momentum (GeV/c)

Figure 16: Percentage of particles called a given type which are correctly identified assuming that the ratio of $\pi/k/p$ is 10/1/1 for all momenta.

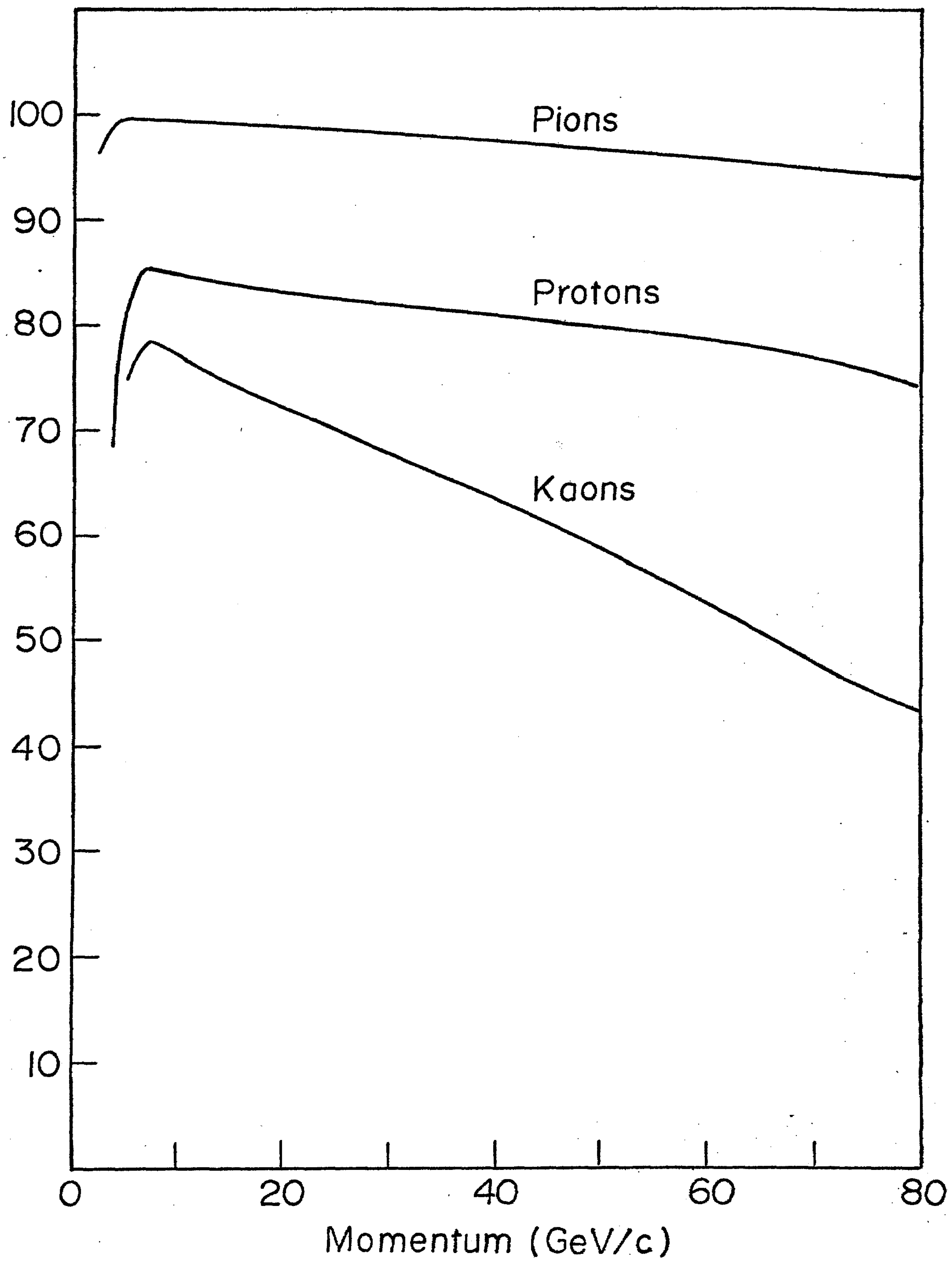

100
90
80
70
60
50
40
30
20
10
Pions
Protons
Kaons
0
20
40
60
80
Momentum (GeV/c)

Table I

PERCENTAGE OF TRACKS WHICH ESCAPE THE MAGNET AND TRAVERSE THE ENTIRE LENGTH OF ISIS-1 FOR VARIOUS DIMENSIONS OF ISIS IN METERS IN THE Y DIRECTION (COLUMNS) AND THE Z DIRECTION (ROWS)

	1.000	1.025	1.050	1.075	1.100	1.125	1.150	1.175	1.200
1.000	96.6	97.0	97.3	97.7	97.9	98.1	98.3	98.4	98.6
1.025	96.7	97.0	97.4	97.7	98.0	98.2	98.3	98.5	98.6
1.050	96.7	97.0	97.4	97.7	98.0	98.2	98.3	98.5	98.6
1.075	96.7	97.0	97.4	97.7	98.0	98.2	98.3	98.5	98.6
1.100	96.7	97.0	97.4	97.7	98.0	98.2	98.3	98.5	98.6
1.125	96.7	97.0	97.4	97.7	98.0	98.2	98.3	98.5	98.6
1.150	96.7	97.0	97.4	97.7	98.0	98.2	98.3	98.5	98.6
1.175	96.7	97.0	97.4	97.7	98.0	98.2	98.3	98.5	98.6
1.200	96.7	97.0	97.4	97.7	98.0	98.2	98.3	98.5	98.6

Table II

PERCENTAGE OF TRACKS WHICH ESCAPE THE MAGNET AND TRAVERSE THE ENTIRE LENGTH OF ISIS-2 FOR VARIOUS DIMENSIONS OF ISIS IN METERS IN THE Y DIRECTION (COLUMNS) AND THE Z DIRECTION (ROWS)

	1.000	1.025	1.050	1.075	1.100	1.125	1.150	1.175	1.200
1.000	79.7	80.5	81.1	81.7	82.5	83.1	83.7	84.3	84.7
1.025	79.9	80.7	81.3	81.9	82.6	83.3	83.9	84.4	84.9
1.050	80.0	80.8	81.4	82.0	82.7	83.4	84.0	84.6	85.0
1.075	80.1	80.9	81.5	82.2	82.9	83.6	84.2	84.7	85.1
1.100	80.2	81.0	81.6	82.2	83.0	83.6	84.2	84.8	85.2
1.125	80.3	81.1	81.7	82.4	83.1	83.8	84.4	85.0	85.4
1.150	80.5	81.3	81.9	82.5	83.2	83.9	84.5	85.1	85.6
1.175	80.5	81.4	82.0	82.6	83.4	84.1	84.7	85.2	85.7
1.200	80.6	81.4	82.1	82.7	83.4	84.1	84.7	85.3	85.7

Table III. Comparison of results both with and without signal wire plane reflection as a function of momentum and primary multiplicity. f_{160} is the fraction of tracks with 160 of 187 cells clear.

Momentum Range	Number of Prongs	f_{160} Reflected	f_{160} Not Reflected
5<p<10	4	.58	.51
	6	.48	.56
	8	.46	.51
	10	.36	.46
	12	.37	.44
10<p<20	4	.75	.91
	6	.72	.87
	8	.66	.83
	10	.64	.80
	12	.50	.74
20<p<70	4	.56	.89
	6	.44	.80
	8	.49	.75
	10	.44	.78
	12	.37	.73

Table IV. Comparison of the track overlap characteristics of the full ISIS with vertical and with horizontal wire orientations. The table gives the percentage of all tracks with $5<p<70$ GeV/c from events with multiplicity greater than or equal to 4 as a function of the percentage of the track which can be resolved from all other tracks in the event.

	% of track which is resolvable				
	90-100%	70-90%	50-70%	30-50%	10-30%
Verticle wire (y)	35%	7%	12%	9%	5%
Horizontal wire (z)	46%	14%	16%	10%	5%

Table V. Comparison of the track overlap characteristics of the full ISIS for the three designs described in the text. The table gives, as a function of momentum, the percentage of all tracks which traverse the entire length of ISIS with at least 90% of the track clear and the percentage of tracks with between 70 and 90% of the track clear. Also given are the average percentage clear for tracks at a given momentum and also the number of tracks in the test sample.

	Momentum	% of track clear		Avg.% Clear	Sample Size
		90-100%	70-90%		
Design A	5-10	27.1	39.7	74.2	1063
	10-20	29.6	35.9	72.5	2431
	20-40	28.0	26.8	65.6	2852
	40-80	26.4	22.4	60.9	2515
Design B	5-10	85.9	5.6	94.2	1063
	10-20	86.0	3.1	92.0	2431
	20-40	80.5	4.0	87.7	2852
	40-80	75.8	5.7	84.6	2515
Design C	5-10	75.8	15.0	90.9	1030
	10-20	80.2	8.9	89.5	2368
	20-40	77.3	7.7	86.5	2647
	40-80	73.5	8.9	83.9	2177

Table VIa-n: The following tables give as a function of momentum and primary multiplicity for ISIS-1, ISIS-2; and the full ISIS (ISIS-3) the fraction of particles with a given percentage of their track clearly resolvable from other tracks in the same event. The table also gives the average percentage of the track which is lost due to overlap or to exiting from the sides of ISIS. The total number of particles used to calculate any particular set of data in the table is also given.

Table VIa: Track resolution characteristics for all particles entering ISIS.

MOMENTUM	PRONGS			0-9	1-30	3-50	5-70	70-	AVE	SAMPLE
5-10 GEV/C	ALL	FLAG1	ISIS1	.596	.234	.053	.027	.090	15.8	2747.
5-10 GEV/C	ALL	FLAG1	ISIS2	.295	.129	.076	.079	.421	50.4	2747.
5-10 GEV/C	ALL	FLAG1	ISIS3	.304	.144	.133	.201	.217	38.7	2747.
10-20 GEV/C	ALL	FLAG1	ISIS1	.713	.164	.014	.016	.093	13.3	2795.
10-20 GEV/C	ALL	FLAG1	ISIS2	.664	.171	.037	.032	.096	15.6	2795.
10-20 GEV/C	ALL	FLAG1	ISIS3	.705	.117	.069	.047	.062	14.7	2795.
20-40 GEV/C	ALL	FLAG1	ISIS1	.691	.123	.018	.015	.153	18.6	2903.
20-40 GEV/C	ALL	FLAG1	ISIS2	.777	.101	.017	.011	.094	12.5	2903.
20-40 GEV/C	ALL	FLAG1	ISIS3	.756	.080	.050	.022	.091	14.4	2903.
40-80 GEV/C	ALL	FLAG1	ISIS1	.676	.095	.022	.026	.181	21.7	2538.
40-80 GEV/C	ALL	FLAG1	ISIS2	.762	.100	.009	.012	.115	14.3	2538.
40-80 GEV/C	ALL	FLAG1	ISIS3	.726	.090	.046	.022	.116	16.7	2538.

Table VIb: Track resolution characteristics for all particles which traverse the entire length of ISIS.

MOMENTUM	PRONGS			0-9	1-30	3-50	5-70	70-	AVE	SAMPLE
5-10 GEV/C	ALL	FLAGO	ISIS1	.665	.240	.025	.011	.059	11.2	2417.
5-10 GEV/C	ALL	FLAGO	ISIS2	.745	.200	.020	.005	.031	8.0	1049.
5-10 GEV/C	ALL	FLAGO	ISIS3	.758	.150	.052	.017	.022	9.1	1030.
10-20 GEV/C	ALL	FLAGO	ISIS1	.717	.164	.013	.015	.091	13.0	2743.
10-20 GEV/C	ALL	FLAGO	ISIS2	.756	.168	.012	.009	.055	9.5	2411.
10-20 GEV/C	ALL	FLAGO	ISIS3	.802	.089	.041	.013	.054	10.5	2368.
20-40 GEV/C	ALL	FLAGO	ISIS1	.691	.125	.018	.013	.153	18.5	2760.
20-40 GEV/C	ALL	FLAGO	ISIS2	.791	.100	.014	.009	.086	11.5	2788.
20-40 GEV/C	ALL	FLAGO	ISIS3	.773	.077	.048	.015	.087	13.5	2647.
40-80 GEV/C	ALL	FLAGO	ISIS1	.676	.093	.023	.023	.185	21.9	2333.
40-80 GEV/C	ALL	FLAGO	ISIS2	.769	.103	.008	.012	.108	13.6	2380.
40-80 GEV/C	ALL	FLAGO	ISIS3	.735	.089	.048	.016	.112	16.1	2177.

Table VIc: Track resolution characteristics for all particles entering ISIS from 4 prong events.

MOMENTUM	PRONGS			0-9	1-30	3-50	5-70	70-	AVE	SAMPLE
5-10 GEV/C	4	FLAG1	ISIS1	.801	.075	.033	.039	.052	9.5	306.
5-10 GEV/C	4	FLAG1	ISIS2	.458	.065	.072	.069	.337	40.5	306.
5-10 GEV/C	4	FLAG1	ISIS3	.458	.101	.108	.212	.121	30.0	306.
10-20 GEV/C	4	FLAG1	ISIS1	.913	.044	.006	.003	.035	4.6	344.
10-20 GEV/C	4	FLAG1	ISIS2	.869	.052	.015	.020	.044	6.9	344.
10-20 GEV/C	4	FLAG1	ISIS3	.887	.029	.035	.029	.020	6.1	344.
20-40 GEV/C	4	FLAG1	ISIS1	.884	.028	.002	.0	.086	9.0	466.
20-40 GEV/C	4	FLAG1	ISIS2	.929	.024	.006	.002	.039	4.5	466.
20-40 GEV/C	4	FLAG1	ISIS3	.897	.015	.045	.006	.036	6.0	466.
40-80 GEV/C	4	FLAG1	ISIS1	.821	.029	.033	.010	.107	13.2	485.
40-80 GEV/C	4	FLAG1	ISIS2	.918	.023	.0	.006	.054	6.1	485.
40-80 GEV/C	4	FLAG1	ISIS3	.845	.058	.037	.0	.060	8.4	485.

Table VId: Track resolution characteristics for all particles from 4 prong events which traverse the entire length of ISIS.

MOMENTUM	PRONGS			0-9	1-30	3-50	5-70	70-	AVE	SAMPLE
5-10 GEV/C	4	FLAGO	ISIS1	.896	.048	.007	.019	.030	4.9	269.
5-10 GEV/C	4	FLAGO	ISIS2	.936	.043	.014	.007	.0	2.1	140.
5-10 GEV/C	4	FLAGO	ISIS3	.921	.043	.036	.0	.0	3.0	139.
10-20 GEV/C	4	FLAGO	ISIS1	.915	.041	.006	.003	.035	4.6	341.
10-20 GEV/C	4	FLAGO	ISIS2	.936	.045	.0	.003	.016	2.5	314.
10-20 GEV/C	4	FLAGO	ISIS3	.955	.006	.019	.003	.016	3.1	312.
20-40 GEV/C	4	FLAGO	ISIS1	.881	.027	.002	.0	.090	9.3	445.
20-40 GEV/C	4	FLAGO	ISIS2	.937	.023	.005	.002	.034	3.9	444.
20-40 GEV/C	4	FLAGO	ISIS3	.905	.012	.045	.005	.033	5.5	423.
40-80 GEV/C	4	FLAGO	ISIS1	.811	.027	.036	.009	.117	14.0	445.
40-80 GEV/C	4	FLAGO	ISIS2	.918	.024	.0	.006	.052	6.0	462.
40-80 GEV/C	4	FLAGO	ISIS3	.841	.057	.038	.0	.064	8.8	422.

Table VIe: Track resolution characteristics for all particles entering ISIS from 6 prong events.

MOMENTUM	PRONGS			0-9	1-30	3-50	5-70	70-	AVE	SAMPLE
5-10 GEV/C	6	FLAG1	ISIS1	.689	.149	.049	.024	.090	13.8	636.
5-10 GEV/C	6	FLAG1	ISIS2	.327	.119	.068	.083	.403	49.0	636.
5-10 GEV/C	6	FLAG1	ISIS3	.347	.121	.132	.204	.195	37.1	636.
10-20 GEV/C	6	FLAG1	ISIS1	.810	.096	.007	.006	.081	9.9	678.
10-20 GEV/C	6	FLAG1	ISIS2	.726	.150	.028	.010	.086	12.4	678.
10-20 GEV/C	6	FLAG1	ISIS3	.786	.086	.043	.040	.046	11.4	678.
20-40 GEV/C	6	FLAG1	ISIS1	.724	.088	.017	.017	.153	18.2	804.
20-40 GEV/C	6	FLAG1	ISIS2	.786	.095	.016	.009	.095	12.1	804.
20-40 GEV/C	6	FLAG1	ISIS3	.784	.058	.044	.026	.088	14.0	804.
40-80 GEV/C	6	FLAG1	ISIS1	.681	.093	.011	.039	.176	21.4	664.
40-80 GEV/C	6	FLAG1	ISIS2	.803	.060	.008	.008	.122	14.1	664.
40-80 GEV/C	6	FLAG1	ISIS3	.748	.071	.038	.024	.119	16.4	664.

Table VIf: Track resolution characteristics for all particles from 6 prong events which traverse the entire length of ISIS.

MOMENTUM	PRONGS			0-9	1-30	3-50	5-70	70-	AVE	SAMPLE
5-10 GEV/C	6	FLAGO	ISIS1	.775	.143	.013	.011	.058	8.9	552.
5-10 GEV/C	6	FLAGO	ISIS2	.804	.160	.012	.0	.024	6.0	250.
5-10 GEV/C	6	FLAGO	ISIS3	.844	.074	.053	.016	.012	7.1	244.
10-20 GEV/C	6	FLAGO	ISIS1	.817	.095	.006	.006	.077	9.5	666.
10-20 GEV/C	6	FLAGO	ISIS2	.808	.128	.010	.002	.052	7.8	600.
10-20 GEV/C	6	FLAGO	ISIS3	.875	.039	.027	.010	.049	8.4	590.
20-40 GEV/C	6	FLAGO	ISIS1	.728	.089	.018	.013	.152	17.9	768.
20-40 GEV/C	6	FLAGO	ISIS2	.795	.093	.015	.008	.089	11.5	776.
20-40 GEV/C	6	FLAGO	ISIS3	.800	.055	.038	.018	.089	13.3	740.
40-80 GEV/C	6	FLAGO	ISIS1	.686	.092	.011	.034	.176	21.2	609.
40-80 GEV/C	6	FLAGO	ISIS2	.814	.061	.008	.006	.111	13.0	622.
40-80 GEV/C	6	FLAGO	ISIS3	.771	.065	.042	.018	.104	14.7	567.

Table VIg: Track resolution characteristics for all particles entering ISIS from 8 prong events.

MOMENTUM	PRONGS			0-9	1-30	3-50	5-70	70-	AVE	SAMPLE
5-10 GEV/C	8	FLAG1	ISIS1	.609	.222	.050	.030	.088	15.6	724.
5-10 GEV/C	8	FLAG1	ISIS2	.291	.141	.068	.086	.414	49.6	724.
5-10 GEV/C	8	FLAG1	ISIS3	.298	.156	.134	.214	.198	38.0	724.
10-20 GEV/C	8	FLAG1	ISIS1	.665	.184	.017	.027	.106	15.6	744.
10-20 GEV/C	8	FLAG1	ISIS2	.617	.192	.056	.042	.093	17.1	744.
10-20 GEV/C	8	FLAG1	ISIS3	.660	.144	.079	.048	.069	16.4	744.
20-40 GEV/C	8	FLAG1	ISIS1	.669	.134	.021	.021	.156	19.5	718.
20-40 GEV/C	8	FLAG1	ISIS2	.773	.103	.014	.011	.099	13.0	718.
20-40 GEV/C	8	FLAG1	ISIS3	.749	.085	.052	.014	.100	15.0	718.
40-80 GEV/C	8	FLAG1	ISIS1	.641	.099	.019	.021	.220	25.0	618.
40-80 GEV/C	8	FLAG1	ISIS2	.702	.131	.015	.015	.138	17.2	618.
40-80 GEV/C	8	FLAG1	ISIS3	.694	.094	.045	.023	.144	19.7	618.

Table V Ih: Track resolution characteristics for all particles from8 prong events which traverse the entire length of ISIS.

MOMENTUM	PRONGS			0-9	1-30	3-50	5-70	70-	AVE	SAMPLE
5-10 GEV/C	8	FLAGO	ISIS1	.667	.234	.025	.012	.062	11.6	645.
5-10 GEV/C	8	FLAGO	ISIS2	.737	.212	.014	.0	.036	8.5	278.
5-10 GEV/C	8	FLAGO	ISIS3	.754	.147	.048	.018	.033	10.0	272.
10-20 GEV/C	8	FLAGO	ISIS1	.669	.186	.017	.023	.105	15.2	726.
10-20 GEV/C	8	FLAGO	ISIS2	.715	.200	.017	.013	.055	10.7	631.
10-20 GEV/C	8	FLAGO	ISIS3	.765	.110	.047	.016	.062	12.2	616.
20-40 GEV/C	8	FLAGO	ISIS1	.672	.136	.021	.018	.154	19.2	676.
20-40 GEV/C	8	FLAGO	ISIS2	.790	.100	.010	.009	.091	12.0	690.
20-40 GEV/C	8	FLAGO	ISIS3	.770	.080	.052	.008	.089	13.7	649.
40-80 GEV/C	8	FLAGO	ISIS1	.643	.096	.017	.019	.224	25.2	572.
40-80 GEV/C	8	FLAGO	ISIS2	.704	.136	.012	.014	.134	16.9	582.
40-80 GEV/C	8	FLAGO	ISIS3	.694	.097	.045	.022	.142	19.5	536.

Table VIi: Track resolution characteristics for all particles entering ISIS from 10 prong events.

MOMENTUM	PRONGS			0-9	1-30	3-50	5-70	70-	AVE	SAMPLE
5-10 GEV/C	10	FLAG1	ISIS1	.520	.311	.053	.029	.086	17.2	546.
5-10 GEV/C	10	FLAG1	ISIS2	.245	.136	.095	.066	.458	53.7	546.
5-10 GEV/C	10	FLAG1	ISIS3	.256	.163	.130	.205	.245	41.3	546.
10-20 GEV/C	10	FLAG1	ISIS1	.640	.215	.022	.018	.105	15.8	503.
10-20 GEV/C	10	FLAG1	ISIS2	.590	.207	.032	.046	.125	19.5	503.
10-20 GEV/C	10	FLAG1	ISIS3	.638	.133	.087	.064	.078	18.1	503.
20-40 GEV/C	10	FLAG1	ISIS1	.567	.213	.029	.011	.179	22.8	441.
20-40 GEV/C	10	FLAG1	ISIS2	.712	.145	.016	.018	.109	15.2	441.
20-40 GEV/C	10	FLAG1	ISIS3	.692	.120	.057	.020	.111	17.6	441.
40-80 GEV/C	10	FLAG1	ISIS1	.611	.114	.024	.041	.211	25.9	370.
40-80 GEV/C	10	FLAG1	ISIS2	.649	.168	.011	.032	.141	19.3	370.
40-80 GEV/C	10	FLAG1	ISIS3	.659	.111	.054	.035	.141	21.4	370.

Table VIj: Track resolution characteristics for all particles from 10 prong events which traverse the entire length of ISIS.

MOMENTUM	PRONGS			0-9	1-30	3-50	5-70	70-	AVE	SAMPLE
5-10 GEV/C	10	FLAGO	ISIS1	.586	.320	.027	.010	.056	12.6	481.
5-10 GEV/C	10	FLAGO	ISIS2	.672	.255	.026	.010	.036	10.0	192.
5-10 GEV/C	10	FLAGO	ISIS3	.686	.218	.048	.021	.027	10.9	188.
10-20 GEV/C	10	FLAGO	ISIS1	.640	.219	.022	.018	.101	15.6	494.
10-20 GEV/C	10	FLAGO	ISIS2	.689	.217	.012	.012	.071	12.0	424.
10-20 GEV/C	10	FLAGO	ISIS3	.740	.130	.050	.022	.058	12.8	416.
20-40 GEV/C	10	FLAGO	ISIS1	.569	.217	.027	.012	.176	22.5	415.
20-40 GEV/C	10	FLAGO	ISIS2	.729	.146	.012	.012	.101	14.0	425.
20-40 GEV/C	10	FLAGO	ISIS3	.715	.120	.050	.015	.100	16.1	400.
40-80 GEV/C	10	FLAGO	ISIS1	.616	.116	.023	.035	.209	25.5	344.
40-80 GEV/C	10	FLAGO	ISIS2	.662	.172	.006	.032	.128	18.1	343.
40-80 GEV/C	10	FLAGO	ISIS3	.682	.104	.053	.025	.135	20.2	318.

Table VIk: Track resolution characteristics for all particles entering ISIS from 12 prong events.

MOMENTUM	PRONGS			0-9	1-30	3-50	5-70	70-	AVE	SAMPLE
5-10 GEV/C	12	FLAG1	ISIS1	.363	.398	.066	.019	.154	24.3	259.
5-10 GEV/C	12	FLAG1	ISIS2	.208	.100	.077	.085	.529	61.0	259.
5-10 GEV/C	12	FLAG1	ISIS3	.189	.131	.151	.174	.355	48.5	259.
10-20 GEV/C	12	FLAG1	ISIS1	.498	.322	.021	.026	.133	20.9	233.
10-20 GEV/C	12	FLAG1	ISIS2	.545	.240	.043	.030	.142	21.4	233.
10-20 GEV/C	12	FLAG1	ISIS3	.541	.215	.086	.069	.090	21.1	233.
20-40 GEV/C	12	FLAG1	ISIS1	.503	.219	.022	.016	.240	29.8	183.
20-40 GEV/C	12	FLAG1	ISIS2	.639	.148	.044	.011	.158	21.2	183.
20-40 GEV/C	12	FLAG1	ISIS3	.596	.131	.077	.044	.153	23.9	183.
40-80 GEV/C	12	FLAG1	ISIS1	.535	.232	.035	.007	.190	24.6	142.
40-80 GEV/C	12	FLAG1	ISIS2	.676	.204	.028	.007	.085	13.9	142.
40-80 GEV/C	12	FLAG1	ISIS3	.627	.162	.085	.049	.077	17.3	142.

Table VII: Track resolution chacteristics for all particles from 12 prong events which traverse the entire length of ISIS.

MOMENTUM	PRONGS			0-9	1-30	3-50	5-70	70-	AVE	SAMPLE
5-10 GEV/C	12	FLAGO	ISIS1	.423	.445	.032	.005	.095	17.8	220.
5-10 GEV/C	12	FLAGO	ISIS2	.712	.219	.014	.0	.055	10.3	73.
5-10 GEV/C	12	FLAGO	ISIS3	.644	.247	.055	.0	.055	12.8	73.
10-20 GEV/C	12	FLAGO	ISIS1	.500	.327	.018	.022	.133	20.7	226.
10-20 GEV/C	12	FLAGO	ISIS2	.628	.250	.026	.010	.087	14.9	196.
10-20 GEV/C	12	FLAGO	ISIS3	.621	.205	.068	.016	.089	17.2	190.
20-40 GEV/C	12	FLAGO	ISIS1	.489	.227	.023	.017	.244	30.4	176.
20-40 GEV/C	12	FLAGO	ISIS2	.638	.147	.045	.011	.158	21.3	177.
20-40 GEV/C	12	FLAGO	ISIS3	.582	.135	.082	.035	.165	24.8	170.
40-80 GEV/C	12	FLAGO	ISIS1	.531	.231	.038	.008	.192	25.1	130.
40-80 GEV/C	12	FLAGO	ISIS2	.684	.203	.023	.008	.083	13.4	133.
40-80 GEV/C	12	FLAGO	ISIS3	.620	.174	.099	.025	.083	17.2	121.

Table VIn: Track resolution characteristics for all particles with momentum between 5 and 80 Gev/c which traverse the entire length of ISIS.

MOMENTUM	PRONGS			0-9	1-30	3-50	5-70	70-	AVE	SAMPLE
5-80 GEV/C	ALL	FLAGO	ISIS1	.689	.156	.019	.015	.121	16.1	10253.
5-80 GEV/C	ALL	FLAGO	ISIS2	.769	.132	.012	.009	.077	11.1	8628.
5-80 GEV/C	ALL	FLAGO	ISIS3	.769	.093	.047	.015	.076	12.8	8222.
5-80 GEV/C	4	FLAGO	ISIS1	.871	.034	.014	.007	.075	8.8	1500.
5-80 GEV/C	4	FLAGO	ISIS2	.930	.030	.003	.004	.032	4.1	1360.
5-80 GEV/C	4	FLAGO	ISIS3	.898	.029	.035	.002	.035	5.7	1296.
5-80 GEV/C	6	FLAGO	ISIS1	.751	.103	.012	.016	.118	14.6	2595.
5-80 GEV/C	6	FLAGO	ISIS2	.805	.101	.012	.005	.078	10.3	2248.
5-80 GEV/C	6	FLAGO	ISIS3	.818	.056	.038	.015	.073	11.6	2141.
5-80 GEV/C	8	FLAGO	ISIS1	.664	.165	.020	.018	.133	17.5	2619.
5-80 GEV/C	8	FLAGO	ISIS2	.739	.153	.013	.010	.085	12.5	2181.
5-80 GEV/C	8	FLAGO	ISIS3	.747	.102	.048	.015	.087	14.3	2073.
5-80 GEV/C	10	FLAGO	ISIS1	.603	.226	.025	.018	.128	18.4	1734.
5-80 GEV/C	10	FLAGO	ISIS2	.692	.189	.012	.017	.090	13.8	1384.
5-80 GEV/C	10	FLAGO	ISIS3	.711	.133	.051	.020	.085	15.3	1322.
5-80 GEV/C	12	FLAGO	ISIS1	.480	.322	.027	.013	.158	22.9	752.
5-80 GEV/C	12	FLAGO	ISIS2	.655	.204	.029	.009	.104	15.9	579.
5-80 GEV/C	12	FLAGO	ISIS3	.612	.182	.078	.022	.106	19.0	554.

Table VIm: Track resolution characteristics for all particles entering ISIS with momentum between 5 and 80 Gev/c.

MOMENTUM	PRONGS			0-9	1-30	3-50	5-70	70-	AVE	SAMPLE
5-80 GEV/C	ALL	FLAG1	ISIS1	.669	.155	.027	.021	.128	17.3	10983.
5-80 GEV/C	ALL	FLAG1	ISIS2	.624	.126	.035	.034	.181	23.2	10983.
5-80 GEV/C	ALL	FLAG1	ISIS3	.623	.108	.075	.073	.121	21.1	10983.
5-80 GEV/C	4	FLAG1	ISIS1	.855	.041	.018	.011	.075	9.4	1601.
5-80 GEV/C	4	FLAG1	ISIS2	.823	.037	.019	.020	.101	12.4	1601.
5-80 GEV/C	4	FLAG1	ISIS3	.795	.047	.052	.049	.056	11.3	1601.
5-80 GEV/C	6	FLAG1	ISIS1	.726	.105	.020	.021	.127	15.9	2782.
5-80 GEV/C	6	FLAG1	ISIS2	.670	.106	.029	.026	.169	21.1	2782.
5-80 GEV/C	6	FLAG1	ISIS3	.676	.082	.062	.070	.110	19.2	2782.
5-80 GEV/C	8	FLAG1	ISIS1	.646	.162	.027	.025	.139	18.6	2804.
5-80 GEV/C	8	FLAG1	ISIS2	.592	.143	.039	.039	.187	24.5	2804.
5-80 GEV/C	8	FLAG1	ISIS3	.597	.121	.079	.077	.127	22.4	2804.
5-80 GEV/C	10	FLAG1	ISIS1	.582	.223	.033	.024	.138	19.9	1860.
5-80 GEV/C	10	FLAG1	ISIS2	.530	.163	.042	.042	.222	28.5	1860.
5-80 GEV/C	10	FLAG1	ISIS3	.543	.134	.086	.089	.147	25.5	1860.
5-80 GEV/C	12	FLAG1	ISIS1	.463	.307	.038	.018	.174	24.6	817.
5-80 GEV/C	12	FLAG1	ISIS2	.482	.169	.051	.039	.258	32.6	817.
5-80 GEV/C	12	FLAG1	ISIS3	.457	.160	.104	.093	.186	29.8	817.

Table VIIa-n: The following tables give as a function of momentum and primary multiplicity for ISIS-1, ISIS-2, and the full ISIS (ISIS-3) the fraction of particles with a given percentage of their track clearly resolvable from other tracks in the event and the simulated background. The table also gives the average percentage of the track which is lost due to overlap or to exiting from the sides of ISIS. The total number of particles used to calculate any particular set of data in the table is also given.

Table VIIa: Track resolution characteristics for all particles entering ISIS.

MOMENTUM	PRONGS			0-9	1-30	3-50	5-70	70-	AVE	SAMPLE
5-10 GEV/C	ALL	FLAG1	ISIS1	.333	.277	.149	.094	.148	29.8	2747.
5-10 GEV/C	ALL	FLAG1	ISIS2	.169	.153	.119	.106	.454	57.1	2747.
5-10 GEV/C	ALL	FLAG1	ISIS3	.146	.180	.175	.194	.305	47.7	2747.
10-20 GEV/C	ALL	FLAG1	ISIS1	.433	.252	.097	.069	.150	26.5	2795.
10-20 GEV/C	ALL	FLAG1	ISIS2	.391	.262	.145	.077	.126	27.0	2795.
10-20 GEV/C	ALL	FLAG1	ISIS3	.359	.278	.180	.096	.087	26.7	2795.
20-40 GEV/C	ALL	FLAG1	ISIS1	.449	.201	.094	.055	.201	30.1	2903.
20-40 GEV/C	ALL	FLAG1	ISIS2	.493	.223	.105	.055	.124	23.5	2903.
20-40 GEV/C	ALL	FLAG1	ISIS3	.421	.257	.152	.058	.112	25.6	2903.
40-80 GEV/C	ALL	FLAG1	ISIS1	.437	.204	.077	.054	.229	32.1	2538.
40-80 GEV/C	ALL	FLAG1	ISIS2	.507	.214	.080	.043	.155	24.9	2538.
40-80 GEV/C	ALL	FLAG1	ISIS3	.411	.267	.127	.050	.145	27.1	2538.

Table VIIb: Track resolution characteristics for all particles which traverse the entire length of ISIS.

MOMENTUM	PRONGS			0-9	1-30	3-50	5-70	70-	AVE	SAMPLE
5-10 GEV/C	ALL	FLAG0	ISIS1	.373	.295	.135	.081	.115	26.0	2417.
5-10 GEV/C	ALL	FLAG0	ISIS2	.425	.320	.147	.058	.050	20.3	1049.
5-10 GEV/C	ALL	FLAG0	ISIS3	.370	.321	.199	.072	.038	22.1	1030.
10-20 GEV/C	ALL	FLAG0	ISIS1	.434	.252	.097	.069	.148	26.4	2743.
10-20 GEV/C	ALL	FLAG0	ISIS2	.446	.280	.139	.053	.082	21.8	2411.
10-20 GEV/C	ALL	FLAG0	ISIS3	.409	.292	.168	.063	.068	23.1	2368.
20-40 GEV/C	ALL	FLAG0	ISIS1	.447	.199	.096	.055	.203	30.3	2760.
20-40 GEV/C	ALL	FLAG0	ISIS2	.502	.222	.106	.053	.116	22.7	2788.
20-40 GEV/C	ALL	FLAG0	ISIS3	.427	.259	.154	.054	.105	24.9	2647.
40-80 GEV/C	ALL	FLAG0	ISIS1	.433	.201	.079	.051	.235	32.7	2333.
40-80 GEV/C	ALL	FLAG0	ISIS2	.510	.218	.081	.044	.146	24.3	2380.
40-80 GEV/C	ALL	FLAG0	ISIS3	.413	.267	.131	.049	.139	26.9	2177.

Table VIIc: Track resolution characteristics for all particles entering ISIS from 4 prong events.

MOMENTUM	PRONGS			0-9	1-30	3-50	5-70	70-	AVE	SAMPLE
5-10 GEV/C	4	FLAG1	ISIS1	.461	.216	.131	.088	.105	24.1	306.
5-10 GEV/C	4	FLAG1	ISIS2	.268	.170	.111	.088	.363	47.5	306.
5-10 GEV/C	4	FLAG1	ISIS3	.222	.212	.160	.186	.219	39.5	306.
10-20 GEV/C	4	FLAG1	ISIS1	.538	.224	.070	.058	.110	20.2	344.
10-20 GEV/C	4	FLAG1	ISIS2	.544	.198	.142	.061	.055	18.6	344.
10-20 GEV/C	4	FLAG1	ISIS3	.480	.244	.183	.052	.041	19.0	344.
20-40 GEV/C	4	FLAG1	ISIS1	.592	.159	.062	.045	.142	21.8	466.
20-40 GEV/C	4	FLAG1	ISIS2	.607	.185	.107	.041	.060	16.0	466.
20-40 GEV/C	4	FLAG1	ISIS3	.545	.236	.116	.047	.056	17.8	466.
40-80 GEV/C	4	FLAG1	ISIS1	.563	.151	.087	.039	.151	23.6	485.
40-80 GEV/C	4	FLAG1	ISIS2	.612	.177	.085	.033	.093	17.7	485.
40-80 GEV/C	4	FLAG1	ISIS3	.507	.262	.115	.033	.082	19.5	485.

Table VIId: Track resolution characteristics for all particles from 4 prong events which traverse the entire length of ISIS.

MOMENTUM	PRONGS			0-9	1-30	3-50	5-70	70-	AVE	SAMPLE
5-10 GEV/C	4	FLAGO	ISIS1	.520	.212	.112	.074	.082	20.5	269.
5-10 GEV/C	4	FLAGO	ISIS2	.557	.293	.093	.036	.021	13.5	140.
5-10 GEV/C	4	FLAGO	ISIS3	.460	.309	.180	.043	.007	15.5	139.
10-20 GEV/C	4	FLAGO	ISIS1	.537	.223	.070	.059	.111	20.3	341.
10-20 GEV/C	4	FLAGO	ISIS2	.583	.210	.137	.045	.025	14.8	314.
10-20 GEV/C	4	FLAGO	ISIS3	.513	.250	.186	.029	.022	16.4	312.
20-40 GEV/C	4	FLAGO	ISIS1	.587	.155	.065	.045	.148	22.4	445.
20-40 GEV/C	4	FLAGO	ISIS2	.613	.180	.110	.041	.056	15.5	444.
20-40 GEV/C	4	FLAGO	ISIS3	.544	.236	.121	.047	.052	17.6	423.
40-80 GEV/C	4	FLAGO	ISIS1	.551	.157	.090	.038	.164	25.0	445.
40-80 GEV/C	4	FLAGO	ISIS2	.617	.180	.082	.032	.089	17.2	462.
40-80 GEV/C	4	FLAGO	ISIS3	.495	.263	.126	.033	.083	20.0	422.

Table VIIe: Track resolution characteristics for all particles entering ISIS from 6 prong events.

MOMENTUM	PRONGS			0-9	1-30	3-50	5-70	70-	AVE	SAMPLE
5-10 GEV/C	6	FLAG1	ISIS1	.388	.244	.145	.086	.137	27.7	636.
5-10 GEV/C	6	FLAG1	ISIS2	.200	.154	.105	.105	.436	55.5	636.
5-10 GEV/C	6	FLAG1	ISIS3	.176	.178	.170	.187	.289	46.0	636.
10-20 GEV/C	6	FLAG1	ISIS1	.468	.237	.114	.063	.118	23.3	678.
10-20 GEV/C	6	FLAG1	ISIS2	.435	.251	.137	.066	.111	24.6	678.
10-20 GEV/C	6	FLAG1	ISIS3	.403	.291	.149	.090	.068	24.0	678.
20-40 GEV/C	6	FLAG1	ISIS1	.476	.195	.091	.055	.183	28.4	804.
20-40 GEV/C	6	FLAG1	ISIS2	.527	.215	.095	.047	.116	21.8	804.
20-40 GEV/C	6	FLAG1	ISIS3	.461	.251	.141	.037	.109	23.8	804.
40-80 GEV/C	6	FLAG1	ISIS1	.423	.211	.066	.075	.224	32.7	664.
40-80 GEV/C	6	FLAG1	ISIS2	.532	.202	.071	.032	.164	24.6	664.
40-80 GEV/C	6	FLAG1	ISIS3	.434	.244	.114	.056	.152	27.1	664.

Table VIIf: Track resolution characteristics for all particles from 6 prong events which traverse the entire length of ISIS.

MOMENTUM	PRONGS			0-9	1-30	3-50	5-70	70-	AVE	SAMPLE
5-10 GEV/C	6	FLAGO	ISIS1	.440	.257	.121	.076	.105	23.6	552.
5-10 GEV/C	6	FLAGO	ISIS2	.496	.284	.128	.052	.040	18.1	250.
5-10 GEV/C	6	FLAGO	ISIS3	.430	.303	.172	.066	.029	20.1	244.
10-20 GEV/C	6	FLAGO	ISIS1	.471	.237	.114	.063	.114	23.0	666.
10-20 GEV/C	6	FLAGO	ISIS2	.483	.255	.130	.057	.075	20.6	600.
10-20 GEV/C	6	FLAGO	ISIS3	.449	.288	.144	.056	.063	21.4	590.
20-40 GEV/C	6	FLAGO	ISIS1	.477	.193	.095	.052	.184	28.4	768.
20-40 GEV/C	6	FLAGO	ISIS2	.536	.211	.097	.045	.111	21.2	776.
20-40 GEV/C	6	FLAGO	ISIS3	.470	.251	.139	.035	.104	23.2	740.
40-80 GEV/C	6	FLAGO	ISIS1	.422	.209	.067	.074	.228	33.1	609.
40-80 GEV/C	6	FLAGO	ISIS2	.527	.212	.074	.032	.154	24.0	622.
40-80 GEV/C	6	FLAGO	ISIS3	.437	.247	.123	.056	.136	26.3	567.

Table VIIg: Track resolution characteristics for all particles entering ISIS from 8 prong events.

MOMENTUM	PRONGS			0-9	1-30	3-50	5-70	70-	AVE	SAMPLE
5-10 GEV/C	8	FLAG1	ISIS1	.359	.265	.145	.087	.144	28.7	724.
5-10 GEV/C	8	FLAG1	ISIS2	.162	.166	.104	.122	.448	56.7	724.
5-10 GEV/C	8	FLAG1	ISIS3	.144	.191	.180	.200	.286	47.2	724.
10-20 GEV/C	8	FLAG1	ISIS1	.415	.259	.090	.065	.171	28.2	744.
10-20 GEV/C	8	FLAG1	ISIS2	.355	.277	.160	.085	.124	28.2	744.
10-20 GEV/C	8	FLAG1	ISIS3	.320	.304	.187	.094	.095	28.0	744.
20-40 GEV/C	8	FLAG1	ISIS1	.425	.194	.102	.064	.216	32.0	718.
20-40 GEV/C	8	FLAG1	ISIS2	.471	.230	.096	.063	.141	25.6	718.
20-40 GEV/C	8	FLAG1	ISIS3	.387	.259	.164	.067	.123	27.6	718.
40-80 GEV/C	8	FLAG1	ISIS1	.427	.207	.066	.036	.264	33.9	618.
40-80 GEV/C	8	FLAG1	ISIS2	.463	.220	.092	.049	.176	27.6	618.
40-80 GEV/C	8	FLAG1	ISIS3	.401	.252	.129	.049	.168	29.5	618.

Table VIIh: Track resolution characteristics for all particles from 8 prong events which traverse the entire length of ISIS.

MOMENTUM	PRONGS			0-9	1-30	3-50	5-70	70-	AVE	SAMPLE
5-10 GEV/C	8	FLAGO	ISIS1	.397	.285	.132	.076	.110	25.1	645.
5-10 GEV/C	8	FLAGO	ISIS2	.406	.338	.129	.065	.061	21.6	278.
5-10 GEV/C	8	FLAGO	ISIS3	.371	.342	.162	.066	.059	22.7	272.
10-20 GEV/C	8	FLAGO	ISIS1	.416	.260	.091	.063	.169	28.1	726.
10-20 GEV/C	8	FLAGO	ISIS2	.410	.304	.147	.055	.082	22.8	631.
10-20 GEV/C	8	FLAGO	ISIS3	.373	.318	.164	.068	.076	24.5	616.
20-40 GEV/C	8	FLAGO	ISIS1	.422	.195	.102	.065	.216	32.2	676.
20-40 GEV/C	8	FLAGO	ISIS2	.480	.230	.096	.061	.133	24.7	690.
20-40 GEV/C	8	FLAGO	ISIS3	.393	.265	.169	.060	.112	26.6	649.
40-80 GEV/C	8	FLAGO	ISIS1	.427	.203	.068	.033	.269	34.4	572.
40-80 GEV/C	8	FLAGO	ISIS2	.462	.223	.091	.050	.174	27.4	582.
40-80 GEV/C	8	FLAGO	ISIS3	.399	.252	.131	.050	.168	29.7	536.

Table VIIi: Track resolution characteristics for all particles entering ISIS from 10 prong events.

MOMENTUM	PRONGS			0-9	1-30	3-50	5-70	70-	AVE	SAMPLE
5-10 GEV/C	10	FLAG1	ISIS1	.269	.333	.150	.099	.148	31.0	546.
5-10 GEV/C	10	FLAG1	ISIS2	.137	.141	.136	.097	.489	60.0	546.
5-10 GEV/C	10	FLAG1	ISIS3	.119	.170	.168	.214	.328	50.1	546.
10-20 GEV/C	10	FLAG1	ISIS1	.392	.270	.097	.078	.163	28.8	503.
10-20 GEV/C	10	FLAG1	ISIS2	.342	.286	.131	.072	.169	30.5	503.
10-20 GEV/C	10	FLAG1	ISIS3	.324	.260	.197	.109	.109	29.8	503.
20-40 GEV/C	10	FLAG1	ISIS1	.340	.256	.122	.050	.231	34.5	441.
20-40 GEV/C	10	FLAG1	ISIS2	.408	.245	.141	.059	.147	27.4	441.
20-40 GEV/C	10	FLAG1	ISIS3	.336	.286	.175	.075	.129	29.6	441.
40-80 GEV/C	10	FLAG1	ISIS1	.346	.232	.081	.070	.270	37.7	370.
40-80 GEV/C	10	FLAG1	ISIS2	.435	.249	.065	.068	.184	29.5	370.
40-80 GEV/C	10	FLAG1	ISIS3	.316	.303	.141	.062	.178	32.1	370.

Table VIIj: Track resolution characteristics for all particle s from 10 prong events which traverse the entire length of ISIS.

MOMENTUM	PRONGS			0-9	1-30	3-50	5-70	70-	AVE	SAMPLE
5-10 GEV/C	10	FLAGO	ISIS1	.301	.360	.137	.079	.123	27.4	481.
5-10 GEV/C	10	FLAGO	ISIS2	.365	.344	.182	.057	.052	22.1	192.
5-10 GEV/C	10	FLAGO	ISIS3	.319	.330	.213	.101	.037	24.6	188.
10-20 GEV/C	10	FLAGO	ISIS1	.391	.273	.097	.079	.160	28.6	494.
10-20 GEV/C	10	FLAGO	ISIS2	.399	.316	.130	.040	.116	24.3	424.
10-20 GEV/C	10	FLAGO	ISIS3	.377	.291	.188	.065	.079	25.2	416.
20-40 GEV/C	10	FLAGO	ISIS1	.347	.248	.123	.051	.231	34.6	415.
20-40 GEV/C	10	FLAGO	ISIS2	.416	.247	.141	.056	.139	26.6	425.
20-40 GEV/C	10	FLAGO	ISIS3	.350	.280	.175	.075	.120	28.7	400.
40-80 GEV/C	10	FLAGO	ISIS1	.346	.238	.081	.064	.270	37.4	344.
40-80 GEV/C	10	FLAGO	ISIS2	.449	.245	.067	.073	.166	28.4	343.
40-80 GEV/C	10	FLAGO	ISIS3	.324	.308	.142	.060	.167	31.0	318.

Table VIIk Track resolution characteristics for all particles entering ISIS from 12 prong events.

MOMENTUM	PRONGS			0-9	1-30	3-50	5-70	70-	AVE	SAMPLE
5-10 GEV/C	12	FLAG1	ISIS1	.189	.305	.178	.093	.236	38.9	259.
5-10 GEV/C	12	FLAG1	ISIS2	.131	.085	.131	.085	.568	66.5	259.
5-10 GEV/C	12	FLAG1	ISIS3	.081	.147	.162	.162	.448	57.1	259.
10-20 GEV/C	12	FLAG1	ISIS1	.305	.330	.086	.099	.180	32.9	233.
10-20 GEV/C	12	FLAG1	ISIS2	.313	.253	.163	.086	.185	33.1	233.
10-20 GEV/C	12	FLAG1	ISIS3	.283	.266	.176	.150	.124	32.9	233.
20-40 GEV/C	12	FLAG1	ISIS1	.333	.240	.060	.055	.311	40.6	183.
20-40 GEV/C	12	FLAG1	ISIS2	.388	.257	.109	.071	.175	30.7	183.
20-40 GEV/C	12	FLAG1	ISIS3	.317	.251	.164	.082	.186	33.9	183.
40-80 GEV/C	12	FLAG1	ISIS1	.366	.275	.113	.028	.218	32.2	142.
40-80 GEV/C	12	FLAG1	ISIS2	.458	.282	.099	.056	.106	22.6	142.
40-80 GEV/C	12	FLAG1	ISIS3	.352	.324	.169	.063	.092	25.6	142.

Table VIII: Track resolution characteristics for all particles from 12 prong events which traverse the entire length of ISIS.

MOMENTUM	PRONGS			0-9	1-30	3-50	5-70	70-	AVE	SAMPLE
5-10 GEV/C	12	FLAGO	ISIS1	.218	.350	.182	.082	.168	33.6	220.
5-10 GEV/C	12	FLAGO	ISIS2	.466	.260	.151	.055	.068	22.1	73.
5-10 GEV/C	12	FLAGO	ISIS3	.288	.370	.233	.055	.055	25.1	73.
10-20 GEV/C	12	FLAGO	ISIS1	.310	.327	.088	.097	.177	32.6	226.
10-20 GEV/C	12	FLAGO	ISIS2	.362	.265	.179	.061	.133	28.0	196.
10-20 GEV/C	12	FLAGO	ISIS3	.316	.295	.163	.121	.105	29.7	190.
20-40 GEV/C	12	FLAGO	ISIS1	.324	.239	.063	.057	.318	41.4	176.
20-40 GEV/C	12	FLAGO	ISIS2	.390	.260	.107	.068	.175	30.6	177.
20-40 GEV/C	12	FLAGO	ISIS3	.318	.241	.176	.076	.188	34.3	170.
40-80 GEV/C	12	FLAGO	ISIS1	.354	.277	.115	.031	.223	33.0	130.
40-80 GEV/C	12	FLAGO	ISIS2	.459	.293	.098	.053	.098	21.8	133.
40-80 GEV/C	12	FLAGO	ISIS3	.355	.322	.182	.050	.091	25.4	121.

Table VIIm: Track resolution characteristics for all particles entering ISIS with momentum between 5 and 80 Gev/c.

MOMENTUM	PRONGS			0-9	1-30	3-50	5-70	70-	AVE	SAMPLE
5-80 GEV/C	ALL	FLAG1	ISIS1	.413	.234	.104	.068	.181	29.6	10983.
5-80 GEV/C	ALL	FLAG1	ISIS2	.389	.213	.113	.071	.214	33.1	10983.
5-80 GEV/C	ALL	FLAG1	ISIS3	.334	.245	.159	.100	.161	31.8	10983.
5-80 GEV/C	4	FLAG1	ISIS1	.547	.184	.084	.054	.131	22.4	1601.
5-80 GEV/C	4	FLAG1	ISIS2	.530	.182	.109	.052	.127	23.1	1601.
5-80 GEV/C	4	FLAG1	ISIS3	.458	.241	.139	.071	.092	22.7	1601.
5-80 GEV/C	6	FLAG1	ISIS1	.441	.220	.103	.069	.166	28.0	2782.
5-80 GEV/C	6	FLAG1	ISIS2	.431	.207	.102	.061	.199	30.8	2782.
5-80 GEV/C	6	FLAG1	ISIS3	.375	.242	.143	.089	.151	29.7	2782.
5-80 GEV/C	8	FLAG1	ISIS1	.406	.233	.102	.064	.196	30.6	2804.
5-80 GEV/C	8	FLAG1	ISIS2	.358	.224	.114	.081	.223	34.7	2804.
5-80 GEV/C	8	FLAG1	ISIS3	.310	.252	.167	.104	.168	33.2	2804.
5-80 GEV/C	10	FLAG1	ISIS1	.334	.278	.116	.076	.196	32.6	1860.
5-80 GEV/C	10	FLAG1	ISIS2	.316	.226	.122	.075	.261	38.2	1860.
5-80 GEV/C	10	FLAG1	ISIS3	.265	.248	.172	.123	.192	36.1	1860.
5-80 GEV/C	12	FLAG1	ISIS1	.285	.293	.114	.075	.234	36.4	817.
5-80 GEV/C	12	FLAG1	ISIS2	.297	.206	.130	.077	.290	41.3	817.
5-80 GEV/C	12	FLAG1	ISIS3	.239	.235	.168	.124	.235	39.5	817.

Table VIIn: Track resolution characteristics for all particles with momentum between 5 and 80 Gev/c which traverse the entire length of ISIS.

MOMENTUM	PRONGS			0-9	1-30	3-50	5-70	70-	AVE	SAMPLE
5-80 GEV/C	ALL	FLAGO	ISIS1	.423	.237	.102	.064	.175	28.8	10253.
5-80 GEV/C	ALL	FLAGO	ISIS2	.479	.249	.113	.051	.107	22.6	8628.
5-80 GEV/C	ALL	FLAGO	ISIS3	.411	.279	.158	.058	.095	24.6	8222.
5-80 GEV/C	4	FLAGO	ISIS1	.553	.181	.082	.051	.133	22.3	1500.
5-80 GEV/C	4	FLAGO	ISIS2	.601	.199	.105	.038	.057	15.7	1360.
5-80 GEV/C	4	FLAGO	ISIS3	.512	.256	.144	.038	.050	17.8	1296.
5-80 GEV/C	6	FLAGO	ISIS1	.455	.222	.099	.065	.160	27.1	2595.
5-80 GEV/C	6	FLAGO	ISIS2	.515	.231	.103	.045	.105	21.5	2248.
5-80 GEV/C	6	FLAGO	ISIS3	.451	.266	.140	.050	.092	23.2	2141.
5-80 GEV/C	8	FLAGO	ISIS1	.415	.237	.099	.060	.189	29.8	2619.
5-80 GEV/C	8	FLAGO	ISIS2	.446	.264	.114	.057	.120	24.5	2181.
5-80 GEV/C	8	FLAGO	ISIS3	.386	.288	.157	.061	.109	26.3	2073.
5-80 GEV/C	10	FLAGO	ISIS1	.347	.284	.111	.069	.189	31.4	1734.
5-80 GEV/C	10	FLAGO	ISIS2	.412	.281	.125	.056	.126	25.7	1384.
5-80 GEV/C	10	FLAGO	ISIS3	.348	.297	.176	.072	.107	27.5	1322.
5-80 GEV/C	12	FLAGO	ISIS1	.294	.305	.114	.072	.215	35.0	752.
5-80 GEV/C	12	FLAGO	ISIS2	.406	.269	.135	.060	.130	26.6	579.
5-80 GEV/C	12	FLAGO	ISIS3	.321	.294	.181	.083	.121	29.6	554.

Table VIII. Comparison of the track overlap characteristics of the full ISIS for 0.5cm and for 1.0cm spacial resolution. The table gives, as a function of momentum, the percentage of all tracks which traverse the entire length of ISIS with at least 90% of the track clear and the percentage of tracks with between 70 and 90% of the track clear. Also given are the average percentage clear for tracks at a given momentum and also the number of tracks in the test sample.

Minimum Track Resolution Distance	Momentum	% of Track Clear		Avg.% Clear	Sample Size
		90-100%	70-90%		
1.0cm	$5<p<10$	75.8	15.0	90.9	1030
	$10<p<20$	80.2	8.9	89.5	2368
	$20<p<40$	77.3	7.7	86.5	2647
	$40<p<80$	73.5	8.9	83.9	2177
0.5cm	$5<p<10$	88.8	7.7	95.2	1030
	$10<p<20$	90.4	4.1	94.5	2368
	$20<p<40$	87.5	4.2	92.8	2647
	$40<p<80$	86.4	3.1	90.8	2177

Table IX. Comparison of the track overlap characteristics of the full ISIS for the signal wires from the two signal wire planes connected as described in the text. The table gives, as a function of momemtum, the percentage of all tracks which traverse the entire length of ISIS with at least 90% of the track clear and the percentage of tracks with between 70 and 90% of the track clear. Also given are the average percentage clear for tracks at a given momentum and also the number of tracks in the test sample.

Description of Wire Connections	Momentum	% of track clear		Avg.% Clear	Sample Size
		90-100%	70-90%		
all signal wires separate	5-10	75.8	15.0	90.9	1030
	10-20	80.2	8.9	89.5	2368
	20-40	77.3	7.7	86.5	2647
	40-80	73.5	8.9	83.9	2177
signal wires connected as described in the text for test 1	5-10	37.2	39.9	80.4	1032
	10-20	43.5	31.7	79.1	2368
	20-40	39.5	26.4	73.9	2650
	40-80	33.5	24.9	68.8	2181
signal wires connected as described in the text for test 2	5-10	35.9	41.9	80.3	1030
	10-20	39.4	37.1	79.1	2368
	20-40	37.1	30.6	74.0	2647
	40-80	35.3	24.6	69.6	2177

FNAL Experimental
Proposal 393 (revised)
Spokesman: Irwin A. Pless

HIGH STATISTICS STUDY OF π^0 PRODUCTION IN 150 GeV/c π^- - p INTERACTIONS

Brown University: M. Heller, A. M. Shapiro, M. Widgoff
Illinois Institute of Technology: R. A. Burnstein, C. Fu, M. Nazaretz, H. A. Rubin
University of Illinois: J. W. Cooper, R. Plumer, R. D. Sard, J. Tortora
Indiana University: E. D. Alyea, Jr.
Johns Hopkins University: L. Bachman, C.-Y. Chien, P. Lucas, L. Madansky, A. Pevsner, R. A. Zdanis
Massachusetts Institute of Technology: J. Bober, J. E. Brau, T. Frank, J. Grunhaus, E. S. Hafen, R. I. Hulsizer, U. Karshon, V. Kistiakowsky, P. A. Miller, A. Napier, I. A. Pless, J. P. Silverman, J. Wolfson, R. K. Yamamoto
University of Padova/University of Rome*: S. Centro, G. Ciapetti*, M. DeGiorgi, D. Pascoli, L. Ventura, D. Zanello*, L. Zanello*
Rutgers University/Stevens Institute*/SUNY**, Albany: E. B. Brucker*, P. F. Jacques, M. D. Jones*, E. L. Koller*, T. C. Ou, R. J. Plano, P. Stamer*, C. Sun**, S. Taylor*, T. L. Watts
University of Tennessee/Oak Ridge National Laboratory*: J. Barwick, W. M. Bugg, H. O. Cohn*, G. Condo, T. Handler, E. Hart, R. D. McCulloch*
Yale University/Fermilab*: D. Bogert*, M. Johnson*, G. Koizumi*, H. Kraybill, D. Ljung, T. Ludlam, J. Mayersohn, H. Taft

20 January 1976 (revised)

SUMMARY

We propose a high statistics study of two, four, six, and eight charged particle final state channels in which a single forward going π^0 is also produced in 150 GeV/c $\pi^- p$ interactions. We will also perform high statistics studies of the four, six, and eight charged particle channels without neutrals and inclusive studies of π^0 production as a function of rapidity. We will also study the forward going electromagnetic energy associated with the two-charged prong topology in 150 GeV/c $\pi^- p$ interactions. We believe that there is evidence of a new phenomenon associated with these photons based on previous data (E-154) which cannot be explained on the basis of known reactions with known particles. We propose adding a gamma ray detector behind the last PWC plane in the Fermilab 30" hybrid system. This gamma ray detector should have an energy resolution $\frac{\Delta E}{E} < 1\%$ and a spatial resolution of less than $\pm$ 3mm. We request 10^6 frames taken in the 30" hybrid system with an incident π^- beam of 150 GeV/c. In this exposure there will be $\sim$ 9000 two prong events with electromagnetic energy greater than 20 GeV of which 3000 will be the events associated with the new phenomenon. The precise information on the photons should allow us to determine what is the character of the beam diffraction reaction and whether or not it represents a new phenomenon. This part of the experiment will be performed first and a quick answer should be possible.

Introduction

The purposes of this experiment are twofold: 1) a high statistics study of π^0 production and 2) a study of the forward going neutral energy associated with the two charged particle topology, both in $\pi^- p$ interactions at 150 GeV/c. We propose a change in the experiment discussed in the original version of this proposal (submitted 14 May 1975), replacing operation with a triggered bubble chamber light flash to untriggered operation in which the events of interest are selected in off-line analysis of the forward going neutrals. We still request 10^6 expansions of the 30-inch hybrid system but now replace our original estimate of $\sim 10^5$ pictures with a request for 10^6 pictures. A scan for tagged two charged-particle events would be done first and permit an expeditious elucidation of the second topic listed above.

High Statistics Study

Based on our previous experience in experiment 154 ($\pi^- p$ at 147 GeV/c), we believe that it is possible to use a slightly higher incident flux and therefore request 10^6 pictures with ten tracks per picture of $\pi^- p$ interactions at 150 GeV/c. Table I gives an estimate of the number of events we expect for the various topologies based on our E-154 results. It is seen that this experiment also would permit high statistics studies of the channels in which no neutral particles were produced for the four, six, and eight charged prong topologies.

The primary purpose of this proposed experiment is a study of channels in which one or more π^0's is produced. In order to accomplish this we propose to add to the proportional wire hybrid bubble chamber system a lead glass hodoscope downstream of the last proportional wire chamber that will have a resolution $\frac{\Delta E}{E} \sim 1\%$ and a spatial resolution less than $\pm$ 3mm. It is expected that the prototype device associated with E-299 (see E-299 agreement and other plans - attached) will suffice and, hence, that we will have suitable equipment for this experiment as soon as the test run with E-299 is completed (spring 1976). We should be able to reconstruct π^0 and η^0 mesons and should be able to distinguish up to six gamma rays ($3\pi^0$). Thus, we would be able to perform a study of the two, four, six, and eight charged prong topologies where one π^0 is observed allowing four constraint (4C) fits. These are channels of which there have not been previous studies. This experiment together with E-154 also would permit high statistics studies of the four, six, and eight charged prong topologies with no neutral particles and comparison with the corresponding channels with π^0 mesons should prove extremely fruitful. For example, our E-154 study of the four charged-particle 4C sample has shown that more than 92% of the cross section is due to beam and target diffraction dissociation. $\rho^0\pi^-$ events make an important contribution to the beam dissociation cross section in the A_1 and A_2 mass region and there is some evidence for a contribution from $f^0\pi^-$. Higher statistics should permit a resolution of the latter question as well as yielding a better understanding of the three-pion system in all invariant mass regions. It would obviously be of great interest to obtain results for the four charged prong, one π^0 channel at a similar level of statistics.

This experiment will also permit an inclusive study of π^0 production as a function of rapidity. Such a study is extremely important in order to verify the previous evidence for the existence of clusters and to determine whether they consist mainly of two pions ("ρ" like) or three pions ("ω" like). Light would also be shed on the question of transverse momentum conservation along the rapidity axis. In particular, the question of local transverse momentum conservation could be answered, whereas with charged-particle rapidity studies only, this is virtually impossible.

Two Charged Prong Events with Forward π^0 Mesons

Another facet of this experiment is the examination of the forward going neutral energy associated with the production of two charged particles. From experiment 154 we have 376 two-prong inelastic events with an identified proton which we find can be classified into three distinct groups. One group is beam fragmentation, and a second, target fragmentation. The third group is not easily categorized and consists of events shown in figure 1. We had in our PWC system for E-154 a crude gamma ray detector consisting of a two-radiation thick piece of lead followed by three PWC planes. By counting the number of wires that fired in these chambers, we can get a crude idea of the intensity of the electromagnetic energy incident on the lead converter. We have arbitrarily defined a scale ranging from 0-6 where 0 indicates no fired wires and 6 indicates more than 100 fired wires. In the beam fragmentation region, there is essentially always some electromagnetic energy incident on the lead converter with the vast majority of the events having intensity six. In the target fragmentation region, there is almost no electromagnetic energy incident on the lead converter with the vast majority of the events having intensity zero. In the third region, half the events have an electromagnetic intensity zero and the other half have electromagnetic intensity six. This is shown in figure 2.

This in itself is interesting but not unexpected. However, when we look at the beam fragmentation events in detail, within our limited statistics (212 events), we find rather unexpected distributions. The first is that for the P_{lab} of the π^-. Although the statistics are poor, there is an accumulation of events with P_{lab} of the π^- at 110 GeV/c. There is another accumulation at 40 GeV/c and another at 10 GeV/c. This is shown in figure 3. For comparison, figure 4 shows the π^- laboratory distribution for all events. In this distribution, a high momentum peak which includes the leading particle signal (target fragmentation) is clearly visible.

A second unexpected feature is the energy distribution of the missing neutrals (beam fragments) which pass through our gamma detector. This distribution has accumulations at 140 GeV/c and 100 GeV/c. This, of course, is the reflection of the π^- distribution and conservation of energy. This distribution is shown in figure 5.

The physics questions we would like to answer are: What is the composition of the neutral energy shown in figure 5? Does the accumulation at 140 GeV/c consist of a single π^0 or several π^0's? What are the invariant mass distributions between the neutral π^0 or π^0's and the π^-?

We have investigated the possibility that the phenomena we see result from a known reaction, such as A^- production. If this were the case, given that the A^- is an I spin 1 particle and that it decays into two I spin 1 particles, we would expect to have similar behavior in the four-prong sample containing an identified proton. In particular, the events in the beam fragmentation region of the four prongs, the π^+ plays the same role as the π^- in the two-prong sample. Figure 6 shows the distribution of this π^+. As can be seen, this distribution (within the statistics) is quite different from the π^- distribution (fig. 3), particularly in the high energy region.

We believe that the above comments indicate a new phenomenon is occurring in the two-prong events and that a detailed study of this phenomenon is called for. We have tried many Monte Carlo calculations to simulate a final state that might explain our data. These include:

1) $\pi^- + p \rightarrow$ "A^-" $+ P$

$\quad\quad\quad\quad \hookrightarrow$ "ρ^-" $+ \pi^0$

$\quad\quad\quad\quad\quad \hookrightarrow \pi^- + \pi^0$

2) $\pi^- + p \rightarrow$ "A^-" $+ p$

"f^0" $+ \pi^-$

$\pi^0\pi^0$

To match the data with reaction 1), one requires "A^-" with widths less than 100 MeV, "ρ^-" with widths less than 10 MeV and angular distributions like $\cos^6\theta$. We have not found parameters that allow us to match the data with reaction 2). Hence, we believe one has to study in detail the electromagnetic energy associated with the two-prong events.

We would use the information from the photon detector to identify those frames in which there was an event with at least 20 GeV of photon energy. These frames would be scanned for two prongs, and we estimate that we will find 9000 two prongs for an exposure of 10^6 frames at ten tracks per frame. Approximately one third of these will be beam fragmentation events. Hence, the data reduction part of this experiment is quite modest and since the scan of preselected frames for two prongs would have the first priority, we should be able to perform this part of the experiment in a short time.

The gamma ray data will allow us to determine π^0 four vectors and form relevant invariant mass distributions. If there is narrow structure in this final state, we will be able to detect it. In any event, we will be able to determine the character of this final state in an exclusive manner and determine if there are any new physical phenomena involved.

Scope of the Experiment

This experiment will be accomplished by use of the Fermilab 30-inch bubble chamber hybrid system with the addition of a gamma ray detector behind the last PWC plane. A total of 10^6 pictures of π^-p interactions at 150 GeV/c is requested. The film will first be scanned for two-prong events associated with at least 20 GeV of forward going electromagnetic energy and the measurement and analysis of the $\sim$9000 events expected could be completed quickly. Then the film will be scanned for all events associated with forward going electromagnetic energy and for all four, six, and eight-prong events. This scanning and the measurement of the events will be carried out by the groups forming the Proportional Hybrid System Consortium (PHSC). If necessary, the number of groups involved in the experiment could be expanded to permit a more rapid reduction of the data.

Table I

Number of Events for 10^6 Pictures with Ten Incident π^- Mesons Per Picture for $\pi^- p$ Interactions at 150 GeV/c

Number of Charged Particles	Number of Events
2	55,000
elastic	35,000
inelastic	20,000
4	46,000
4C	6,300
6	52,000
4C	1,600
8	49,000
≥ 10	75,000
All events	280,000 (11.6 events/μb)

FIGURE CAPTIONS

Figure 1: Scatter plot of the laboratory momentum of the π^- versus the center of mass value of the Feynman x parameter for the proton. The sample is all the inelastic two-prong (π^-, p) events. Shown are our definition of beam fragmentation and target fragmentation regions. Also indicated is the definition of Region III.

Figure 2: For each of the three regions shown in figure 1, we have estimated the electromagnetic intensity seen in the forward direction. The detecting device was two radiation lengths of lead followed by proportional wire planes. The intensity was estimated by the number of struck wires. Bin 0 implies no struck wires and bin 6 implies more than 100 fired wires. As might be expected, in the beam fragmentation region there is relatively more electromagnetic energy seen downstream than for the target fragmentation region.

Figure 3: π^- laboratory momentum for the beam fragmentation region.

Figure 4: π^- laboratory momentum for the whole two-prong inelastic (π^-, p) sample.

Figure 5: For the beam fragmentation region we calculated the missing mass four vector. If this four vector was aimed towards our gamma ray detector, we computed the energy of the missing mass and entered it into this histogram.

Figure 6: The data for this histogram comes from the four-charged prong sample with an identified proton. We made the same cut on the proton as for the two-charged prong sample and then plotted the laboratory momentum of the π^+. Note the events in this sample may or may not have associated missing neutrals.

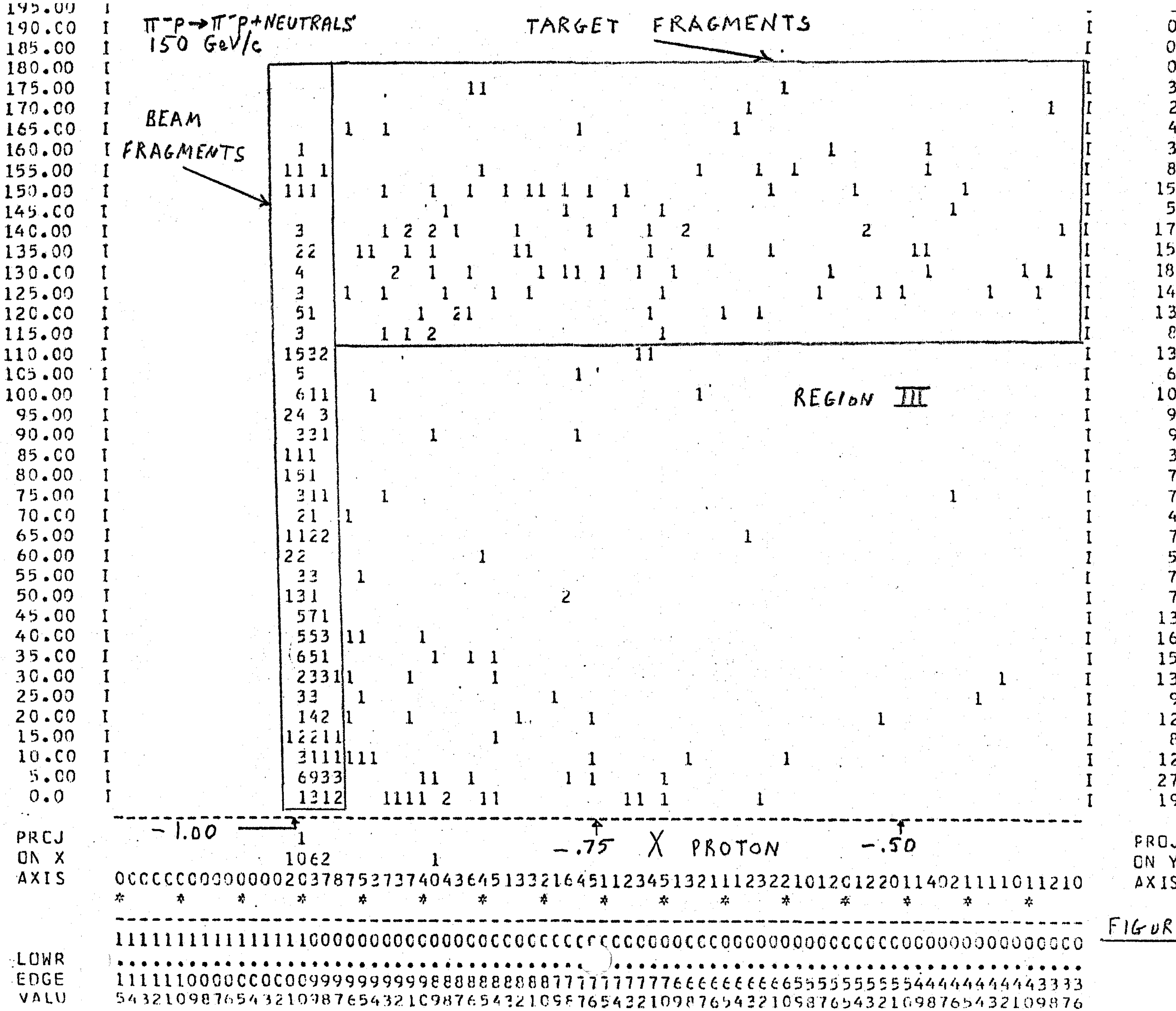
P_{LAB} π^-
$\pi^- p \to \pi^- p$ + NEUTRALS
150 GeV/c
TARGET FRAGMENTS
BEAM FRAGMENTS
REGION III
−1.00
−.75
−.50
X PROTON
PROJ ON X AXIS
PROJ ON Y AXIS
LOWR EDGE VALU

FIGURE 1

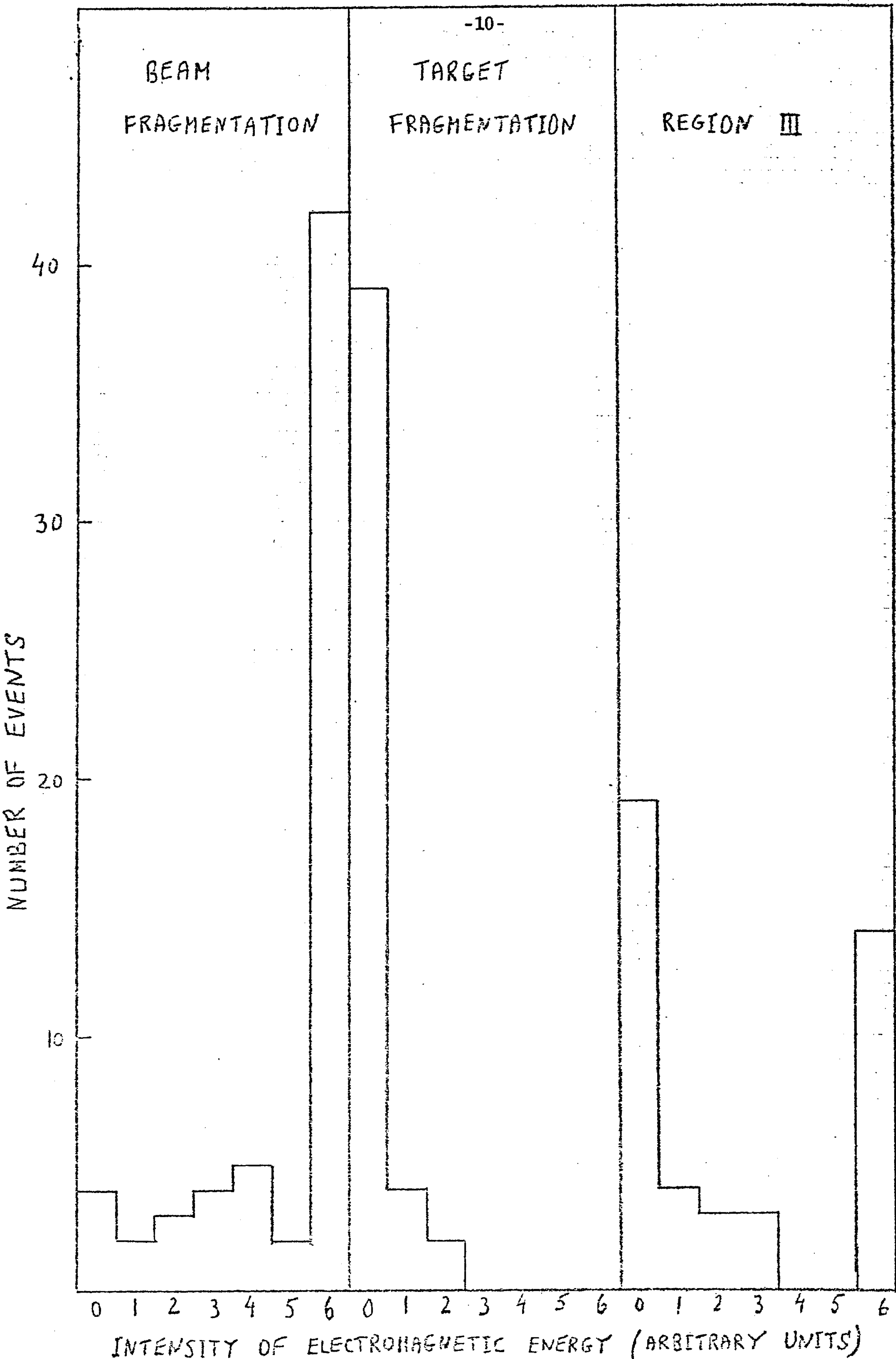

BEAM FRAGMENTATION
TARGET FRAGMENTATION
REGION III
NUMBER OF EVENTS
40
30
20
10
0 1 2 3 4 5 6 0 1 2 3 4 5 6 0 1 2 3 4 5 6
INTENSITY OF ELECTROMAGNETIC ENERGY (ARBITRARY UNITS)

FIGURE 2

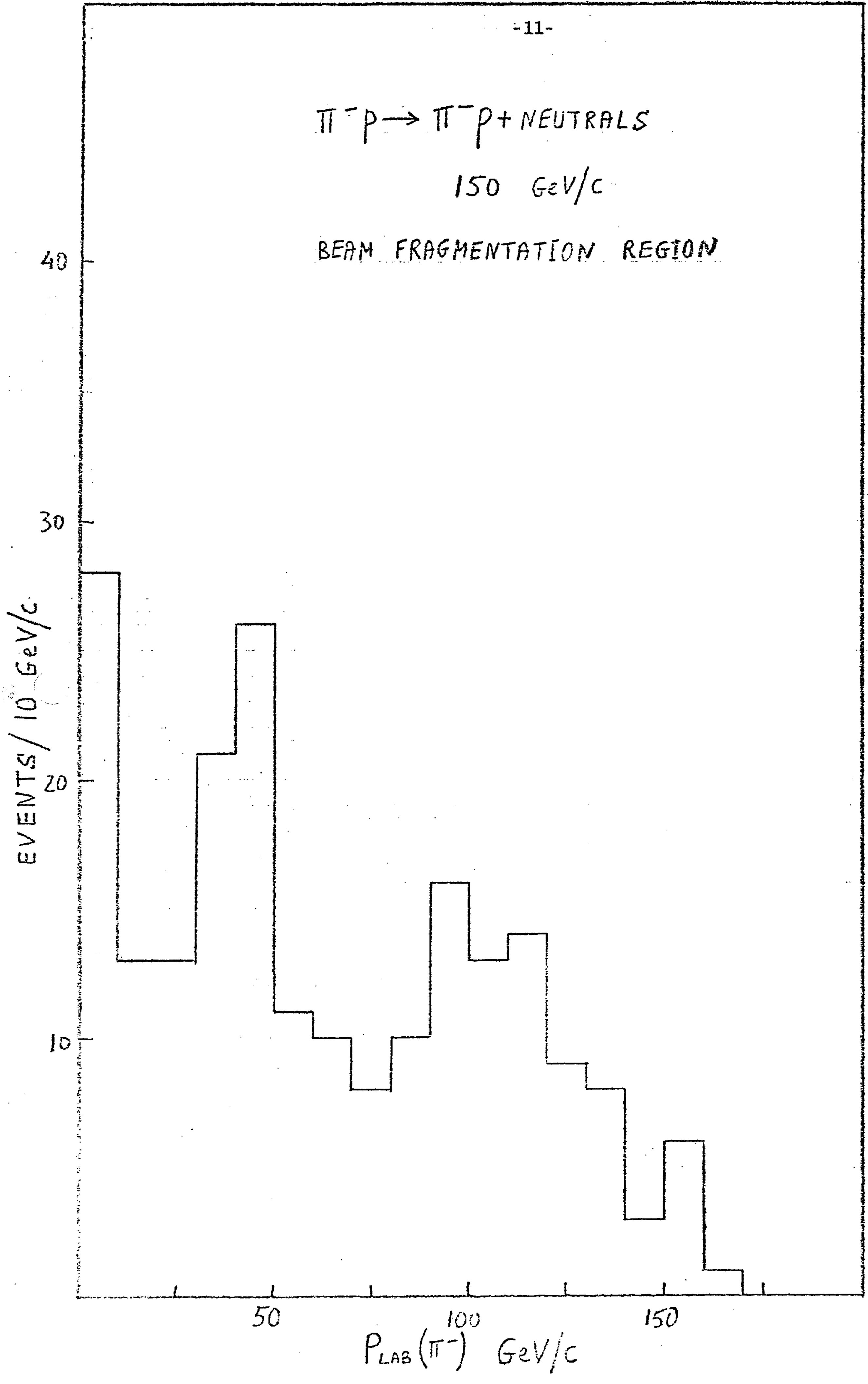
π⁻p → π⁻p + NEUTRALS
150 GeV/c
BEAM FRAGMENTATION REGION
40
30
20
10
EVENTS / 10 GeV/c
50
100
150
$P_{LAB}(\pi^-)$ GeV/c

FIGURE 3

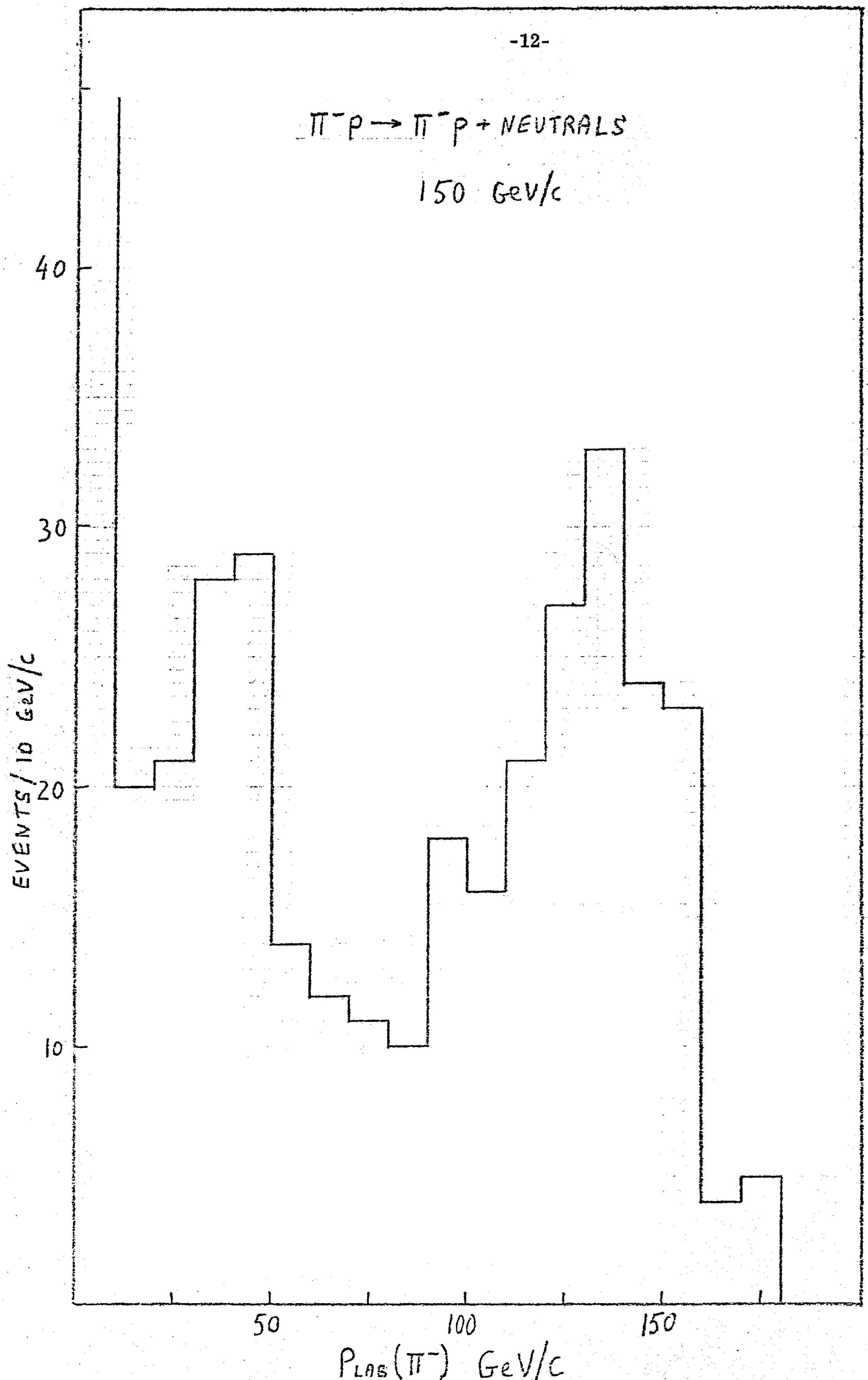
$\pi^- p \rightarrow \pi^- p$ + NEUTRALS
150 GeV/c
EVENTS / 10 GeV/c
40
30
20
10
50
100
150
$P_{LAB}(\pi^-)$ GeV/c

FIGURE 4

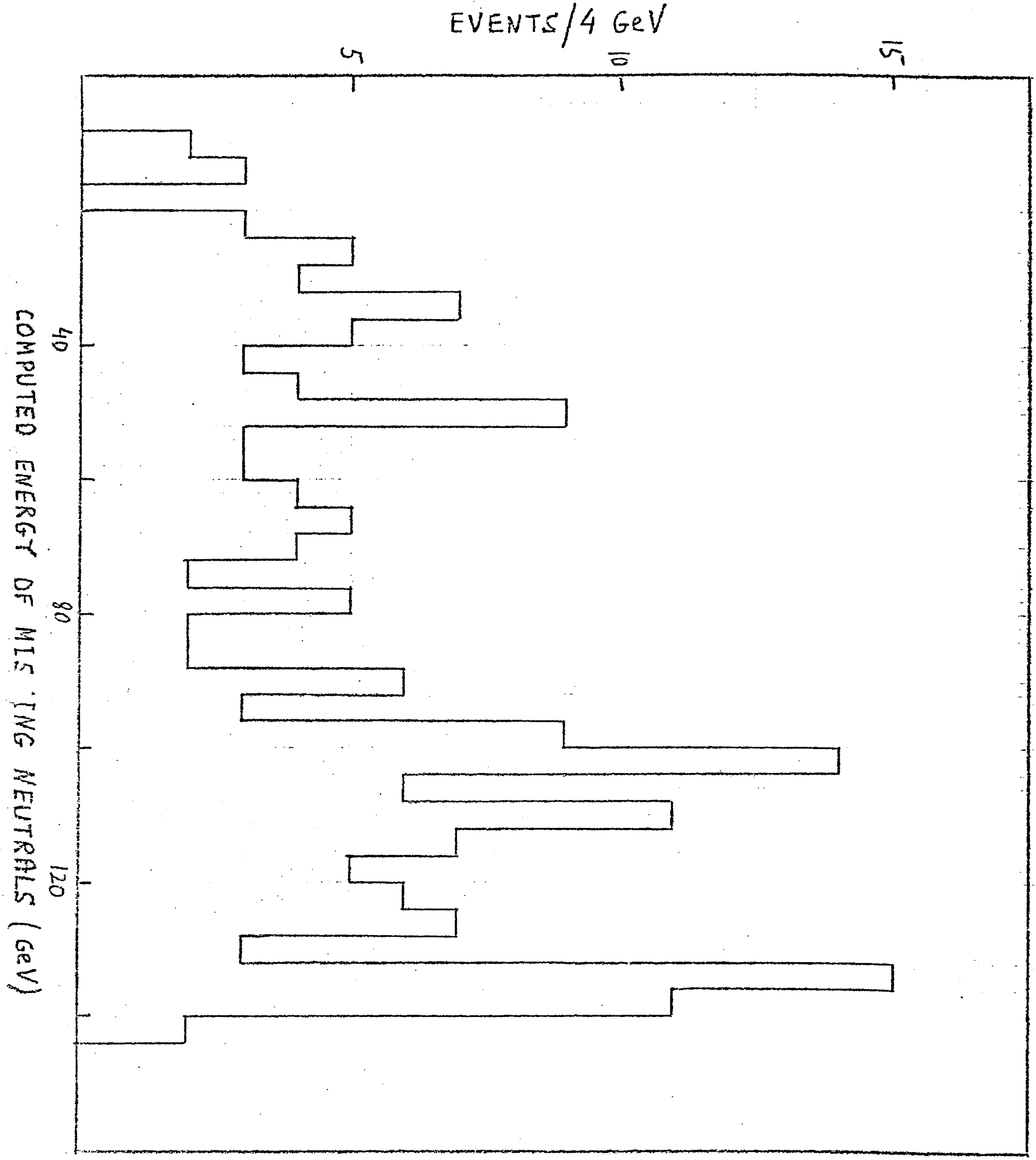
EVENTS/4 GeV
5
10
15
40
80
120
COMPUTED ENERGY OF MIS'ING NEUTRALS (GeV)

FIGURE 5

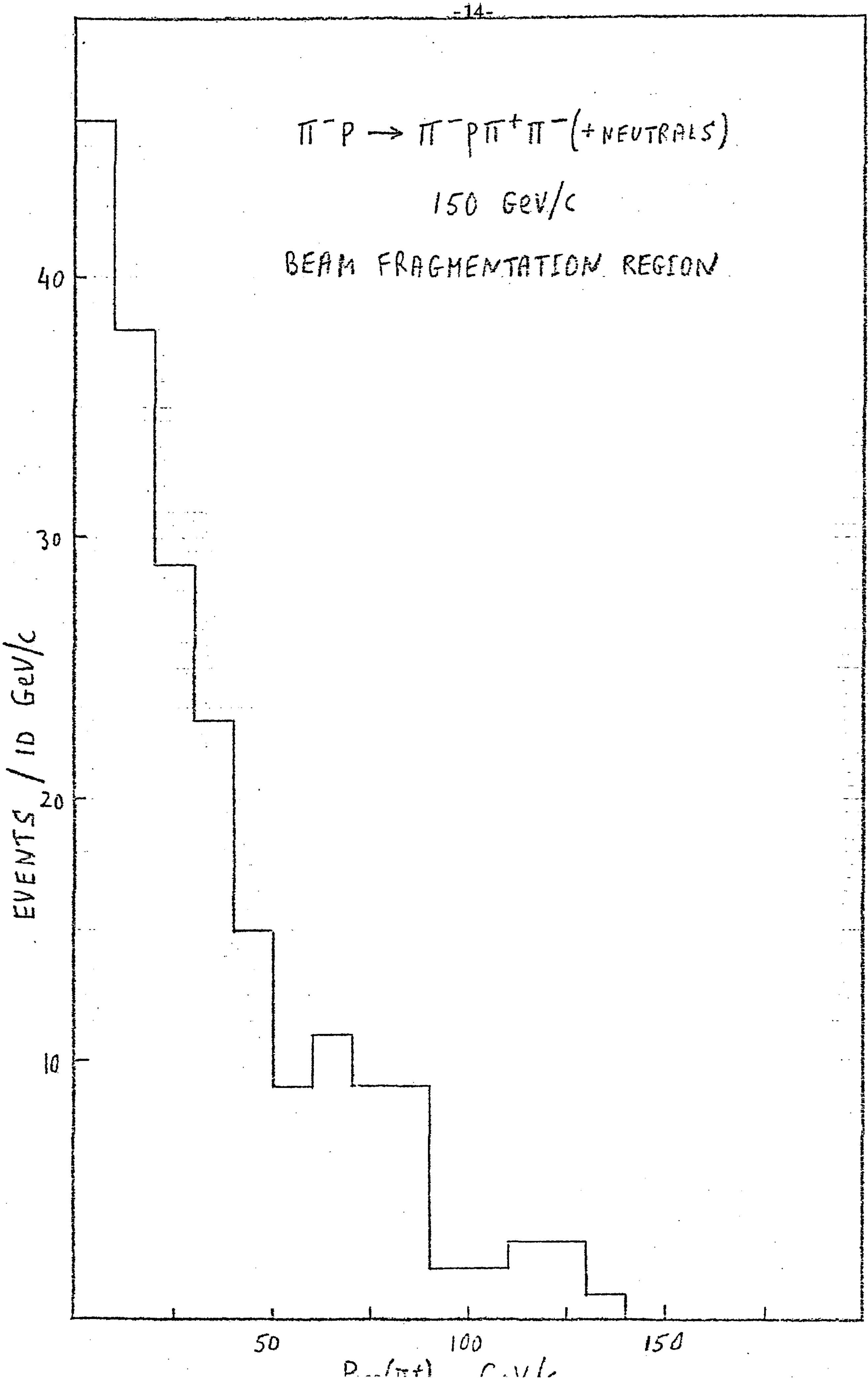

$\pi^- p \to \pi^- p \pi^+ \pi^-$ (+NEUTRALS)
150 GeV/c
BEAM FRAGMENTATION REGION
EVENTS / 10 GeV/c
40
30
20
10
50
100
150

FIGURE 6

This is an Agreement between Fermi National Accelerator Laboratory and the experimenters of Proposal No. 299. This document contains an enumeration of the major items needed for the proper execution of Experiment No. 299 as expressed in the proposal for the experiment and subsequent correspondence. A one page summary describing the current research objectives of this experiment as expressed by the experimenters is given in Appendix I.

A. Personnel

1. The experimenters committed to this experiment are:

D.G. Fong, M. Heller, A. Janos, A.M. Shapiro, M. Widgoff, Brown University; J.W. Cooper, R. Plumer, R.D. Sard, A.E. Snyder, J. Tortora, University of Illinois; R.A. Burnstein, C. Fu, H.A. Rubin, Illinois Institute of Technology; E.D. Alyea, Indiana University; L. Bachman, C.-Y. Chien, P. Lucas, L. Madansky, A. Pevsner, R.A. Zdanis, Johns Hopkins University; J.E. Brau, J. Grunhaus, E.S. Hafen, R.I. Hulsizer, U. Karshon, V. Kistiakowsky, P.A. Miller, A. Napier, I.A. Pless, P.C. Trepagnier, J. Wolfson, R.K. Yamamoto, Massachusetts Institute of Technology; S. Centro, G. Ciapetti, M. De Giorgi, D. Pascoli, L. Ventura, D. Zanello, Padova/Rome; E.B. Brucker, P.F. Jacques, M.D. Jones, E.L. Koller, T.C. Ou, R.J. Plano, C. Sun, S. Taylor, T.L. Watts, Rutgers University/Stevens Institute/SUNY, Albany; J. Barwick, W. Bugg, H. Cohn, G. Condo, T. Handler, E. Hart, R.D. McCulloch, University of Tennessee/Oak Ridge; D. Bogert, M. Johnson, H. Kraybill, D. Ljung, T. Ludlam, H. Taft, Yale University/Fermilab.

2. In addition, the university groups expect to involve three other physicists, six engineers, three draftsmen, and twelve technicians during various phases of the experiment. In addition, the universities will supply at least two full-time people stationed at Fermilab during the testing and installation period of the drift chambers and gamma ray detectors at Fermilab.

3. R.K. Yamamoto was chosen to be Project Manager to direct all aspects of the design, construction, installation, testing, and initial operation of the drift chamber and gamma ray detector.

4. The scientific spokesman for this Experiment is I.A. Pless.

5. The presently assigned Fermilab liaison physicist is L. Voyvodic

B. Equipment and Beam:

1. The instrumentation and experiment will be done using the N3 beam to the 30-inch hybrid bubble chamber facility located in the neutrino area.

2. The beam will be equipped with appropriate quadrupoles, bending magnets, collimators, and with additional instrumentation as described herein.

3. Fermilab will provide:

a. The secondary beam and beam enclosures	----
b. Instrumentation for tuning and controlling the beam, including Čerenkov counters	(30.0K)
c. The 30-inch Fermilab bubble chamber with manpower for bubble chamber operation and beam line technicians. It is understood that the experimenters will assist in these efforts.	----

d.	The film and film processing will be provided by Fermilab. Test strip developing facilities will be available for use during the exposure.	
e.	Proportional wire planes with 2" radius active area	$(14.6K)
f.	Upstream system and interfaces	(23.3K)
g.	Cables, power supplies, etc.	(13.0K)
h.	Proportional wire planes with 6" radius active area for downstream system	(19.4K)
i.	Downstream systems and interfaces	(10.0K)
j.	Cables and power supplies for downstream system	(15.0K)
k.	Enclosure for detectors	(2.0K)
l.	Data tagging computer - existing PDP-11	(80.0K)
m.	The experimenters request the use of an existing computer in Lab A for debugging equipment. Cables and serial read-out equipment must be installed to Enclosure 114.	6.0K
n.	Space in bubble chamber high bay area for downstream detecting equipment	-
o.	Standard PREP electronics, CAMAC crate and modules (see Appendix II)	78.7K
	PREP equipment presently assigned to E154	(1.3K)
p.	Cables from bubble chamber high bay area to Laboratory A	(5.0K)
q.	Lead glass photo tubes - 48 pieces (existing)	(15.0K)
r.	Rigging	5.0K
s.	Fast turn around CDC 6600 time (50 hours)	-
	New Costs	$ 89.7K
	Existing Value	$(228.6K)
	Total	$ 318.3K

4. The University experimenters and Oak Ridge National Laboratory will provide:

a. Drift chamber with 1.2 meter diameter active area and read out system	40.0K
b. Lead glass gamma ray detector with .75 meter x .75 meter active area and read out system	80.0K
Total New Equipment	$120.0

5. The Fermilab Physics Department will provide:

a. Computing time on IBM 370/195 (10 hours)	3.5
b. Three (3) scanner/measurer-months on Film Analysis Facility with PDP-10. To be decided later.	---
c. Funds towards item 4. above	5.0K
Total Cost	8.5K

C. Funding

1. Fermilab funds are available in FY 76 and FY77 for items in Category B3. The Fermilab Neutrino Department budget codes for this experiment are ENU (operating) and EAH (equipment).

2. The budget codes of the university experimenters at Fermilab are ___ (operating) and ___ (equipment). The budget codes for the Fermilab experimenters through the Physics Department are ___ (operating) and ___ (equipment).

3. Each university will approach its funding agency (ERDA, NSF) for an incremental increase of at least $10K. This will provide a base of $90K or greater to fund this experiment. R.K. Yamamoto was chosen to be the treasurer to monitor the university funds. (ORNL will provide $30K to augment the university funds which will be spent mainly on item B. 4a).

D. Special Considerations:

1. It is recognized that the physics under investigation in Experiment #299 has been expressed in two phases. It is understood that Phase II of this investigation is contingent on completion of Phase I and on the approval of a separate proposal by Fermilab.

   a. Phase I - 600 x 10^3 pictures: (approved)

      i. 500 x 10^3 pictures with a mixture of π^+ and p. at 150 GeV/c (158 x 10^3 pictures already have been taken as of the signing of this document)

      ii. 100 x 10^3 pictures of π^- at 150 GeV/c

   b. Phase II - 600 x 10^3 pictures: (requiring a new proposal)

      1. 400 x 10^3 pictures with a mixture of π^+ and p at 150 GeV/c

      ii. 200 x 10^3 pictures of π^- at 150 GeV/c

2. As part of the ongoing program to improve the Fermilab 30-inch hybrid bubble chamber system, the experimenters will design, construct and bring into operation a large drift chamber and a gamma ray detector. These two devices will increase the acceptance of the hybrid system for charged particles and give information on the direction and energy of gamma rays. The experimenters will furnish the equipment described in the body of this document and when the devices are installed, documented and operational, they will be turned over to Fermilab to be operated as a part of the Fermilab bubble chamber spectrometer system.

3. Beam characteristics and bubble chamber operation.

   a. Beam will use the available filter to optimize the π^+/p ratio. This will nominally be 1/3 or greater.

   b. The nominal beam spill to the bubble chamber should be 100 microseconds or longer.

   c. The experimenters will be provided with 35 mm film. The bubble chamber will be operated in a multi-pulse mode during each accelerator cycle.

   d. The 30-inch magnet will be operated at approximately 25

   e. The film is the property of the Fermi National Accelerator Laboratory and is on loan to the experimenters for an eighteen (18) month period starting with the date of exposure. Following this period the film is to be returned to Fermilab for possible reassignment to other approved research groups unless an extension of the loan has been arranged.

   f. The picture count is to be determined by the frame counter. Reasonable care will be taken by the beam line technicians and bubble chamber crews to provide quality pictures.

4. Testing time

   a. Experimenters estimate that the installation of the gamma ray detector and drift chamber will take one month. On site testing of the system will require two months. A beam spill of 100 microseconds or longer required. Beam will be available on a parasitic basis only.

b. A short test run with 5,000 correlated bubble chamber pictures will be required to fully certify the installation.

5. The experimenters will provide all programs, magnetic tapes and consumable items for the on-line computer system.

6. Six (6) copies of all publications or preprints for work done at Fermilab will be sent by the Scientific Spokesman for this experiment to the Director of Fermilab.

E. Experimental Planning Milestones (tentative)

	Relative Time	Estimated Date
1. Construction of prototype lead glass hodoscope	t_o-10 mos.	1 Sept, 197
2. Beam testing of prototype lead glass system (requiring about 1 week of prime running in N3 hadron beam at 50 GeV)	t_o-9 mos.	1 Oct, 1975
3. Construction of prototype drift chamber	t_o-7 mos.	1 Dec, 1975
4. Test prototype drift chamber (requiring parasitic use of N3 hadron beam)	t_o-6 mos.	1 Jan, 1976
5. Construction of drift chambers	t_o-4 mos.	1 Mar, 1976
6. Construction of gamma ray detector	t_o-4 mos.	1 Mar, 1976
7. Installation of equipment	t_o-3 mos.	1 Apr, 1976

8.	Test of equipment	t_o-2 mos.	1 May, 19
9.	Data collection	t_o	1 July, 1
10.	Completion of experiment	t_o+6 mos.	1 Jan, 19

This Agreement is mutually acceptable to both the experimenters and Fermilab. Circumstances and needs will change as the experimental program develops. This Agreement will be amended when necessary.

James R. Sanford 9/29/75

James R. Sanford (Date)
Fermi National Accelerator Laboratory

Irwin A. Pless 10/10/75

I. A. Pless (Date)
Massachusetts Institute of Technology

Appendix I

Current One-Page Summary of Physics Objectives and Experimental Techniques for Experiment 299

Precision Study of High Energy Collisions Induced by Incident 150 GeV/c Pions and Protons

The experiment will be performed using the Fermilab Proportional Wire Hybrid 30" Bubble Chamber System. A total of 600,000 pictures will be taken of which 500,000 will be with π^+ and protons on hydrogen at 150 GeV/c, and 100,000 with π^- on hydrogen, also at 150 GeV/c.

The objective of the experiment is the study of the following topics:

1) Charged particle multiplicity moments
2) Production spectra for charged and neutral particles
3) Leading particle and diffraction phenomena
4) Correlating in momentum and rapidly among the produced particles
5) Factorization of production amplitudes with respect to the quantum numbers of the incident particle.

In addition, we expect to make a preliminary study of $K^{\pm}p$ and $\bar{p}p$ interactions.

Appendix II

New PREP Equipment for Experiment #299

PREP REQUEST FILE/ SORT BY AFFILIATION

AFFILIATION E299

TYPE CODE	QTY	MFGR	MODEL #	DESCRIPTION	UNIT COST	TOTAL COST
AA	2	ORTEC	401A	NIM BIN	182	364
AB	2	BL PACK	1011	NIM BIN PWR SUPPLY	362	724
AD	5	LECROY	621AL	QUAD DISCRIMINATOR	795	3975
AE	3	LECROY	364AL	4-FOLD LOGIC UNIT	675	2025
AF	2	LECROY	429	LOGIC FAN-IN/FANOUT	545	1090
CA	13	STD ENGR	1CS	CAMAC CRATE	695	9035
CB	13	STD ENGR	1410	CAMAC PWR SUPPLY	850	11050
CG	10	LECROY	2249	CAMAC ADC	2000	20000
CI	13	JORWAY	70A	CRATE CONTROLLER	855	11115
CI	3	GEC-ELL	CBF6501	CAMAC B-H EXTENDER	1000	3000
CJ	3	STD ENGR	MM816C	CAMAC MEMORY CORE	2795	8385
FP	5	POW DES	1570	H V POWER SUPPLY	595	2975
FD	5	FERMILAB	FS-7092	HV DISTRIBUTION BOX	1000	5000

TOTAL QUANTITY IS 79 ITEMS AT A TOTAL COST OF $ 78738

TOTALS:

ALL ITEMS	$ 78738	ALL DELIV ITEMS	$ 0
ALL 'A' ITEMS	$ 7975	ALL OWED ITEMS	$ 78738

Exploratory discussion for setting up a beam line test for the 299 lead glass hodoscope

The following is a suggested outline for determining the important energy and special characteristics of the lead glass hodoscope suggested for the 299 gamma ray detector. This outline is meant to be a reference point of discussion and not a firm commitment on any party.

1. Beam line - Fermilab
   - a) Flux density of e^- up to 100 cts/mm^2 in a "few hours" at most.
   - b) $\frac{\Delta p}{p} \sim 0.3\%$
   - c) $25 < p < 200$ GeV/c
   - d) PDP-11 computer plus scope
   - e) NIM LOGIC - borrowed
   - f) beam counters
2. Remote CAMAC System - Fermilab
   - a) CAMAC CRATE
   - b) serial crate controller system
   - c) parallel to serial converter
   - d) 12 channel A to D converter (borrowed or bought)
3. 5 element x, 5 element y 2 dimensional lead glass hodoscope - Fermilab
   - a) glass and photo tubes
   - b) box
   - c) movable carriage
   - d) calibration tubes and pulser
   - e) cross slide
4. Calibration system and data - PHSC
   - a) similar to that described in FGD and PHSC - Fermilab agreement
   - b) provide phototube + source + neutral density filter and mount.
   - c) use Fermilab neon tube and pulser
5. Binary glass system - Fermilab
   - a) glass 12" x 12" by $\frac{1}{4}$", $\frac{1}{2}$", 1", 1"
   - b) mount for above

6. Hole counter system - PHSC

   a) two counters

      i) 1" diameter
      ii) $1\frac{1}{2}$" diameter with 3.6 mm diameter hole in center

   b) photo tubes - 56 AVP

   c) bases - 5 nanosecond pulse

   d) two-dimensional cross slides with 4" travel

7. Software - PHSC

   a) data gathering

   b) histograms

8. Off-line computer time - Fermilab-PHSC

As noted above, the outline is not meant to be an agreement but rather the basis for discussion so that an agreement can be reached. The enclosed sketch is just a rough idea of how the test might go.

M. Johnson
I. A. Pless

11 February 1975

Outline for the Joint Construction between the European FGD Collaboration and the American PHSC-Fermilab of a Forward Gamma Detector

The following outline is the result of discussions between Gigi Ventura and Irwin Pless. These discussions followed presentations to the whole PHSC-Fermilab and a subgroup of the PHSC-Fermilab.

The purpose of this outline is to delineate construction ideas and preliminary responsibilities for accomplishing two objectives. The first objective is a preliminary study of the critical parameters of the system. This will involve a test period in the Fermilab beams with a prototype representing a minimal configuration. The second is the construction, installation, and operation of a full-size Forward Gamma Detector in the Fermilab 30" Hybrid Bubble Chamber System, to be used for physics experiments. It is anticipated that the equipment will remain at Fermilab through 1 January 1977.

I. Preliminary Test

A. Size:

1. Full-size along beam direction

2. One quarter area perpendicular to beam direction

B. Components:

1. 4 block 15 x 15 x 60 cm^3

a. Responsibility

i. FGD

2. 30 x 30 cm^2 two coordinate scintillation hodoscope

a. Responsibility

i. FGD

3. 31.5 x 31.5 cm^2 two coordinate lead glass hodoscope

a. Responsibility

i. PHSC-Fermilab

I. B.   4. 30 x 30 cm^2 three coordinate PWC hodoscope

a. Responsibility

i. PHSC-Fermilab

5. 64 Channel ADC - 10 bit

a. Responsibility

i. FDG - borrowed

ii. PHSC-Fermilab - borrowed

6. NIM Logic

a. Responsibility

i. PHSC-Fermilab

7. Calibration phototubes - 2 each

a. Responsibility

i. FGD

8. Movable Carriage

a. Responsibility

i. PHSC-Fermilab

II. Operational Hardware

A. Size:

1. 30 radiation lengths along beam direction

2. 60 x 60 cm^2 perpendicular to beam direction

B. Components

1. Lead glass counter

i. 16 blocks 15 x 15 x 60 cm^3

a. Responsibility

i. FGD

ii. PHSC-Fermilab

$\bar{2}$. Calibration tube and two-dimensional remote control [1]

a. Responsibility

i. FGD

ii. PHSC-Fermilab

$\bar{3}$. Nitrogen box

a. Responsibility

i. PHSC-Fermilab

2. Vertex hodoscope

$\bar{1}$. 60 x 60 cm^2 three coordinate scintillation hodoscope

a. Responsibility

i. FGD

b. Calibration tube and remote control system [1]

a. Responsibility

i. FGD

$\bar{2}$. Nitrogen box

a. Responsibility

i. FGD

3. Lead glass hodoscope

$\bar{1}$. 62.5 x 62.5 cm^2 two coordinate lead glass hodoscope

a. Responsibility

i. PHSC-Fermilab

$\bar{2}$. Calibration tube and one-dimensional remote control [4]

a. Responsibility

i. FGD

ii. PHSC-Fermilab

$\bar{3}$. Nitrogen box

a. Responsibility

i. PHSC-Fermilab

4. Drift chamber

   1. 120 x 120 cm^2 drift chamber

      a. Responsibility

         i. PHSC-Fermilab

5. Mechanical mount

   1. Two-dimensional remote control mechanical mount for items 1, 2, 3, 4, and 5.

      a. Responsibility

         i. PHSC-Fermilab

6. Calibration device [6 each]

   1. Tubes - nuclear services - ADC - Self Trigger - LED

      a. Responsibility

         i. FGD

This document just records, as mentioned above, informal discussions between Drs. Ventura and Pless. This document is not meant to be a binding commitment but,rather, a basis for discussion before any final commitments are made. In particular, the attached rough sketch is only that; much effort must be expended before these crude ideas become a working scheme.

G. Ventura

I. Pless

30 January, 1975

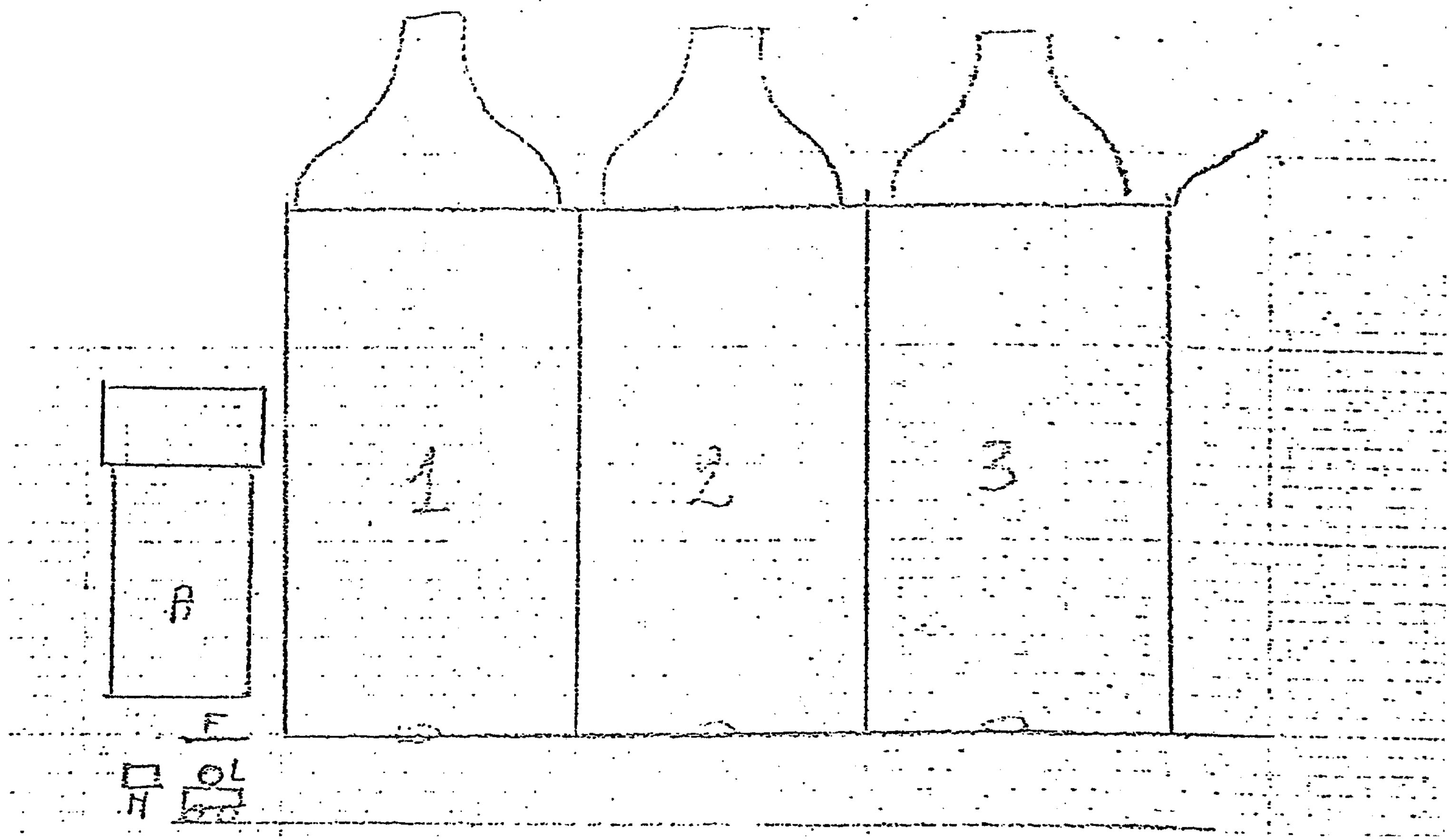

A is a reference PM, whose gain is kept constant by monitoring the light pulses from the NaI (Am 241 doped) source N. The LED L can be moved, by computer control, over the central region of the faces of lead glass blocks 1, 2, 3, etc. to control the stability of their gains, and over A to check for shifts in the light output of L itself. Since for the lead glass counters a pulse intensity is needed equivalent to the light from a shower of several tens GeV, while the pulses from N correspond to or ~ 1 GeV shower, an attenuating filter F is set between L and the photocathode of A, so as to roughly equalize its outputs for L and N.

#570 Update
2-7-78

FERMILAB PROPOSAL P-570

Appendix III

Yields of Events for Various Projectile Particles at 200 GeV/c

The following table gives estimated yields of interactions in the bubble chamber target of the hybrid system, for the various projectile particles whose interactions we are proposing to study. These figures were obtained using the following experimental parameters:

(a) The positive beam is to consist of 10% K^+, with the remainder evenly divided between p and π^+.

*(b) The negative beam is to consist of ~ 5-10% $\bar{p}$, the remainder π^-.

(c) Exposures of 10^6 pictures in the positive beam and 10^6 in the negative beam are proposed.

(d) We plan to run with an average of 6 tracks per frame. In order to have sufficient track length for analysis of both incoming and outgoing tracks in the bubble chamber, only events with primary vertices in a 35 cm long fiducial volume will be included in the experimental data. The hydrogen density is taken to be 0.0627 gm/cm^3.

(e) The inelastic cross sections used are from D. S. Ayres et al., Phys. Rev. D15, 3105 (1977), with cross sections at 200 GeV/c obtained by linear extrapolation from the data at 140 and 175 GeV/c.

Table III-I gives the expected number of events induced by each incident beam.

* Note that this differs from the main body of the proposal. The actual percentage achievable will depend on a careful test.

TABLE III-I

Yields of Events with Various Projectile Particles at 200 GeV/c

Projectile Particle	Events per Microbarn	Inelastic Cross Sections at 200 GeV/c (mb)	Numbers of Events from Proposed Exposures
π^+	3.54	20.4	7.2×10^4
K^+	0.79	17.3	1.4×10^4
p	3.54	31.8	11.3×10^4
π^-	6.29	20.9	13.1×10^4
$\bar{p}$	~ .39 - .79	34.6	$\sim 1.4 - 2.8 \times 10^4$

International Hybrid Spectrometer Consortium

Outline of Procedures for Experiment 299 and 393

These experiments currently involve the following institutions:

299		393	
1.	Brown	1.	Brown
2.	Illinois	2.	Illinois
3.	I. I. T.	3.	I. I. T.
4.	Johns Hopkins	4.	Johns Hopkins
5.	Nijmegen/Cambridge/Mons	5.	M. I. T. / Indiana
6.	M. I. T. / Indiana	6.	Padova/CERN/Pavia/Trieste/Rome
7.	Rutgers/Stevens/Albany	7.	Rutgers/Stevens/Albany
8.	Tennessee/Oak Ridge	8.	Tel-Aviv/Technion/Weizmann
9.	Yale/Fermilab	9.	Tennessee/Oak Ridge
		10.	Yale/Fermilab

An institution including more than one individual laboratory is considered to be a single institution. No institution may add individual laboratories without the approval of the Consortium. Meetings of the Consortium will normally be held in the United States and it is expected that each institution will be represented by its spokesperson or that person's delegate.

The Consortium functions through the work of four committees (or boards):

(a) The Institutions Executive Committee (IEC) consisting of one spokesperson per institution.

(b) The Consortium Board (CB) consisting of all physicists participating in the experiment.

(c) A Data Center Control Board (DCCB) consisting of

(i) a representative from each Data Center

(ii) the Consortium spokesperson (ex-officio and non-voting).

(iii) the film and tape controller as chairperson.

(d) A Quality Monitor Committee (QMC) consisting of

(i) a representative from each Data Center,

(ii) a chairperson not representing any Data Center,

(iii) ad hoc experts.

I. Processing Responsibilities

There will be four types of laboratory processing sites:

(α) Sites where scanning, IPD'ing and measurement are done,

(β) Sites where scanning and IPD'ing are done,

(γ) Sites where scanning and measurement (without IPD) are done,

(δ) Sites where only measurements are done.

Each laboratory will make a choice among these possibilities at the outset of the experiment. This choice may be modified in the course of the experiment with the approval of the I. E. C. Institutions are grouped into Data Centers. The following six Data Centers are defined:

Center 1 - M.I.T./Indiana; Brown; Yale/Fermilab
Center 2 - Johns Hopkins; Rutgers/Stevens/Albany; Tennessee/Oak Ridge
Center 3 - Illinois (until Oct. 1, 1976); I.I.T.
Center 4 - Nijmegen/Cambridge/Mons
Center 5 - Padova/CERN/Pavia/Trieste/Rome
Center 6 - Tel-Aviv/Technion/Weizmann

1. Duties of a Laboratory Processing Site

A. Sites of type α, β, and γ

1. Common responsibilities

Sites where one stage of the operation consists of scanning should scan according to common criteria as determined by the DCCB. Each such site is expected to provide a minimum of two scanner shift-years and to scan up to 1/n of the film, where n is total number of sites of type α, β, and γ in the experiment.

2. Additional responsibilities of sites where scanning, IPD'ing, and measuring are done (type α).

   a.) IPD according to common criteria and format as determined by the DCCB. Furnish film and IPD tapes to Data Centers as instructed by the DCCB.

   b.) Check and correct IPD type measurement failures as directed by the DCCB.

   c.) Act as part of a Data Center according to the rules and procedures set up by the DCCB.

3. Additional responsibilities of sites where scanning and IPD'ing are done (type β)

   a.) same as 2a and 2b.

4. Additional responsibilities of sites where scanning and measurement are done without IPD'ing (type γ)

   a.) Furnish all data from the normal operation of the site requested by the DCCB in a format determined by the DCCB.

   b.) Act as part of a Data Center according to the rules and procedures set up by the DCCB.

B. Sites of type δ (measurement only)

   1. Act as part of a Data Center according to the rules and procedures set up by the DCCB.

C. Sites which can measure, including those with hand measuring machines

   1. Each laboratory site having measurement capability will be asked to remeasure an equal number of failures. It is not yet known what form the remeasurements may take, but it is likely that for some fraction, at least, precision hand measuring capability will be required. Each site in the Consortium should therefore inform its spokesperson of the extent of their access to such facilities and the time periods of such access.

   2. Definitions and Duties of Data Centers

      The task of a data center is to transform raw film into a Geometry

Summary Tape (GST). Each DC should contain a sufficient mix of sites of the type α, β, γ and δ to make this task possible. Each DC is expected to handle up to 1/M of all film, where M is the number of active data centers in an experiment. Each DC performs the above task (and its different steps) under the rules and procedures given by the DCCB.

3. Duties and Responsibilities of Data Center Control Board

The DC Control Board is the executive committee for all data processing. It allocates all film to sites or DC for scanning, IPD'ing and/or measurement. Where applicable, it allocates IPD data to Data Centers. It specifies all formats and has sole authority, subject to approval by the IEC, to initiate, authorize and require all format and program changes.

It is the responsibility of the DCCB to certify the presently foreseen and all future Data Centers, subject to approval by the IEC.

The DCCB will establish the Quality Monitor Committee. It is the responsibility of the DCCB to investigate any concerns raised by the QMC and to recommend any necessary changes in procedure. The DCCB should meet frequently at scheduled intervals.

4. Duties and Responsibilities of the Quality Monitor Committee

The QMC will have five functions. First, this committee should establish procedures whereby measures of quality on both input to and output from Data Centers may be obtained. Second, using these measures it should advise the DCCB as to certification and should continuously check the quality of the input and output data and report to the Data Center Control Board any problems with or concerns about data quality. Third it should, through continuous checking, ensure that the output of the Data Centers is uniform. Fourth, it should provide technical aid in resolving conflicts between data centers. Fifth, it should prepare implementation of data processing improvements and recommend certification of all such improvements.

5. Processing Responsibility Flow Chart

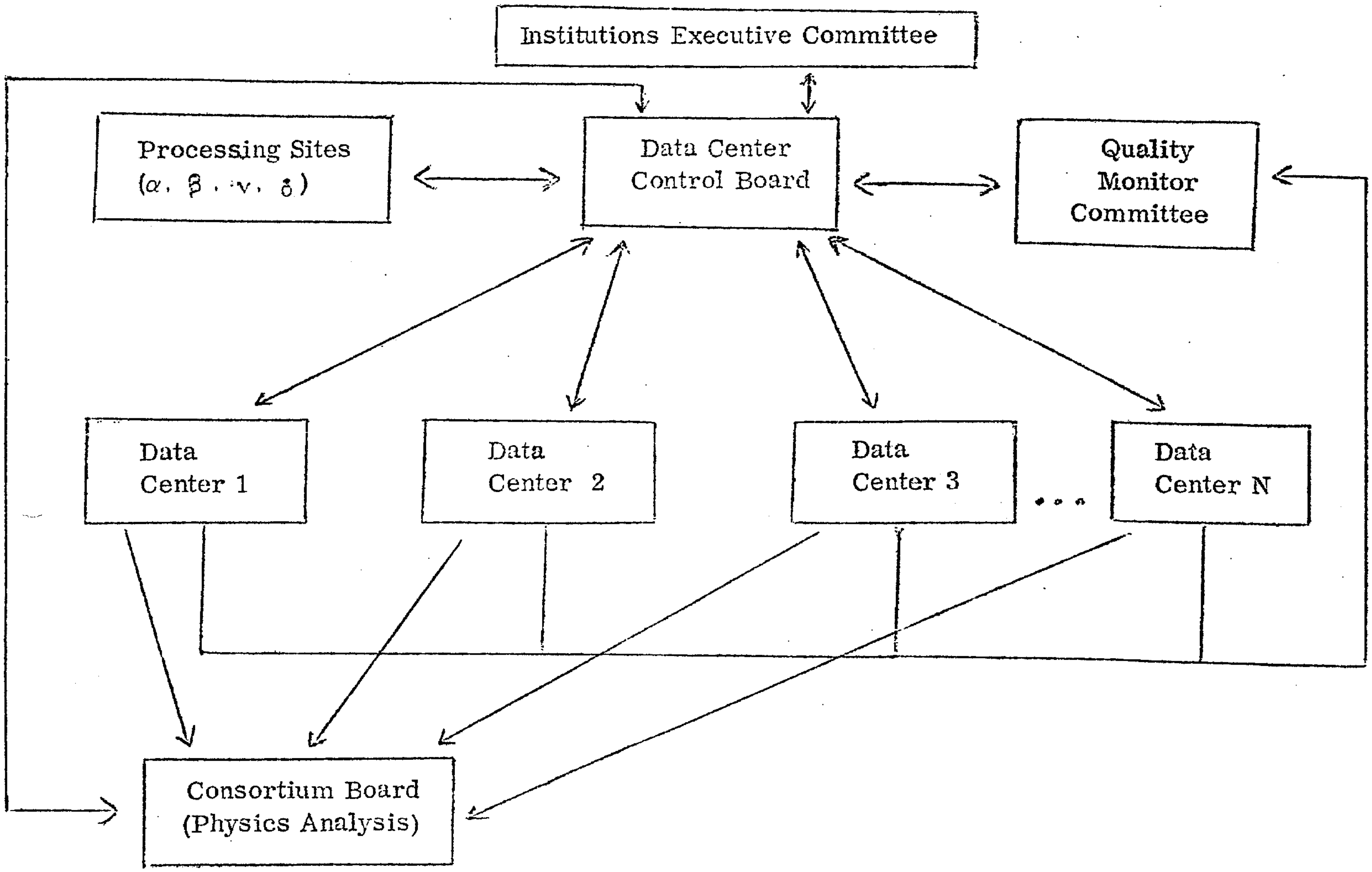

II. Staffing

1. Each institution selects its own representative on the IEC following a procedure of its own choice.

2. The Consortium Board consists of all Consortium members, i.e. all physicists whose names appear on a list established at the start of the experiment. Adding new names to a laboratory requires the approval of the Consortium Board.

3. The Consortium spokesperson is I.A. Pless. The spokesperson serves as Chairperson of the Consortium Board and of the I.E.C.

4. Each Data Center selects its own representative on the DCCB following a procedure of its own choice; this selection is subject to ratification by the IEC.

5. Each Data Center selects its own representatives on the QMC following a procedure of its own choice; this selection is subject to ratification by the IEC.

6. The film and tape controller and the ad hoc experts on the QMC are selected and appointed by the IEC.

III. Operational Procedures

A. Access to Consortium Data

All laboratories in the Consortium have equal access to the data of the experiment. The Data Centers have the obligation to provide expeditiously to laboratories within the Consortium who wish to receive them, current data and program tapes with appropriate inventory. The receiving group has the obligation to provide the physical tapes and, if the Data Center so requests, an operator qualified to use their computer complex.

B. Certification of Consortium Tapes

1. Data Centers will have the responsibility to declare tapes "correct".

2. Data Center Control Board has responsibility to "certify" that tapes are correct.

3. No tapes are usable for publication purposes unless steps B.1 and B.2 have been carried out.

C. Communications

1. Data Center Control Board will issue regular internal progress reports. The contents of the progress reports will be determined by the Institutions.

2. Consortium members shall be responsible for submitting to the Data Center Control Board all useful and pertinent results for inclusion in the internal progress reports

IV. Physics and Publications

A. Publication Policy

1. We define a "completed GST" (Geometry Summary Tape) as a GST for which no further measurements or remeasurements are expected to be entered. The period up to the production of such a completed GST is defined to be Period I. The IEC will decide at what date the GST is considered to be "completed". During this period:

a.) No Institution may withdraw from a publication without explicit approval of the IEC. However. Institutions consisting of more than one individual laboratory may remove the name of one or more laboratories associated with those Institutions from publications.

b.) Individual laboratories will be asked to submit names to be associated with each publication. The Consortium Board reserves the right to set a maximum limit on the number of names any laboratory may submit on any individual publication.

2. Period II is defined to be the year following Period I. During this period:

a.) Every physicist in the Consortium is invited to participate in preparing individual papers.

b.) Publication will be by those persons (representing laboratories within the Consortium) who participated in preparing the paper.

Period III is defined to be the one year following Period II. During this period:

a.) Each institution may publish independently or in collaboration with other institutions of the Consortium b.) No person may publish results from this experiment in collaboration with persons outside of the Consortium without approval of the Consortium Board.

c.) The duration of Period III can be extended by a decision of the Consortium Board.

After Period III:

a.) There are no constraints on the use of the GST.

B. Contributed Papers, Invited Papers and Colloquia or Seminars

The following understandings apply to Period I, Period II and Period III.

1. Contributed papers at APS meetings and other conferences

a.) Nomination policy

i. The IEC will make a selection of candidates to present the talks.

ii. Additional candidates can be nominated by any three persons belonging to the Consortium.

iii. A vote will be taken by the Consortium Board or their representatives to decide which candidates will give each talk.

iv. The speaker will distribute a copy of the talk or clearly labelled transparencies to the Consortium.

2. Invited papers at APS meetings and other conferences.

a.) Invitations to present invited papers must be forwarded to the IEC.

b.) The IEC will make a list of candidates for all invited papers.

c.) Additional candidates may be nominated for an invited paper by any six physicists belonging to the Consortium.

d.) A vote will be taken by the Consortium Board to select the person to give the invited talk.

e.) The speaker will distribute a copy of the talk to the Consortium.

3. Seminars and Colloquia

a.) Any member of the Consortium may give talks at seminars or colloquia as long as such talks deal with published or formally presented data or data submitted for publication.

b.) Approval of the IEC is required before any member may give talks of any kind involving data which have not yet been published, formally presented, or submitted for publication.

C. Arrangement for Ph.D. thesis topics

1. Each laboratory will inform the Consortium Board if all proposed thesis projects. These projects should be coordinated by the I.E.C.

MASSACHUSETTS INSTITUTE OF TECHNOLOGY
LABORATORY FOR NUCLEAR SCIENCE
CAMBRIDGE, MASSACHUSETTS 02139
575 Technology Square, Room 408

November 16, 1977

Dear Colleagues:

At our November 12 meeting we chose chairmen of physics topics and added a new topic, and they are:

A. Topological Cross Sections and Multiplicity Distributions
Chairpersons: E. B. Brucker
R. E. Ansorge

B. Elastic Scattering and Inelastic Two Prongs
Chairpersons: W. M. Bugg
V. Henri

C. Four Constraint Fits - Four and Six Prongs
Chairpersons: O. Benary
R. Van de Walle

D. Neutral Strange Particles
Chairpersons: T. L. Watts
D. R. Ward

E. Δ^{++}
Chairpersons: A. Levy
E. S. Hafen

F. Correlations and Clustering
Chairpersons: W. Kittel
H. A. Rubin

G. Charm
Chairpersons: E. L. Hart
F. Grard

H. Beam Diffraction
Chairpersons: J. W. Cooper
J. Grunhaus

J. M_x^2 and Multiplicity
Chairpersons: V. Kistiakowsky
U. Karshon

K. Forward Diffractive π^0 and γ
Chairpersons: R. K. Yamamoto
P. Herquet

N. Vector Mesons
Chairpersons: T. Ludlam
W. Metzger

P. Gammas
Chairpersons: B. M. Whyman
L. Bachman

Q. Leading Particles
Chairperson: M. Widgoff

R. Generalized Inclusive Studies
Chairperson: S. Ratti

The GST 154 has been defined to be complete and E-154 is now in phase 2 of our agreements. It has been decided that the next meeting of the IHSC will be in early February and part of that meeting will be a preview of the presentation to the PAC, which will be around February 23. All the other documents should be self-explanatory, and if there are any new developments everyone will be kept informed.

Sincerely yours,

Irwin A. Pless

Irwin A. Pless
for the IHSC

IAP:fh
Enclosures:
Courier Report, I.A. Pless trip to Europe/Israel, Oct. 9-28, 1977
Minutes of IHSC mtg. at Fermilab Nov. 12, 1977, R.I. Hulsizer
Ltr. J. Rushbrooke to I. A. Pless, Sept. 22, 1977
Abstracts submitted to San Francisco mtg. of APS Jan. 22-26, 1978
Notes by P. F. Jacques and T. L. Watts on Progress of Neutrals Physics E299, 10/4/77
"Updated GEOMAT and GEOMAT Tape", DAS 77-4, L. E. Morecroft

Courier Report for the Trip to Europe/Israel

October 9 - 28, 1977

Irwin A. Pless

Cambridge - 10 October 1977

Summary of Data Reduction.

Measured on SWEEPNIK	7 Rolls
Scanned and checked	1 Roll
Scanned; checking in progress	1 Roll
Scanned; to be checked	1 Roll

This is the first Fermilab film to be measured on SWEEPNIK. Data will be processed at Nijmegen after Vézelay conference. GEOMAT is working on MIT test data. Bugs in GEOMAT system have been noted and will be delivered to Linda Morecroft. One PWC tape sent to Cambridge seems to be in error and three PWC tapes seem to be completely missing. The courier will check this at M.I.T. Cambridge would like a copy of the beam log including Čerenkov pressure curves. The spokesperson will be asked to furnish this. Cambridge would like a copy of the M.I.T. GST for 299. Cambridge would also like a copy of E. S. Hafen's weighting program.

Padova - 15 October 1977

Summary of Data Reduction.

Padova has not yet received its film. It is in Customs and will soon be released (hopefully). Elio Calligarich (Pavia) has been designated spokesperson for the "Italian" group (CERN, Padova, Pavia, Rome, Trieste). Pavia would like the official scan rules and the official STYX Format. (These have been furnished.) They would also like the M.I.T. GST. The spokesperson will be requested to furnish this.

Israel (Tel-Aviv, Weizmann, Technion) - 15-17 October 1977

Summary of Data Reduction.

Measured on spiral reader	1 Roll
Scanned and checked; hand measurement in progress	2 Rolls
Just arrived	2 Rolls

This group expects to finish the first round of spiral reader measurements in one month. They have used the spiral reader in a p, π^+ on deuterium experiment. They have GEOMAT operational but were using wrong version of STYX Format. This should be cleared up now. They have put their measurements through their TVGP, PWC and TRACK ORGANIZER chain. The data looks reasonable. They expect to have complete results through GEOMAT chain in one month. They have a list of errors in the GEOMAT chain which will be delivered to Linda Morecroft. This group would like a copy of the M.I.T. GST. The spokesperson will be asked to furnish this. Professor Karshon would like a reply to the letter he sent Professor Hulsizer about the STYX Format. The courier will check on this. (Bob has sent a reply.)

Nijmegen - 18 October 1977

Summary of Data Reduction.

Measured on hand machines	2 Rolls
Measurement on hand machines; in progress	1 Roll
Measurement on PEPR; in progress	1 Roll
Scanned and checked	6 Rolls

This is the first Fermilab film that this group is processing. They have 100 events of 299 measured on PEPR processed through GEOMAT and GEOHYB. It was possible to compare the two outputs and they are comparable. They have found a number of errors in the GEOMAT chain and these errors will be delivered to

Linda Morecroft. There seems to be some confusion about the new GEOMAT PAM; a clarification will be sent by telex to Crijns. (This has been done.) They have also seemed to notice a shift in the fiducials on View 1 on roll 1722 when measured with PEPR. The dispersion seems to be between 1.7 - 4.8 microns. They wish to know the experience of M.I.T. on this matter. The courier will investigate this. They also want the M.I.T. GST. The spokesperson will be asked to furnish this. This group expects to finish all its film and produce a GST by 1 January 1978.

Mons - 21 October 1977

Summary of Data Reduction.

Measured on SWEEPNIK	3 Rolls
Scanned, checked; measurement in progress	1 Roll
Scanned, checked	2 Rolls
Scanning in progress	2 Rolls
To be scanned	1 Roll

This is the first time that this group is processing Fermilab film. Roll 1720 (first frame number 6402, last frame number 8834) and PWC tape 1720 do not match. This is the region of the experiment where logging errors were made. The courier will check on this. This group also would like the M.I.T. ionization versus momentum plot for a roll of film near roll 1700 if possible. They would like this to help with their certification techniques. Three rolls of PWC tapes seem not to be at Mons. The courier will check on this. Mons wishes to know if DAS-76-9 is the latest LEM Format. The courier will check on this and inform Nijmegen. (This has been done.) Mons expects to have their nine (not 10) rolls of film measured once and processed through GEOMAT and GEOHYB (at Nijmegen) by 1 February 1978.

Since R. J. Plano will be at CERN to talk to F. Bruyant and others about GEOHYB he will be in the best position to report on the CERN situation. Therefore, this courier report ends with the discussion on Mons.

November 14, 1977

IHSC Meeting

November 12, 1977

Curia II, Fermilab

The meeting was opened at 9:30 by Pless with a report of his trip as the October courier. A written report of his trip is being prepared and will be distributed. He lso gave a brief report on the status of the European Hybrid System (EHS) as learned from his visit to CERN and to the EHS workshop at Vezelay.

Bugg then reported on the measurement of the magnetic field of the 30" B.C. magnet. The measurement was started on September 2 and finished on September 25. It was undertaken because a study of beam tracks from E-299 indicated that there might be errors of 1.0 to 1.5 percent in the field map, possibly due to the effect of having enlarged the exit hole in the iron. Between E-154 and E-299 the exit hole had been opened up to an angle of $\pm 7^0$.

In 1973 Notre Dame had mapped the field for E-154 and E-2B, using Hall probes. For this measurement Alyea, Hart and Rubin re-calibrated the Hall probe and used it for mapping the field inside the bubble chamber. For the exit and entrance volumes outside the chamber, Bugg, Burnstein, Condo, Handler, Hart, Rubin and Yamamoto used a set of three mutually orthogonal passive search coils positioned by a digitized lathe bed. There were 450 runs in which the coils were moved from 11 inches outside the iron in to the chamber window along a straight line, measurements being made every 0.16 inches along the way. 200,000 data points were taken in all.

The Notre Dame parametrization assumed that $B_z = f(r)$, not $f(r.z)$. The measurements indicate that this is not true. A fit of the new data to the Notre Dame parametrization will be available by December 1. A better parametrization is being sought.

For a given magnet current the absolute value of the field is suspected to be 1.77% higher than the 1973 Notre Dame value, despite the decreased iron. It might be noted that 1.0177×147 GeV/c = 149.60 GeV/c.

Widgoff then reported that the film for E299/50 and E299/60 has been almost completely scanned. One-third of the film has been measured. Four measuring centers are now in production and three are producing geometry results.

Pless reported that a preliminary GST of 20 rolls is now available from MIT. It is not a certified GST and no guarantees of quality or receptiveness to complaints are provided. There was then a discussion of how to proceed on determining the quality of the events and when it would be appropriate to start re-measuring bad events. Pless said that it is ultimately the responsibility of the chairpersons of the various physics topics committees to request the DCCB to request the centers to do re-measurements. The response of the DCCB will be dependent on competing priorities. Pless expressed the opinion that the greatest payoff in results at the present time would result from pushing through first measurements of all the film rather than going back to re-measure failed events.

A coffee break followed.

Then the subject of re-measurement procedures followed. Since GEOMAT and GEOHYB crash on an event if a failed track has no IPD points, it was agreed that all tracks should have points put in its IPD bank even if they are only rough measurements by the scanner or the measurement operator. Hafen has developed a technique for estimating the contribution of a failed track to an event, using the data from the IPD points for the failed track, so having the IPD points not only prevents the geometry program from collapsing, but also enables all events to be used in the analysis of the physics. The conclusion of these recommendations is therefore a new policy: there will be no failed events, only failed tracks and all tracks, including the failed tracks, will have measured points in their IPD point banks.

Hart then reported on the scan results for the QMC. He has received scan results from 52 rolls, 27 of which have check and correction results.

Bugg, speaking for the QMC, reminded everyone that each center must not only report scan results, but also topological distributions, rejects for various causes, and a scatter plot of ionization vs. momentum for all tracks of each roll. He also reported on the status of data center certification:

MIT has measured both certification rolls and has provided the results on a GST.

Rutgers has measured both certification rolls.

Hopkins and Illinois have each measured one certification roll.

Bugg then reported on GEOHYB certification. The QMC met on October 19 to compare GEOMAT 3.21 vs. GEOHYB. Both are good on beam tracks. Both underestimate errors, but GEOHYB's errors are only low by about 30% whereas GEOMAT's errors are low by more than a factor of two.

Brucker then reported on a comparison of GEOHYB (GH) vs. GEOMAT 3.21 (GM) for 100 events from roll 797 of E-154.

Of the 100 events, 50 were essentially identically treated.

10 events had evenly split differences between GM and GH.

6 events had better hook-ups with GH than GM, the difference being on low momentum tracks.

31 events had more hook-ups with GM than with GH, the difference being on tracks that had a view missing.

3 events untabulated.

On 32 additional events that were examined in detail:

25 had identical matches

3 had better matches by GM than GH

2 had better matches by GH than GM

2 were inconclusive

Bugg then reported that the same differences between treatment of errors that was clear on beam tracks appears to be occurring on secondary tracks; namely, GH much better than GM. Crijns then asked if the number of tracks hybridized by GH and GM was equal. Brucker answered that they were about the same.

LUNCH

After lunch Plano reported that he had three versions of GEOHYB at Rutgers dated July, September and November. The July version has run on the Rutgers PDP-10, on the Brown 360 and the CERN 7600 with the same input data. The results were the same from all three computers. The PAM for the 360/65 utilizes double precision arithmetic where needed. This impressive result was not achieved without pain, however. Fiducial failures caused disastrous trouble, and it is absolutely essential that the measurements placed in the integer-format STYX track banks be scaled so as to preserve the full precision of the measurements, e.g., one micron or better. The results of these runs have been sent to QMC. GEOHYB takes 30 seconds per event to run on a PDP-10 (KA-10). Plano also reported that Bruyant is coming to the U.S. in 1978 to discuss programming of data from ISIS and FGD.

Crijns then reported on the work on geometry at Nijmegen. In August they had GEOMAT working on some E-154 test events, but it never worked on E-299 data. Cause unknown. Work on GEOHYB was started in July. In a September workshop at CERN, the parameters were tuned. Beam tracks and fiducials were then measured, optics calculated with PYTHYD and BCCONST and FITROT titles were calculated by

October. Then test runs were made on roll 797 and an E-299 roll, measured at Nijmegen. After tuning the parameters, one roll from each lab (Cambridge, Mons and Nijmegen) was run. A comparison of data from 797 was made and a GEOHYB histogram package was written to prepare results for the QMC. In comparing GEOHYB with GEOMAT on 73 events, they find that GH had 118 hybridized tracks compared with GM's 101. The momenta were essentially identical. GH produced more 5-plane tracks, while GM could handle tracks with one view missing. Also GH hybridized tracks from two neutral V's; GM cannot do that.

The performance of four European measuring machines are given below:

	Nij Hand	Nij PEPR	Cambridge	Mons
% triplets	95	88	92	91
% hybridized	21	20	22	26
missing	2	6	2	3
R.M.S. (μ)	5	4	3	5

The vertex reconstructions errors ran as follows:

Δx 60μ

Δy 40μ

Δz 30μ

The success rate as a function of topology was:

No. of prongs	Nijmegen Hand measure	Nijmegen PEPR
2	93	84
10	50	
12		40
14	13	

The Northern European Data Center hopes to achieve final certification by December 1.

Pless then announced that the group heads for E-154 have reported that the E-154 GST is complete as of November 12, 1977 and that period B of the E-154 contract (similar to period 2 of the E-299 contract) is now in effect, for one year. Pless read the rules regarding the three periods to refresh the memories of those present. They deal with procedures for working on and publishing results from the GST data, and determination of authors.

Pless then invited everyone to review the list of physics topics and physicists signed up on them that had been written on the blackboards. Changes were declared to be in order. Ratti proposed a new topic, "Generalized Inclusive Studies".

The revised lists are appended.

A partial list of those attending the meeting is also appended. It is incomplete because during the meeting the test run of ISIS was going on in the 30" B.C. building and many members of the IHSC dropped in to this meeting from time to time, but were not apprehended by the secretary for their signatures.

The meeting adjourned at 3:30 p.m., a new record of brevity for the IHSC.

Respectfully submitted,

Bob Hulsizer

Robert I. Hulsizer
Secretary pro tem

RIH:fh
Encs.

A. Topological Cross Sections and Multiplicity Distributions

π1	topological cross sections
π2	multiplicity distributions
K1	topological cross sections
K6	multiplicity distributions
p12	topological cross sections
p22	multiplicity distributions

Cambridge:	R. E. Ansorge (Co-chairperson), J. G. Rushbrooke, B. M. Whyman
I.I.T.:	R. A. Burnstein, H. A. Rubin
M.I.T.:	R. I. Hulsizer
Mons:	F. Grard, J. Hanton, J. Skura
Nijmegen:	F. Crijns, C. Pols
Stevens:	E. B. Brucker (Chairperson), E. L. Koller, P. E. Stamer, S. Taylor
Technion:	S. Dado, J. Goldberg, B. Lev, S. Toaff
Tel-Aviv:	J. Grunhaus, A. Levy, D. Lissauer, Y. Oren
Tennessee:	E. L. Hart

B. Elastic Scattering and Inelastic Two Prongs

π24	elastic scattering
π25	inelastic two-prong events
K21	elastic scattering
K24	inelastic two-prong
p17	inelastic two-prong events
p18	elastic scattering

Brown:	A. M. Shapiro
Cambridge:	J. R. Carter
M.I.T.:	R. I. Hulsizer, J. Silverman
Mons:	V. Henri (Co-chairperson), J. Kesteman
Pavia:	E. Calligarich, D. Scannicchio
Tennessee:	W. M. Bugg (Chairperson)

C. Four Constraint Fits - Four and Six Prongs

π10 4P - 4C, 6P - 4C
K2 4P - 4C, 6P - 4C
p19 4P - 4C, 6P - 4C

Cambridge:	J. R. Carter
Fermilab:	D. Bogert, J. Wolfson
M.I.T.:	O. Benary (Chairperson), P. Trepagnier
Mons:	J. Lesceux
Nijmegen:	R. Van de Walle (Co-chairperson), H. de Bock, W. Kittel
Rutgers:	R. J. Plano
Stevens:	E. L. Koller
Technion:	Berny, L.
Tel-Aviv:	S. Dagan, Y. Gnat, J. Grunhaus
Tennessee:	T. Handler
Weizmann:	D. Hochman, E. E. Ronat, R. Yaari
Yale:	H. Taft

D. Neutral Strange Particles

π7 inclusive K^0 production
π8 inclusive Λ^0 production
π9 inclusive $\bar{\Lambda}^0$ production
K4 inclusive K^0 production
K5 inclusive nK^0 production, $n \geq 2$
K8 inclusive $\bar{\Lambda}^0$ and Λ^0 production
p10 inclusive Λ^0 and $\bar{\Lambda}^0$ production
p11 inclusive K^0 production

Cambridge:	D. R. Ward (Co-chairperson), W. W. Neale, J. G. Rushbrooke, B. M. Whyman
Johns Hopkins:	L. Bachman
M.I.T.:	F. Barreiro, O. Benary
Mons:	P. Gillis, F. Grard, J. Hanton, P. Herquet
Nijmegen:	W. Metzger, R. Van de Walle
Rutgers:	T. L. Watts (Chairperson), P. F. Jacques, T. C. Ou
Stevens:	E. B. Brucker, E. L. Koller, P. E. Stamer, S. Taylor
Tennessee:	E. L. Hart
Yale:	D. Ljung

E. Δ^{++}

π5 inclusive Δ^{++} production
K7 inclusive Δ^{++} production
K13 inclusive $p \rightarrow p\pi\pi$
p9 inclusive Δ^{++} production

Brown:	D. Brick, A. M. Shapiro
Cambridge:	D. R. Ward
M.I.T.:	E. S. Hafen (Co-chairperson), J. Silverman
Mons:	V. Henri, R. Windmolders
Nijmegen:	F. Crijns, H. de Bock, W. Metzger, M. Schouten
Technion:	S. Dado, J. Goldberg, Berny, L., Toaff, S.
Tel-Aviv:	A. Levy (Chairperson), S. Dagan, Y. Oren
Tennessee:	T. Handler
Weizmann:	Y. Eisenberg, E. E. Ronat, A. Shapira

F. Correlations and Clustering

π4	n-body correlations $n \geq 2$
π19	clustering studies
π20	search for neutral plateaus (or lack thereof)
K9	Kopylov effect
K14	many body correlations
K20	clustering studies
K28	search for neutral plateau (or lack thereof)
p15	clustering studies
p16	search for neutral plateau (or lack thereof)
p21	n-body correlations $n \geq 2$

Brown:	M. Heller, M. Widgoff
I.I.T.:	H. A. Rubin (Co-chairperson), R. A. Burnstein
Illinois:	J. W. Cooper, R. L. Plumer, R. D. Sard
Indiana:	E. D. Alyea
M.I.T.:	J. Brau, R. K. Yamamoto
Mons:	P. Gillis, J. Skura
Nijmegen:	W. Kittel (Chairperson), H. de Bock, C. Pols, J. Schotanus, M. Schouten
Pavia:	G. Cecchet, R. Dolfini
Rutgers:	R. J. Plano
Tennessee:	T. Handler
Yale:	T. Ludlam

G. Charm

K11 neutral 4-prong decays (D^0 decay)

M.I.T.:	V. Kistiakowsky, I. A. Pless
Mons:	F. Grard (Co-chairperson)
Oak Ridge:	H. O. Cohn
Pavia	A. Piazzoli, S. Ratti
Tennessee:	E. L. Hart (Chairperson)

H. Beam Diffraction

$\pi 27$ $\pi^+ + p \rightarrow p + (\pi^+)^* + X$ where $(\pi^+)^*$ is diffractive
K12 inclusive $K \rightarrow K^0 \pi^+ \pi^0$
p20 $p + p \rightarrow p_s + p^*$ where p^* is diffractive
$\hookrightarrow p_f + p^*$

Illinois:	J. W. Cooper (Chairperson), R. D. Sard
M.I.T.:	P. Miller, I. A. Pless, J. Silverman
Mons:	V. Henri, J. Lesceux
Tel-Aviv	G. Alexander, Y. Gnat, J. Grunhaus (Co-chairperson)
Weizmann	Y. Eisenberg, U. Karshon, E. E. Ronat, A. Shapira

J. M_x^2 and Multiplicity

π11	M_x^2 versus multiplicity;	$\pi^+ + p \to \pi^+ M_x^2$
π12	M_x^2 versus multiplicity;	$\pi^+ + p \to p + M_x^2$
π13	M_x^2 versus multiplicity;	$\pi^+ + p \to \Lambda^0 + M_x^2$
π14	M_x^2 versus multiplicity;	$\pi^+ p \to K^0 + M_x^2$
π23	M_x^2 versus multiplicity;	$\pi^+ p \to \Delta^{++} + M_x^2$
K15	M_x^2 versus multiplicity;	$K^+ + p \to p + M_x^2$
K16	M_x^2 versus multiplicity;	$K^+ + p \to K^+ + M_x^2$
K17	M_x^2 versus multiplicity;	$K^+ + p \to K^0 + M_x^2$
K18	M_x^2 versus multiplicity;	$K + p \to \Lambda^0 + M_x^2$
K23	M_x^2 versus multiplicity;	$K^+ p \to \Delta^{++} + M_x^2$
p2	M_x^2 versus multiplicity;	$p + p \to p_f + M_x^2$ $\hookrightarrow p_s + M_x^2$
p3	M_x^2 versus multiplicity;	$p + p \to K^0 + M_x^2$
p4	M_x^2 versus multiplicity;	$p + p \to \Lambda^0 + M_x^2$
p23	M_x^2 versus multiplicity;	$pp \to \Delta^{++} + X$
p24	M_x^2 versus multiplicity;	$pp \to \pi^+ + X$

Brown:	M. Widgoff
Cambridge:	R. E. Ansorge
M.I.T.:	V. Kistiakowsky (Chairperson), O. Benary
Mons:	P. Gillis, F. Grard, J. Lesceux
Nijmegen:	F. Crijns, C. Pols, J. Schotanus, R. Van de Walle
Stevens:	P. E. Stamer
Technion:	S. Dado
Tel-Aviv	G. Alexander, D. Lissauer
Weizmann	U. Karshon (Co-chairperson), Y. Eisenberg, E. Kogan
Yale:	D. Ljung

K. Forward Diffractive π^0 and γ

π29	inclusive and semi-inclusive π^0 and γ production in forward diffractive processes
K19	inclusive and semi-inclusive π^0 and γ production in forward diffractive processes
p1	inclusive and semi-inclusive π^0 and γ production in forward diffractive processes

Brown:	D. Brick
Cambridge:	J. R. Carter, T. O. White
Fermilab:	D. Bogert, J. Wolfson
Illinois:	J. W. Cooper, R. D. Sard
Indiana:	E. D. Alyea
Johns Hopkins:	L. Bachman
M.I.T.:	R. K. Yamamoto (Chairperson), F. Barreiro, J. Brau, A. Napier, P. Trepagnier
Mons:	P. Herquet (Co-chairperson), J. Kesteman
Pavia:	E. Calligarich, S. Ratti
Rutgers:	R. J. Plano
Stevens:	E. B. Brucker
Tel-Aviv:	Y. Gnat, A. Levy, D. Lissauer, Y. Oren
Tennessee:	W. M. Bugg
Weizmann:	D. Hochman, U. Karshon, E. Kogan, R. Yaari
Yale:	T. Ludlam

N. Vector Mesons

π15	inclusive ρ^0 production
π16	inclusive ρ^+ and p^- production
π21	inclusive η^0 and ω^0 production
K26	inclusive ρ^0 production
K30	inclusive η^0 and ω^0 production
K32	vector meson production
K33	$K^+p \rightarrow pK^*$, $K^* \rightarrow \pi^+ K^0$
p6	Inclusive ρ^0 production
p7	inclusive ρ^+ production
p8	inclusive ρ^- production
p14	inclusive ω^0 production

Brown:	A. M. Shapiro
Cambridge:	D. R. Ward, T. O. White
Fermilab:	D. Bogert, J. Wolfson
Indiana:	E. D. Alyea
M.I.T.:	F. Barreiro, E. S. Hafen
Nijmegen:	W. Metzger (Co-chairperson), W. Kittel, J. Schotanus, M. Schouten
Technion:	J. Goldberg, S. Toaff
Tel-Aviv	G. Alexander, S. Dagan
Tennessee:	G. T. Condo
Weizmann:	D. Hochman, E. Kogan, A. Shapira
Yale:	T. Ludlam (Chairperson), D. Ljung, H. Taft

P. Gammas

$\pi 6$ Inclusive π^0 and γ production
K29 inclusive π^0 and γ production
p5 inclusive π^0 and γ production

Cambridge	B. M. Whyman (Chairperson), R. E. Ansorge, W. W. Neale J. G. Rushbrooke, T. O. White
Johns Hopkins:	L. Bachman (Co-chairperson)
M.I.T.	E. S. Hafen
Mons:	J. Hanton, P. Herquet
Tennessee:	W. M. Bugg

Q. Leading Particles

$\pi 3$ single leading particle cross sections
K31 single leading particle cross sections
p13 single leading particle cross sections

Brown:	M. Widgoff (Chairperson), D. Brick
M.I.T.	V. Kistiakowsky, I. A. Pless, P. Trepagnier, R. K. Yamamoto
Tennessee:	G. T. Condo, H. O. Cohn

R. Generalized Inclusive Studies

ORNL:	H. O. Cohn
Pavia:	S. Ratti (Chairman), E. Calligarich, G. Cecchet, R. Dolfini, A. Piazzoli

<u>APC Programming Notes</u> (1975-1977)

1. GEOMAT - Part I, E. S. Hafen, DAS 75-1, February 6, 1975.

2. The NPLOT Package for Analysis of PWHS Experiment DST's, C. H. Hafen, Jr. and U. Karshon, DAS 76-1, July 24, 1975.

3. Using the Michigan Plotter Program, MPLOT, on the LNS 360/65, M. Matzka, DAS 76-2, July 24, 1975.

4. Output Format of CHARON, P. Trepagnier, DAS 76-3, August 4, 1975.

5. A Comparison of the Performance of MATCH-TVGP with GEOMAT, J. Wolfson, DAS 76-8, March 25, 1976.

6. Updated GEOMAT and GEOMAT Tape Format for Use with GEOMAT Version 3.2, L. E. Morecroft, DAS 76-9, August 1, 1976.

7. IPD Rules for Fermilab Experiment 299 π^+/p 150 GeV/c, Exp. 60 with 30-inch Hydrogen Bubble Chamber, E. Hafen, R. Hulsizer, DAS 77-2, December 27, 1976.

8. IPD and HM Output Tape Format, R. I. Hulsizer, DAS 77-3, Exp. 60, January 10, 1977.

9. Updated GEOMAT and GEOMAT Tape Format for Use with GEOMAT Version 3.21 (Update of DAS 76-9), L. E. Morecroft, DAS 77-4, March 1, 1977.

10. First Revised Scan Rules for Fermilab $\pi^+/K^+/p$ 150 GeV/c Experiment E-299 with the Fermilab Hybrid Spectrometer, E. S. Hafen and R. I. Hulsizer, DAS 77-5, Exp. 60, March 11, 1977.

11. GEOMAT 3-21 Information., L. E. Morecroft, DAS 77-6, March 8, 1977.

12. Documentation for a High Energy SQUAW, J. P. Silverman, DAS 77-7, March 25, 1977.

13. TRACKORGANIZER Documentation, J. Brau, DAS 77-8, March 7, 1977.

14. A Weighting Scheme for Incomplete Events, E. S. Hafen, DAS 77-9, June 24, 1977.

PHSC/IHSC NEWSNOTES

"Upstream PWC Readout Electronics Group" (Hardware Design Approach)	B. Wadsworth et al.	No. 1	7-14-71
"Upstream Magnet System Monitoring"	Chih-Yung Chien et al.	No. 2	7-12-71
"Proportional Chamber Station Facilities"	D. Bogert et al.	No. 3	7-19-71
"Proportional Chamber Station Facilities"	E. D. Alyea et al.	No. 4	7-20-71
"Downstream PWC Chambers and Electronics"	J. Wolfson et al.	No. 5	8-2-71
"Upstream PWC Chambers and Amplifiers"	R. Downing et al.	No. 6	8-2-71
"Scintillation Telescope and Master Gate"	A. Shapiro	No. 7	8-9-71
"PWC Power, Cooling, Gas Flow Monitoring"	C. Ellis et al.	No. 8	8-20-71
"On-Line Software"	V.D. Bogert et al.	No. 9	8-23-71
"Cerenkov Tagging"	H. Rubin et al.	No. 10	8-23-71
"PWC Mounts, Space and Conduit Availability" (Drawings for PWC Mounting Stands)	V. D. Bogert et al.	No. 11	9-1-71
"Computer Interface"	R. J. Piano et al.	No. 12a (to replace No. 12)	11-5-71
"PWC Power, Cooling, Gas Flow Monitoring" (Diagram for Gas Flow Monitoring System)	C. Ellis et al.	No. 13	9-25-71
"Upstream PWC Chambers and Amplifiers" (Upstream PWC Drawings)	R. Downing et al.	No. 14	10-6-71
"On-Line Software"	T. Ludlam et al.	No. 15	10-29-71
"PWC Mounts, Space and Conduit Availability" (PWC Triplet Assembly and B.C. Bracket)	V. D. Bogert et al.	No. 16	12-1-71
"Upstream PWC Readout Electronic Group" (Dataway Commands Required for Readout Electronics)	B. Wadsworth et al.	No. 17a (to replace No. 17)	2-2-72

"Proposed Physical Requirements for Experiment No. 154"	R. K. Yamamoto	No. 18	1-4-72
"PHS Coordinate System; Conventions for Locating PWC Planes; Preliminary Specifications of PWC Positions and Orientations"	T. Ludlam	No. 19a (replaces No. 19)	6-13-72
"Downstream PWC Development"	J. Wolfson	No. 20	3-25-72
"Upstream PWC Readout Electronics Group" (Computations for Beam Line Cabling)	B. Wadsworth et al.	No. 21	3-15-72
"NAL 30 in. B. C."	T. W. Ludlam et al.	No. 22	5-30-72
"Position Errors in Upstream Proportional Wire Chambers"	A. Snyder et al.	No. 23	6-26-72
"30" B.C. data Box Readout for PHS"	D. V. Petersen	No. 24	7-14-72
"Track Reconstruction in the 30" B.C."	P. Trepagnier	No. 25	9-8-72
"Track Trajectories in Some Typical N.A.L. Events"	R. Hulsizer	No. 26	6-25-73
"30" Bubble Chamber Beam Description and Tuning Procedure"	D. Petersen	No. 27	Fall '73
"Utility Programs and System Performance Exp. 154 Sept. (200 GeV Protons) and Nov. (150 GeV Protons) Runs"	W. M. Bugg	No. 28	1-15-74
"Updated GEOMAT/PWGP Tape Format"	C. Hafen et al.	No. 29	3-18-74
"Brief Summary of Survey Results for Experiment 154"	W. M. Bugg	No. 30	8-9-74
"Summary of Performance Characteristics of Hybrid-PWC Compared to Hybrid-Wide Gap System	W. M. Bugg	No. 30a	8-74
"Selection of .2 GeV/c to 1.4 GeV/c Protons Using PEPR ionization Measurements"	D. Ljung	No. 31	10-10-74
"Pivot Points on Trajectories of Tracks Leaving a Magnetic Field; Accuracy of Momentum of Tracks in the Hybrid Chambers at FNAL"	T. L. Watts	No. 32	11-8-74

"A Brief Description of Track Organizer and The Meaning of MULT on the DST"	D. G. Fong	No. 33	12-4-74
"Study of the Feasibility of Using SQUAW to Fit 4C Events at 150 GeV/c Part I"	J. Grunhaus	No. 34	12-13-74
"Input Formats of Cerberus 2"	P. Trepagnier	No. 34a	2-17-75
"Geometrical Acceptance of the Forward Gamma Detector"	R. L. Plumer	No. 35	5-21-75
"Secondary Tracks in Multiwire Proportional Counters at the NAL 30" Bubble Chamber"	D. Fong et al.	No. 36	5-73
"Removal of Ambiguities by Track Organizer"	D. G. Fong	No. 37	8-18-75
"The Modifications to the SQUAW Input Bank Made by Track Organizer"	D. G. Fong	No. 38	7-2-75
"How Bubble Chamber and PWC Data are Merged by Track Organizer"	D. G. Fong	No. 39	7-29-75
"K^+ Beam Enrichment Studies"	H. Rubin T. Ludlam	No. 40	9-75
"Description of Programs STXPRT-4, STYXIN-4 and STY2T4"	P. Lucas	No. 41	1-21-77
"A Modification in How Bubble Chamber and PWC Data are Merged by Track Organizer"	J. E. Brau	No. 42	3-10-77
"Version 2 of Scan Rules for Fermilab $\pi^+/K^+/p$ 150 GeV/c Experiment E-299 with the Fermilab Hybrid Spectrometer	E. S. Hafen R. I. Hulsizer	No. 43	5-2-77
"In Search of H Production in π^-p Interactions at 147 GeV/c"	O. Benary	No. 44	5-20177

Technical Notes - PHSC

1. Measurement Errors Using Downstream Detectors with the 30-inch Bubble Chamber at NAL, T. Ludlam, April 21, 1971.

2. Summary of 6/22/71 Discussions with Lach and Co., R. K. Yamamoto, June 24, 1971.

3. Software Projects for Phases I and II, R. K. Yamamoto, June 24, 1971.

4. Survey Requirements for Proportional Wire Chamber Hybrid Spectrometer, I. A. Pless, 1971.

DPI (ISIS) Notes

1. The Downstream Particle Identifier for the Fermilab Hybrid Spectrometer, V. Kistiakowsky et al., DPI Note No. 1, January 12, 1977.

2. ISIS Bibliography, V. Kistiakowsky, DPI Note No. 2, January 2, 1977.

3. High Voltage Breakdown Studies for the Fermilab, J. B. McManus et al., July 14, 1977.

4. Fermilab ISIS Electric Field Study, Seog Oh, DPI Note No. 4, June 1977.

5. Acceptance and Resolution Studies for the Fermilab ISIS, T. B. Stoughton et al., DPI Note. No. 5, July 27, 1977.

Engineering Notes

1. Effects of Stress on Glass Fiber Light Guides, J. T. Bober and J. Mayersohn, APC Eng. Note No. 4, June 1975.

2. A Study of the Properties of a Strobe/Lead-Glass/Phototube System, J. T. Bober and J. Mayersohn, APC Eng. Note No. 5, June 1975.

3. A Drift Chamber Scheme for High Event Rate, High Multiplicity Applications, B. F. Wadsworth and P. Marcato, APC Eng. Note 76-1, July 28, 1975.

4. Implementation of Beam Time Encoding for Drift Chambers Using Various Digitizing Schemes, P. Marcato and B. F. Wadsworth, APC Eng. Note 76-2, July 28, 1975.

5. A 5 x 5 Lead Glass Block Hodoscope, J. T. Bober and T. A. Frank, APC Eng. Note 76-5, June 1, 1976.

6. A Study of the Properties of a LightGuide/Prism/Lead Glass System, N. Cronin, APC Eng. Note 77-1, October 5, 1976.

7. PWCMUX, P. Marcato, APC Eng. Note 77-3, July 18, 1977.

APC Engineering Note 76-1

Bernard Wadsworth and Paolo Marcato

28 July 1975

A Drift Chamber Scheme
for High Event Rate, High Multiplicity Applications -

a study presented in part at a meeting of the PHS Consortium

held 16 April 1975

at 575 Technology Square, Cambridge, Massachusetts

The APC Engineering Notes are a form of aide memoire for the Accelerator Physics Collaboration and are intended primarily for internal circulation.

Laboratory for Nuclear Science

MASSACHUSETTS INSTITUTE OF TECHNOLOGY

Summary

A drift chamber has been included in the improvements proposed for the Proportional Hybrid System (PHS) at Fermilab. A preliminary study of digitizing techniques and system configurations for the readout electronics has been made with a view to selecting the combination most likely to meet the requirements imposed on the drift chamber in this application.

A byproduct of this study is the subject of this note: the development of a new approach to handling digitized information from drift chambers, which we call Beam Time Encoding. For a very minimal increase in hardware, beam-time encoding greatly enhances the event rate capability of a drift chamber and allows greater freedom in the choice of some of the chamber parameters. Other advantages to be gained by using this technique include continuous monitoring of the chamber drift velocity and discrimination against background particles.

Contents

		Page
	Summary	(i)
1.	Introduction	1
	1.1 Outline of existing PHS hardware	1
	1.2 Proposed improvements for PHS	2
2.	Beam Time Encoding: a new approach to handling digitized information from drift chambers	4
	2.1 Review of properties of a single drift plane	4
	2.2 Proposed changes in digitizing information	6
	2.3 Sorting algorithms	7
	2.4 System requirements	10
	2.5 Extension to 3-plane/2 coordinate configuration	12
	2.6 Minimum temporal separation of beam particles	15
	2.7 Inclined tracks	18
3.	Conclusion	25
4.	Acknowledgments	28
5.	References	28

1. Introduction

1.1 Outline of existing Proportional Hybrid System (PHS) hardware.

The proportional hybrid system installed and operating at FNAL consists of a system of proportional wire chambers (PWC's) used in combination with the 30-inch bubble chamber. The essential beam-line components of the system are shown schematically in figure 1.

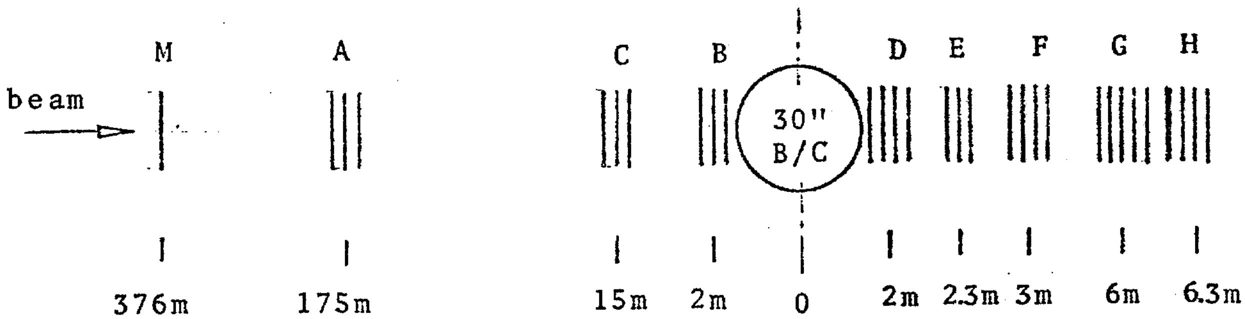

Figure 1
Proportional Hybrid System: Existing Beam Line Components

The upstream portion is a beam telescope consisting of 3 PWC's, A, B, and C. Each chamber contains 3 planes oriented at 120^0 intervals. Each plane measures 9.6 cm x 9.6 cm and contains 48 wires with 2mm wire spacing. A similar plane, m, with only 20 sense wires activated, is positioned at the momentum slit 326 m upstream. Signals from a scintillator telescope (detectors at A and B) provide a master gate which strobes the sense wire data into temporary storage in the readout electronics. A Çerenkov counter located approximately 463 m upstream provides tagging information which is transmitted to the readout electronics and stored along with the coordinate data from the PWC's.

Downstream from the 30-inch bubble chamber, there are 5 PWC's, D through H. The planes in these positions measure approximately 31 cm x 31 cm and contain

156 wires with 2mm wire spacing. The planes in a given chamber are oriented at 120^0 intervals. At the more critical orientations, there are actually 2 planes staggered by an amount equal to half the wire spacing to give increased spatial resolution. The coordinate axes of the chambers are all rotated (about the beam axis) slightly with respect to one another to minimize the redundancies in the system and to facilitate unscrambling of the coordinate data from multiparticle events.

Chamber H is a gamma detector: a lead sheet, approximately 6mm thick, is placed in front of 3 planes. In each plane, the sense wires are connected in groups of 3 to provide 6mm spatial resolution.

Sense wire data for up to 16 beam tracks/beam spill can be accepted at a 10MHZ rate (50nsec wide master gate, followed by 50nsec dead-time) and stored in the readout electronics pending transmission to the computer at the end of the beam spill.

The whole system was designed in 1971 and contains some 3100 wires. The upstream portion was installed in 1972 and became an FNAL user facility in December 1972. The downstream portion was installed in mid 1973 and has been used in 6 experiments to date.

1.2 Proposed improvements for PHS

Possible improvements in the PHS detector components have been studied and reported on by the Plano Committee.[1] Basically, three areas of improvement are proposed:

1) Increased acceptance to be obtained by increasing the size of the downstream detectors from their present 0.3m to 1.2 - 1.5m. The detectors will consist of a mix of PWC's, which can trigger the B/C flash lamps on events of interest, and drift chambers for economy and increased spatial resolution.

2) A forward gamma detector (FGD) with the ability to detect and measure the angles and energies of γ rays.

3) A spectrometer arm to provide accurate momentum measurements of tracks with momenta above 50 GeV/c.

Our concern in this note is the drift chamber which is to be used in conjunction with the Forward Gamma Detector shown in figure 2.

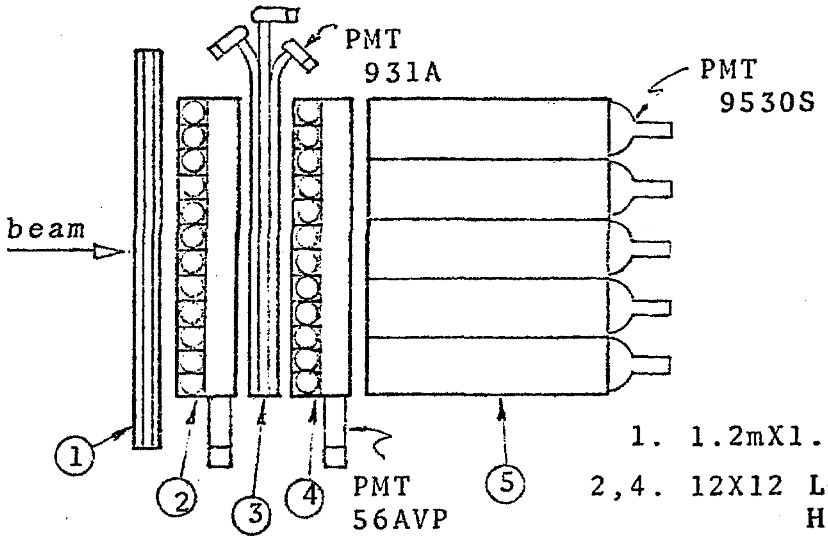

1. 1.2mX1.2m Drift Chamber

2,4. 12X12 Lead Glass Block Hodoscope

3. 75cmX75cm Vertex Detector Scintillation Hodoscope

5. 5X5 Lead Glass Block Hodoscope.

Figure 2. Forward Gamma Detector

In addition to providing greater acceptance in the downstream system, the drift chamber will tag charged particles entering the FGD.

The drift chamber proposed in the committee report was to have the following properties:

3 planes oriented at 120^0 intervals

drift space 2cm
drift velocity 5cm/μsec } max drift time 400nsec

overall dead-time 1μsec
using beam spill time of 300 μsec and 10 beam particle/spill } 3% of events will be lost

2. New approach to handling digitized information from drift chambers.

In this section, we consider the requirements imposed on a drift chamber in our particular application which is characterized by high event rates and high multiplicities. We propose a scheme by which the event rate capability of the drift chamber can be increased from 1MHz (implied by the 1μsec dead-time quoted in the committee report) to approximately 50MHz. This would more than match the performance already achieved with the PWC's in the system.

2.1 Review of properties of the single-plane drift chamber.

Figure 3 shows a partial cross section (orthogonal to the sense wires) of a drift chamber and serves to illustrate two shortcomings of the single plane drift chamber.

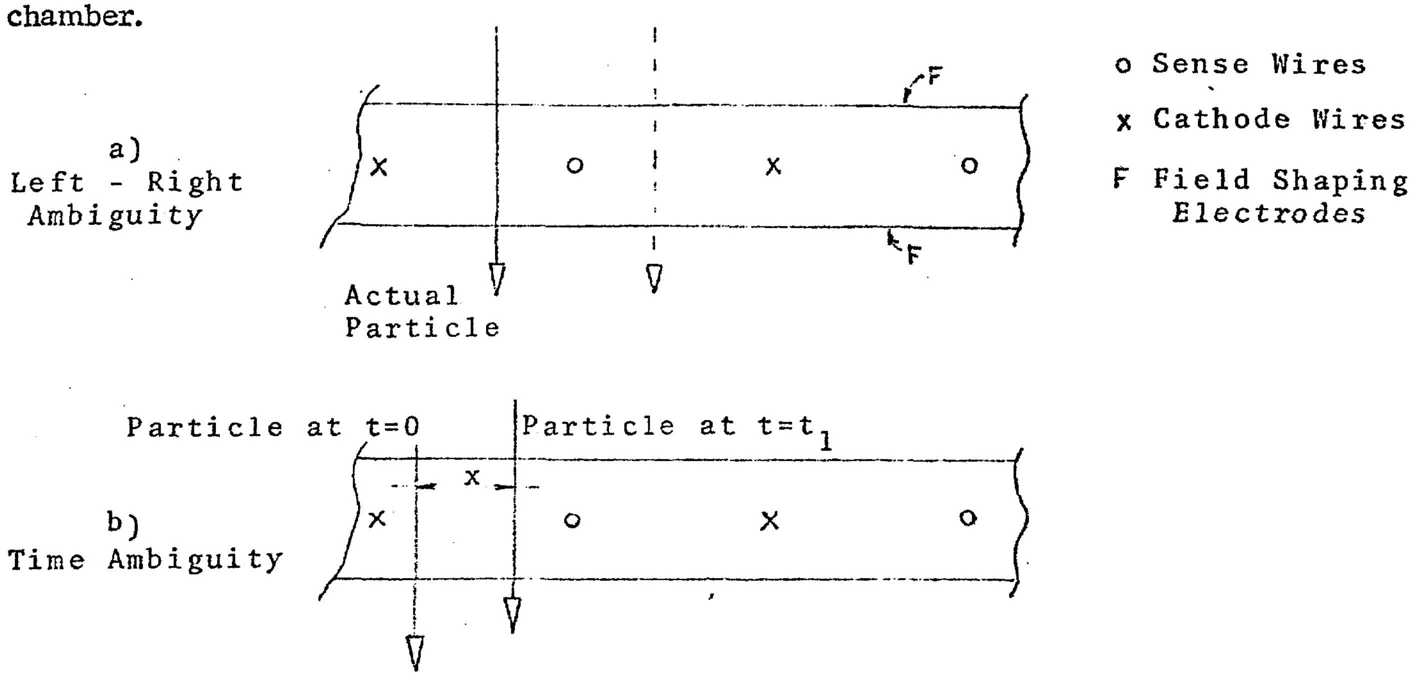

Figure 3. Ambiguities in Data From a Single Drift Plane

In practice, an external trigger signals the instant a particle traverses the chamber. With this as a reference, the electronics associated with each sense wire digitizes the time of arrival of the primary electrons at the wire. Wire signals are admitted to the digitizing channels until the maximum drift time has expired, at which point the time reference is reset to zero.* For a given particle and its associated digitized drift time, there are two possible locations of the track: one on either side of the sense wire and spaced equidistantly from it, giving rise to the so-called left-right ambiguity.

A further complication arises when two or more particles traversing the plane are separated in time by an interval less than the maximum drift time. The timing electronics is referenced to the passage of the first particle and there is no way of correctly associating the signals received at the sense wire with one or other of the particles. For example, in fig. 3(b), the particles are separated in time by t_1 and in space by a distance x. If the drift velocity v_d is such that $\frac{x}{v_d} > t_1$, the primary electrons from the second track will actually be the first to arrive at the sense wire.

Even if there is only one particle in the cell, due to one of two beam particles which entered the system in quick succession, there is still the problem of assigning this particle to the correct beam particle. Thus, the size of the drift space would appear to place a limit on the maximum event rate the plane can handle.

Drift chambers, in addition to providing increased spatial resolution as compared with PWC's, are also supposedly more economical: for a given detector size, the drift chamber requires fewer sense wires and sense amplifiers and fewer digitizing channels.** The next section discusses a new approach to handling drift chamber data which effectively frees the cell size from event rate considerations and which therefore allows further economies to be exploited.

---

* In the remainder of the note, this is referred to as the conventional approach.

** However, the digitizing channels of a drift chamber are necessarily more complex than those required for a PWC; and it seems to us the major portion of the savings achieved by using the drift chamber comes as a result of the need for fewer sense amplifiers.

2.2 Proposed changes in digitizing information.

To illustrate the new approach, we restrict our attention to a single coordinate system. We begin by adding a second plane in which the sense wires are parallel to those in the first, but offset as shown in figure 4. For the time being, we consider only tracks normal to the drift planes.

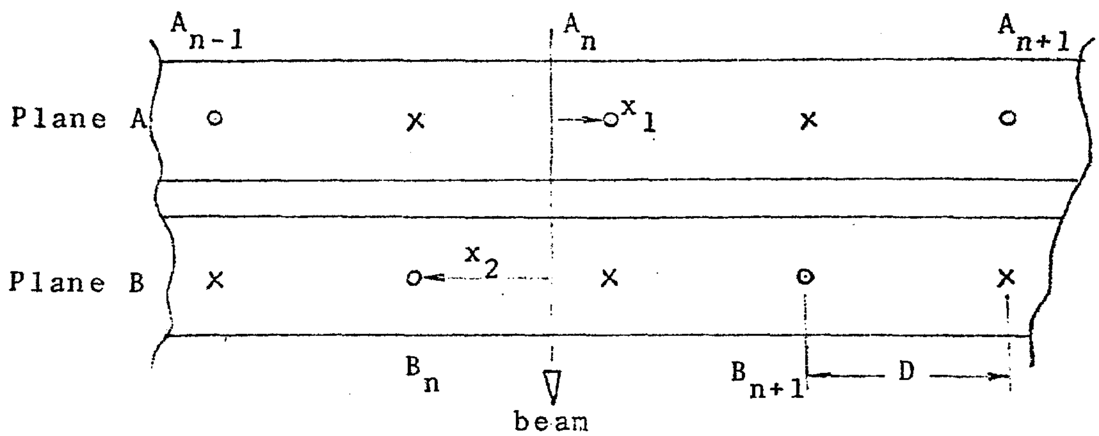

Figure 4. 2-Plane, Single Coordinate System

The first benefit obtained from such a configuration is removal of the left-right ambiguity and this aspect has been noted previously in the literature.[2] In the example shown in the figure, signals at sense wire A_n (wire n of plane A) and sense wire B_n will unambiguously place the track in the space between those two sense wires.

Another aspect of this configuration is that a tight constraint is imposed on the time digitizings recorded in channels A_n and B_n: the sum of the drift times, $t_1 + t_2$, is constant and equal to the maximum drift time.*

To make use of the constraint provided by the addition of a second plane, we digitize the time of arrival of the beam tracks at the system. This requires one additional channel of readout electronics and the use of a real time clock providing digitizings referenced to the beginning of the beam spill. The time of arrival

---

* This assumes the drift time is a linear function of the drift distance, which in practice is not the case. It is the sum of the actual drift distances, $x_1 + x_2$, which is constant and equal to half the cell size. The point is clarified in Section 2.3.

of sense wire signals is also digitized according to the same time reference We now have information that is not available in the conventional system; namely, the time between beam tracks. This added information, in conjunction with the constraint described above, is sufficient to allow unscrambling of sense wire data for any number of tracks arriving in an interval equal to the maximum drift time.

2.3 Sorting algorithms

The data recorded for a beam spill are the digitized time of arrival of signals at each sense wire during the spill, plus an additional channel containing the digitized time of arrival of beam tracks at the system. Figure 5 shows a partial listing.

Plane A, wire n A_n	Plane B, wire n B_n	Beam Time (corrected)
t_{An1}	t_{Bn1}	t_{b1}
t_{An2}	t_{Bn2}	t_{b2}
t_{An3}	t_{Bn3}	t_{b3}
t_{An4}	t_{Bn4}	t_{b4}
t_{An5}	t_{Bn5}	t_{b5}
		.
		.
		.
		.
		t_{bn}

Figure 5. Partial Listing of Data at end of beam spill

The number of entries in the beam time channel is just the number of beam particles which entered the system during the beam spill. The number of entries in channels A_n and B_n can be more or less than the number of beam particles. Channels A_n and B_n do not necessarily contain the same number of entries since each can contain information not associated with the other, e.g., channel B_n can contain information related to entries in channel A_{n-1}.

The data are examined off-line using algorithms which attempt to correctly associate the data in the two columns with the data recorded in the beam channel. The data are taken in triads and tested: e. g., for the triad t_{Anj}, t_{Bnk}, t_{bm}

$$(t_{Anj} - t_{bm}) + (t_{Bnk} - t_{bm}) = \text{Max. drift time, } T_d \quad \ldots 2.3.1$$

Drift time for jth signal received at wire A_n if this were associated with mth beam particle

Drift time for kth signal received at wire B_n if this were associated with mth beam particle

If equ. 2.3.1 is satisfied, then we have correctly associated two sense wire signals with a beam particle, and entries t_{Anj} and t_{Bnk} can be removed from the bank.

Two important qualifications apply to equation 2.3.1

a) the beam time is derived from a scintillator telescope. Consequently, a correction should be applied to the entries in the beam channel when testing data in planes A and B to account for the time of flight from the beam telescope to planes A and B, as well as for relative delays in the signal cabling and electronics.

b) as mentioned in the footnote on p. 6, drift time vs. drift distance will generally be nonlinear. For a given chamber construction, the relation of drift time vs. drift distance will be a measurable and known function. That is, we can express the drift distance by $x = f(t)$, in which case equation 2.3.1 is replaced by the more rigorous equation 2.3.2.

$$f(t_{Anj} - t_{bm}) + f(t_{Bnk} - t_{bm}) = \text{Max. drift distance, } D \quad \ldots 2.3.2$$

If a triad of data fails the test, then the data must be retained but a new combination tried. Figure 5 shows that several attempts were necessary before determining that t_{An_2} and t_{Bn_3} were associated with t_{b_2}, and that t_{An_3} and t_{Bn_2} were associated with t_{b_3}. This indicates that the second and third beam particles were separated in time by an amount less than the maximum drift time.

Since only some fraction of the data will be generated by bunched beam tracks, the off-line sorting can be accomplished more quickly in two steps.

1) The beam time encodings should be examined. If, for example, $t_{b_2} - t_{b_1} > T_d$, then all the sense wire data related to the first beam particle can be separated from the table and moved to a secondary bank by testing individual entries: $t_{b_1} < t_{entry} < t_{b_1} + T_d$.

Using figure 5 as the example, $t_{b_3} - t_{b_2} < T_d$, so we expect intermingled data for the second and third beam tracks.

Next, $t_{b_4} - t_{b_3} > T_d$, therefore the intermingled data are restricted at this point to only the second and third beam tracks. The data for these beam tracks are moved to another secondary bank by testing individual entries $t_{b_2} < t_{entry} < t_{b_3} + T_d$.

Next, $t_{b_5} - t_{b_4} > T_d$, therefore all data for the fourth beam track can be separated by testing $t_{b_4} < t_{entry} < t_{b_4} + T_d$. And so on.

2) The data in each secondary bank are tested according to equation 2.3.2. This will correctly pair the sense wire data and, in addition, correctly associate these pairs with the proper beam particle in the case of intermingled data.

The purpose of the first step is to provide a first order separation of the data, thereby restricting the range of entries to which the more complicated second step is applied.

The final result is that all the data have been correctly associated with the proper beam particles where these particles can be separated by as little as the pulse-pair resolution of an individual digitizing channel, namely, 25-50nsec. Entries which remain in the primary bank and which cannot be paired successfully can be caused by:

a) one of two particles in a multiparticle event which generate the same measurement in one of the planes. That is, two of the particles traversed a plane at the same distance from a particular sense wire, either on the same or opposite sides of it.

To check this, the remaining piece of data is tested with entries (already successfully paired with other data) for the appropriate wires in the other plane, generated by the same beam track.

b) a beam track trailing another by less than t_r, the pulse-pair temporal resolution of the digitizing channels. A flag generated elsewhere (in the PWC system) indicates the presence of such a closely spaced beam track. If this flag is set, the remaining data might be paired successfully by using a beam time equal to the leading beam track's time plus $\frac{t_r}{2}$, and relaxing the tolerance on the constraint equation by an amount equivalent to t_r.

or c) failing a and b above, the remaining data must be due to incoherent background.

2.4 System requirements.

We now consider in a little more detail what is involved in incorporating this proposed digitizing scheme into the system.

First, consider the basic parameters of the drift chamber as proposed

Size of chamber/plane	1.2m	
Drift space* (anode-cathode wire spacing)	5cm	
Drift velocity	5cm/μsec.	2 nsec. least count
Least count	100 μ	
Maximum number of beam particles/spill	16	
Beam spill duration	300 μsec.	

Capacity of the real-time clock:

The real-time clock introduced in section 2.2 above measures time from the beginning of the beam spill which is defined for us by the arrival of the first beam particle. The clock is not run continuously throughout the beam spill, as its

* We take advantage of the new scheme to increase the drift space from 2 to 5 cm. The cell size (left plus right drift spaces) is therefore 10cm, which implies a total of 36 wire signal channels for the chamber.

name might lead one to suspect: with a least count of 2nsec and a beam spill duration of 300μsec, this would require a scaler capacity of 18 bits if the scaler were to run continuously.

It should be clear by now that an important function of the clock is to time the interval between bunched tracks. And if the interval is greater than T_d, then we are not interested in the actual time between the beam particles; it is sufficient to know that they are separated 'cleanly.'

Consequently, the beam particles are used to generate gates which allow the digitizing channels to accept data from the sense wires. The clock is run during the gating interval and continues to run for a short time following the termination of the gating interval, see figure 6. Signals from the sense amplifiers are admitted to the system for a time equal to the maximum drift time, 1μsec., and the clock is allowed to run for, say 1.1μsec.

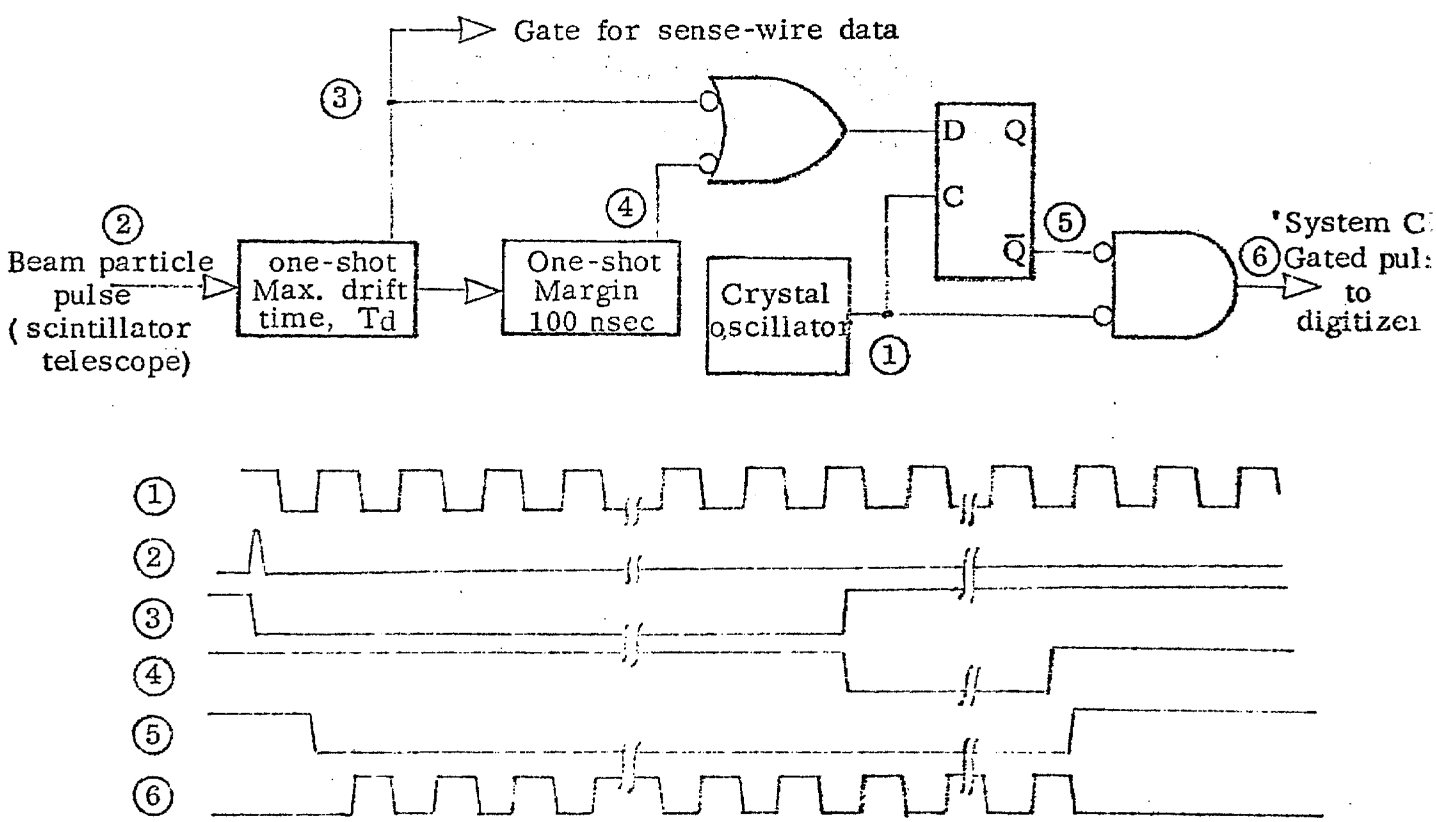

Figure 6. Pseudo real-time clock.

This conserves the 'real time' clock scaler capacity and therefore minimizes the number of bits which must be stored as sense wire data. But, it also provides enough margin so that in the off-line sorting of the data, most of the entries can be sorted on an individual basis as described in step 1, section 2.3.

Gating the sense wire data into storage using the beam track information means that no increase in the number of storage locations is required over that required for a conventional system.

We allow the real time clock to run for 1.1μsec. and provision is made for a maximum of 16 beam particles. Therefore, the maximum running time of the clock is 16 x 1.1 = 17.6μsec. With 2nsec. least counts, this implies time digitizings of 1 part in 8800, or 14 bits.

As a comparison, a conventional digitizing scheme for a drift chamber would require time digitizings of $\frac{1\mu sec.}{2nsec.}$, i.e., 1 part in 500, or 9 bits. Plus 4 bits to associate the data with one of 16 beam tracks, for a total of 13 bits.

2.5 Extension to 3-plane/2 coordinate configuration.

In section 2.2, we considered a simple 2-plane/single coordinate configuration and showed how the spatial constraint it offers, in conjunction with beam-time encoding, enables us to correctly associate sense wire data with the proper beam track.

A similar spatial constraint can be obtained by using 3 planes oriented at 120° intervals. Figure 7 illustrates the familiar Dalitz constraint provided by such a configuration. S_1, S_2, S_3 are sense wires in three separate, superimposed planes.

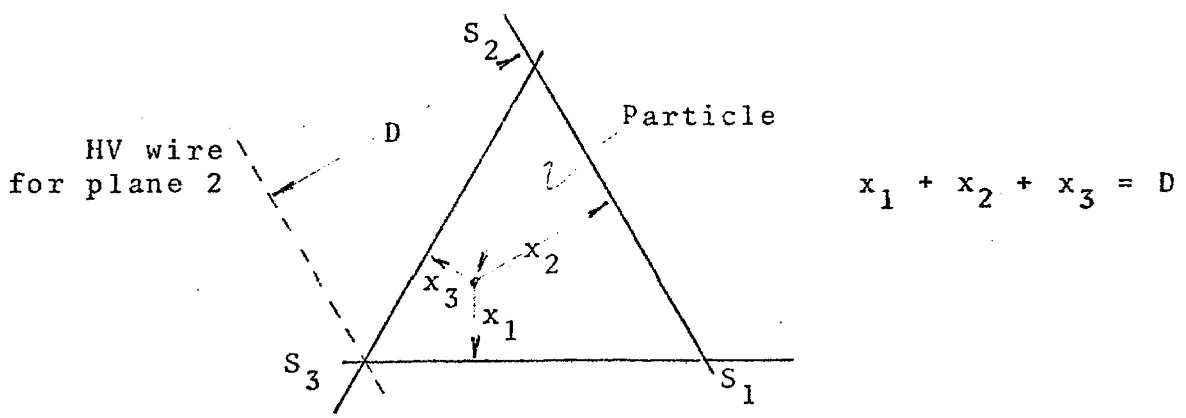

Figure 7. Superposition of 3 drift planes at 120° intervals to provide spatial constraint on drift distances.

Figure 8 shows the basic cell formed by three sense wires. If a particle generates data on the three sense wires S_1, S_2, and S_3, it must have traversed the planes in one of four possible regions, labelled a, b, c, or d.

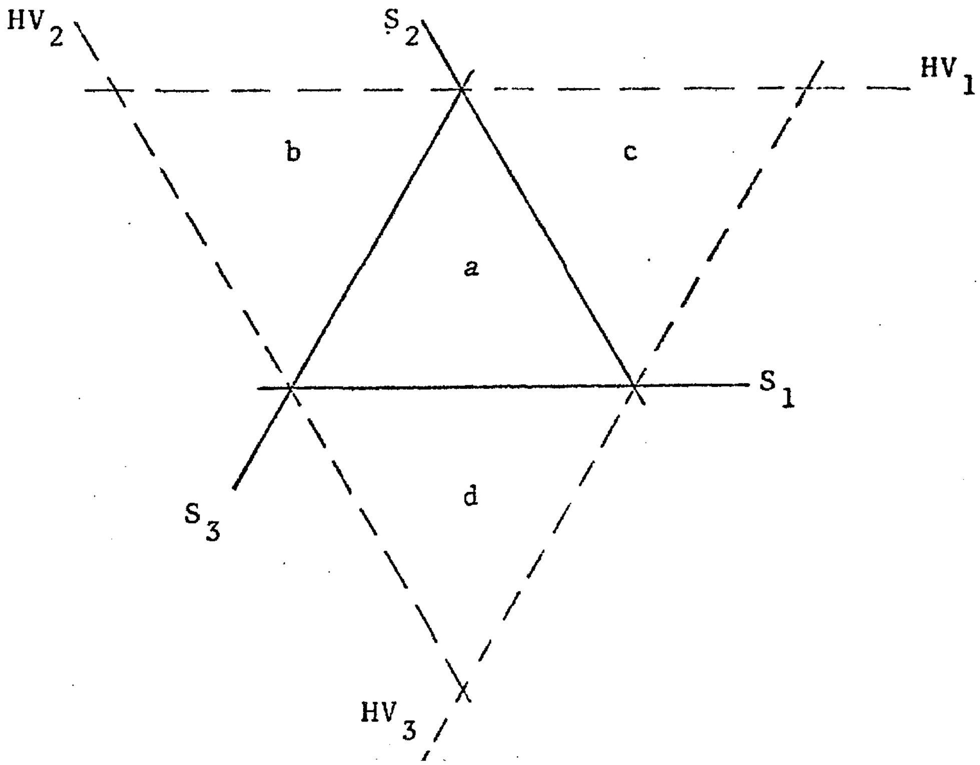

Figure 8. Four regions associated with sense wires S_1, S_2, S_3

In region a: $x_1 + x_2 + x_3 = D$

However, in regions b, c, and d, the Dalitz condition is modified slightly

$x_1 + x_2 - x_3 = D$ in region b

$x_1 - x_2 + x_3 = D$ in region c

$-x_1 + x_2 + x_3 = D$ in region d

In other words, each group of data (3 sense wire data + 1 beam-time encoding) must be examined in as many as four different ways before one can say whether or not it belongs to a single particle. The two-step sorting process as described in section 2.3 is seen to be even more desirable in this case.

---

* The aligament of the three planes as shown in fig. 8 is important. Specifically, one must not align the planes such that a projected triplet of sense wires intersects at a common point: if this were the case, 75% of the chamber's surface would yield ambiguous data.

Figure 9 illustrates a tendency towards ambiguity where a particle passes close to any HV wire. Figure 9(a) shows an overall view of the sense-wire triplet, a particle passing through point P, and the pairs of ordinate (dotted) lines generated in each plane. Figure 9(b) is an expanded view of the two regions P and P'. One combination of the ordinate lines intersects at P, but another set forms a small triangular region P'. When the dimensions of the triangle are comparable to the uncertainties in the track's location in each of the three planes, then P' represents an ambiguity. In our application (see Section 2.7), this uncertainty (a combination of measurement error, due mainly to thermal diffusion, and uncertainty in the track's orientation) can be as great as 0.5mm. That is, in a chamber with a 5cm drift space, ~ 1% of its area is susceptible to ambiguities.

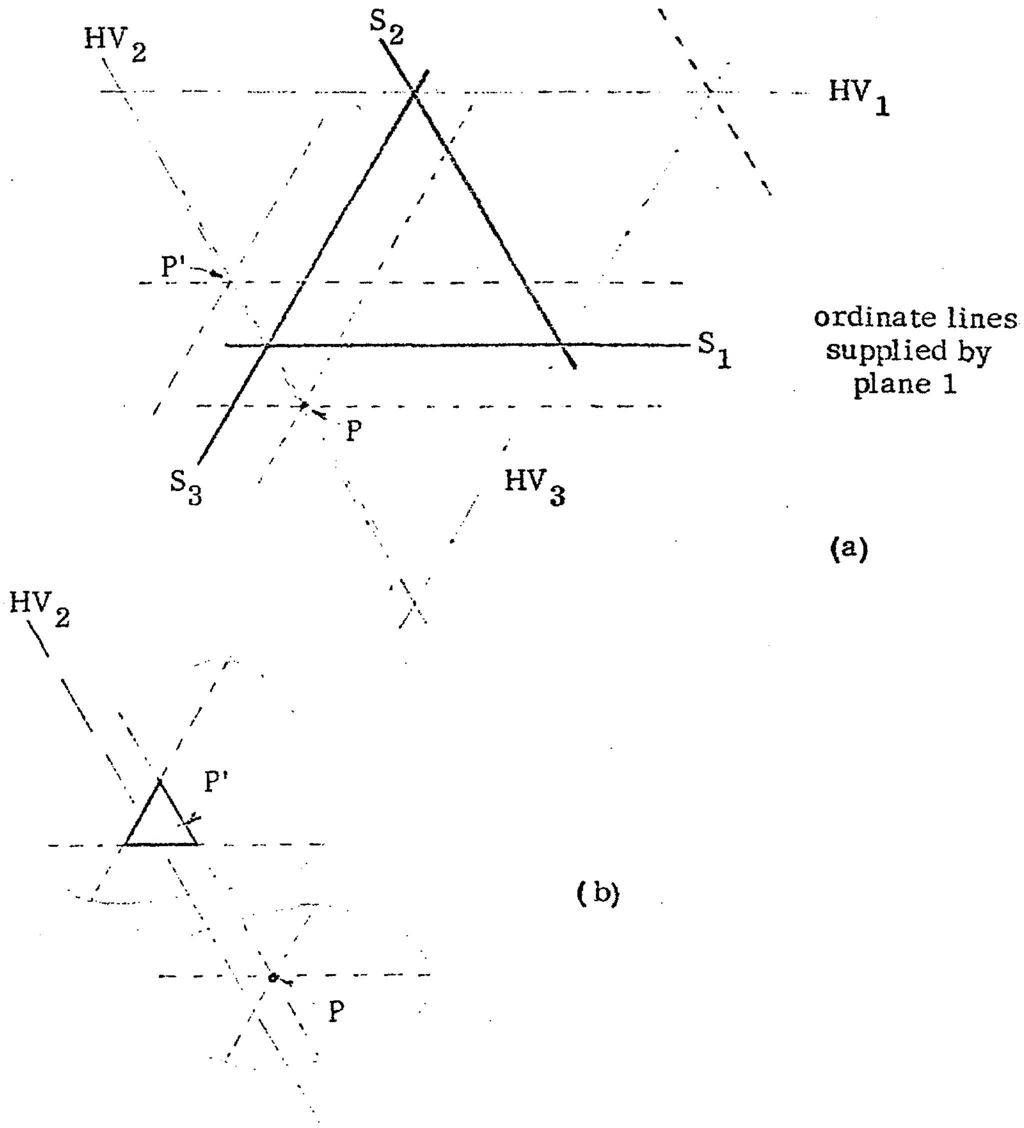

Figure 9 Showing tendency towards ambiguity.

2.6 Minimum beam track separation.

The minimum temporal separation of beam tracks which beam time encoding can handle, can be estimated from the following considerations.

We assume the accuracy of the individual drift time measurements is determined mainly by diffusion broadening of the primary ion swarm.

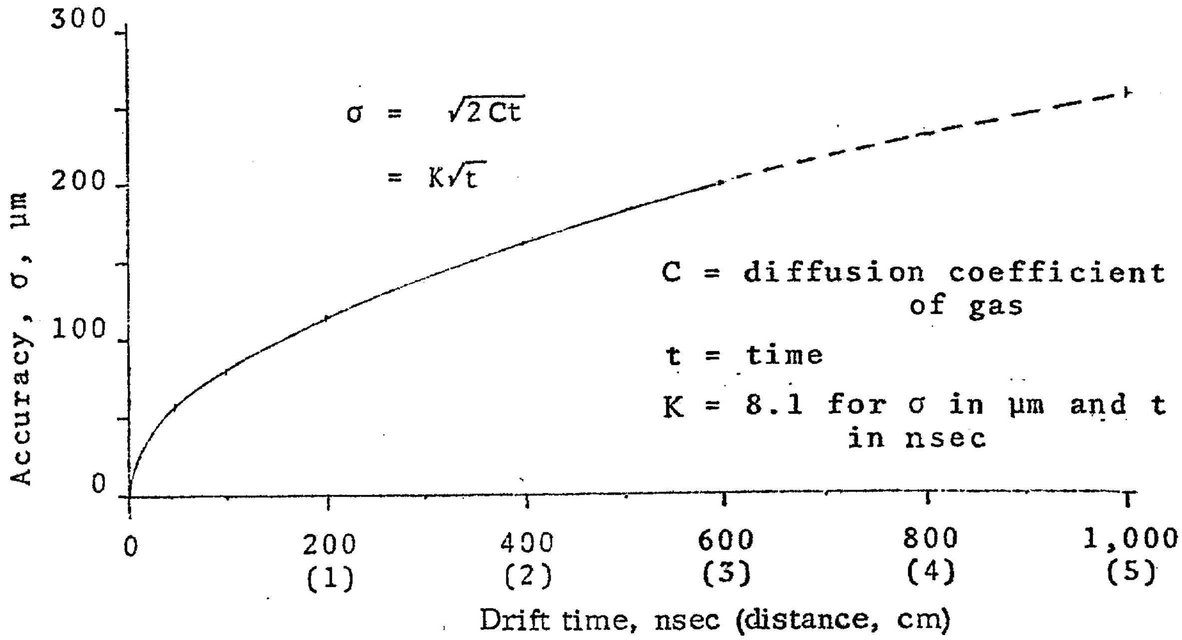

Figure 10.

Figure 10 shows a plot of the Einstein formula (describing the diffusion process) normalized to fit experimental data from a chamber with a drift space of 2.4mm.[3) *] We further assume that the accuracy of measurement over greater distances can be estimated by extrapolating the normalized curve; in which case, the intrinsic accuracy is approximately 260μ at 5cm.

If the appropriate error is applied to the individual ordinate measurements from each of the cells in a triplet, it is found that the overall error on the sum of ordinates is essentially constant at 260μ.

---

* The drift rate reported in Reference 3 was 4cm/μsec. Throughout this note we consider a drift rate of 5cm/μsec. Therefore, the independent variable (mm) in fig. 8, Ref. 3 is interpreted in terms of time (nsec) for fig. 10 of this note. Corresponding distances are also shown: they are computed for a drift rate of 5cm/μsec and are based on the assumption that C/μ (diffusion coefficient /electron mobility) for the gas remains constant as the drift rate is increased from 4 to 5cm/μsec.

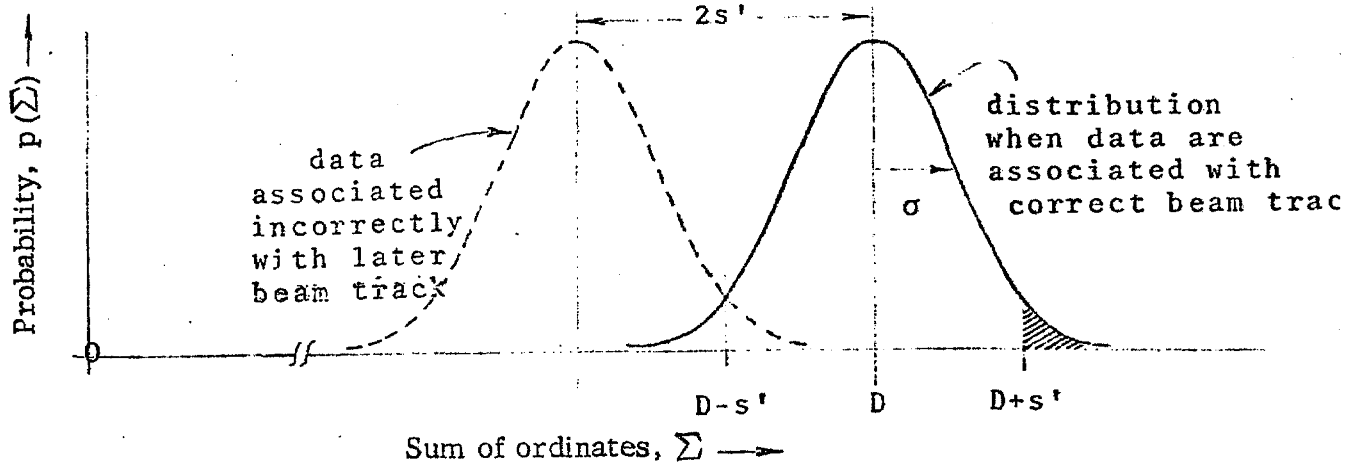

Figure 11. Probability distribution of sums of ordinates for particle generated by one of two closely spaced beam tracks.

Figure 11 shows the normal distribution of possible values for the sums of ordinates generated by a particle when associated with the correct beam track. The distribution peaks at D, the constant on the right-hand side of the constraint equation (2.3.2, p8). Shown also is the distribution generated by the same particle when associated with an incorrect (trailing) beam track. The separation of the two distributions is 2s', and it is clear that any measurement which falls to the right of D+s' in the correct distribution would certainly appear more acceptable (i.e., closer to the central value D) if the data were associated with the later beam track. If the closely spaced beam track is leading the beam track which generated the particle in question, there is no difficulty in correctly assigning the particle on the basis of a measurement falling in the upper portion of the distribution: an attempt to associate the particle with the earlier beam track will generate a sum of ordinates further removed from the desired value, D. Similar, complementary arguments apply to the samples lying below D-s' in the distribution.

The separation of the distributions can be expressed as $2m\sigma$ (i.e., $s'=m\sigma$) where m is a parameter we can vary to investigate the behavior of the system. For example, for $m=2$, the separation is 4σ and a total of approximately 4.6% of the samples lie outside the range $D - 2\sigma$ to $D+2\sigma$. Of these, 2.3% will be incorrectly associated as explained above.

A separation of 4σ or $4 \times 260\mu$ in the sum of ordinates is caused by an increment of $\frac{1040\mu}{3} = 347\mu$ in each of the three ordinates. At a drift velocity of 50μ/nsec. this represents a time difference of 7 nsec. That is, in situations where beam particles are separated by 7 nsec, particles in the drift chamber will be assigned to an incorrect beam particle about 2% of the time.

Considering other values of m allows one to make a plot, see figure 12, showing confidence level (that a given particle will be associated with the correct beam particle) versus temporal separation of the beam tracks.

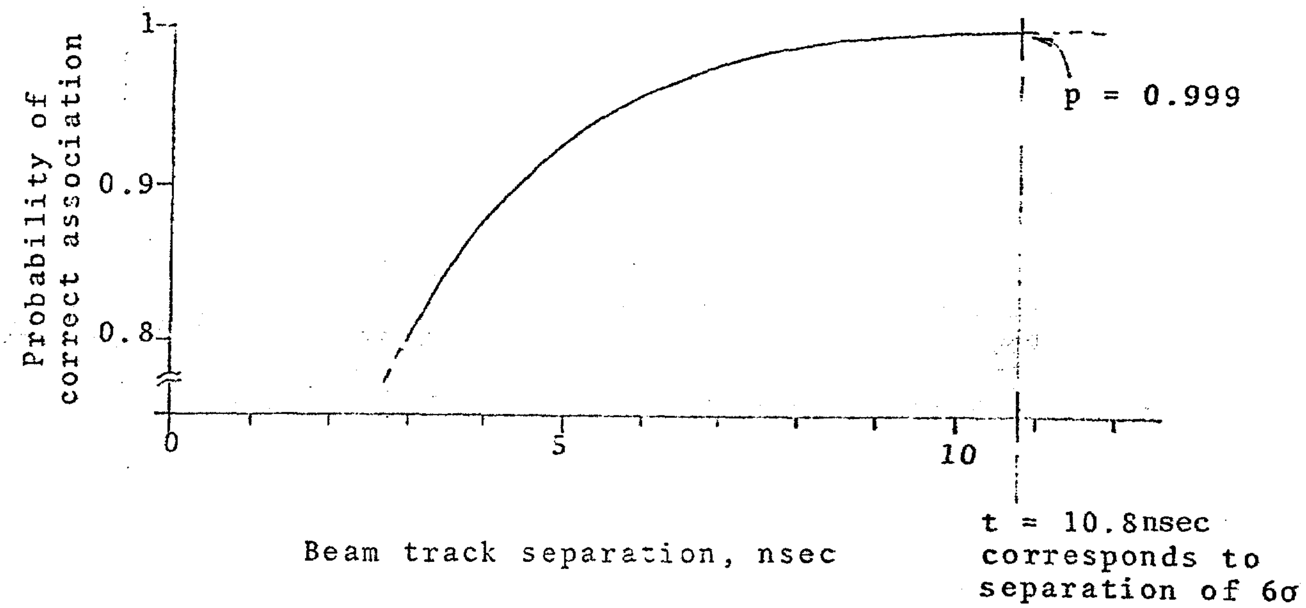

Figure 12. Confidence curve for correct association of data

2.7 Inclined tracks

The discussion so far has been based on tracks normal to the drift planes. In this section we examine the effects of inclined tracks.

Figure 13 shows the relevant geometry of the bubble chamber and drift chamber.

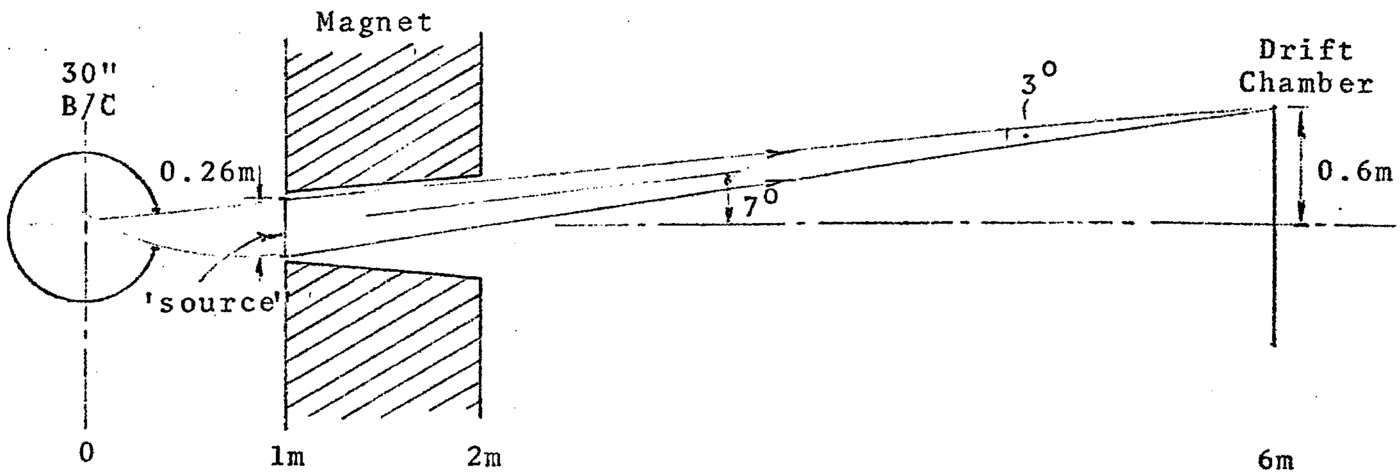

Figure 13. Relative positions of 30-inch B/C and Drift Chamber on FGD.

The modified chamber/magnet combination, referred to in the committee report[1], is shown. Taking into account the curvature of tracks due to the bubble chamber's magnetic field, the drift chamber can be considered illuminated by a source at the inside edge of the aperture in the bubble chamber magnet. This 'source' has a dimension of 0.26m and subtends a full angle of approximately 3^{0} at any point on the drift chamber. That is, one can compute the mean angle for the trajectory of a track entering a particular point in the drift chamber by constructing a line from that point to the center of the 'source'. This mean angle has a maximum value of 7^{0} at the edge of the drift chamber. But added to this, there is an uncertainty of $\pm 1.5^{0}$.

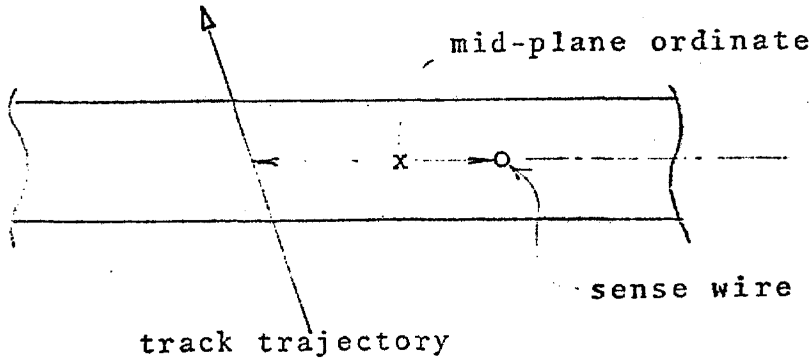

Figure 14. Inclined track passing through drift plane.

In dealing with an inclined track, see figure 14, we first assume that it is possible to compute the midplane coordinate x from the information supplied by the digitizing channel. Experimental results have been reported[4], which indicate that tracks up to 45^0 give predictable results in terms of track location provided the angle is known to within 10^0. For the chamber construction described in reference 4, the chamber signals behaved as simple geometrical considerations predicted. The error in track location was found to be ~ 0.5mm for an angle of 30^0 (not much greater than that reported for straight through tracks in the same series of tests).

In our application, we are considering angles up to 7^0 which are known to within 1.5^0 and, therefore, our starting assumption appears reasonable.

To apply beam time encoding to the data generated by a triplet of drift planes, the relative positions of the planes must first be adjusted to account for the mean track angle. Figure 15 shows the midplane points recorded by an inclined track passing through a triplet of cells, and the adjustment of the plane positions to arrive at the situation where the three midplane ordinate lines intersect at a point. Since we deal with the midplane ordinates, and since the drift still takes place in the plane of the drift chamber and not in the plane normal to the particle trajectory, the sense wires in this adjusted view remain oriented at exactly 0^0, 120^0, and 240^0.

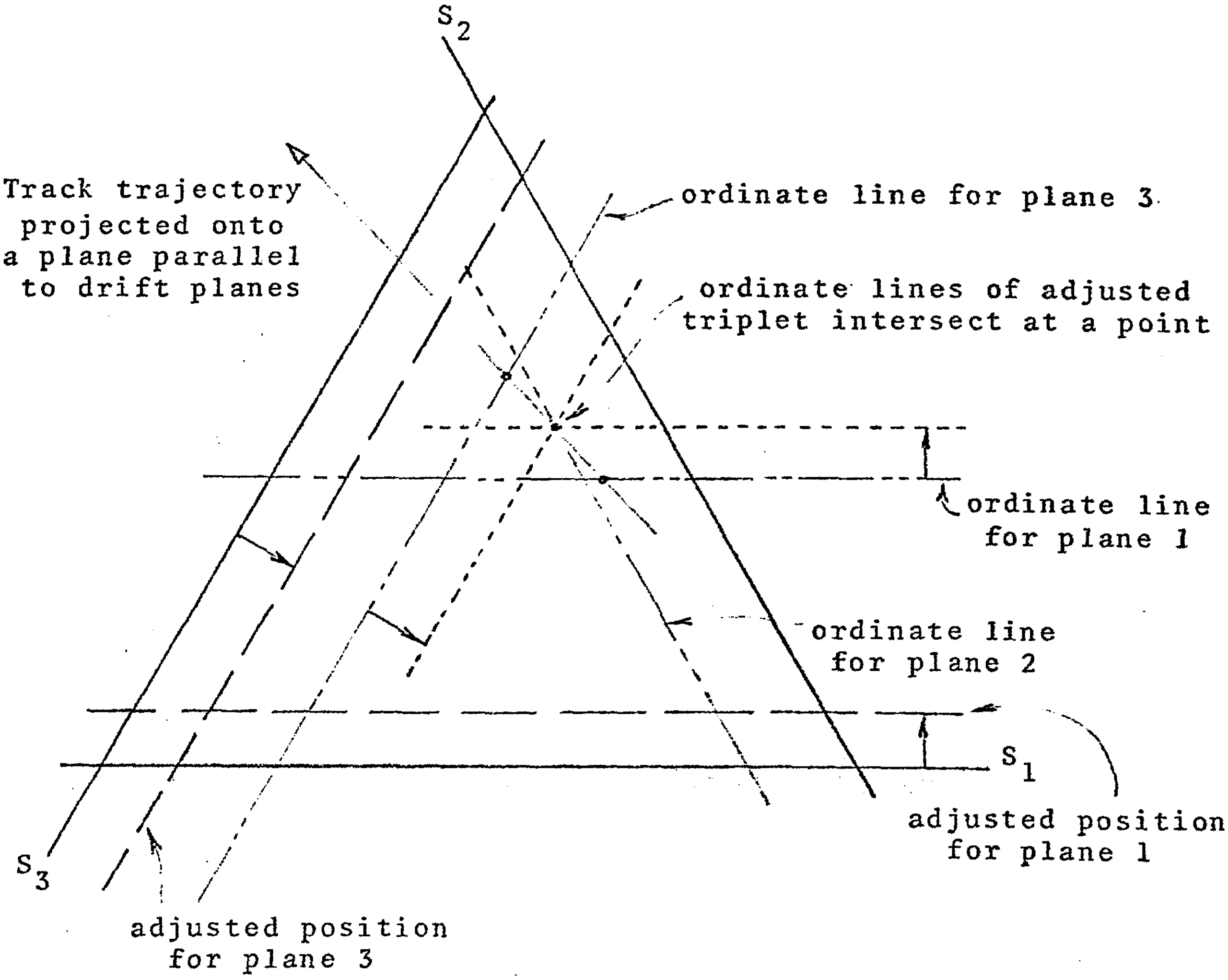

Figure 15. Cell triplet showing adjustments necessary to accommodate an inclined track. The adjustments are relative to plane 2 which is used as a reference.

Figure 16 shows a wider view of the triplet of planes, in this case adjusted to account for a track trajectory of mean angle 10^0 (to exaggerate the effect).

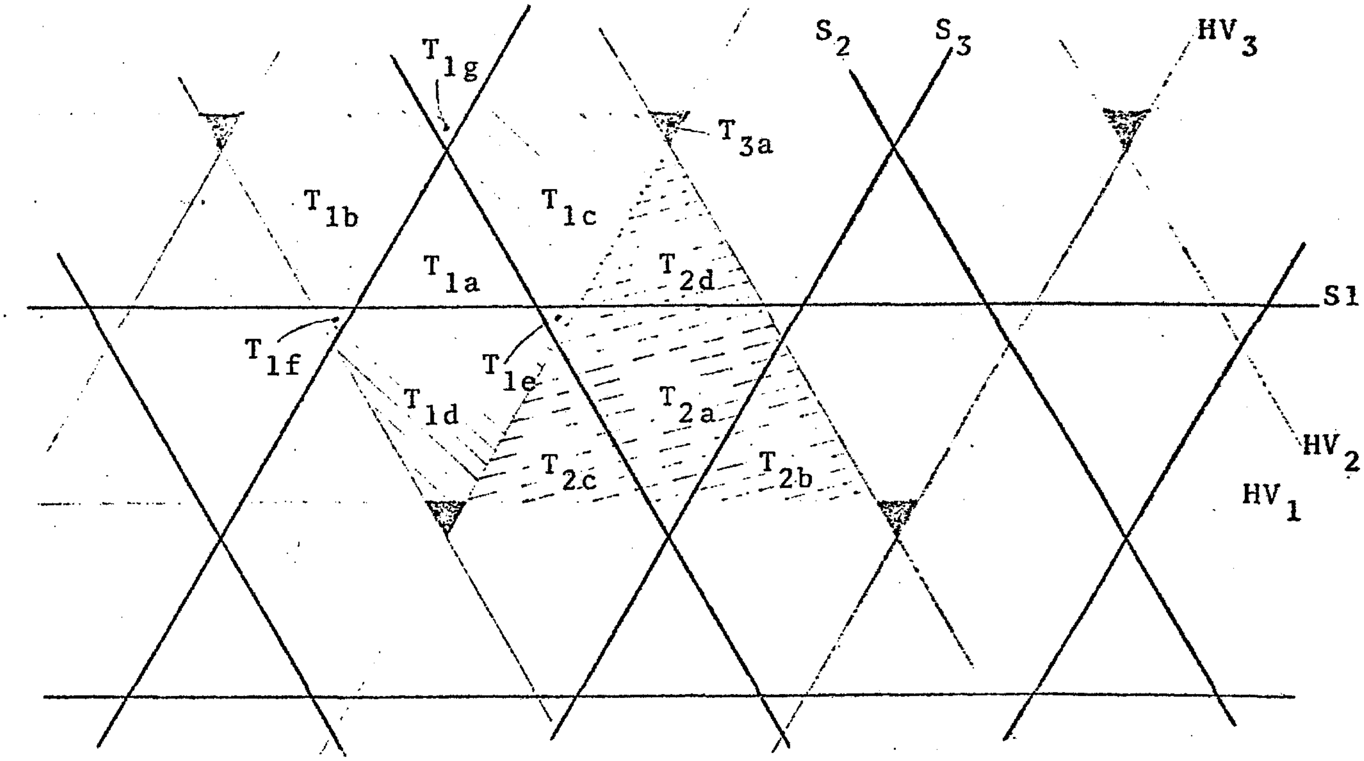

Figure 16. Triplet of planes adjusted for an inclined track.

The figure illustrates one immediate consequence of dealing with inclined tracks: the simple cell shown in figure 8 for a straight through track becomes the more complex pattern seen in figure 16, solid cross-hatched area or dashed cross-hatched area. Associated with each triplet of wires, there are now as many as seven regions which require consideration in the sorting process:

a) $$x_1 + x_2 + x_3 = K \qquad \ldots 2.6.1$$

b) $$x_1 + x_2 - x_3 = K \qquad \ldots 2.6.2$$

c) $$x_1 - x_2 + x_3 = K \qquad \ldots 2.6.3$$

d) $$-x_1 + x_2 + x_3 = K \qquad \ldots 2.6.4$$

e) $$-x_1 - x_2 + x_3 = K \qquad \ldots 2.6.5$$

f) $$-x_1 + x_2 - x_3 = K \qquad \ldots 2.6.6$$

g) $$x_1 - x_2 - x_3 = K \qquad \ldots 2.6.7$$

Data from cell triplet labelled T_1 require testing in only the first four constraint equations; data from the cell triplet T_2 must be tested in all seven. The constant K for each of these two cases is different. In fact, there is a small region (T_3, solid black in figure 16) in which tracks develop signals on a triplet of wires forming a larger triangle. The constant K will be correspondingly larger, and of course only equation 2. 6. 1 is applicable in this region.

In any case, for a track of known angle, the spatial constraint can still be applied with a tolerance limited only by the error on the individual ordinate measurements. *

The uncertainty in the angle of the inclined track requires a larger tolerance in the application of the spatial constraint as demonstrated in figures 17 and 18. Figure 17 is a cross section of the triplet in the plane defined by the actual track trajectory and the mean ray (the line to the center of the 'source'). Assuming the planes are no thicker than 15mm**, the effective offset of the midplane points is 0.4mm for an angle of 1.5^0. This is shown in figure 18, where the resulting ordinate lines form a small triangle. The sum of the ordinates is the left hand side of the constraint equation, and simple geometry shows this sum varies $\pm 0.4\sqrt{3}$, i.e., ± 0.7mm.

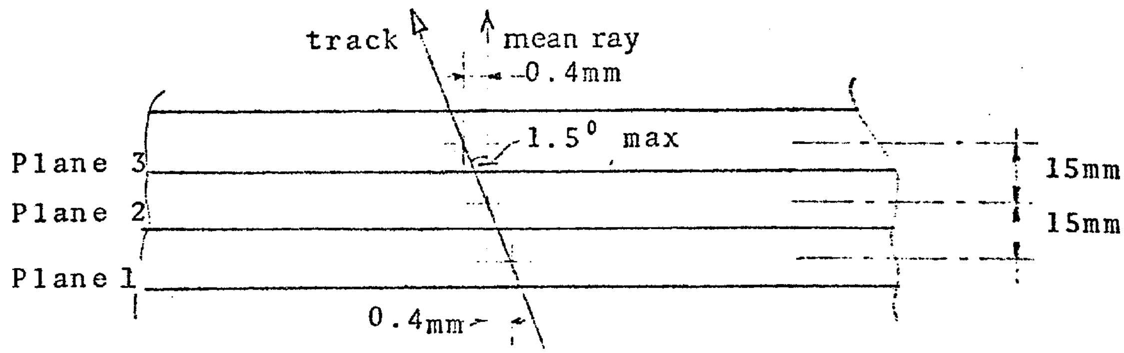

Figure 17. Cross-section of triplet adjusted to account for nominal angle of inclined track.

---

* Perhaps as much as 100-150μ greater than that obtained for straight through tracks. See, for example, figs. 8, 9 p378 of reference 4, fig. 22 p. 20 of reference 5.

** See for example the 12mm plane (which includes electrostatic shielding) in fig. 10, p. 197 of reference 6.

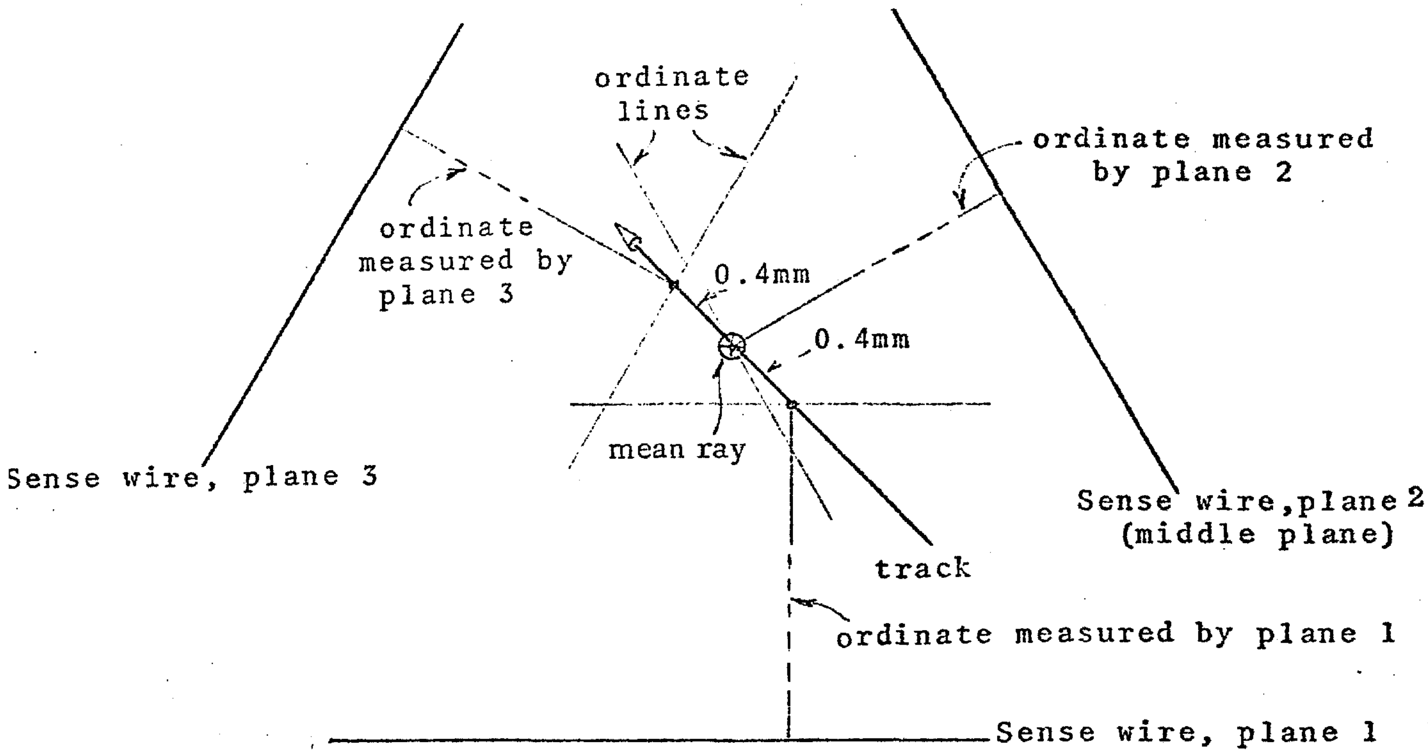

Figure 18. Adjusted triplet showing measured ordinates for a track with max. angle of uncertainty.

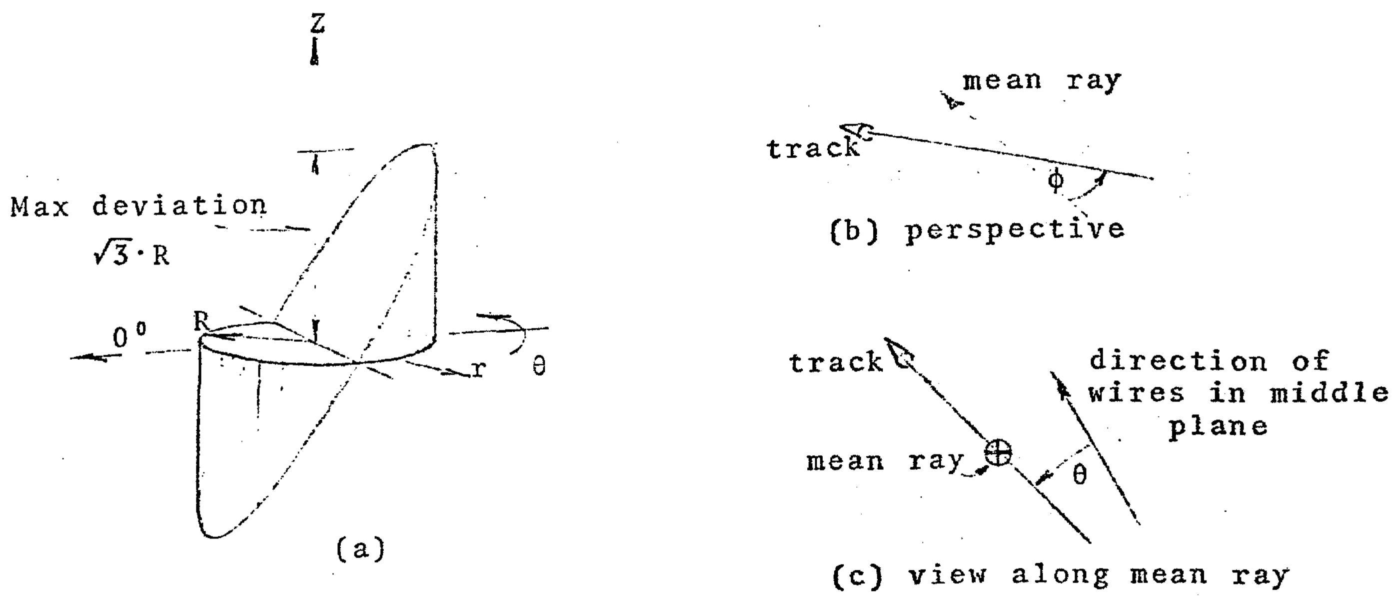

Figure 19. Deviation of sum of ordinates generated by inclined track as a function of the orientation of the track trajectory.

The deviation in the sum as a function of track orientation is represented pictorially in figure 19(a). Figures 19(b) and (c) indicate the angles which define the track's trajectory: (b) is a perspective showing the track inclined at an angle ϕ

to the mean ray; (c) is a view along the mean ray showing the track inclined at angle θ to the direction of the wires in the central drift plane (2).

The deviation $z = \sqrt{3}.\, r \cos\theta$, where r is the 'offset' between points of intersection of the track with successive mid-planes. For a drift plane separation of 15mm, this offset is 15. ϕmm. $r_{max} = R = 0.4$mm for the maximum angle of uncertainty, 1.5^0.

Assuming that from any point in the drift plane, the particle 'source' appears uniformly illuminated, the mean square deviation is given by

$$\overline{z}^2 = \frac{1}{\pi R^2}\int_0^{2\pi}\int_0^{R} z^2 \cdot r d\theta \cdot dr$$

$$= \frac{1}{\pi R^2}\int_0^{2\pi}\int_0^{R} (\sqrt{3}\cdot r\cos\phi)^2 r d\theta \cdot dr$$

$$= 3/4\ R^2$$

i. e., the rms deviation $= \frac{\sqrt{3}.\, R}{2}$

$= 0.35$mm for $R = 0.4$mm

Combining the independent errors, one due to diffusion broadening (see sec. 2. 6) including an additional 100μ to account for the angle of the track at the edge of the chamber (see first footnote p. 22), and the other due to the uncertainty in the track's orientation, we can estimate the overall rms deviation in the sum of ordinates as $\sqrt{(360)^2+(350)^2}$ or 500μ.

There are two consequences of the uncertainty in the track's orientation:

1) Degradation of the intrinsic temporal discrimination of the drift chamber. It is difficult to obtain an exact quantitative measure of this degradation (in the form of a confidence curve similar to that produced in section 2. 6) since the error component due to the uncertainty in the track's orientation does not have a normal

distribution. As an estimate, however, consider a track separation such that the two possible sums of ordinates are separated by 3000μ, i.e., 6 x overall rms deviation. For a normal track, this gave a confidence level of 0.999 for association with the correct beam track, see fig. 12. We estimate that in the present case, the confidence level should be at least this high, as the orientation error component distribution is more compact (i.e., has no long tails) compared with the normal distribution. A shift of 3000μ in the sum is contributed by an increment of 1000μ in each of the three ordinates, which in turn can be caused by associating the data with another beam track separated in time by $\frac{1000\mu}{50\mu/\text{nsec}}$, i.e., 20nsec.

For 16 beam particles spread randomly over a 300μsec beam spill, the probability of two or more beam particles occurring in the same 20nsec time slot is 0.8%. Assuming a 10% probability that a beam particle interacts in the bubble chamber, the probability that the drift chamber event data cannot be correctly associated with its proper beam track is quite negligible.

2) An increased tendency towards ambiguity. Figure 9 (b) shows the situation with a particle passing near the HV wire in one of the planes. A tendency towards ambiguity is indicated by the small triangle labelled P' if the distance of the true particle P from the HV wire is such that this secondary triangle is comparable in size with that* shown in fig. 18, then indeed it is difficult to determine, on the basis of the data presented by the drift chamber alone, whether the actual particle passed through P or P'.

3. Conclusion

Summarizing the advantages of beam time encoding used in conjunction with plane configurations which provide spatial constraints:

1) Removes left-right ambiguity normally encountered in a single plane. This advantage derives from the plane configuration alone.

2) Provides high beam (event) rate capability. In a collimated beam, beam time encoding provides temporal resolution limited by

*The triangle formed by the ordinate lines.

a) the measurement error in an individual plane

b) how well one knows the position of the wires in the chamber, and how stable this position is with time

and c) the pulse-pair temporal resolution in the digitizing channel handling the beam.

Assuming one can initially measure the relative placement of the wires in each triplet using a collimated beam, and that thereafter each wire remains within 100μ of its measured position, the combined effect of a and b is still largely dominated by diffusion broadening. It was shown in section 2.6 that this limits the temporal resolution to about 10 nsec. Therefore, in practice, the actual limit on temporal resolution achieved with beam time encoding will very likely be determined by c, which in turn depends on the degree of sophistication of the electronics in the beam digitizing channel.

In an uncollimated beam, the performance of beam time encoding depends largely on the extent of the angular spread of the beam. For the drift chamber attached to the FGD in our application, the intrinsic temporal resolution is degraded to approximately 20nsec, which is comparable with the pulse pair resolution of the individual digitizing channels.

3) Provides continuous (beam spill by beam spill) calibration of the chamber drift velocity. In any beam spill, there will be sense wire data derived from 'isolated' particles (either straight through beam tracks or a secondary not sharing a cell with any other secondaries) which can be used as a check on the drift rate. Such an arrangement would require provision for good uniformity of the gas mixture within the set of three planes. Straight through beam tracks are to be preferred for calibration because they are essentially normal to the planes and therefore permit tighter tolerances to be imposed. For a 5cm drift space, an rms error of 260μ on individual ordinate measurements and an uncertainty of $\pm 50\mu$ in the position of the

sense wires, it should be possible to detect a variation of about 1% in the drift velocity on the basis of observations from a single beam track. Averaging over 100 beam tracks, one can follow the short term ($\sim$20 secs) behavior of the drift velocity extremely well.

4) Provides protection against asynchronous background. Any background which arrives at a sense wire during the drift time interval associated with an actual beam track requires storage but can be sifted out during the off-line sorting.

5) Provided the asynchronous background rate is such that the additional storage space in the readout electronics is tolerable, the drift space dimension need no longer be constrained by event rate considerations. The cell size is now limited by other factors, perhaps the diffusion broadening of the drifting electrons and the accuracy required of the measurement.

An intrinsic accuracy of 300μ for measurements of distances of about 10cm* has been achieved in experimental set-ups.[2)]

Very little has been said about ambiguities, temporal and spatial: a study of this aspect of beam time encoding seems best handled by computer modeling. A Monte Carlo study of the problem is in progress and results should soon be available.[7)]

In any case, it would seem that employing beam time encoding does not burn any bridges: all the information collected in a conventional digitizing system will still be available using the approach described in this note.

---

*The curve of fig. 10 would yield a corresponding figure of 360μ if extrapolated to 10cm.

4. Acknowledgments

We would like to thank Professors Irwin Pless and Richard Yamamoto for their encouragement in this work and for useful discussions during its formative stages.

5. References

1) Improved 30-inch BC-Hybrid System, Committee Report, R. J. Plano, Chairman, 27 September 1974.
2) Very large Proportional Drift Chambers with High Spatial and Time Resolutions, D. C. Cheng et al., Nucl. Instr. and Meth. 117(1974) 157-169.
3) Very High Accuracy Drift Chambers in Magnetic Fields, A. Breskin et al., Proc. Int. Conf. on Instrumentation for High Energy Physics, Frascati, 8-12 May 1973, pp 301-304.
4) The Multiwire Drift Chamber, a New Type of Proportional Wire Chamber, A. H. Walenta et al., Nucl. Instr. and Meth. 92(1971) 373-380.
5) Further Results on the Operation of High-Accuracy Drift Chambers, A. Breskin et al., Nucl. Instr. and Meth. 119(1974) 9-28.
6) Recent Observations and Measurements with High-Accuracy Drift Chambers, A. Breskin et al., Nucl. Instr. and Meth. 124(1975) 189-214.
7) Private communication, Austin Napier and Richard Yamamoto.

IHS CONSORTIUM

NEWSNOTE

NO. 43

Version 2 of Scan Rules for Fermilab $\pi^+/K^+/p$ 150 GeV/c Experiment E-299 with the Fermilab Hybrid Spectrometer

(Supersedes DAS-77-1)

E. S. Hafen and R. I. Hulsizer

Massachusetts Institute of Technology

2 May 1977

TABLE OF CONTENTS

I.	Summary	Page 1
II.	IPD Instructions	2
III.	Hand Measurement Instructions	8
IV.	Definitions	9

Figure 1:	Fiducials in view 1	13
Figure 2:	Fiducials in view 2	14
Figure 3:	Fiducials in view 3	15
Figure 4:	Fiducials in view 4	16
Figure 5:	Fiducial Volume	17
Figure 6:	Sample Measurement	18

Appendix I:	NACOM Definitions	19
Appendix II:	Vertex Types	20
Appendix III:	IPD Reject Codes	21
Appendix IV:	Beam Count and Second Scan	22

I. SUMMARY

This document presents the IPD rules agreed upon for FNAL Experiment 299. The university numbers of the groups participating in the IPD'ing of this film are given in the STYX format writeup.

A complete scan shall be done of the bubble chamber film for all events inside the fiducial volume (fig. 5). All such events shall be IPD'ed except those falling into the reject categories specified in Sections II B-D. A prong count at the primary vertex shall be recorded for each event found in the scan, including rejected events, until further notice. A reference ionization track shall be IPD'ed with measured events. All tracks from the primary vertex of an event shall be IPD'ed even if superimposed. Tracks from secondary interaction vertices shall not be IPD'ed except for a scattered slow proton without a visible recoil or with a visible recoil less than 135 microns on film in all views. Secondary tracks from a decay shall always be IPD'ed. V's, straight gammas, and curly gammas shall be IPD'ed in association with each event for which they point back to the primary vertex. The output of the IPD'ing shall be a tape in the STYX format version 4.

After the complete scan and IPD have been performed, as above, there will be a check and correction scan. For this scan the scanner will be provided with a list of frames on which events were found on the original scan, but no other information. The scanner will then examine those frames and record the roll, frame, and event number and the complete topology of the event as given in the STYX format words NATOP and NATOP2. When this check scan is complete, the topological description of the events from the original scan and the check scan will be compared. Differences between the two lists will be adjudicated and the STYX output tape corrected. If the error is in the original scan, and if the error resulted in incorrect IPD'ing, the event will be re-IDP'ed and new measurements inserted in the STYX tape to replace the erroneous ones. The result of this check and correction scan will be a single file in STYX format for each roll with the corrections made and with the events ordered by ascending roll-frame-event number.

II. IPD INSTRUCTIONS

A. MASTER FIDUCIAL MEASUREMENT

At the beginning of each day or when starting a new roll of film, a master fiducial measurement shall be done. This consists of measuring fiducials M_1 through M_4 defined in figs. 1-4, in the order M_1, M_2, M_3, M_4, in each view of one frame. The scanner comment number NACOM shall have the digit F set to 1 for this record.

B. SCANNING INSTRUCTIONS

The first frame scanned on a roll should be recorded even if there is no event on it. The record should have the digit S set to 1 in the scanner comment word NACOM. The last frame scanned on a roll should be recorded even if there is no event on it. The record should have the digit S set to 2 in the scanner comment word NACOM. If there is an extended section of bad frames on a roll, these frames may be removed from the experiment as a block by the following procedure. Record the last good frame scanned before the bad section with the digit S set to 2 in the scanner comment word NACOM. The first good frame scanned after the bad section shall be recorded with the digit S set to 1 in the scanner comment word NACOM. The minimum required length for a section to be rejected in this manner is left to the discretion of the individual laboratories. Each frame shall be scanned for interactions of beam tracks (events) in the fiducial volume defined on p. 10 and in fig. 5. If there is an event in the fiducial volume, the frame should be checked to see that it is good. A bad frame is one for which one or more of the following is true:

1) One or more views is missing. (IPD digit in NATRB set to 1)

2) The beam tracks have on the average fewer than 15 bubbles per mm on film. (IPD digit in NATRB set to 1; this replaces the old "faint view" criterion.)

3) There are more than 16 incoming beam and secondary tracks which cross the front edge of the fiducial volume. A single track which makes multiple crossings

of the front edge of the fiducial volume (e.g., electron spiral) is to be counted only once. Beam tracks and incoming secondary tracks are defined in Section IV (IPD digit in NATRB set to 2).

4) There are more than two events in the fiducial volume (IPD digit in NATRB set to 6).

C. EVENTS IN BAD FRAMES

If the frame is bad, each event in the fiducial volume shall be recorded individually with the correct topology words and then rejected with the appropriate reject code. At a later time, QMC may eliminate the requirement that the events in the bad frames be identified.

D. ACCEPTED EVENTS

If an event in the fiducial volume has been accepted as being in a good frame, then it shall be examined to see if it is an acceptable event. The following events are to be rejected:

1) Events having a secondary scatter less than 225 microns on film from the primary vertex in any view (IPD digit in NATRB set to 4).

2) Events having more than two beam tracks which are not associated with the event and which lie within a band 180 microns wide on film, centered on the event's beam track in any view (IPD digit in NATRB set to 3).

Rejected events are to be recorded individually with the correct topology words and the appropriate IPD reject code, as given above, but no IPD measurements.

Acceptable events shall be IPD'ed as in the following discussion and in fig. 6. Each view is to be completed before the next view is begun, and the tracks are not to be matched. Each view should have the same number of tracks IPD'ed from the primary vertex. Vertices downstream from the primary vertex shall be IPD'ed and recorded in the topology word only if they are in the visible region in all three views and the track which gives rise to the vertex does not turn through more than 120^0 before the vertex occurs. If they are in the visible region in all three views, they should be measured as well as possible even if obscured by other tracks or some imperfection in the picture

E. MEASURING (IPD'ING) ACCEPTED EVENTS

1) TRACK COUNT

The number of charged tracks emanating from the primary vertex shall be entered as the track count on the first view measured. The track count does not include identified electrons. It must be the same in all views. (See II. E. 4, page 5.)

2) EVENT COMMENTS

If there is a beam track within 45 microns on film of the interacting beam track in any view, the digit C should be set to 1 in the scanner comment word NACOM. If there is evidence of turbulence in the picture, the digit T should be set to 1 in the scanner comment word NACOM.

3) FIDUCIALS, BEAM TRACK, AND IONIZATION REFERENCE TRACK

This information is referred to as generation 1 data; it shall consist of at least six points: fiducials M_1 and M_2, the primary vertex (V), a clear point (C) on the beam track, and two points (I_1 and I_2) on an ionization reference track. Additional clear points, an upstream hald point (H) and an end point (E) may be put on the beam track, if desired. If the primary vertex (V) is obscured, an upstream halt point should be used subsequently on all outgoing tracks, but a best guess inside the confusion should be measured for the vertex as the first point on the beam track. The second beam track point should be a clear point on the beam track or should be guessed if no part of the beam track is clear. The clear point should be placed approximately half-way between the vertex and either the beginning of the beam track or any obstruction, whichever is closer to the vertex. If there is no confusion, the clear point should be no more than 5mm on film from the vertex, even if the beam track is long and clear. The last two points, designated by I_1 and I_2 for "ionization points", should be measured along a nearby beam track which is clear and does not interact in the region of the outgoing tracks to be measured. The purpose of this track is for comparison of its ionization with that of the outgoing tracks. The first ionization point measured should be in the region of the outgoing tracks and the second ionization point measured should be in the region of (but slightly upstream of) the interaction vertex. An ionization track should be as close to the original beam track as possible, but further than 135 microns on film from any beam track. If there is no suitable separate beam track to be used as an ionization reference track, the beam track of the event should itself be remeasured as the ionization reference track.

4) GENERATION 2 TRACKS

Generation 2 information shall include IPD points on all tracks from the primary vertex. Each track may have up to eight points measured on it.

If the track is simple, with no confusion, then only two points are required: a clear point (C) and an end point (E). The clear point must be between the vertex and the end point and in a region of the track which is as clear as possible of other tracks and confused areas of the film. The end point should be placed on the last point of the track seen in the bubble chamber unless the track turns through more than 120^0, in which case the end point should be put on the track near where the track has turned through 120^0.

If the track is confused, then there can be up to eight points on the track. A halt point may be used to indicate that the region of the track near the vertex is obscured by confusion. A halt point should be placed as near the vertex as possible, but downstream of the obscured region. If other parts of the track are obscured, a clear point must be placed near the center of each clear region (up to a total of six clear regions). No clear points should be placed at a turning angle of more than 120^0 from the vertex; in this case the end point should be put at 120^0.

The number of tracks IPD'ed must be the same in all three views. If two tracks are superimposed so that it is not possible to find a clear region, the double track should be IPD'ed twice. If a track cannot be found at all in a view, then the missing track should be measured by IPD'ing the vertex twice.

5) SLOW PROTONS

If a positive, densely ionized track appears to end inside the chamber (a "stopping" track), it should be labeled as a stopping track and the end point should be on the end of the track. If there is a secondary scatter of a slow proton with no change in bubble density and no recoil, or a recoil shorter than 135 microns on the film in all views, then the proton track before the scatter shall be measured with the end point on the scatter vertex (vertex type 7; proton kink); the portion of the proton track after the proton kink is a generation 3 track, but shall be measured like a generation 2 track. The invisible or short recoil is a generation 3 track, but should not be measured. If the portion of the proton track after the kink stops in the chamber it should be labeled as a stopping track, and the end point of the scattered track should be on the end of the track. If the kink is not apparent in all views, it should be measured in the view(s) where visible and a best guess made in the other view(s). In this case the end point of the portion before the scatter is not a corresponding point, so it should not be put in the vertex bank, but the track ID word should be set to 10. Stopping track ends are given vertex type 10. Notice that a sigma phi decay might be classed as a proton with a kink.

6) GENERATION 2 TRACKS WITH SECONDARY INTERACTIONS

Such tracks shall be measured like other generation 2 tracks, but the end point shall be on the secondary vertex (vertex type 2). The tracks from the secondary interaction shall not be IPD'ed unless the generation 2 track is a slow proton (see II. E. 5).

7) TRACKS WITH DECAYS

If a positive, densely-ionized track has a kink such that the direction changes by more than 2^0 and the ionization is observed to change, or if any other type of track has a kink such that the direction changes by more than 2^0 and/or the ionization is observed to change, it shall be taken as a one-prong decay unless the decay is clearly identifiable as a π-μ-e decay (see II. E. 8). The track before the decay point shall be

IPD'ed like a generation 2 track, but the end point shall be on the decay point (vertex type 4). The track emanating from the decay point is a generation 3 track and must be IPD'ed like a generation 2 track. A three-prong decay should also have all outgoing generation 3 tracks IPD'ed like generation 2 tracks; its decay vertex is type 12.

8) π-μ-e DECAYS

If a generation 2 track has a decay that is clearly identifiable as a π-μ-e decay, the track is a pion and shall be IPD'ed like a generation 2 track. If a generation 3 track has a decay that is clearly identifiable as a π-μ-e decay, the track is a pion and shall be IPD'ed like a generation 2 track. In neither case are the muon and electron to be IPD'ed. If the π-μ decay vertex is in the visible region in all three views, and the π track does not turn through more than 120^0, the end point of the π track is to be on the vertex and it is to be given vertex type 8.

For sections II.E. 6-8, if the relevant vertex is outside the visible region in one or two views or the track turns through more than 120^0, then the end point cannot be at the vertex in all three views and is therefore not labeled as a vertex, but the track identifier word for that track is set to the value the vertex identifier would have been given had the end point been a corresponding point.

9) V TRACKS

If there is a V which points to the primary vertex with a nonzero opening angle where neither of the charged tracks is identifiable as an electron (see II.E.10 and II.E. 11), this feature shall be taken as an associated V and measured after all charged tracks from the primary vertex have been completed. The neutral track will not be in the STYX track banks. The vertex of the V shall be measured and given the type 3. The tracks from the V vertex shall be IPD'ed as generation 2 tracks. If a V points back to more than one primary vertex, it shall be IPD'ed with each of these events. Both events shall have the ambiguity digit A in the scanner comment number, NACOM, set as described in Appendix I.

10) CURLY GAMMA (ELECTRON PAIR)

A curly gamma (electron pair) is identified by zero opening angle and at least one prong which is minimum ionizing and which is observed to spiral by at least 180^0. The neutral track will not be in the STYX track banks. The vertex of the curly gamma shall be measured and given the vertex type 6. The tracks of the electron and positron shall be measured as generation 2 tracks. If a curly gamma points back to more than one primary vertex, it shall be taken with each of these events. Both events shall have the ambiguity digit A in the scanner comment number, NACOM, set as described in Appendix I.

11) STRAIGHT GAMMAS

A V with zero opening angle in all three views, where neither track can be identified as an electron or positron, is a straight gamma. The neutral track will not be in the STYX track banks. The vertex of the straight gamma shall be measured and given the vertex type 5. The tracks from the straight gamma vertex are IPD'ed as generation 2 tracks. If a straight gamma points back to more than one primary vertex, it shall be taken with each of these events. Both events shall have the ambiguity digit A in the scanner comment number, NACOM, set as described in Appendix I.

12) DALITZ PAIRS

If either the electron or positron or both tracks of a Dalitz pair can be identified as an electron or positron (minimum ionizing tracks which spiral by at least 180^0), then such tracks shall be labeled as Dalitz electrons (upstream vertex type 9) and IPD'ed like (a) generation 2 track(s). The quantity E in NATOP is to contain the number of electrons and positrons identified at the vertex.

III HAND MEASUREMENT INSTRUCTIONS

Hand measurements of events follow the same procedures as the IPD measurements of events except that 5 fiducials are to be measured on each frame in the order 13, 19, 21, 16, 1 (see figs. 1-4). At least 7 points are to be measured on each charged track. There are no reference ionization track measurements; instead, an ionization code is recorded for each track in each view. The ionization codes are:

(1 to 1.3) x minimum is code 1

(1.3 to 1.8) x minimum is code 2

(1.8 to 2.5) x minimum is code 3

(2.5 to 4) x minimum is code 4

(> 4) x minimum is code 5

unknown is code 0

IV. DEFINITIONS

1) BEAM TRACK

A beam track is a track which is in the fiducial volume, has minimum ionization, and is parallel to the beam track direction to within 1/400th of a radian. For frames having more than one beam track, this means that the real beam tracks deviate from being parallel by less than 45 microns on film in traversing the fiducial volume. For a frame with only one track, its trajectory should be compared to a template positioned relative to the fiducials. The template should be marked with beam track trajectories from other frames.

2) CURLY GAMMA

A curly gamma is a V-shaped topology which has zero opening angle between the tracks, is produced at a distance from a primary vertex, points back to the vertex, and has either or both of the positron and the electron identifiable as electrons.

3) DALITZ PAIR

A dalitz pair is a positron-electron pair which emanates from an interaction vertex and has one or both of the positron and electron identified.

4) DECAY

A decay is the end point of a track with a kink which is not a proton kink (see IV. 14), where the direction changes by more than 2^0 and/or the ionization changes. A three-prong decay is the end point of a track which has three charged particles emerging from the decay vertex.

5) ELECTRON/POSITRON

An electron or positron is a track which has minimum ionization and which is observed to spiral by at least 180^0.

6) EVENT

An event is an interaction of a beam track.

7) EVENT REJECTION CRITERIA

a. Events with a secondary scatter less than 225 microns on film from the primary vertex in any view (IPD reject code 4).

b. Events having more than two beam tracks, not associated with the event, within ± 90 microns on film of the event's beam track in any view (IPD reject code 3).

8) FIDUCIAL VOLUME

The fiducial volume is the region in view one (1) within which events are considered for measurement. The fiducial volume is bounded by the arc of a circle and three straight lines. The arc of the circle forms the upstream edge. Its center is fiducial 12 and the arc passes through fiducial 7.

To construct the two lines forming the sides of the volume, take the following steps, as illustrated in fig. 5. Draw a line from fiducial 18 to fiducial 22. On that line mark one point 3/20 of the distance from fiducial 18 to fiducial 22 (point A). Mark a second point 17/20 of the distance from fiducial 18 to fiducial 22 (point B). Now draw a line which is parallel to the line which joins fiducials 17 and 18 and that passes through the first point described above (point A). Then draw a line which is parallel to the line which joins fiducials 19 and 22 and that passes through the second point described above (point B). These two lines define the sides of the fiducial volume.

The downstream edge of the fiducial volume is constructed by the following steps. Draw a line connecting fiducials 17 and 12 and mark on it a point that is one-quarter (1/4) of the distance from fiducial 17 to fiducial 12 (point C). Then draw a line which is parallel to the line joining fiducials 17 and 19 and that passes through point C. This line defines the downstream edge of the fiducial volume.

9) FIDUCIALS

Fiducials are defined in figs. 1-4. Fiducials M_1-M_4 are the IPD Master fiducials. Fiducials M_1 and M_2 are in the IPD event fiducials.

10) FRAME REJECTION CRITERIA

a. One or more of the views is missing (IPD reject code 1).

b. The beam tracks have, on the average, fewer than 15 bubbles per mm on film (IPD reject code 1).

c. There are a total of more than 16 incoming beam and secondary tracks that cross the front edge of the fiducial volume. Multiple crossing of the front edge by a single track (e.g., electron spiral) is not to be counted (IPD reject code 2).

d. There are more than two events in the fiducial volume (IPD reject code 6).

11) INCOMING SECONDARY TRACK

An incoming secondary track is a track which enters the upstream edge of the fiducial volume and has more than minimum ionization or has a distinguishably smaller radius of curvature than the beam tracks or which is nonparallel with the beam tracks by more than 1/400th of a radian.

12) IONIZATION REFERENCE TRACK

An ionization reference track is a clear track more than 135 microns on film away from any beam track and which does not itself interact in the region of the outgoing tracks from the event. The purpose of this track is for comparison of its ionization with the outgoing tracks from the event.

13) π-μ-e

A π-μ-e is a track consistent with a pion which decays into another particle which has a short track and which in turn decays into an electron. See fig. 6 for an example (track 5).

14) PRIMARY VERTEX

A primary vertex is the interaction point of a beam track.

15) PROTON KINK

A proton kink is the point where a positive densely ionized track changes its direction by more than 2^0 but the ionization does not change, and which has either no visible recoil or a recoil shorter than 135 microns on film in all views.

16) SECONDARY INTERACTION

A secondary interaction is the end point of a track which emanates from a primary vertex and which interacts in the bubble chamber resulting in an even number of outgoing tracks. The point of interaction is the secondary interaction vertex.

17) STOPPING TRACK

A stopping track is a positive track which appears to end in the bubble chamber volume and which has ionization greater than minimum, consistent with the hypothesis that it is a proton.

18) STRAIGHT GAMMA

A straight gamma is a V-shaped topology with zero opening angle, produced at a distance from the primary vertex, which points back to the primary vertex but has neither particle identifiable as an electron or positron.

19) TRACK COUNT

The track count is the number of charged tracks emanating from the primary vertex excluding all tracks identified as electrons. The track count may be odd.

20) V

A V is a V-shaped topology with nonzero opening angle, produced at a distance from a primary vertex, which points back to the vertex, and in which neither track can be identified as a positron or electron.

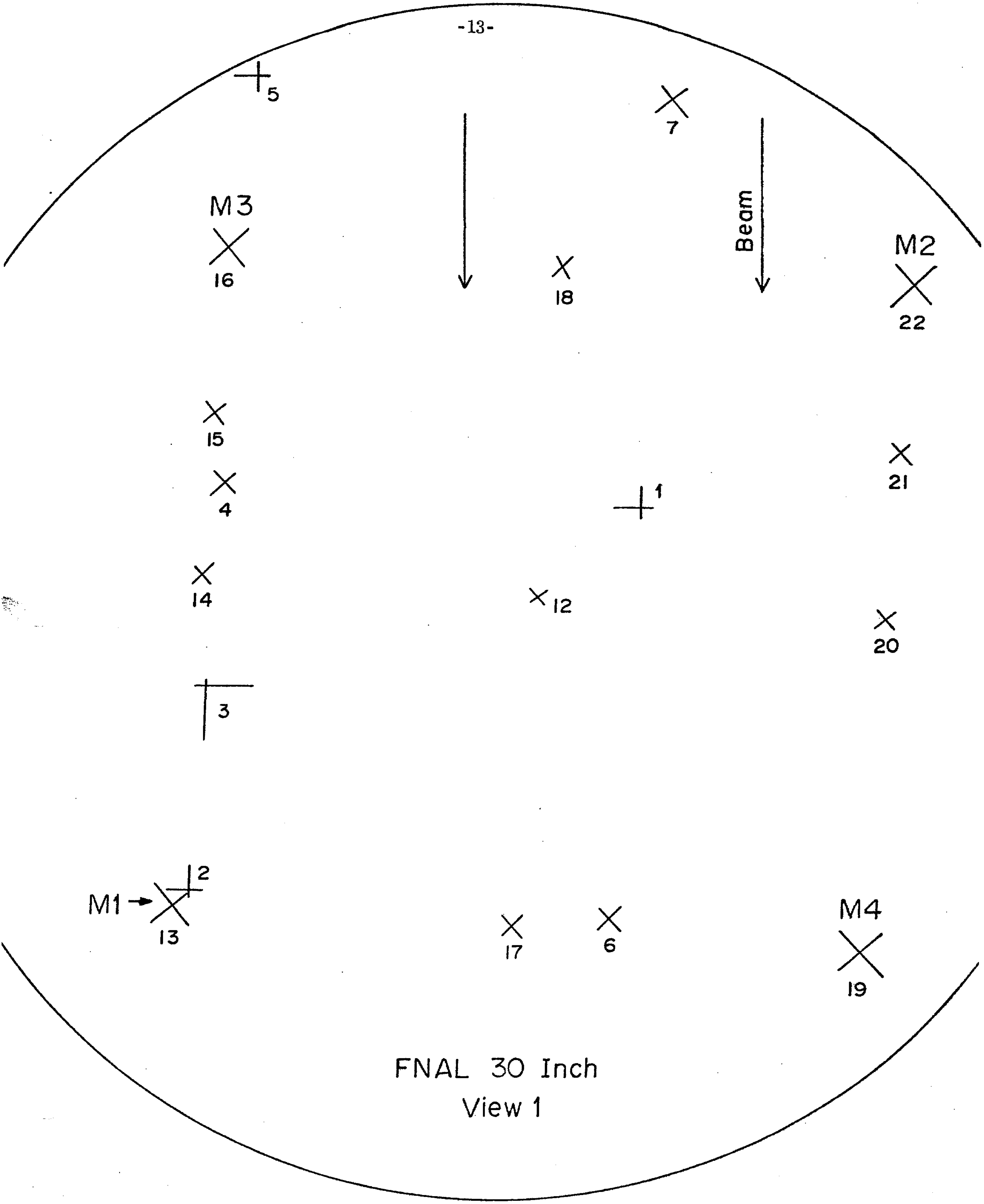
5
7
Beam
M3
16
18
M2
22
15
21
4
1
14
12
20
3
2
M1
13
17
6
M4
19
FNAL 30 Inch
View 1

Figure 1

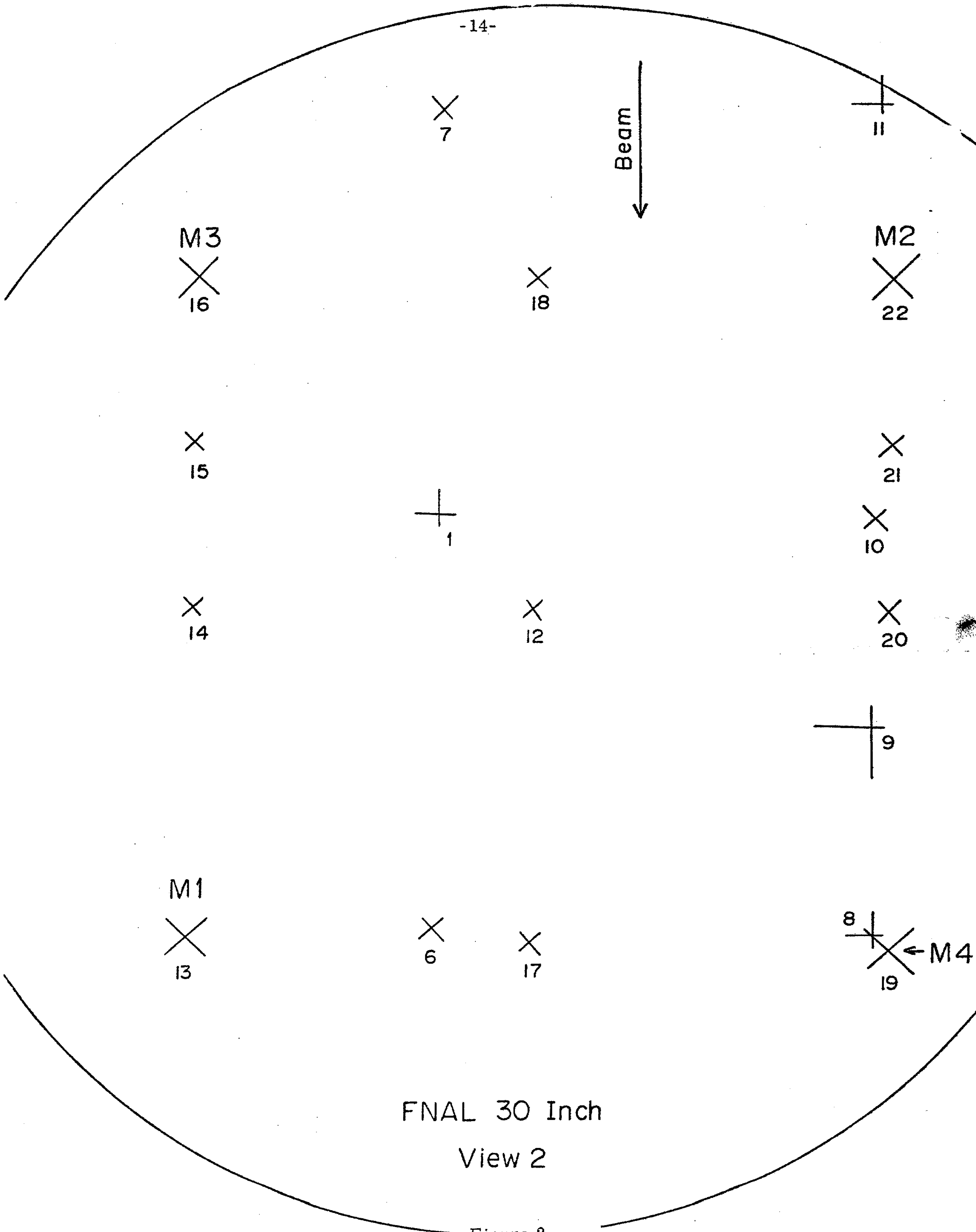

Beam
7
11
M3
16
18
M2
22
15
21
1
10
14
12
20
9
M1
13
6
17
8
M4
19
FNAL 30 Inch
View 2

Figure 2

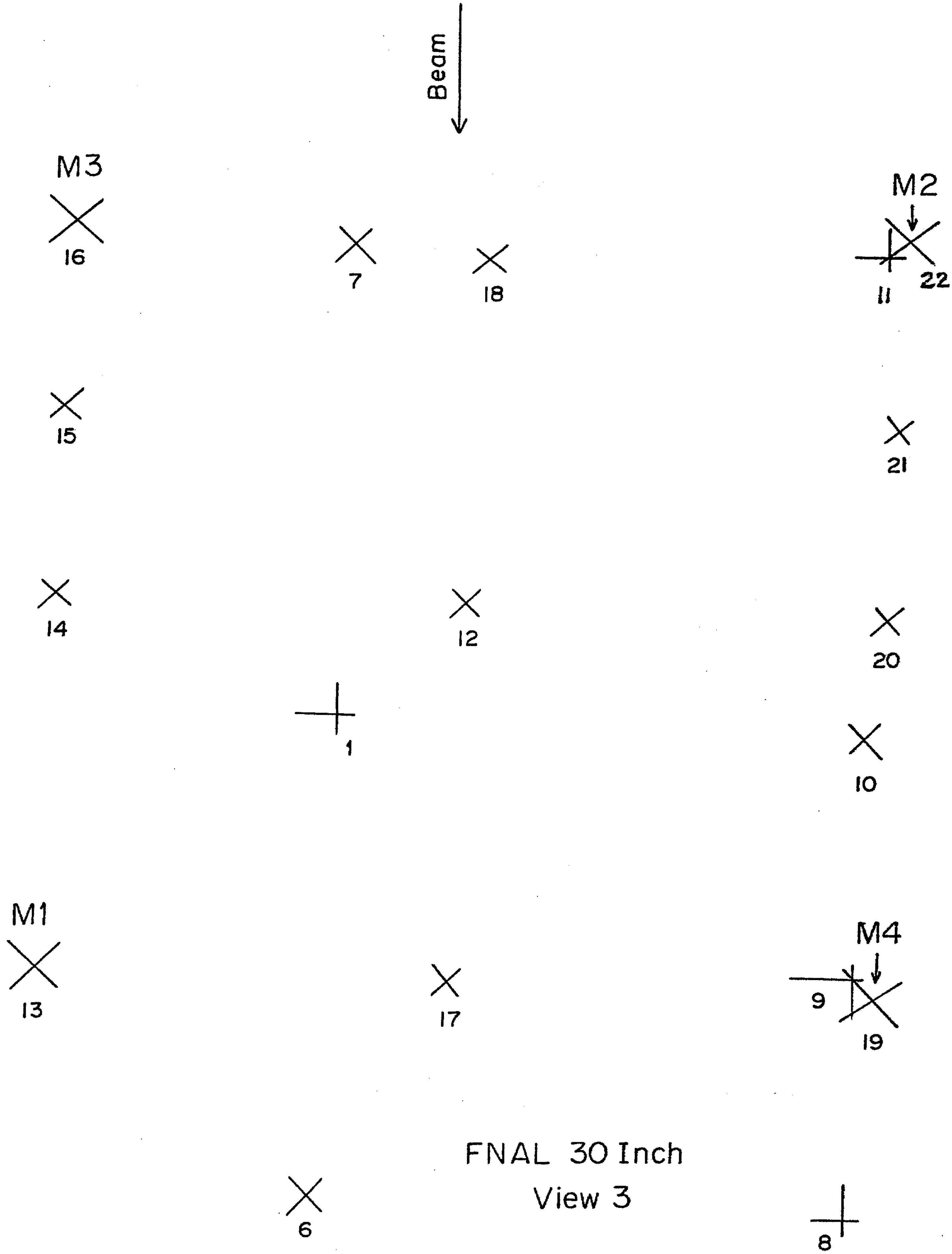
Beam
M3
16
7
18
M2
22
11
15
21
14
12
20
1
10
M1
13
17
M4
9
19
FNAL 30 Inch
View 3
6
8

Figure 3

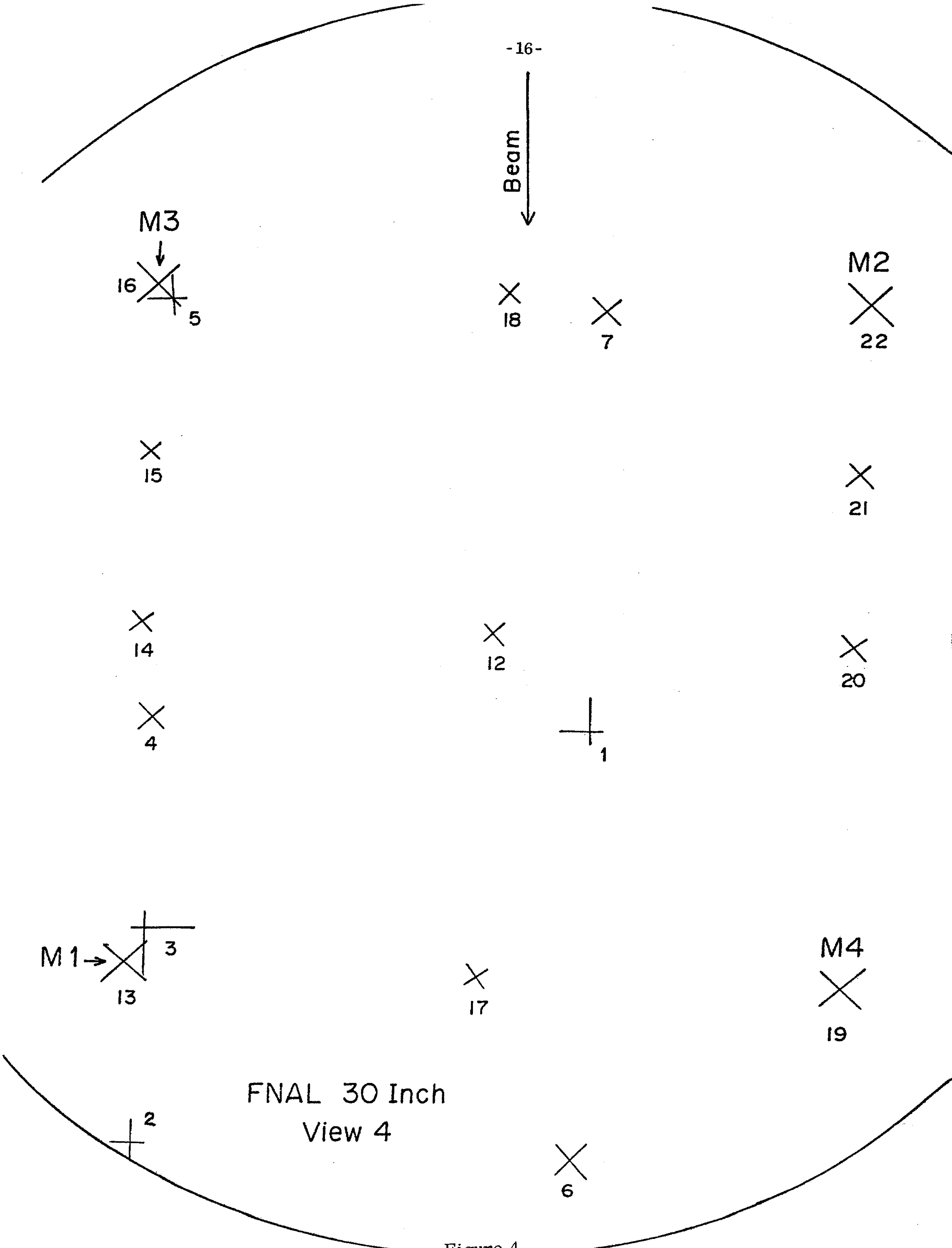
Beam
M3
16
5
18
7
M2
22
15
21
14
12
20
4
1
3
M1
13
17
M4
19
FNAL 30 Inch
View 4
2
6

Figure 4

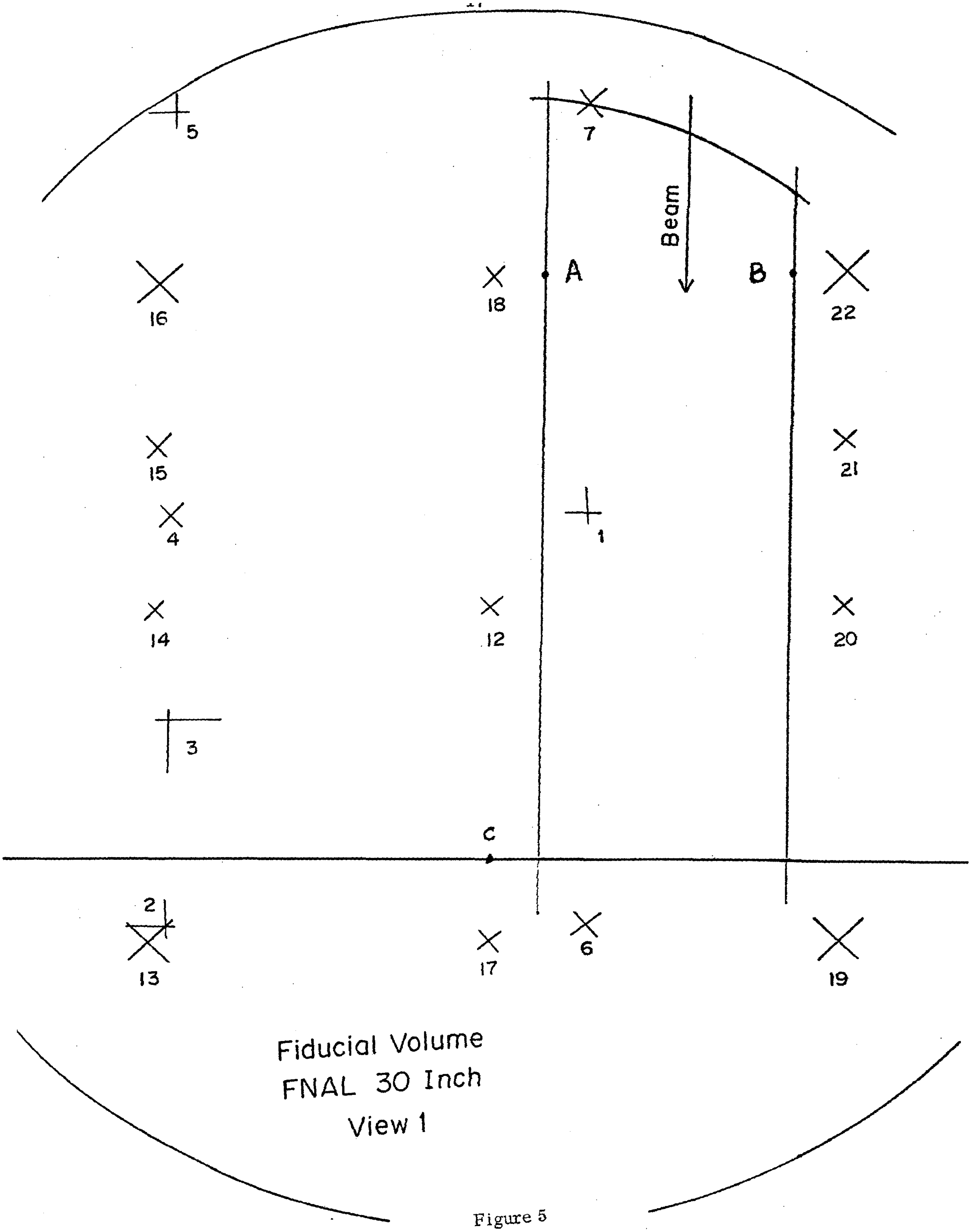

5
7
Beam
A
B
16
18
22
15
21
4
1
14
12
20
3
C
2
13
17
6
19
Fiducial Volume
FNAL 30 Inch
View 1

Figure 5

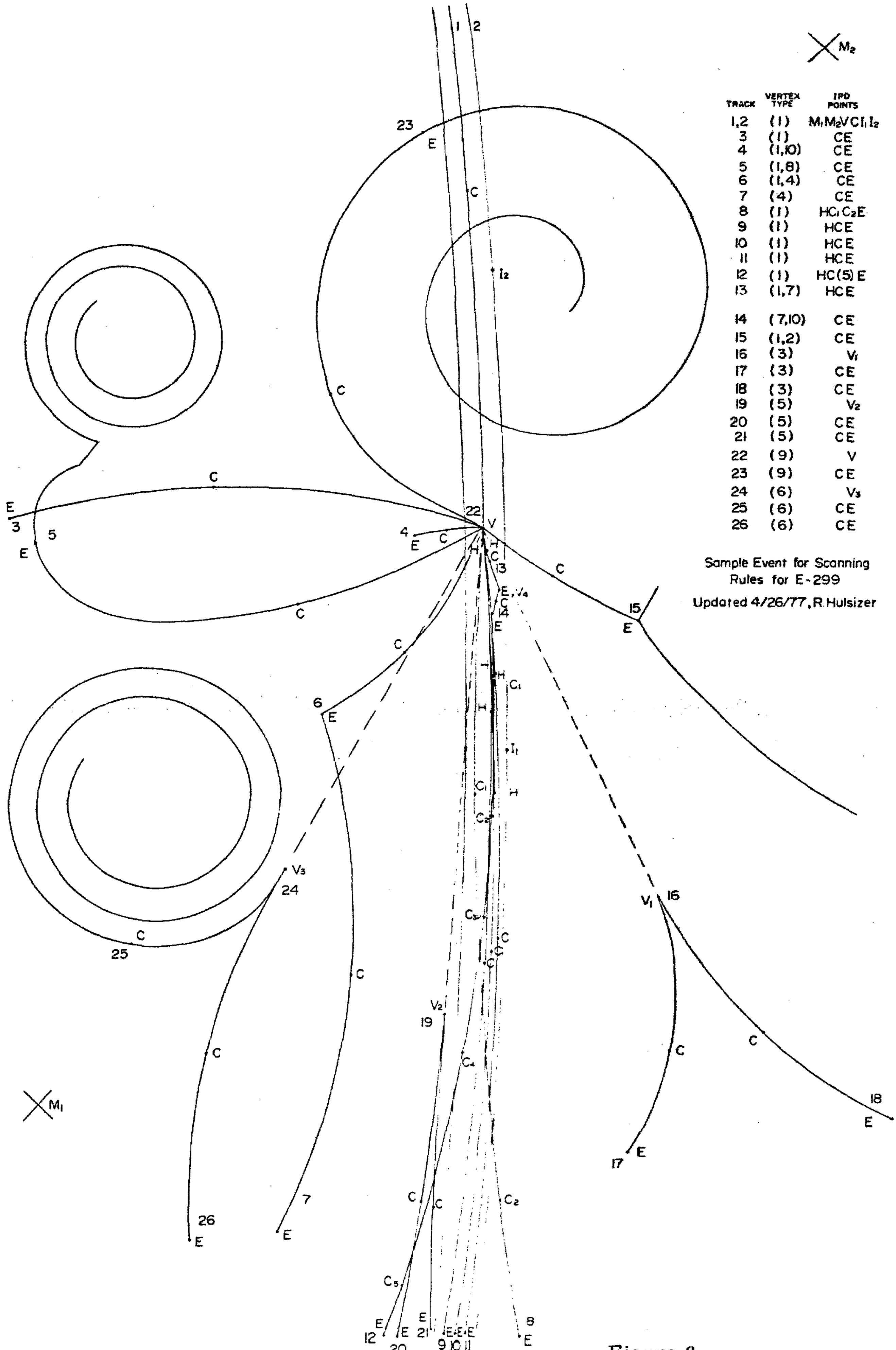

TRACK	VERTEX TYPE	IPD POINTS
1,2	(1)	$M_1M_2VCI_1I_2$
3	(1)	CE
4	(1,10)	CE
5	(1,8)	CE
6	(1,4)	CE
7	(4)	CE
8	(1)	HC_1C_2E
9	(1)	HCE
10	(1)	HCE
11	(1)	HCE
12	(1)	HC(5) E
13	(1,7)	HCE
14	(7,10)	CE
15	(1,2)	CE
16	(3)	V_1
17	(3)	CE
18	(3)	CE
19	(5)	V_2
20	(5)	CE
21	(5)	CE
22	(9)	V
23	(9)	CE
24	(6)	V_3
25	(6)	CE
26	(6)	CE

Sample Event for Scanning Rules for E-299

Updated 4/26/77, R. Hulsizer

Figure 6

Appendix I - NACOM Definitions

The STYX word NACOM is for scanner comments. It is to have the following decimal structure: TPCABSF. The digits have the following definitions:

F: 1 - Master fiducial record

2 - Event found on rescan

S: 1 - First frame scanned on a roll

2 - Last frame scanned on a roll

B: 1 - First frame scanned after a series of unscanned bad frames

2 - Last frame scanned before a series of unscanned bad frames

A: 1, 2, 3 - This number indicates the number of types of neutral decays in this frame which are ambiguously associated with this event and another event in the frame. The types of neutral decays are V's, curly gammas, and straight gammas.

C: 1 - A beam track is within 45 microns on film of this event's beam track in some views.

P: 1 - A positive track from the primary vertex of this event disappears in the liquid without stopping. Such a track is probably a positron annihilating with an atomic electron.

T 1 - There is evidence of turbulence in this frame.

Appendix II - Vertex Types

1 - Main Vertex

2 - Secondary Interaction Vertex

3 - V vertex

4 - One prong decay vertex

5 - Straight gamma vertex

6 - Curly gamma vertex

7 - Proton kink vertex

8 - End of stopping pi track that decays into a muon and then an electron

9 - Dalitz electron pair at primary vertex

10 - Stopping track end

11 - Not used in E-299

12 - Three pronged decay vertex

Appendix III - IPD Reject Codes

These code numbers are to be placed in the least significant decimal digit of the STYX word NATRB. The reject code to be placed therein is the code for the first cause of reject that is found, following the order listed.

1 - View missing on this frame or the bubble density is less than 15 per mm on film on the beam tracks.

2 - Too many incoming tracks in this frame (> 16).

3 - Event with more than two beam tracks, not associated with the event, within 90 microns on film of the event's beam track in any view.

4 - Event with secondary scatter less than 225 microns on film from the primary vertex in any view.

5 - Three or more events in the fiducial volume of this frame.

Appendix IV - Beam Count and Second Scan

A - Beam count - a beam track count will be made on every roll of the experiment. The procedure will be that every tenth frame in each roll will be examined. If it is an acceptable frame by the criteria used in the scan rules, then the number of beam tracks crossing the front edge of the fiducial volume will be recorded. If the frame does not satisfy the criteria for an acceptable frame, then it will be recorded as a rejected frame. For the present, it is proposed that records of the beam track count be kept by hand, not as records on magnetic tape. For reference, the criteria for an acceptable frame are summarized below.

1) All views are present.
2) The beam tracks have on the average 15 bubbles or more per mm on film.
3) There are fewer than 17 incoming beam and secondary tracks crossing the front edge of the fiducial volume.
4) There are at most two events in the fiducial volume.

B - Second scan - Every fourth roll shall be scanned a second time. The scan rules will be exactly the same as for the first scan, including the check and correction scan, but no IPD measurements will be made. Each event will have the digit F of STYX word NACOM set to 2.

APC Programming Note
DAS 77-4

Updated GEOMAT and GEOMAT Tape Format for Use With GEOMAT Version 3.21

(Update of DAS 76-9)

Linda E. Morecroft
March 1, 1977

Laboratory for Nuclear Science
Massachusetts Institute of Technology
Cambridge, Massachusetts

Table of Contents

New Features in GEOMAT 3.2	1
GEOMAT Printed Output Format	3
GEOMAT Tape Format	4
PWGP/TRKOR Tape Format	9
SQUAW Tape Format	12
Notes	18

New Features in GEOMAT 3.2

1) An SP bank is now used to describe groups of IPD points.

2) NALG41 has been replaced by NALG50, and patch SLAC17 modifies SLAC13; both changes are modifications for positive tracks.

3) Neutral mass hypotheses have been added. Modifications have been made to the mass hypotheses on charged tracks (see Note 13), and to the vertex labels (see Note 10).

4) Processor FF updates the mass hypotheses if the sign of curvature has changed during any fit. This allows a proton hypothesis on some low momentum straight tracks.

5) FFM now updates the starting parameters between mass hypotheses for non-stoppers. This rescues a few pathological measurements from the "overstop" condition and does no harm to good measurements.

6) A variable buffer size is used in X154 to include all PEPR points and IPD point groups in the output record.

7) Processors CC and PMS have been modified to match vertices within type class.

8) Processor EST requires a minimum number of points in each view. This eliminates a few spurious matches, primarily those with high transverse momentum.

9) Minor bugs have been fixed.

10) The following constants have been altered:

(i) Z = TTINSIDM, ZMIN and ZMAX - making the underestimated chamber smaller.

(ii) Z = TTINSIDP, ZMIN and ZMAX - making the overestimated chamber larger.

(iii) Z = TTPTOR, SCALE; Z = TTXSQN, SCALE - hydrogen density was too large.

(iv) Z = TTFNAT, ICHBM; Z = TTBXYZ, SCFLX; Z = TTXSQN, ICHBM - π^+ beam

and (v) Z = TTXSQN, OKDELP - has been added. This is the threshold value of DELP/P ratio to change the track charge.

11) The following constants in the DATA BLOCK have been added:

(i) Z = TTCC0, PSEP
Z = TTMIT0, PSEP - minimum separation required between points.

(ii) Z = TTEST0, KILLVW - minimum number of points required per view in ESTHLX.

GEOMAT Printed Output Format: output header line*

1) Roll No.
2) Frame No.
3) Event No. (see Note 1)
4) Remeasurement No. (see Note 2)
5) Measuring device No. (see Note 3)
6) Topology (see Note 4)
7) Prep serial No. (see Note 5)
8) Input event sequence No.
9) Output event sequence No.
10) Reject/report conditions for this event (see Notes 6 and 7)

*N.B. When reporting problems with events please give items 1-9 of the output header line (all of which are also on the output tape) and as much of item 10 as is available.

GEOMAT Tape Format

1) R. K. Yamamoto word (see Note 22)

2) N = No. words following in record (integer)

All subsequent words are floating point

HEADER BLOCK

1) NWH = No. words in header block = 30

Header Block (one/event)

1) Experiment No.
2) Source flag (see Note 8)
3) Roll No.
4) Frame No.
5) Event No. (see Note 1)
6) Remeasurement No. (see Note 2)
7) PREP serial No. (see Note 5)
8) Packed report conditions (see Note 7)
9) "
10) Reject code (see Note 6)
11) Prong count
12) No. measured tracks Vw. 1
13) No. measured tracks Vw. 2
14) No. measured tracks Vw. 3
15) No. measured tracks Vw. 4

(12–15: at primary vertex, including beam track)

16) Event type code-topology (see Note 4)
17) Measuring device (see Note 3)
18) IPD date (all dates in form YYMMDD)
19) Measuring device version No.
20) Measuring device run date
21) GEOMAT version No.
22) GEOMAT run date

23-24) Spare

25-28) Relative Ionization, Views 1-4

29-30) Spare

POINT BLOCK

1) NPF = No. reconstructed space points (vertices, stopping points)

2) NWPF = No. words/space point = 13 (see Note 9)

NWPF words repeated NPF times:

- 1) Vertex label (see Note 10)
- 2) Vertex type (see Note 10)
- 3) X
- 4) Y
- 5) Z
- 6-11) Error matrices

  $(\Delta X)^2$, $\Delta X \Delta Y$, $\Delta X \Delta Z$, $(\Delta Y)^2$, $\Delta Y \Delta Z$, $(\Delta Z)^2$

- 12) Chi^2 of original fit to vertex point
- 13) Vertex flag (see Note 12)

RECONSTRUCTED TRACK BLOCK

1) NTF = No. reconstructed tracks

2) NWTF = No. words in mass-independent block (NWTF = 15)

3) NWMF = No. words in mass-dependent block (NWMF = 20)

    1) NMASS = No. mass interpretations for this track

    2) MULT = No. views used in reconstruction

    3) Label 1 (label of vertex from which track starts--see Note 10)

    4) Label 2 (track label-see Note 11)

    5) No. measured points each Vw (V4, V3, V2, V1) (see Note 14)

    6) Nature (see Note 15)

    7) Length of track

    8-11) Measured ionization each Vw

    12-15) Spare

    1) Mass Code (see Note 13)

    2-4) $1/P$, λ, ϕ

    5-10) Error matrix at vertex:

    $(\Delta 1/P)^2$, $\Delta 1/P\, \Delta\lambda$, $\Delta 1/P\, \Delta\phi$, $(\Delta\lambda)^2$, $\Delta\lambda\Delta\phi$, $(\Delta\phi)^2$

    11) Residual (RMS point scatter)

    12) Chi-squared

    13) Expected ionization (reference view)

    14-16) X, Y, Z end

    17-19) $1/P$, λ, ϕ end

    20) Spare

Repeat NMASS Times

Repeat NTF Times

TRACK IMAGE BLOCK

1) NTI = No. Track images (see Note 16)

2) NWTIB = Total No. of words in block of track images

- 1) No. of words in this track image
- 2) Vertex label
- 3) Track label (see Note 17)
- 4) View number
- 5) Nature (see Note 15)
- 6) Measured ionization
- 7) IPD = 2*NMEAS + 9 = pointer to start of IPD points
- 8) NIPDG = No. IPD point groups
- 9) NMEAS = No. precision measured points (PEPR points)
- 10-11) x, y
- 12-13) x, y

NMEAS precision measurements

. .
. .
. .
. .

one/track image

- 1)' NIPD = No. IPD points of this type
- 2)' Type (see Note 18)
- 3'-4)' x, y

. .
. .
. .
. .

NIPD IPD points

repeat for NIPDG types

repeat for NTI track images

PWGP/TKORG Tape Format

PWGP/TKORG format is the same as GEOMAT format with the following exceptions:

A) Header Block

(i) NWH = No. words in header block = 35

(ii) 23) PWGP version No.

24) PWGP run date

(iii) 31) Date of spill

32) Time of spill

33) Accel. cycle count — from PWC tape

34) Spill No. (1-3)

35) Trigger No. (1-16)

B) Reconstructed Track Block (see next page)

RECONSTRUCTED TRACK BLOCK (PWGP)

1) NPWC = No. tracks reconstructed in downstream planes (PWGP) (see Note 19)

2) NWT = No. words in mass-independent block (NWT = 15)

3) NWM = No. words in mass-dependent block (NWM = 20)

Repeat for NPWC Tracks

- 1) NMASS = 1
- 2) MULT (see Note 20)
- 3) Label 1 (see Note 10)
- 4) Label 2 (see Note 11)
- 5) No. Planes traversed by this track
- 6) Nature (see Note 15)
- 7-9) X, Y, Z at first downstream chamber
- 10) ΔY
- 11) ΔZ
- 12) a_Y fitted downstream slopes
- 13) a_Z fitted downstream slopes
- 14-15) Δa_Y, Δa_Z

one mass-dependent block for downstream tracks

- 1) Mass code (see Note 21)
- 2-4) 1/P, λ, ϕ at vertex — from BCMAG
- 5-10) Error matrix at vertex — from BCMAG
- 11) Spare
- 12) Downstream χ^2
- 13) Spare
- 14-16) X, Y, Z last chamber
- 17-20) Spare

RECONSTRUCTED TRACK BLOCK (TKORG)

The TKORG reconstructed track block is the same as the PWGP track block with the following exceptions:

When

(i) <u>MULT = -1</u>

2) MULT = -1

8) Y
9) Z
} at first downstream chamber with FITALL solution

10) ΔY
11) ΔZ
} differences between FITALL and PWGP solutions

12) a_Y
13) a_Z
} slopes from FITALL

14) Δa_Y
15) Δa_Z
} differences between FITALL and PWGP

Mass dependent block:

2-4) 1/P, λ, ϕ at vertex
5-10) Error matrix at vertex
} from FITALL

11) Residue (RMS point scatter) of FITALL solution in bubble chamber

12) χ^2 of overall fit

15) Y
16) Z
} at last chamber with FITALL solution

20) Label of the GEOMAT track hooked up

(ii) <u>MULT = -2</u>

2) MULT = -2

11) If zero - solution is pure BCMAG

If non-zero - solution from FITALL

SQUAW Output Format

HEADER BLOCK

1) R. K. Yamamoto word (see Note 22)

BLOCK 1 - RECORD CHECK

1) No. of words following
2) No. of words in whole record (including 1)
3) No. of words in block 1 (including 1)
4) No. of words in block 2
5) No. of words in block 3
6) No. of words in block 4
7) No. of words in block 5 (see Note 23)

BLOCK 2 - EVENT INFORMATION

1) No. of words following in this block

2) Input event sequence No.

3) Scale factor used by PTOR and RTOP. Set in D = CONSTANT

4) X coordinate of primary vertex (cm)

5) Y coordinate of primary vertex (cm)

6) Z coordinate of primary vertex (cm)

7) Primary vertex χ^2

8) Roll No.

9) Frame No.

10) Event No.

11) Event type word 1 } (see Note 24)

12) Event type word 2 }

13) Measurement information (see Note 25)

14) Table (T)/Scanner (S)/University (U) No., TTSSUU

15) Reject code from GEOMAT/CERBERUS/PEPR (see Note 6)

16) Setting error on film (see Note 26)

17) Measuring device version No.

18) Measuring device run date

19) Geometry version No.

20) IPD date

21) Prep serial No.

22) Packed report conditions from GEOMAT (see Note 7)

23) Packed report conditions from GEOMAT (see Note 7)

24) Reject code (as 15 above)

25) Experiment No.

26) Non-fatal codes from PEPR

27) Geometry run date

28) No. of SQUAW fits (set to 0)

29) Status word (see Note 27)

BLOCK 3 - INDEX TO TRACK OUTPUT BLOCK

1) No. of words for track 1 (including all mass hypotheses)

2) No. of words for track 2 (including all mass hypotheses

: for all tracks in this event)

BLOCK 4 - TRACK OUTPUT BLOCK

Track information is in two groups. Group 1 contains indicative mass independent information and Group 2 information for each mass tried.

Group 1 - for track K

1) No. of words in Group 1

2) Track number (1, 2, 3, etc. Beam track, if present, is first)

3) Point measure code (see Note 28)

4-6) No. points measured in views 1, 2 and 3

7-9) No. points used in fit in views 1, 2 and 3 (if negative it is equal to -IFAIL code (see note 27) for that view)

10) No. points going into fit (set = 2 for 2-pointers)

11) Scan/measure packed data word for this track (see Note 29)

12) HX at track center (kilogauss)

13) HY at track center (kilogauss)

14) HZ at track center (kilogauss)

15) Spare

16-21) Ionization data (2 words/view) (see note 30)

Group 2 - for track K (repeat for each mass hypothesis)

1) No. of words in Group 2

2) IFAIL code (see note 27)

3) K-PANG test (set to 99. for non-stopped and to 0. for stoppers)

4) Mass used in this test(carries sign of charge). MeV.

5) LSZ for this mass test (see definition in note 28)

If event failed, Group 2 ends here.

6) Length of track for this mass test, in cms

7) RMS deviation of measured points on film (microns), or for 2-point tracks, first point fit χ^2

8) Expected multiple scattering contribution to RMS, or for 2-point tracks, second point fit χ^2

9) Beginning space X, in cms

10) Beginning space Y, in cms

11) Beginning space Z, in cms

12) Beginning azimuth, in radians

13) Beginning slope (tangent of dip)

14) Beginning K (= 1. / (MOM * COS (DIP))), MOM in MeV/c

For a 2-point track or a stopping track:

15) Beginning D(AZ) * D(AZ)

16) Beginning D(AZ) * D(SLP)

17) Beginning D(AZ) * D(K)

18) Beginning D(AZ) * D(LNG)

19) Beginning D(SLP) * D(SLP)

20) Beginning D(SLP) * D(K)

21) Beginning D(SLP) * D(LNG)

22) Beginning D(K) * D(K)

23) Beginning D(K) * D(LNG)

24) Beginning D(LNG) * D(LNG)

25) End space X, in cms

26) End space Y, in cms

27) End space Z, in cms

28) Beginning D(AZ) * end D(AZ)

29) Beginning D(AZ) * end D(SLP)

30) Beginning D(SLP) * end D(SLP)

This is meaningful only for charged 2-point non-stoppers

Note: - For charged 2-point tracks or stoppers, all K-information and error matrix is from length (not curvature). For non-stoppers use curvature, and for neutral 2-pointers use nothing.

Block 4 ends here for a 2-point or stopping track.

For regular non-stopping tracks:

15) Beginning D(AZ) * D(AZ)

16) Beginning D(AZ) * D(SLP)

17) Beginning D(AZ) * D(K)

18) Beginning D(SLP) * D(SLP)

19) Beginning D(SLP) * D(K)

20) Beginning D(K) * D(K)

21) End space X, in cms

22) End space Y, in cms

23) End space Z, in cms

24) End azimuth, in radians

25) End slope

26) End K

27) End D(AZ) * D(AZ)

28) End D(AZ) * D(SLP)

29) End D(SLP) * D(SLP)

30) Beginning D(AZ) * end D(AZ)

31) Beginning D(SLP) * end D(AZ)

32) Beginning D(K) * end D(AZ)

33) Beginning D(AZ) * end D(SLP)

34) Beginning D(SLP) * end D(SLP)

35) Beginning D(K) * end D(SLP)

36) Error in length

N.B. All errors and beginning/end correlations between errors are coulomb corrected.

NOTES

Note 1 Event Number

The event number is defined as

0 = 1st event on the frame

1 = 2nd event on the frame, etc.

Note 2 Remeasurement Number

The remeasurement number is set to

0 for the first measurement of the roll

1 for the second measurement of the roll, etc.

Note 3 Measuring Device Number

The measuring device number is defined as:

1 = PEPR measured

2 = hand measured

Note 4 Topology

Topology is defined as:

100* prong count + 10* No. Vee Zeros + No. electron pairs

Note 5 Prep Serial Number

Prep serial number = event sequence number through IPD

Note 6 Reject Codes

The reject code is normally set to zero, except for the following cases:

(i) 99 - Hydra system condition. Insufficient memory space

(ii) 100 - Event failed in PEPR stage

(iii) 134 - Event failed by scanner (unbiased)

(iv) 135 - Event failed by scanner (biased)

(v) 352 - All vertices failed in processor PMS

Note 7 — Report Conditions

Packed Cond. No.	Report No.	Description	Processor
3	301	Fewer than 2 matched fiducials	- FDC
5	302	Residual too big (reject one fiducial first if possible)	- FDC
4	303	Stretch too big	- FDC
22	304	One fiducial rejected	- FDC
23	305	Measured fiducial not found in title	- FDREF
14	351	Vertex measured on fewer than 2 views	- PMS
1	352	No PF created	- PMS
13	353	Fewer than 2 vertex measurements available	- PAP
7	354	Point refit	- CC
15	355	Unmatched vertices remain in at least one view	- PMS
11	357	Point match ambiguity	- PMS
17	361	Space point candidates difficult to resolve	- PMU
20	363	Labeled double fails test	- PMU
16	371	First approximation not precise enough, iterate	- PFT
18	372	No convergence in point fit	- PFT
6	373	Point fit attempted using one view only	- PFT
8	381	Convex failure	- CVM
2	382	No primary vertex	- X154
21	385	No convergence in convex	- CVX
12	401	Not enough views for track match	- MIT/MBTA
24	402	Incomplete multiple	- MIT/MBTA
9	403	Restart matching	- MIT
19	412	Incompatible labeled doubles	- MU
26	451	No mass fit accepted	- FF
25	461	Change of sign of curvature during iteration	- FFM
10	481	2-point track final fit failure	- TWP/TWPS

The report conditions generated by each event are converted to a packed condition code (from 1 to 26). This packed condition code represents the priority of the report condition, 1 being the first in priority and 26 the last.

Conditions 1 and 2 mean no track reconstruction can be done.

Conditions 3-9 mean the entire event is at best questionable.

Conditions 10-21 mean the event is at worst questionable.

Conditions 22-26 happen often, depending on the experiment.

A maximum of 8 report conditions may be packed into the output record (4 per word); if more than 8 have been generated, the 8 with the highest priority are selected. For example, if report conditions 354, 371, 373, 402 and 451 are generated for one event, these are equivalent to packed condition codes 7, 16, 6, 24 and 26. On the output record the packed condition codes appear as 803046 and 26. These are represented in binary as:

11000 10000 00111 00110

and 11010

Bits 1-5 of the first word represent packed condition code 6

Bits 6-10 of the first word represent packed condition code 7

Bits 11-15 of the first word represent packed condition code 16

Bits 16-20 of the first word represent packed condition code 24

and

Bits 1-5 of the second word represent packed condition code 26

Note 8 Source Flag

The source flag is zero for GEOMAT format record.

Note 9 Space Point Words

If a block of data contains no entries, the length specification words still appear. Thus, if there are no reconstructed space points: NPF=0, NWPF=13, and these two words are immediately followed by NTF, the number of reconstructed tracks.

Note 10 Space Point Types

1 = primary vertex

2 = secondary vertex

3 = V^0 vertex

4 = decay vertex (kink)

5 = ambiguous neutral, straight gamma

6 = electron pair

7 = proton kink

8 = π - μ - e decay vertex

9 = Dalitz pair vertex

10 = stop point

11 = short stub

12 = Tau decay

The vertex label is defined as:

Label = 10 * Type + I

where I = integer from 0 - 9

e. g. I = 0, first vertex of this type

I = 1, second vertex of this type

The exception to this rule is for Type 7.

I = 0, Ionization reference track

I = 1, first vertex for Type 7

I = 2, second vertex for Type 7

Note 11 Track Label

The track label is set by CERBERUS to:

1 - for beam tracks

10 * vertex type - for downstream vertex of unique type

0 - for non-unique or no downstream vertex

In processor MIT, if the track label is zero from input, it is given a value of TFLAB + I, where TFLAB is the starting value for track autolabels (set in block data, Z = TTMIT0) and I is incremented by 1 for each track.

Note 12 Vertex Flag

This is normally set to zero. GEOMAT 2.1 allowed tracks to be reconstructed for failed vertices. In this case the flag was set to 1, indicating a bad vertex.

Modifications may be made to STEER and CC to allow for this in GEOMAT 3.2.

Note 13 Mass Codes

The following mass codes are used:

$1 = \gamma$

$4 = e^{\pm}$

$5 = \mu$

$6 = \pi^{0}$

$7 = \pi^{\pm}$

$8 = K^{\pm}$

$9 = K^{0}$

$10 = p$

$13 = \Sigma^{+}$

$15 = \Sigma^{-}$

Mass assignment is based on the beginning and end vertex types (see Note 10) for the fit. If there is no beginning vertex, or the type is undefined, the track is treated as coming from the primary vertex.

Some beginning and end types suggest simple cases for mass assignment. The others are determined by comparing the momentum (P) with cutoff values, PCUTML and PCUTMH (set in the CONSTANT deck), and checking whether bit 3 of the TF bank (- charge) has been set.

Beginning Vertex Type	Mass Assignment
1	check end type
2	check end type
3	e, π or e, π, p (if P<PCUTMH)
4	e, π (if negative OR if positive and P>PCUTMH) or e, π, p (if positive and P<PCUTMH)
5	e, π or e, π, p (if P<PCUTMH)
6	e
7	p
8	μ
9	e

End Vertex Type		Mass Assignment
		π (if P > PCUTML and negative or P > PCUTMH and positive)
1	or	π, p (if PCUTML < P < PCUTMH and positive)
2	or	π, K (if P < PCUTML and negative)
10	or	π, K, p (if P < PCUTML and positive)
3		K^0
4		K^-, Σ^- (if negative)
	or	K^+, Σ^+ (if positive)
5		γ
6		γ
7		p
8		$\pi^{\pm}$
9		π^0

These hypotheses are those necessary to obtain a reasonable parametrization of the track. In some cases additional mass hypotheses are added to the output by XSQMAS for SQUAW's convenience.

Note 14 **Number of Measured Points Each View**

This word contains the number of measured points used in the final fit for each view.

Bits 1- 5, number of points used in view 1

6-10, number of points used in view 2

11-15, number of points used in view 3

16-20, number of points used in view 4

e.g. 19024 on the output record is represented as:

10010 10010 10000

in binary, and indicates:

0 PEPR points view 4

18 PEPR points view 3

18 PEPR points view 2

16 PEPR points view 1

Note 15 **Nature**

Nature is the status word of the TF bank for reconstructed tracks and of the TK bank for track images. Each bit, if set, carries a different piece of information about the track. Bit 1 is the least significant bit.

Bit 1 - Spare

2 - Track is positive

3 - Track is negative

4 - Track is doubly charged

5 - Beam track

6 - Track is incident at this vertex

7 - Direction unknown

8 - Definite stopping track

9 - Possible stopping track

10 - Straight track

11 - 2-point track

12 - Connecting track

13 - Matched (for track images)

14 - Ambiguous match (for reconstructed tracks)

15 - IPD points only (for track images)

Note 16 Track Images

A track image consists of the measurement information for a given track in a given view. All precision measured points (denoted by "PEPR points", although any device might have been used) appear first, followed by all IPD point groups. A track image appears on the output tapes for all measured tracks in the "forward jet" (space angle and curvature criteria) and for all track images not used in the reconstruction.

Note 17 Track Label

Track Label = 0 for track images not used in the GEOMAT reconstruction, otherwise it is the same as the track label for the corresponding track in the reconstructed track block.

Note 18 IPD Point Types

0 = Unspecified

1 = Upstream halt point

2 = Clear point

3 = Neighbor point

4 = End point

5 = Upstream vertex

6 = Downstream vertex

Note 19 No. of Tracks Reconstructed in Downstream Planes

For PWGP output the downstream tracks are added onto the existing GEOMAT event record; for TKORG, tracks reconstructed from bubble chamber measurements (GEOMAT) may be replaced by PWC reconstructed tracks and the two types of blocks intermixed. The word MULT determines the source of the reconstruction and hence the format of the block:

MULT > 0, bubble chamber (GEOMAT) reconstruction

MULT < 0, PWC reconstruction

Note 20 MULT

MULT is defined as:

3 - Three view GEOMAT reconstruction

2 - Two view GEOMAT reconstruction

1 - Possible GEOMAT mismatch

0 - PWGP track not originating from primary vertex

-1 - Track successfully reconstructed by both GEOMAT and PWGP

-2 - Track from primary vertex detected by PWC, but not reconstructed by GEOMAT (although track image exists)

Note 21 Mass Code

The mass code is set to 0 if Čerenkov gives no information. Otherwise the code is the same as the GEOMAT code (see Note 13) for the incoming beam track.

Note 22 R. K. Yamamoto Word

This is set to 2 for SQUAW and

1 for GEOMAT

Note 23 Block 5

This word is set to 0 by GEOMAT. SQUAW output fills block 5 with fit information and this word gives the number of words in block 5. The SQUAW output is the same up to this block.

Note 24 Event Type

Word 1:

10^6 * NELPR + 10^5 * NDLPR

+ 10^4 * NSCATN + 10^3 * NSCATP + 10 * NTRK

+ 5 * NPIMUN + NPIMUP

Word 2:

10^6 * NKPRO + 10^5 * NSTRAN + 10^4 * NDKIN + 10^3 * NDKIP

+ 10^2 * NDK3N + 10 * NDK3P + NVEE

where NKPRO = No. of proton kinks

NELPR = No. of electron pairs

NDLPR = No. of dalitz pairs

NSCATN = No. of negative scatters

NSCATP = No. of positive scatters

NTRK = No. of charged prongs at primary vertex

NPIMUN = 1 for a $\pi^- - \mu^- - e^-$ decay

NPIMUP = 1 for a $\pi^+ - \mu^+ - e^+$ decay

NSTRAN = No. of strange topologies in the event

NDK1N = No. of negative 1-prong decays

NDK1P = No. of positive 1-prong decays

NDK3N = No. of negative 3-prong decays

NDK3P = No. of positive 3-prong decays

NVEE = No. of vee zeros

Note 25 Measurement Information

The measurement information is defined as:

10^5 * prong count + 10^3 * remeasurement No.

+ measuring device No.

Note 26 Setting Error on Film

Setting error = TMEASR cms on unit reference plane (URP), where TMEASR is included in sequence Z = TTFFM0, set in block data.

Setting error on film (microns)

= TMEASR * FOCAL * 10^4, where

FOCAL is the scale factor from URP to film, and is set in sequence Z = OPTICS. Each view has a different value of FOCAL; an average value is used here.

Note 27 Status Word

The status word is set to:

10001 if GEOMAT O.K.

or 9000 + GEOMAT/CERBERUS/PEPR reject code otherwise

Reject conditions are also set by XSQN - series 600, 700 and 800.

Reject 600 - no primary vertex

710 - charge not balanced at primary vertex after VRTFIX

800 - number of reconstructed tracks greater than scanner prong count

800 + vertex label - unmatched track occurring in all three views at this vertex (match failure)

Note 28 Point Measure Code

The point measure code, J, is defined as:

J = 2 for 1st track (beam track if present)

J = 3 if LSZ = 1

J = 10 * IVUN + IVDN if LSZ > 1

where LSZ = 0, regular non-stopping track

= 1, stopping track

= 2, 2-point non-stopping track

= 3, charged 2-point non-stopping track

IVUN = originating vertex no.

0 - track originates from outside the chamber

1 - track originates from the primary vertex

2, 3 . . . track originates from vertex 2, 3 . . .

The vertices are labeled consecutively for identification only

IVDN = final vertex no.

0 - track leaves the chamber

1 - track ends on the primary vertex

2, 3 . . . track ends on the vertex labeled IVUN

Note 29 Scan/Measure Packed Data Word (Afterword)

This is defined as:

10^5 * IVXU + 10^2 * IVXD + 10 * IVUN + IVDN

where IVXU = vertex label (see Note 10)

IVXD = track label (see Note 11)

$\left.\begin{array}{l}\text{IVUN = originating vertex no.}\\ \text{IVDN = final vertex no.}\end{array}\right\}$ (see Note 28)

Note 30 Ionization Data

Word 1 = 2^{16} * lacunarity (%)

Word 2 = number of sweeps

Note:

a) In "beam track to close events", beam ionization is from the ionization reference track.

b) Number of sweeps = -1, indicates a possible pepr output error in the ionization record length.